I. MECHANISM OF ETHYLIDYNE FORMATION ON Ni(111)

and

II. DESIGN OF A MOLECULAR BEAM-SURFACE SCATTERING AND SURFACE ANALYSIS INSTRUMENT

by

THEODORE ROBERT TRAUTMAN

B. S. North Dakota State University
(1990)

SUBMITTED TO THE DEPARTMENT OF CHEMISTRY
IN PARTIAL FULFILLMENT OF THE REQUIREMENTS
FOR THE DEGREE OF
DOCTOR OF PHILOSOPHY

at the

MASSACHUSETTS INSTITUTE OF TECHNOLOGY

September 1996

Signature of Author ____

Department of Chemistry
September 25, 1996

Certified by _____

Sylvia T. Ceyer
Thesis Supervisor

Accepted by _____

Dietmar Seyferth
Chairman, Department Committee

This thesis has been examined by a committee of the Department of Chemistry as follows:

Professor Sylvia T. Ceyer_____

Thesis Supervisor

Professor Moungi G. Bawendi_____

Professor Robert G. Griffin_____

Chairman

I. MECHANISM OF ETHYLIDYNE FORMATION ON Ni(111)

and

II. DESIGN OF A MOLECULAR BEAM-SURFACE SCATTERING AND SURFACE ANALYSIS INSTRUMENT

by

THEODORE ROBERT TRAUTMAN

Submitted to the Department of Chemistry
on September 25, 1996 in partial fulfillment of the
requirements for the Degree of Doctor of Philosophy in
Chemistry

ABSTRACT

The synthesis and spectroscopic identification of ethylidyne ($-CCH_3$) on a nickel single crystal surface are demonstrated for the first time. Ethylidyne bound to Ni(111) is formed by the reaction of gas phase hydrogen atoms with adsorbed acetylene, ethylene or ethane. The ethylidyne formation reaction competes with displacement and/or hydrogenation of the hydrocarbon by the incident gas phase H atoms to yield gas phase hydrocarbons. Independent of the hydrocarbon reactant, a small amount of acetylene is observed to be coadsorbed with ethylidyne. This observation is explained by a dynamic equilibrium between adsorbed ethylidyne and adsorbed acetylene in the presence of gas phase H atoms. Ethylidyne is also synthesized by the reaction of adsorbed acetylene and hydrogen emanating from the bulk to the surface. With the assumption that these four reactions which yield ethylidyne proceed via the same intermediates, the mechanism for ethylidyne formation is determined to be reaction of the adsorbed hydrocarbon with a gas phase or bulk H atom to form vinyl ($-CHCH_2$), which in turn reacts to form ethylidene ($-CHCH_3$), which in a final step, reacts to form ethylidyne.

The ethylidyne adsorbate is identified through analysis of its vibrational spectrum measured by high resolution electron energy loss spectroscopy (HREELS). Four isotopomers of ethylidyne are synthesized and their vibrational spectra measured. Analysis of the observed vibrational features is shown to be consistent with those of ethylidyne. A normal modes analysis is also performed to confirm the assignment of the vibrational features to those of ethylidyne. The calculated normal mode frequencies of ethylidyne equal the measured frequencies within experimental error, and the force constants employed which yield the best fit to the observed frequencies are close in value to those used in previous normal modes calculations of an ethylidyne moiety. The normal modes analysis also sheds

light on the explanation for the unexpected upward shift in the frequency of the C-C stretching mode of ethylidyne upon deuteration observed in this and previous studies. The calculated normal mode displacements show extensive mixing of the C-C stretching and the symmetric CH_3 deformation modes which causes the frequency of the C-C stretching mode to shift downward in the unlabeled ethylidyne species and upward in the deuterated ethylidyne species. Analysis of the dipole activity of the observed vibrational features reveals the symmetry of the ethylidyne adsorbate to be C_3 or C_{3v}. The symmetry of ethylidyne in turn leads to determination of its adsorption site on the Ni(111) surface to be a three-fold hollow site. The observed vibrational spectra are also shown to be inconsistent with any other adsorbed C_2 hydrocarbon.

Attempts to synthesize a different hydrocarbon adsorbate, ethyl ($-CH_2CH_3$), have been carried out. A variety of approaches using ethyl halides, ethylene and ethane as precursors to ethyl have been undertaken. No vibrational features assignable to ethyl have been observed in the HREELS spectra measured after the attempted ethyl synthesis reaction. The features observed in the vibrational spectra are assigned to those of the precursor hydrocarbon molecule or those of ethylene. A large number of the attempted synthetic routes to an adsorbed ethyl species yield ethylene which suggests that the ethyl species is not a stable adsorbate on Ni(111) at the temperatures employed in the reactions, 40 - 120 K. It is therefore proposed that the barrier for thermal decomposition of adsorbed ethyl to produce adsorbed ethylene and surface bound hydrogen is very low or nonexistent.

These studies have been carried out on a custom built experimental apparatus which combines supersonic molecular beam techniques with surface sensitive spectroscopies. A new experimental apparatus has been designed which should prove to be even more powerful for the study of gas-surface dynamics because it includes a triply-differentially pumped detector, a rotatable molecular beam source and the capability of reflection absorption infrared spectroscopy in addition to the stationary molecular beam source and the surface spectroscopies in the present apparatus. Supersonic molecular beams allow the direction and energy of the incident molecule to be controlled. Surface analytical spectroscopies can be used to identify and characterize the adsorbed reaction product of the gas-surface interaction. The triply-differentially pumped detector coupled with a time-of-flight chopper can be used to identify scattered or desorbing products of the gas-surface interaction and to characterize their angular and translational energy distributions. Included in the design of the detector is the ability to ionize molecules with laser light through multi-photon ionization (MPI). Multi-photon ionization of specific rovibrational states allows the internal energy distribution of gas molecules which scatter or desorb from the surface to be measured. The combination of these techniques into one experimental apparatus should prove to be a powerful tool with which to probe gas-surface reaction dynamics.

Thesis Supervisor: Sylvia T. Ceyer

Title: Professor of Chemistry
W. M. Keck Foundation Professor of Energy

To My Parents

Acknowledgments

I would first like to thank my advisor, Professor Sylvia Ceyer. Sylvia's demand for excellence and attention to detail shows in all that she does including research, presentations, scientific publications, apparatus design and undergraduate teaching. I thank Sylvia for instilling in me the desire to produce quality work in all that I attempt. I know my experience at MIT will serve me well in my future scientific career. I would also like to thank Sylvia for the guidance and financial support she has afforded me over the last six years. Lastly, I would like to thank her for keeping a level head and positive attitude after the many mistakes I made in the lab, no matter how disastrous they may have been.

I thank Art Utz and Sean Daley for teaching me the details of operating the apparatus which was used to perform the experiments described in this work. Art showed great patience with my many questions of how the electronics worked, even the second and third time through. Sean was not only a good teacher in lab, but was and still is a great friend outside of lab. We have had many good times together which allowed me to blow off a lot of steam to relieve the stresses of graduate school. Sean was also very supportive in my final months of graduate school, always telling me I would make it through. Well Sean, you were right. I made it.

Kerstin Haug and Thomas Burgi deserve credit for helping me obtain a lot of the data which is presented in this thesis. I am very grateful for their help. Both were also available to discuss scientific problems and to bounce ideas around about chemistry. Kerstin especially showed me there is more than one way to look at a particular problem. I also thank Thomas for helping me with the normal modes analysis computer program. Without his help, I'm afraid I would still be programming.

I also want to thank the "Big Machine People" for putting up with me for the last six years. David 'Shmool' Pullman was always more than willing to answer any of my questions about surface science or chemistry in general. He was also a good source of humor

throughout his stay at MIT. Julius Yang's sincere interest in people was always apparent and appreciated. David Gosalvez has taught me a lot, especially about the little things in life such as proper place mat folding, the karma of parking and Spanish dancing (it's all in the knees). He has also been a true friend, and I wish him luck writing his thesis as he is next in line. Thanos Tsekouras kept my statements accurate, and I thank him for helping me troubleshoot electronics problems after the other electronics pros had left the group. Matthew Tate has impressed me with his ability to keep up with lab experiments, surface science literature and Ceyer Group catch phrases. I trust he will carry on the traditions when I am gone. I am thankful for Matt's help in preparing this manuscript as he has carefully read each chapter to catch my many mistakes. Stacey Eckman continually displayed a positive attitude which helped to keep my spirits up. I wish her luck carrying on the work of the new "Middle Machine".

Outside the Ceyer Group there are many people I would like to thank, but none are as special as Danna Leard. Danna has been a constant source of support and often cheered me up when I was down. Over the years we have shared countless experiences together, and I hope that they will continue far into the future. Whether I was catching a movie, sitting around a campfire or just making dinner at home, it was always more fun with Danna. I especially thank her for putting up with me near the end of my graduate work as I was probably not the most pleasant person to be around.

My first year at MIT I made a great friend, Chris Murray. I don't know if I would have made it through the early years without his companionship. Marc Wefers, Andy Pete, Bob Murry and Dave Kayes are also great friends with whom I shared some fun times. I have made many more friends while at MIT, but unfortunately, I cannot list them all.

Lastly, I thank my parents, my grandmother, and the rest of my family for their constant support and their confidence in me throughout my academic career.

Table of Contents

List of Figures

List of Tables

CHAPTER I:
MECHANISM OF ETHYLIDYNE FORMATION ON Ni(111)

I. Introduction

The interaction of hydrocarbons with metal surfaces is one focus of surface science. The goal of these studies is to better understand heterogeneous catalytic processes such hydrogenation, hydrogenolysis and dehydrogenation. Because of their relative simplicity, smaller hydrocarbons are typically studied as model systems for understanding the interaction of larger hydrocarbon molecules with metal surfaces.

The interaction of ethylene with Pt[1-17], Pd[18,19], Ru[20,21], Rh[22-24] and Ir[25] metals is an example of a model hydrocarbon-transition metal surface system that has been widely studied. On the most closely packed surfaces of these transition metals, ethylene adsorbs molecularly at temperatures below 200 K with the C-C bond lying parallel to the surface and each carbon atom forming a bond with the transition metal. Interestingly, at surface temperatures above 270 K, ethylene is observed to transform to ethylidyne ($-CCH_3$), an adsorbed species in which the carbon-carbon bond is perpendicular to the surface. Through the study of reactions like the transformation of ethylene to ethylidyne under single collision conditions of an ultrahigh vacuum environment, it is hoped that fundamental steps involving hydrogen transfer to and from the surface as well as hydrogen migration on the adsorbate can be characterized and that this information can subsequently be applied in the understanding of 'real world' hydrocarbon catalysis. Indeed an adsorbed ethylidyne species has been observed[26,27] to be present during catalytic hydrogenation of ethylene to ethane on Pt(111) and has been suggested as an intermediate in this reaction. Ethylidyne also has been observed with infrared spectroscopy on alumina supported metals: Pt, Rh, Ru, Pd and Ni.[28-30] The identification of ethylidyne on these supported metals is significant because supported metals are similar to the 'real world' catalysts used in hydrogenation reactions. Therefore, the mechanism for the transformation of ethylene to ethylidyne is of interest.

A large number of previous studies, employing a great many surface analytical techniques such as infrared reflection absorption spectroscopy,[9,15] high resolution electron

energy loss spectroscopy,[2] thermal desorption spectrometry,[10,16] near edge x-ray adsorption fine structure,[8] sum frequency generation[31] secondary ion mass spectrometry,[6] laser induced desorption,[12,15] and scanning tunneling microscopy,[13] have been aimed at determining the mechanism of the transformation of ethylene to ethylidyne on Pt(111). However, no experimental evidence has yet been obtained which reveals the mechanism by which ethylene is converted to ethylidyne, and no consensus has been reached as to the intermediates involved. Vinylidene ($-CCH_2$),[2,3,32] vinyl ($-CHCH_2$)[10,33] and ethylidene ($-CHCH_3$)[31,34,35] have all been proposed as intermediates in the conversion of ethylene to ethylidyne, but none have been identified spectroscopically, even with vibrational spectroscopy, the most powerful technique for chemical identification of adsorbates.

Although the binding of ethylene to Ni(111) is similar to that to Pt(111) at low temperatures, the thermochemistry of ethylene on Ni(111) is quite different from that on Pt. Below 150 K ethylene adsorption is molecular.[36,37] Photoelectron diffraction studies have determined that ethylene adsorbs with the C-C bond parallel to the surface and with each carbon atom bound to an atop site on the Ni lattice.[38] Significant rehybridization of the C-C bond is evident by the lower C-C stretching frequency, approximately 1200 cm^{-1},[36,37] for adsorbed ethylene relative to the gas phase value, 1624 cm^{-1}.[39] At surface temperatures above 200 K, ethylene dehydrogenates to form acetylene and surface bound hydrogen for initial ethylene coverages below 0.16 ML.[37] At ethylene coverages higher than 0.16 ML, molecular desorption competes with the decomposition process. Acetylene also adsorbs on Ni(111) with the C-C bond parallel to the surface. However, the carbon atoms are believed to bind to the three-fold hollow site.[38] Again, the low C-C stretching frequency of adsorbed acetylene, 1220 cm^{-1}, indicates the rehybridization of the C-C bond upon chemisorption to the surface.[40] Adsorbed acetylene is stable to approximately 400 K, where at low coverages (0.1 ML) it dehydrogenates to adsorbed carbon, and at high coverages (0.25 ML) it trimerizes to form benzene.[41] To this date, there is no spectroscopic evidence for ethylidyne adsorbed on a

surface of a nickel single crystal, because unlike all the other metals on which ethylidyne has been spectroscopically observed, ethylidyne is not formed by thermal decomposition of adsorbed ethylene. The experimental results of this work demonstrate for the first time the synthesis of ethylidyne on a nickel single crystal surface and its spectroscopic identification. Adsorbed ethylidyne is shown to form from the reaction of gas phase hydrogen atoms with adsorbed ethylene, acetylene, and ethane. In a previous study of the thermal decomposition of high coverages of ethylene and acetylene on Ni(111), a static secondary ion mass spectroscopy CH_3^+ feature has been attributed to that of ethylidyne.[42] However, previous vibrational spectroscopic results do not support this conclusion and instead demonstrate that ethylene thermally decomposes to acetylene[36,37] and acetylene thermally reacts to form benzene on Ni(111).[41]

It is the unique reactivity of gas phase H atoms to be able to abstract H atoms from adsorbed hydrocarbons along with their ability to add to adsorbed hydrocarbons that allows the synthesis of ethylidyne from acetylene, ethylene and ethane. Although these processes have not been directly observed in this study, both abstraction of H atoms from adsorbed hydrocarbons by gas phase H atoms and addition of gas phase H atoms to adsorbed hydrocarbons must be occurring in order for the ethylidyne product to be formed from these three C_2 hydrocarbons. Abstraction of H atoms from adsorbed hydrocarbons by gas phase H atoms[43,44] and addition of gas phase H atoms to adsorbed hydrocarbons[45] have also been indirectly measured in previous studies. Addition of H atoms to unsaturated hydrocarbons in the gas phase is known to take place[46-48] as is abstraction of H atoms from hydrocarbons by gas phase H atoms[46,48]. Hydrogen atom addition has also been directly observed in the reaction of H atoms with solid phase hydrocarbons[49,50] as has the abstraction of H atoms from hydrocarbons in solid matrices by H atoms.[51] In the reaction of gas phase H atoms with adsorbed hydrocarbons discussed here, both H atom addition to and H atom abstraction from adsorbed hydrocarbons will be deduced to be steps in the mechanism of ethylidyne formation.

This chapter also discusses the synthesis of ethylidyne on Ni(111) by reaction of adsorbed acetylene and hydrogen emanating from the bulk to the surface. It is the ability of bulk H to add to adsorbed hydrocarbons that explains the formation of ethylidyne in this reaction. Therefore, four different reactions have been observed to form ethylidyne. With the assumption that the four reactions, gas phase hydrogen atoms with ethylene, acetylene and ethane and bulk hydrogen with acetylene, proceed via the same intermediates to produce ethylidyne, the mechanism for the formation of ethylidyne on Ni(111) is determined and is discussed in this chapter.

Gas phase hydrogen atoms incident on the Ni(111) surface are known both to adsorb to form surface bound hydrogen and absorb to form bulk hydrogen.[52] Therefore, in the determination of the reaction mechanism for the formation of ethylidyne, both the chemistry of surface and bulk hydrogen must be considered. The reactivity of surface bound hydrogen and bulk hydrogen with adsorbed ethylene has been studied previously, and the results of these studies can be used in determining the reactions available in the ethylidyne formation reaction mechanism.[37]

The vibrational spectra of ethylidyne produced from the dehydrogenation of ethylene on Pt(111) exhibit features in addition to those assigned to ethylidyne. The features are tentatively assigned to a hydrocarbon, coadsorbed on the surface with ethylidyne, but the identity of this hydrocarbon has not been determined.[4] Similarly, ethylidyne is not the only product of the four aforementioned reactions on the Ni(111) surface. Competing reactions are also observed, and each reaction product, adsorbed and desorbed (gaseous), is discussed in this chapter. The adsorbed reaction products are characterized by Auger electron spectroscopy, electron energy loss spectroscopy and thermal desorption spectroscopy while the gas phase reaction products are characterized by mass spectrometric measurements during the reaction of gas phase hydrogen atoms with adsorbed hydrocarbons.

Since ethylidyne has been proposed as a hydrogenation intermediate, its reactivity with hydrogen will also be addressed.

II. Experimental

The apparatus utilized in the experiments has been described in detail elsewhere.[53-55] The apparatus consists of an ultrahigh vacuum chamber, referred to as the main chamber, coupled to a supersonic molecular beam source. The nickel single crystal is housed in the main chamber along with the electron spectrometers. The main chamber base pressure is typically $4x10^{-11}$ torr. This low pressure is achieved by pumping with a liquid nitrogen trapped 10" diffusion pump backed by a mechanical (two stage rotary vane) pump. The very low main chamber pressure minimizes the adsorption of residual gases on the crystal during the course of experiments. Ultrahigh vacuum is also necessary for operation of the electron spectroscopic techniques used for surface analysis.

II.A. Analytical Instruments

The analytical techniques used in the experiments discussed in this chapter are Auger electron spectroscopy, high resolution electron energy loss spectroscopy and mass spectrometry. A short description of each technique's application to the present experiment is given in the following sections.

II.A.1. Auger spectroscopy

Auger electron spectroscopy is an elemental analytical technique which is used in these experiments for the measurement of the absolute carbon coverage of both the reactants and products. The intensity of the Auger signal is proportional to the coverage of the adsorbate, but the sensitivity of the spectrometer can be affected by the spectrometer settings and geometry. To minimize scatter in the absolute intensities of the Auger signal, the ratio of the intensity of

the Auger feature from the adsorbate to that of the nickel feature at 850 eV is used as a measure of the adsorbate coverage. Since all adsorbate coverages measured by Auger electron spectroscopy reported in this thesis are those of hydrocarbons, the ratio of the carbon (272 eV) and nickel (850 eV) Auger signals is used to characterize the hydrocarbon coverage. The absolute coverage of carbon adsorbate is determined by comparing the C/Ni Auger signal ratio to a known carbon coverage measured under identical conditions. The saturation coverage of ethylene, 0.25 ML, which has been determined previously by low energy electron diffraction (LEED) is used as the calibrated carbon coverage. Although the LEED pattern of this coverage of ethylene has not been measured in this work, it has been measured with the same experimental apparatus in previous work.[55] Ethylene is used as a calibrant because the sensitivity of its carbon Auger signal is expected to be similar to that of other adsorbed hydrocarbons. Saturation coverage of ethylene is determined in this work to be the coverage at which a sharp transition is seen in the amount of carbon deposited on the surface as a function of ethylene exposure. The C/Ni Auger signal ratio measured at this transition is 0.22. Therefore a carbon coverage of 0.5 ML yields a C/Ni Auger signal ratio of 0.22. The carbon Auger signal is assumed to scale linearly with carbon coverages. Although this relation has been reported previously not to hold for carbon coverages below 0.03 ML,[55] no absolute carbon coverages reported in this work fall within this range. It should be noted there are sometimes discrepancies in the use of the monolayer (ML) unit. For coverages reported in this work, a monolayer is defined as one adsorbate per surface nickel atom. Therefore, a coverage of 0.25 ML of ethylene is one ethylene molecule per four surface nickel atoms. Note that a 0.25 ML ethylene coverage is the same as a 0.5 ML carbon coverage since there are two carbon atoms per ethylene molecule.

The Auger electron spectrometer settings employed for all the measurements described in this thesis are: 2 kV incident electron beam energy, 0.5 μA incident electron beam current, 3

second time constant of the lock-in amplifier, and 3 V modulation amplitude of the lock-in amplifier.

II.A.2. High resolution electron energy loss spectroscopy

High resolution electron loss spectroscopy will be discussed in detail in the experimental section of Chapter II. Briefly, the technique uses the inelastic scattering of low energy electrons from a surface to detect excitation of vibrational modes at the surface. The frequencies and the intensities of the loss features can be used to identify and characterize adsorbates bound to the surface. Some of the spectra shown in this chapter have been measured both in the specular direction and out of the specular direction in order to be able to identify the dipole active features as discussed in Section III.A of Chapter II. All spectra shown use the same incident electron energy, 6.5 eV. The resolution reported in the electron energy loss spectra in this work are measured as the full width of energy of the elastic feature at half its maximum intensity.

II.A.3. Mass spectrometry

Mass spectrometry has been utilized in this work to identify and quantify hydrocarbons desorbing from the crystal. Upon ionization in the mass spectrometer, hydrocarbons crack to a variety of ions. The mass distribution of the relative number of ions is termed the cracking pattern. Table 1.1 shows the relative cracking pattern of ethane, ethylene and acetylene at an electron impact energy of 50 eV.[56] Although ethane is most efficiently cracked to mass 28, mass 30 is used as a measure of the ethane partial pressure because ethylene does not crack to mass 30 and therefore all of the observed mass 30 signal arises from ethane. Mass 27 is used as a measure of the ethylene signal, but because ethane also cracks to mass 27, the observed mass 27 signal can also arise from ethane in addition to ethylene. The ethane cracking ratio of mass 27 to mass 30 can be used to determine for the portion of the mass 27 signal that is due to ethane rather than ethylene. Because of its importance in these studies, the ratio of mass 27

signal to mass 30 signal for ethane cracking in the mass spectrometer with the electron impact energy used in these studies, 70 eV, has been verified to be 1.3 .

Two types of experiments have employed the mass spectrometer for detection of gas phase molecules. The first type is a typical thermal desorption experiment where the increase in the partial pressure at a particular mass is monitored by the mass spectrometer as a function of surface temperature. The desorbing molecules can be used to either identify the adsorbed molecules or identify reactions of the adsorbed molecules which yield gas phase products as a result of increasing the surface temperature. Thermal desorption spectroscopy can also be used to determine relative coverages of adsorbates provided that the adsorbate desorbs from the surface rather than thermally decomposing. Relative coverages of ethane have been monitored in this way in experiments described in this chapter. In all thermal desorption experiments described, the crystal heating rate is 2 K/s.

The second type of experiment which uses the mass spectrometer involves monitoring gas phase hydrocarbon signals during exposure of a hydrocarbon covered surface to gas phase hydrogen atoms. This experiment measures the products which desorb from the surface upon reaction of the H atoms with the adsorbed hydrocarbon.

Mass to charge ratio	Ethane	Ethylene	Acetylene
25	4	11	20
26	23	61	100
27	33	62	3
28	100	100	.2
29	22	2	0
30	26	.1	0

Table 1.1. Mass spectral cracking patterns from reference 56 of ethane, ethylene, and acetylene at an electron impact energy of 50 eV.

II.B. Nickel (111) Single Crystal Surface

All the experiments in this chapter are conducted on a Ni(111) surface. The nickel crystal is mechanically polished to within 0.2° of the 111 plane. A geometrical calculation yields a value for the average width of a terrace before the occurrence of a step as 280 atoms.

Surface purity of the nickel crystal is confirmed with Auger electron spectroscopy and electron energy loss spectroscopy. The typical surface contaminants, sulfur, carbon and oxygen are detected by their Auger signals at 152 eV, 272 eV, and 550 eV, respectively or by their electron energy loss spectroscopy features at 390 cm^{-1}, 300 cm^{-1} and 50 cm^{-1} respectively. The detection limit of Auger electron spectroscopy is approximately 0.01 monolayer (ML).[57] Electron energy loss spectroscopy is a more sensitive detector of these contaminants than Auger spectroscopy, but the actual sensitivity is unknown. Sulfur contamination of the surface has been observed to correlate with gas phase hydrogen atom exposures. It is believed that upon absorption of H atoms into the bulk of the crystal or upon emergence to the H atoms from the bulk, sulfur is displaced from the bulk to the surface of the crystal. Therefore, when sulfur contamination recurs, attempts are made to deplete sulfur from the near surface region of the crystal by bringing it to the surface through multiple exposures to H atoms, each followed by an anneal of the crystal at 1100 K for 5 minutes. This H atom exposure and anneal is repeated several times. The sulfur is then removed from the surface by sputtering with 2 kV argon ions. Surface carbon can usually be removed by its dissolution into the bulk of the crystal by heating the crystal above 1000 K. Occasionally, this procedure does not remove the surface carbon and argon ion sputtering of the surface is necessary. When sputtering does not remove surface carbon, oxidation of the crystal is necessary. Oxidation of the surface is achieved by exposure of the crystal to a molecular beam of pure oxygen as the crystal cools from 1100 K to 500 K. Ideally, the crystal would be held at 1100 K during its exposure to oxygen, but this would require the filament which heats the crystal to remain on during the exposure which would degrade the filament due to oxidation. The carbon removed from the surface by oxidation can

be monitored by measuring CO and CO_2 partial pressures with the mass spectrometer while heating the crystal surface following the O_2 exposure. This process is repeated several times until the amount of CO and CO_2 desorbing from the crystal is greatly reduced and no carbon is detected on the surface by Auger electron spectroscopy. Surface bound oxygen contaminant has not been observed to be a problem with the Ni crystal currently studied except after oxidation of the surface mentioned above. Surface bound oxygen is removed by reduction of the surface by exposure to a molecular beam of hydrogen while the crystal cools from 1100 K. An additional surface contaminant has been observed which gives rise to a feature in the electron energy loss spectra at 730 cm^{-1}. Although the identity of the contaminant is unknown, it has been learned that annealing the crystal at 1100 K for 30 minutes will remove it from the surface.

The crystal is mounted to the sample manipulator via spot welds to two tungsten rods. The tungsten rods are in turn clamped to a copper block. This copper block is in thermal contact with a cryogenic reservoir referred to as a cryotube. The copper block is electrically isolated from the cryotube to allow the crystal to be biased electrically. Use of liquid nitrogen or liquid helium in the cryotube results in crystal temperatures of 80 K or 10 K, respectively. The crystal can also be cooled to 70 K by bubbling gaseous helium through the liquid nitrogen in the cryotube.[58] The helium displaces the nitrogen vapor and therefore lowers the partial pressure of nitrogen in the cryotube which in turn causes the nitrogen to boil at a lower temperature. Heating of the crystal is achieved through use of a tungsten filament at the rear of the crystal. Two different heating mechanisms are employed: radiative heating for temperatures up to 500 K and electron impact heating for temperatures above 500 K. As current is passed through the filament, it is resistively heated, causing emission of light and electrons. In radiative heating, the light emitted from the hot filament heats the crystal. The crystal bias is held equal to that of the filament such that the electrons emitted from the filament are not accelerated into the crystal. In electron impact heating, the crystal is biased positively (typically

600 V) relative to the filament, and therefore the electrons from the filament strike the rear of the crystal with high energy, causing the temperature to rise. With the current geometry, radiative heating cannot yield temperatures higher than 500 K, and therefore electron impact is utilized for heating the crystal to temperatures higher than 500 K. Since a fraction of the high energy electrons used in electron impact heating do make their way to the front of the crystal and can induce chemical changes of the adsorbates, only radiative heating is used in experiments where adsorbates or desorption products are examined during or subsequent to heating. Unless explicitly stated otherwise, 'heating the crystal' referred to in the following sections indicates heating the crystal at a rate of 2 K/s and then immediately cooling the crystal back to its original temperature.

II.C. Adsorbed Hydrocarbons

The experimental studies in this chapter have used three different hydrocarbons as reactant adsorbates: acetylene, ethylene, and ethane. Acetylene (99.6% - MG Industries), ethylene (99.95%- MG Industries) and ethane (99.96% - Matheson) are used as received without further purification. Because high pressures of acetylene are explosive, pure acetylene is never used at pressures higher than 15 psi. Also, only stainless steel is used for acetylene transfer lines because acetylene produces explosive acetylides on copper surfaces. Hydrocarbon adsorption to the surface is achieved by exposure of the surface to a molecular beam of the hydrocarbon. Both pure hydrocarbon beams and 2% hydrocarbon seeded in argon beams have been used. Argon is used as a diluent in order to lengthen the exposure times so they could be more precisely controlled. The stagnation pressure behind the nozzle is 40 psi.

The molecular beam can enter the main chamber through two different size apertures, referred to as the small beam hole and the large beam hole, which defines the cross sections of the beam on the crystal. The cross section is larger than the crystal surface when exposing the crystal in the beam dose position to a beam entering through the big beam hole and therefore the

entire crystal face is exposed to the molecular beam.[54] The molecular beam cross section obtained by using the small beam hole is smaller the size of the crystal and therefore it can be used to expose only the center of the crystal to the hydrocarbons. In the experiments described in this thesis, the entire face of the crystal has been exposed to hydrocarbons unless otherwise stated.

The surface is exposed to ethylene and acetylene at a crystal temperature of 80 K. The surface temperature is held at 70 K for exposure to ethane because ethane desorbes at 80 K. To ensure that argon does not stick to the surface during exposures to the seeded beams, the crystal temperature is maintained at 70 K or above. Argon does not stick to the surface at these temperatures.[55] As mentioned previously, the hydrocarbon coverage is measured by Auger electron spectroscopy.

II.D. Gas phase hydrogen atoms

Hydrogen atoms are formed by thermal dissociation of molecular hydrogen over a hot tungsten filament positioned 0.25" from the crystal surface. The flux of H atoms impinging the surface is a function of H_2 pressure, filament temperature and distance of the filament to the surface. All the experiments described in this thesis have used the same filament temperature and filament distance to the surface. The hydrogen atom dose is therefore characterized by the molecular hydrogen pressure and the length of exposure. With the exception of exposure of ethane to H atoms, all H atom exposures are carried out at a H_2 pressure of $5x10^{-6}$ torr and therefore this parameter will be reported only when a H_2 pressure other than $5x10^{-6}$ torr is utilized.

The sequence of the H atom dose is as follows. The filament is positioned 0.25"' away from the front face of the crystal surface. Molecular hydrogen is leaked into the main chamber to the desired pressure. The potential across the filament is increased rapidly to 3 volts to heat the filament, and thus initiating the H atom exposure. The temperature of the crystal rises

slightly during the H atom exposure due to radiative heating from the hot filament. At the end of the desired exposure time, the filament potential is turned off, the molecular hydrogen leak valve is closed and the filament is moved away from its position in the front of the crystal.

The flux of gas phase hydrogen atoms impinging the surface has not been measured. The H atom flux has been measured in previous work to be $6x10^{13}$ atoms cm^{-2} s^{-1} [52], but the experimental procedure was different in these experiments. Specifically, the molecular beam was used to supply H_2 to the filament rather than leaking H_2 into the main chamber.

II.E. Electron exposures

Adsorbed hydrocarbons have been exposed to electrons to activate C-H bonds in an attempt to synthesize adsorbed hydrocarbon intermediates. The electrons are produced by thermionic emission from a hot tungsten filament positioned 0.25" away from the front face of the crystal such that the electrons are in line-of-sight with the adsorbates. The energy of the electrons impinging the surface is controlled by biasing the crystal relative to the filament. The temperature of the crystal rises slightly during electron exposure due to radiation from the hot filament. The current to the crystal is measured by a picoammeter during the electron exposure and can be used to calculate the flux of electrons to the surface assuming it to be uniform across the surface. Typical electron fluxes are on the order of 10^{14} electrons cm^{-2} s^{-1}

III. Results and Discussion

III.A. Ethylidyne Formation Reactions

III.A.1. Ethylene and Gas Phase Hydrogen atoms

The reaction of adsorbed ethylene with gas phase hydrogen atoms has been studied using a variety of techniques. Both gas phase and adsorbed reactions products have been observed. The gas phase products have been measured mass spectrometrically during the

hydrogen atom exposure, while the adsorbed reaction products have been probed by Auger electron spectroscopy, electron energy loss spectroscopy and thermal desorption spectroscopy following the hydrogen atom exposure. The following sections present the experimental results.

III.A.1.a. Mass spectrometric measurements

Figure 1.1 shows the mass spectrometer signal at 27 amu and 30 amu as a function of the time during exposure of 0.25 ML ethylene adsorbed on Ni(111) to gas phase hydrogen atoms. Specifically, the figure shows the following sequence of exposure to hydrogen atoms. The partial pressure of H_2 in the main chamber is increased to $5x10^{-6}$ torr. Then, the hydrogen atom filament in front of the crystal surface is turned on for a duration of two minutes. After the filament is turned off, the H_2 partial pressure is lowered to its background level of less than $5x10^{-11}$ torr. The mass spectrometer monitors the mass 30 and mass 27 signals as measures of ethane and ethylene, respectively, throughout the duration of the experiment. As discussed in the experimental section, ethane also contributes to the mass 27 signal, but as can be seen in Table 1.1 the ratio of mass 27 to mass 30 signals observed for ethane is approximately 1.3. The mass 27 signal measured in Figure 1.1 is greater than 1.3 times that of the mass 30 signal, and therefore ethane alone cannot account for the mass 27 signal level and some of the signal must be due to ethylene.

A steady rise in the ethylene and the ethane signals is observed as soon as the partial pressure of H_2 is raised to $5x10^{-6}$ torr. Although the origin of this rise in signal has not been investigated, it is most likely due to reactions in the hot ionization region of the mass spectrometer or to displacement of ethylene and ethane from the walls of the vacuum chamber by hydrogen adsorption. The background signal increases steadily with H_2 exposure until the moment the filament is turned on. At that time hydrogen atoms impinge on the ethylene covered

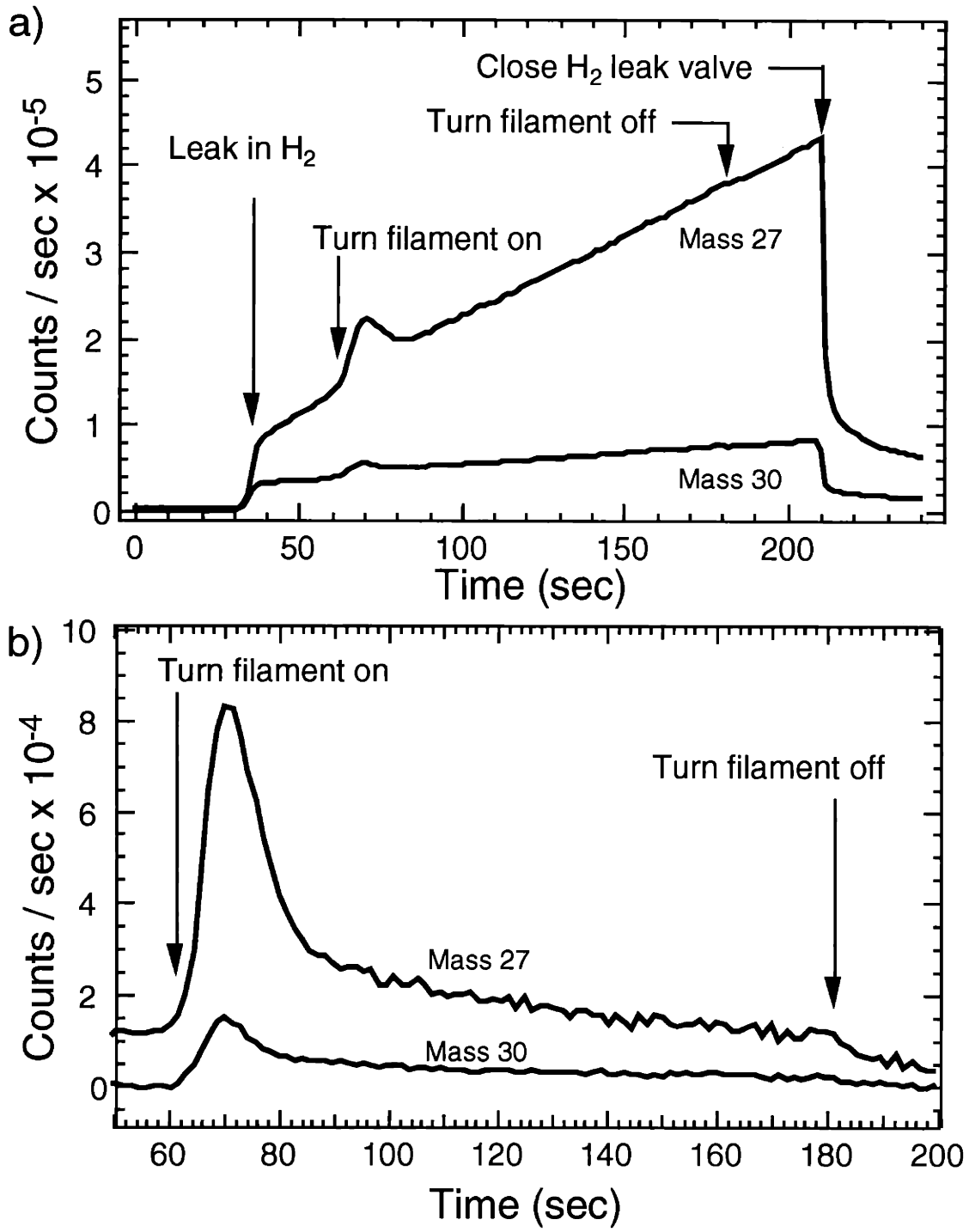

Figure 1.1. **a)** Mass spectrometer signals monitored during exposure of 0.25 ML adsorbed ethylene to gas phase hydrogen atoms. **b)** Same experiment as a), but a linear background has been subtracted from the signal such that the signal resulting from the hydrogen atom exposure are more easily observed.

crystal, and both the ethylene and ethane signals are observed to increase sharply. The impinging H atoms both displace the adsorbed ethylene and hydrogenate it to form ethane.

The following control experiment eliminates the possibility that ethylene and ethane have boiled off of the hot filament or have desorbed from the crystal cold shield due to radiative heating from the hot filament. The experimental conditions are the same as in the previous experiment, shown in Figure 1.1, with the exception of the placement of the hydrogen atom filament. The filament is positioned directly next to the crystal cold shield, rather than in front of the crystal, so that the crystal is not in the line-of-sight of the filament and therefore, no hydrogen atoms impinge the crystal surface. Figure 1.2 show the results of the experiment. The increases in the mass spectrometer signals corresponding to the introduction of the H_2 are seen, but the signal is unaffected when the hydrogen atom filament is turned on and heated to

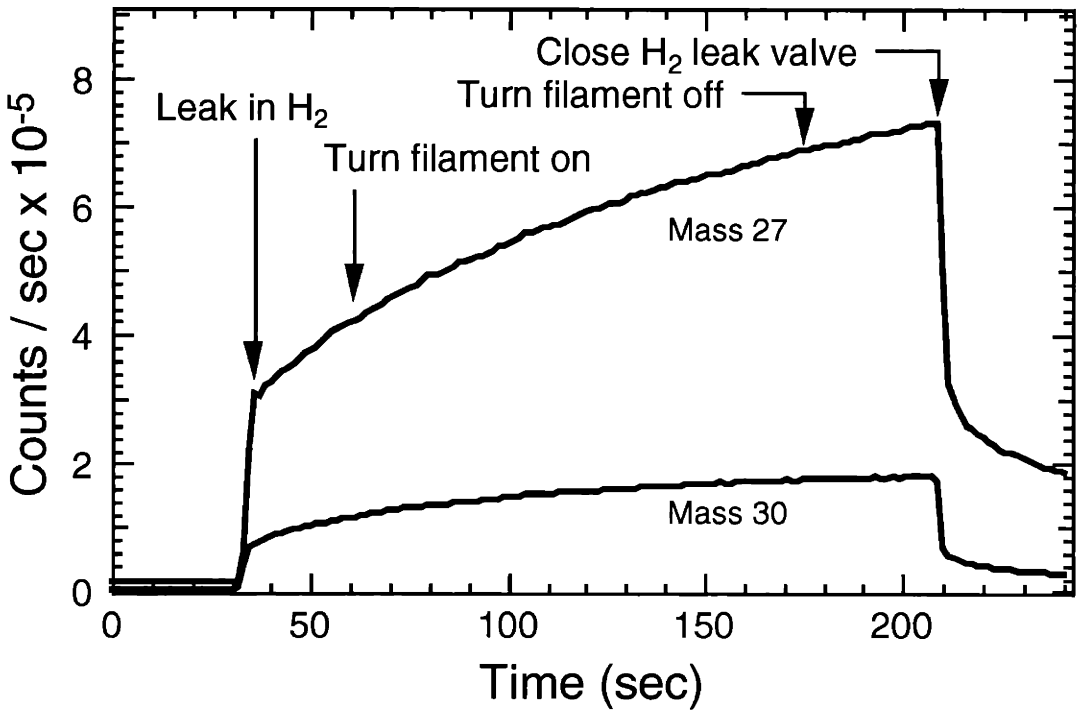

Figure 1.2. Mass spectrometer signal monitored during a gas phase hydrogen exposure with the hydrogen atom filament placed next to the crystal cold shield, out of line-of-site of the crystal. Ethylene is adsorbed on the crystal at a coverage of 0.25 ML.

the same temperature as in the previous experiment. No ethylene or ethane is observed to desorb, confirming that the ethylene and ethane desorbing during the H atom exposure are from the crystal surface and not the filament or the crystal cold shield.

While this control experiment demonstrates that the ethylene is displaced from the crystal by exposure to H atoms, it does not conclusively prove that the hydrogenation of ethylene to ethane is taking place on the crystal. There remains the possibility that the hydrogenation reaction occurs in the gas phase or on the hydrogen atom filament as the ethylene desorbs from the crystal. However, another control experiment shows this not to be the case. H_2 is leaked into the main chamber to maintain a partial pressure of $5x10^{-6}$ torr. The hydrogen atom filament, positioned in the path of the molecular beam, is turned on. Then a molecular beam of 2% ethylene in argon is directed onto the filament. The flux of ethylene in the beam is approximately equal to that desorbing from the surface during exposure of ethylene to H atoms.

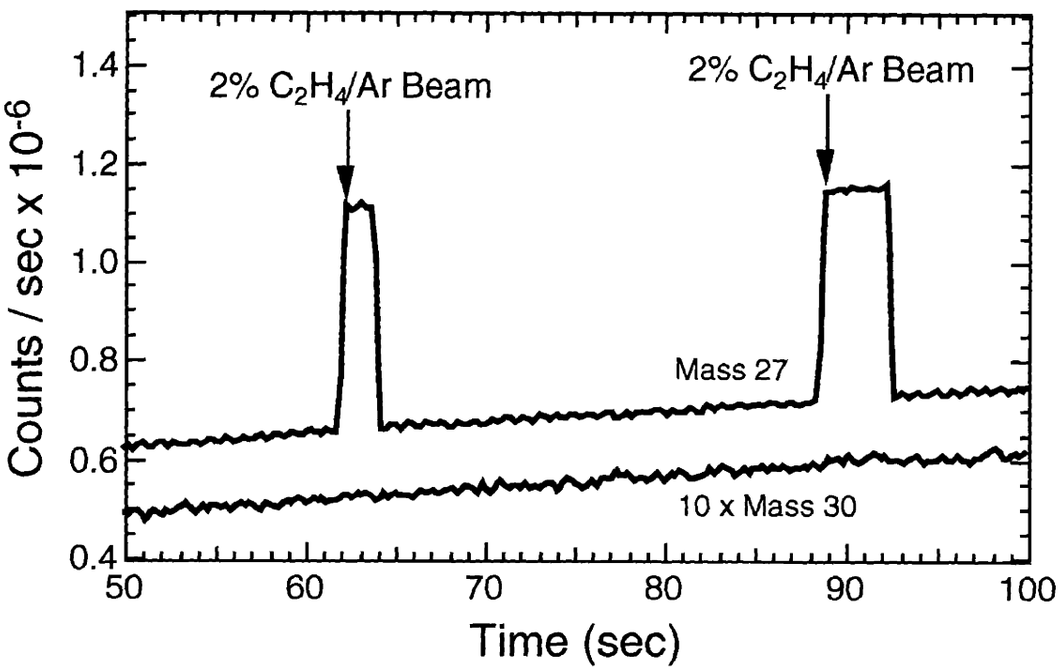

Figure 1.3. Mass spectrometer signal monitored during exposure of a molecular beam of 2% C_2H_4/Ar to the hydrogen atom filament. The filament is on and the H_2 pressure is $5x10^{-6}$ torr.

The 27 amu and 30 amu mass spectrometer signals are shown in Figure 1.3 for a two second and a four second exposure of the molecular beam. No increase in the mass 30 signal is seen, excluding the possibility that the mass 30 signal, observed in Figure 1.1, arises from the reaction of ethylene with hydrogen atoms in the gas phase or on the hydrogen atom filament.

In summary, the exposure of adsorbed ethylene to H atoms results in two processes to produce gas phase products, displacement of ethylene and hydrogenation of ethylene to ethane by H atoms.

III.A.1.b. Auger spectroscopy measurements

The reaction of ethylene and gas phase hydrogen atoms has also been investigated by measuring the amount of carbon remaining on the surface after exposure to H atoms. The carbon Auger signal has been measured as a function of the time of exposure to hydrogen atom. Figure 1.4 shows the results. Each point represents an individual measurement of the C/Ni Auger signals after 0.25 ML ethylene has been exposed to H atoms for the noted time. The temperature of the crystal is 80 K prior to the H atom exposure, but rises to 120 K during the exposure. The Auger measurements are performed at 80 K.

The results in Figure 1.4 show a dramatic drop in the carbon coverage in the first 30 seconds followed by a very slow decrease in the coverage. These results are consistent with the mass spectrometric results in Figure 1.1. Carbon, in the form of ethylene and ethane, is observed to desorb rapidly in the first 30 seconds of the H atom exposure followed by a much lower rate. Apparently, the carbon remaining on the surface after the initial 30 seconds is less reactive with H atoms to produce a product which desorbs than the carbon of the initial reactant, ethylene. The Auger results in Figure 1.4 show that after exposure to 30 seconds or longer of H atoms, the carbon remaining on the surface is approximately half of the carbon initially adsorbed on the surface in the form of ethylene. The Auger signals have also been measured at 80 K after heating the crystal to 300 K and are included in Figure 1.4. The carbon coverage

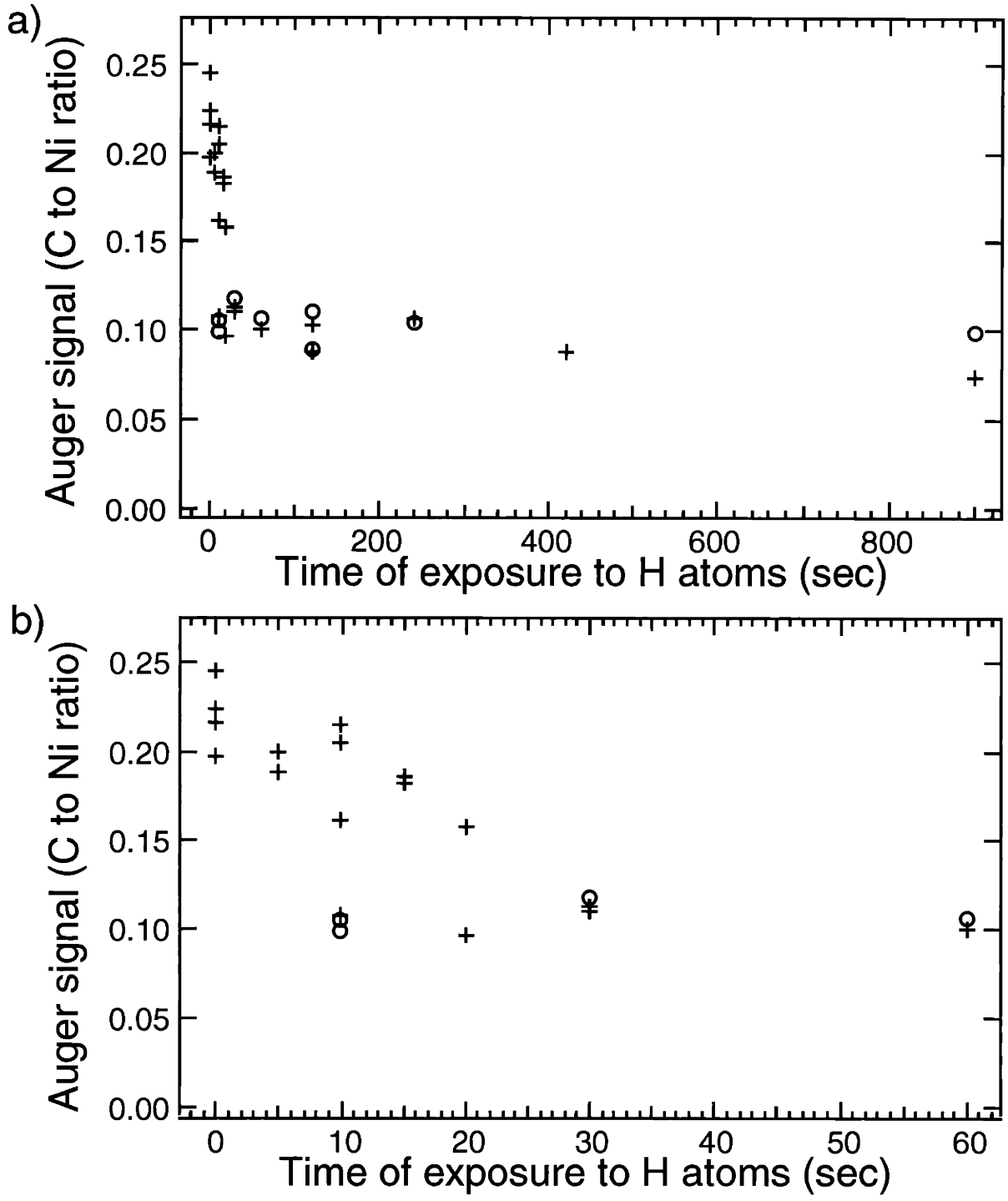

Figure 1.4. **a)** Carbon to nickel Auger signals after H atom exposure to 0.25 ML of adsorbed ethylene. The +'s are measurements after H atom exposure and O's are measurements after H atom exposure and heating the crystal to 300 K. **b)** Expanded time scale of a) showing initial drop in C/Ni ratio.

after exposure to H atoms for 30 seconds or longer is affected very little by heating the surface to 300 K.

The time it takes for the conversion to this less reactive form of carbon, 30 seconds, will be used later in this chapter as a measure of the rate of the reaction of ethylene with H atoms to form this less reactive hydrocarbon. This rate will be important in the discussion of the mechanism for the formation of the hydrocarbon.

The approximately 50% conversion of ethylene to a more unreactive form is independent of the initial coverage of ethylene as shown in Figure 1.5. In these measurements, the exposure of ethylene to H atoms has been held constant at two minutes. It can be seen that, for initial ethylene coverages of 0.25, 0.12 and 0.5 ML, approximately half of the carbon remains on the surface after a 2 minute H atom exposure. Also shown in Figure 1.5 is the carbon coverage after heating the crystal to 300 K. Again, the carbon coverage changes very

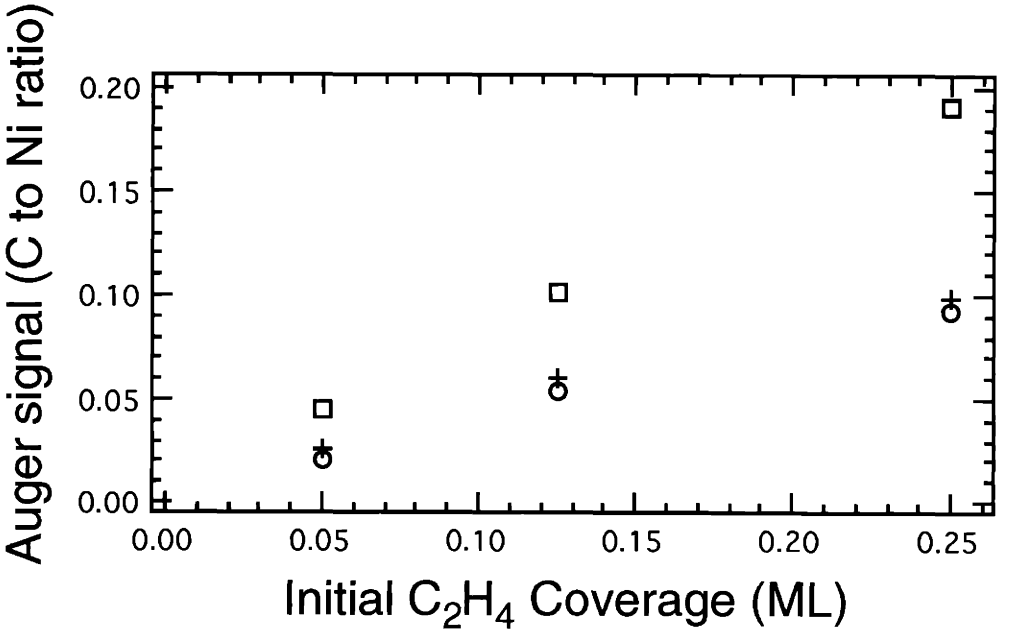

Figure 1.5. C/Ni Auger signals of ethylene after a two minute exposure to H atoms as a function of initial ethylene coverage. The □'s show carbon Auger levels prior to H atom exposure. The +'s are the carbon levels after H atom exposure. The O's are carbon levels after H atom exposure and heating the crystal to 300 K.

little upon raising the surface temperature to 300 K after the two minute exposure to H atoms. The identity of the remaining 50% of the initially adsorbed carbon which is stable to 300 K is given in the next section.

III.A.1.c. High resolution electron energy loss spectroscopy

The electron energy loss spectra provide a great deal of chemical information on the reaction of H atoms with chemisorbed ethylene. The adsorbed reaction products that comprise the 50% remaining surface carbon are identified by their electron energy loss spectra. Figure 1.6 shows electron energy loss spectra of the reaction product of 0.25 ML chemisorbed ethylene after a two minute hydrogen atom exposure. Included in the Figure are the spectra of the same reaction product after heating the crystal to 300 K.

With the exception of the 860 cm^{-1} and the small 700 cm^{-1} features, all the features observed in Figure 1.6 are readily assigned to ethylidyne coadsorbed with hydrogen, as discussed in detail in Chapter II. The vibrational modes of ethylidyne match the features observed: symmetric and antisymmetric C-Ni stretching modes at 260 cm^{-1} and 440 cm^{-1}, a CH_3 rocking mode at 1020 cm^{-1}, a C-C stretching mode at 1130 cm^{-1}, symmetric and antisymmetric CH_3 deformation mode at 1330 and 1400 cm^{-1}, and symmetric and antisymmetric CH_3 stretching modes at 2880 and 2940 cm^{-1}. Additional support for the ethylidyne assignment is provided by the dipole activity. The symmetric C-Ni stretch, the C-C stretch and the symmetric CH_3 deformation modes are all observed to be dipole active, as is expected for an ethylidyne species. The 950 cm^{-1} feature is assigned to the antisymmetric stretching mode of surface bound hydrogen as is discussed in Chapter II.[59]

No new features are seen in the electron energy loss spectra after heating the reaction product to 300 K. However, the intensities of the 860 cm^{-1} and 700 cm^{-1} features decrease upon heating the crystal to 300 K. In fact, it is difficult to see any intensity at 700 cm^{-1} after

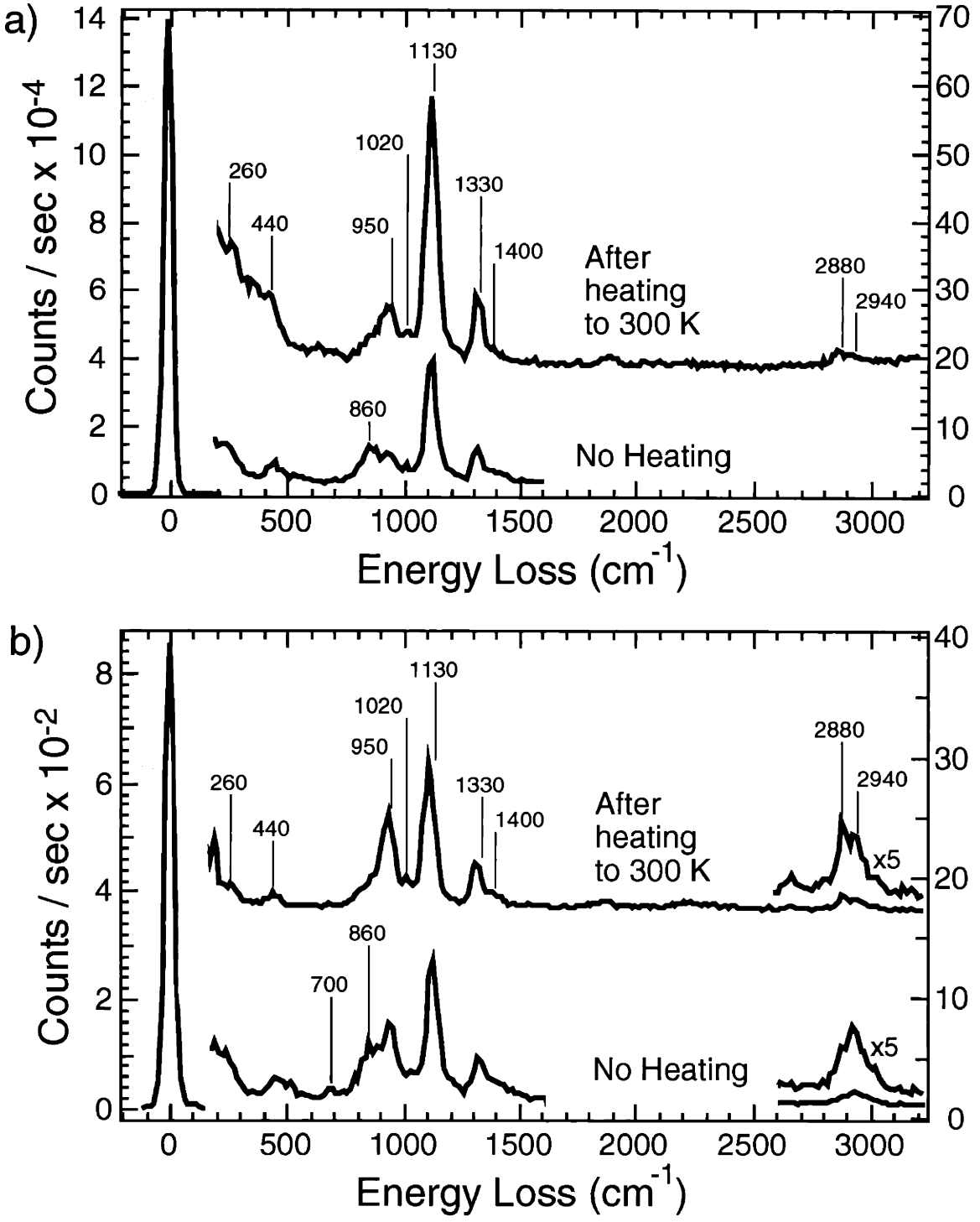

Figure 1.6. Electron energy loss spectra after exposure of 0.25 ML ethylene to two minutes of H atoms, both before and after heating the crystal to 300 K. **a)** on-specular **b)** 10° off-specular

heating. The C-H stretching feature at 2940 cm^{-1} is also lower in intensity after heating to 300 K, allowing the 2880 cm^{-1} C-H stretch feature of ethylidyne to be more easily resolved. Section III.D of this chapter will show that these features which decrease in intensity upon heating to 300 K are due to a small amount of acetylene which is produced in the reaction along with ethylidyne. However, it is appropriate here to address briefly the reasons for the decrease in intensities of the acetylene features upon heating the crystal to 300 K.

Hydrogen atom exposures to a clean Ni(111) surface have been shown previously to produce hydrogen absorbed in the bulk of the nickel crystal[52,60]. The same study showed that hydrogen can be removed from the bulk by heating the crystal. Heating the crystal to 300 K causes the hydrogen to emerge from the bulk to the surface. As it emerges, bulk hydrogen can hydrogenate hydrocarbon adsorbates with the hydrogenation products desorbing into the gas phase.[52,37,61,62] The decrease in intensity of the features attributed to acetylene can be understood by the hydrogenation of acetylene and subsequent desorption of the hydrogenation product. The next section will explore the desorption of hydrocarbons while heating the crystal after the exposure of adsorbed ethylene to H atoms.

Heating the crystal to 300 K also increases the intensity of the dipole active electron energy loss features as observed in the spectra measured in the specular direction. This change in intensity is discussed in Chapter II.

The electron energy loss spectra have also been measured at longer ethylene exposures to H atoms. Figure 1.7 shows the reaction product spectra measured after a seven minute exposure of 0.25 ML ethylene to gas phase hydrogen atoms. The reaction product spectra of a two minute exposure is included for comparison. In both experiments, the crystal is heated to 300 K before the electron energy loss spectra are measured. The spectra in Figure 1.7 show that for H atom exposures as long as 420 seconds, ethylidyne is still the dominant species adsorbed on the surface. This observation, coupled with the Auger measurements, demonstrates that the ethylidyne species is fairly stable in the presence of gas phase hydrogen

atoms. The ethylidyne species reacts only very slowly with H atoms to deplete the amount of carbon on the surface. This conclusion is also consistent with the mass spectrometric measurements; very little desorption of hydrocarbons is observed for H atom exposure times longer than 30 seconds. It appears that all of the adsorbed ethylene reacts with H atoms to from ethylidyne within the first 30 seconds of the exposure, and after ethylidyne is formed it reacts very slowly with H atoms. The time for complete conversion of ethylene to ethylidyne, 30 seconds, will be used as a measure of the rate of this reaction. The rate of the reaction of acetylene with H atoms will be seen to be important in the discussion of the mechanism for ethylidyne formation later in this chapter in Section III.E.

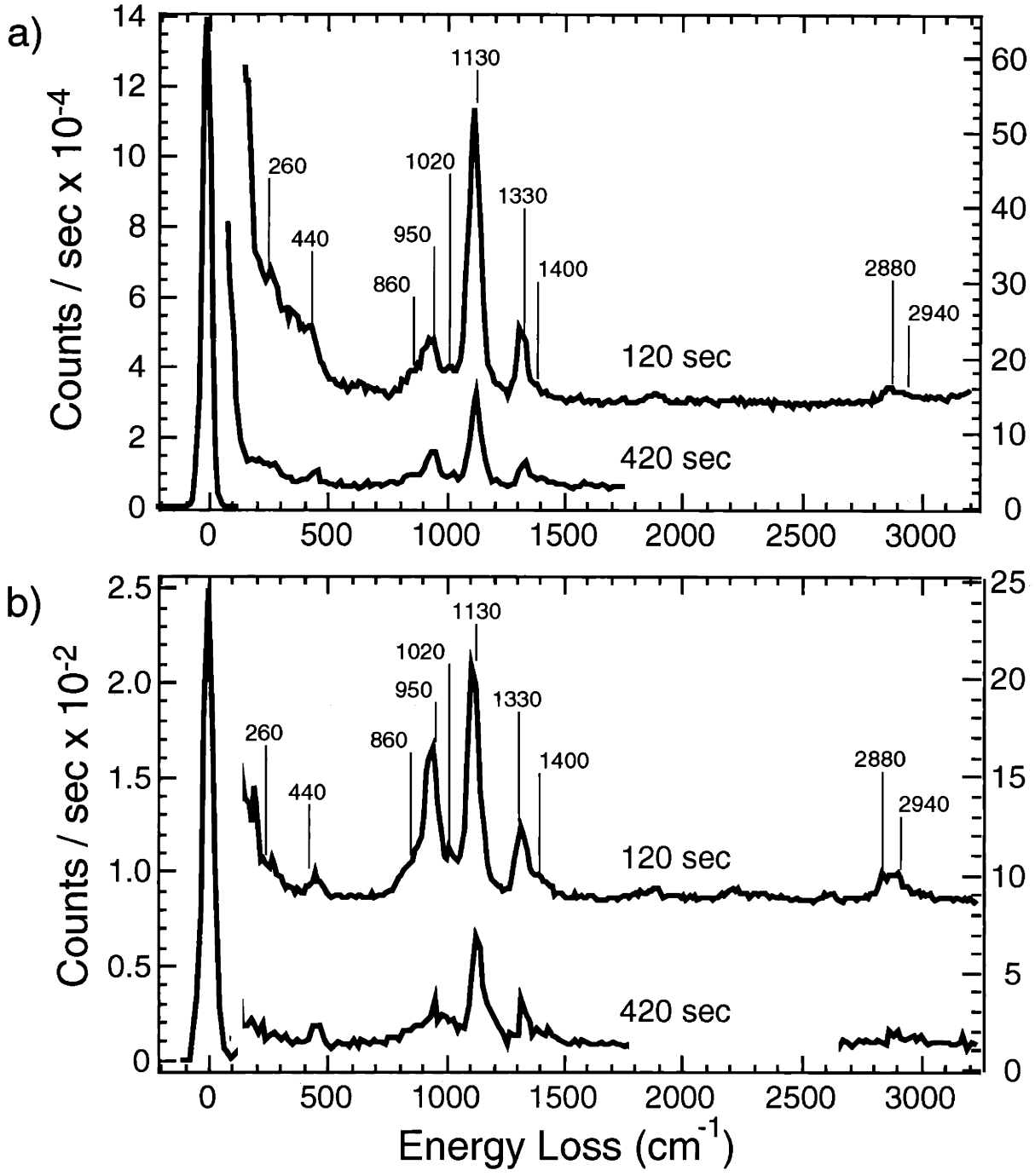

Figure 1.7. Electron energy loss spectra of 0.25 ML ethylene exposed to H atoms. The duration of H atom exposures are shown. **a)** on-specular **b)** 10° off-specular

III.A.1.d. Thermal desorption experiments

Thermal desorption experiments also provide information on the reaction products of chemisorbed ethylene and gas phase hydrogen atoms. Figure 1.8 is a thermal desorption spectra measured after exposure of 0.25 ML ethylene to two minutes of H atoms. The ethylene is exposed to the crystal such that the entire crystal surface is exposed.

There are two major features in the hydrogen signal (mass 2) in Fig 1.8, one at 180 K and one at 350 K. Bulk hydrogen is known to recombinatively desorb from the Ni(111) crystal at 180 K [52,60,63] and therefore the lower temperature feature is assigned to bulk hydrogen. Surface hydrogen recombinatively desorbs from the Ni(111) surface in the 300 - 400 K temperature range,[52,64] and therefore, the higher temperature feature in Figure 1.8 is assigned to hydrogen desorbing from the surface. The shape of the surface hydrogen desorption feature is somewhat different than that observed for hydrogen desorbing from a surface in which no

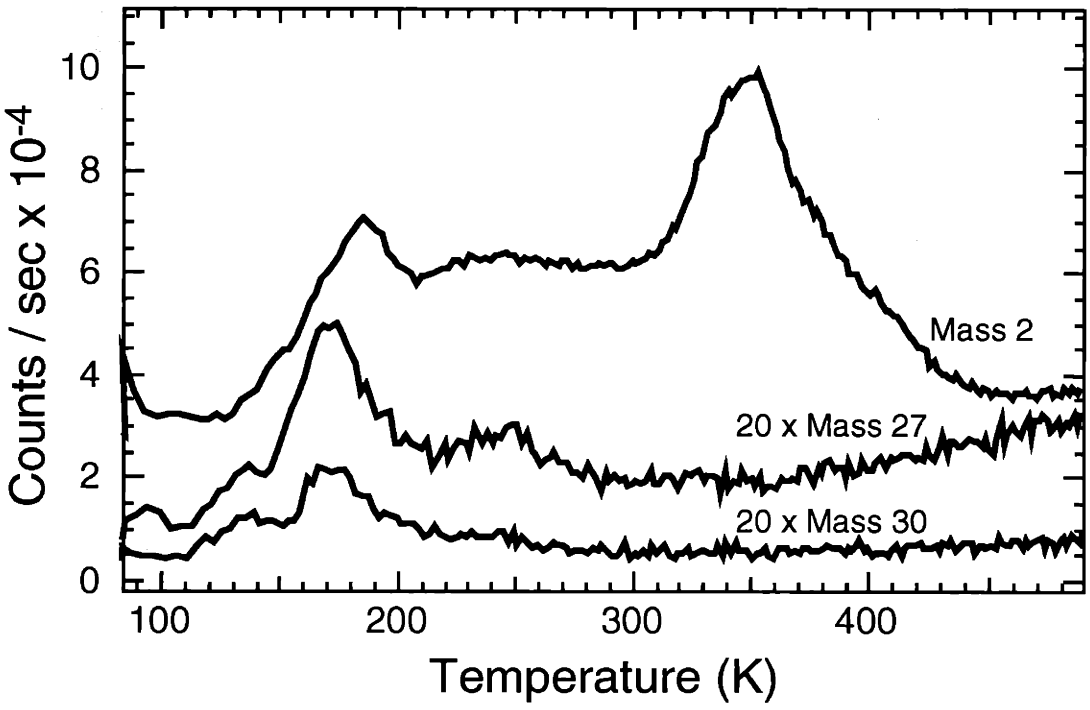

Figure 1.8. Thermal desorption spectrum measured after a two minute exposure of 0.25 ML ethylene to H atoms.

ethylidyne is present. This difference in shape arises from the decomposition of ethylidyne in this temperature range. The decomposition of ethylidyne produces surface hydrogen which then recombinatively desorbs from the surface. Ethylidyne decomposition will be further discussed in Section III.D of this chapter.

As discussed previously, the mass 27 and mass 30 signals are used to measure the partial pressures of ethylene and ethane, respectively. There is a single major feature at 175 K in each of the mass 27 and mass 30 signals. Because these features coincide with the desorption of bulk H at 180 K, they could be assigned to displacement of ethylene and ethane by bulk H emerging to the surface, as bulk hydrogen is known to do as it emerges from the bulk to the surface.[37,62] Instead, they are assigned as hydrogenation products of bulk hydrogen with surface hydrocarbon adsorbates rather than bulk hydrogen displacement products because no ethylene or ethane is observed on the surface in the electron energy loss spectra immediately after ethylene exposure to H atoms and prior to heating the surface. However, as already mentioned and as will be discussed in more detail in Section III.D of this chapter, a small amount of acetylene is identified as a coadsorbate with ethylidyne after the exposure of ethylene to H atoms. Therefore, the products desorbing at 175 K, as observed in Figure 1.8, are assigned to ethylene and ethane formed from hydrogenation of this coadsorbed acetylene. This assignment is also consistent with the observation of a decrease in the intensity of the electron energy loss features at 700 cm^{-1}, 860 cm^{-1}, and 2940 cm^{-1}, features associated with acetylene, after heating the crystal to 300 K. Evidence for hydrogenation of acetylene by bulk H is presented below.

A second, lower intensity feature in the mass 27 signal at approximately 240 K is assigned as ethylene desorbing from the edge of the crystal. This assignment is made by comparing Figures 1.8 and 1.9. Figure 1.9 is a thermal desorption spectrum measured under the same conditions as in Figure 1.8 except that the ethylene is exposed to only the center of the

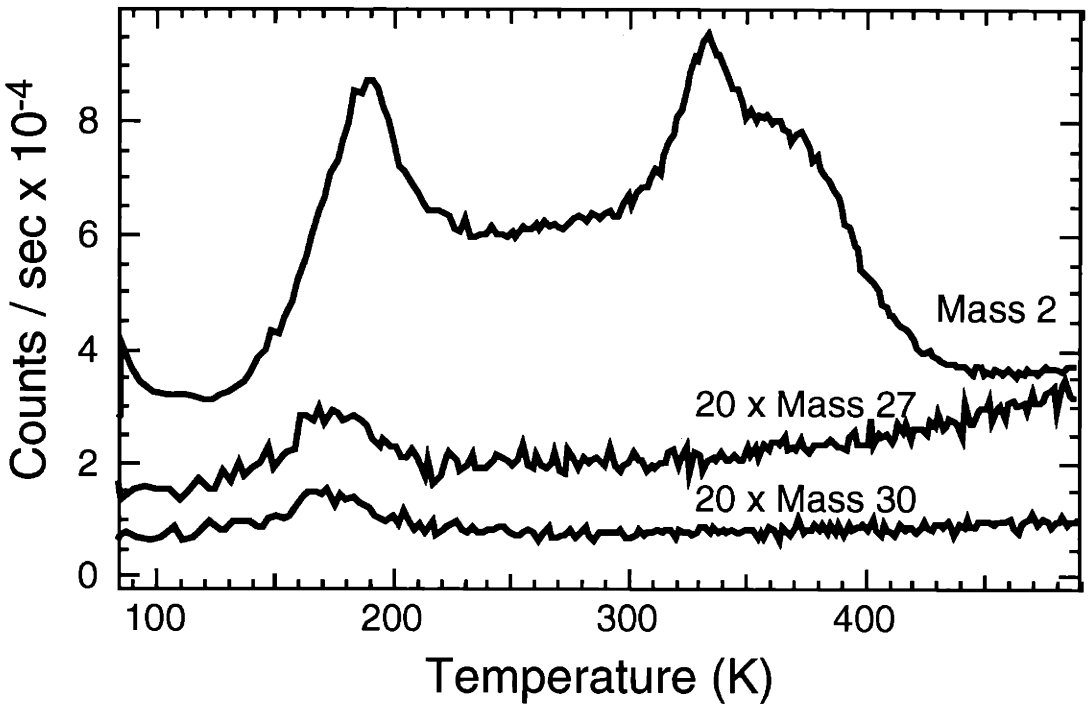

Figure 1.9. Thermal desorption spectrum measured after a two minute exposure of 0.25 ML ethylene to H atoms. The ethylene is exposed only to the center of crystal surface.

crystal; no ethylene is exposed to the crystal edges. No 240 K feature in the mass 27 signal is observed.

A low intensity feature in each of the mass 27 and mass 30 signals is observed at 140 K. The origin of these features is unknown and was not investigated.

Thermal desorption experiments in which hydrogen is prepared in the bulk of the crystal before ethylidyne is formed on the surface have also been carried out. The experimental procedure is as follows. Exposure of a clean crystal to H atoms produces bulk hydrogen, but also produces hydrogen atoms adsorbed on the surface. The surface hydrogen is removed by exposure to a ~140 kcal/mol seeded beam of Xe atoms at an angle of incidence of 40° from the surface normal for 30 minutes. This method of preparing bulk hydrogen without surface hydrogen is documented elsewhere.[52] Ethylene is then exposed to the clean crystal to a coverage of 0.25 ML. Lastly, the ethylene covered, bulk H containing crystal is exposed to gas

phase hydrogen atoms to produce the ethylidyne reaction product. The thermal desorption spectrum is shown in Figure 1.10.

A comparison of the thermal desorption experiments in Figures 1.8 and 1.10 is informative. As is expected, when hydrogen is prepared in the bulk of the crystal prior to ethylidyne formation, more hydrogen desorbs in the bulk hydrogen feature. In addition, more intensity is observed at mass 27 and mass 30. More hydrogenation products are formed at higher bulk hydrogen concentrations, but the question still remains as to the identity of the adsorbed hydrocarbon that is being hydrogenated to produce ethylene and ethane. It was mentioned above that acetylene is concluded to be formed, coadsorbed with ethylidyne, from the reaction of ethylene and H atoms. If this is the case, then the mass 27 and mass 30 signals could arise from hydrogenation of acetylene by bulk hydrogen to ethylene and ethane. The following experiment tests the notion that hydrogen emerging from the bulk to the surface of the

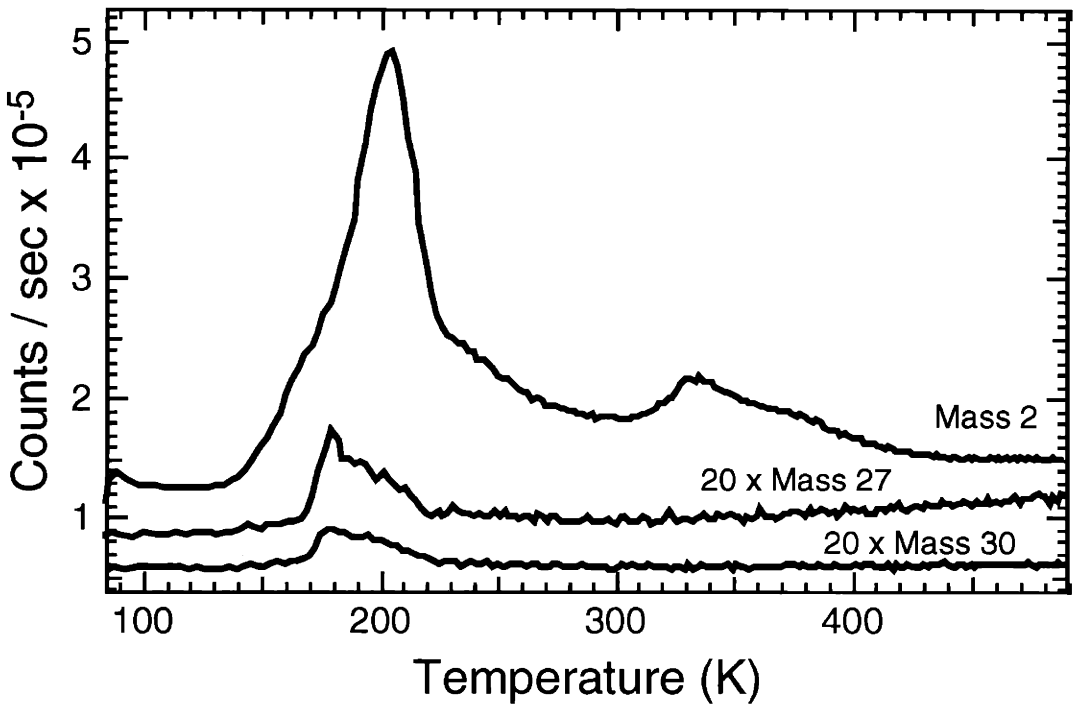

Figure 1.10. Thermal desorption spectrum measured from an ethylidyne covered, bulk H containing crystal.

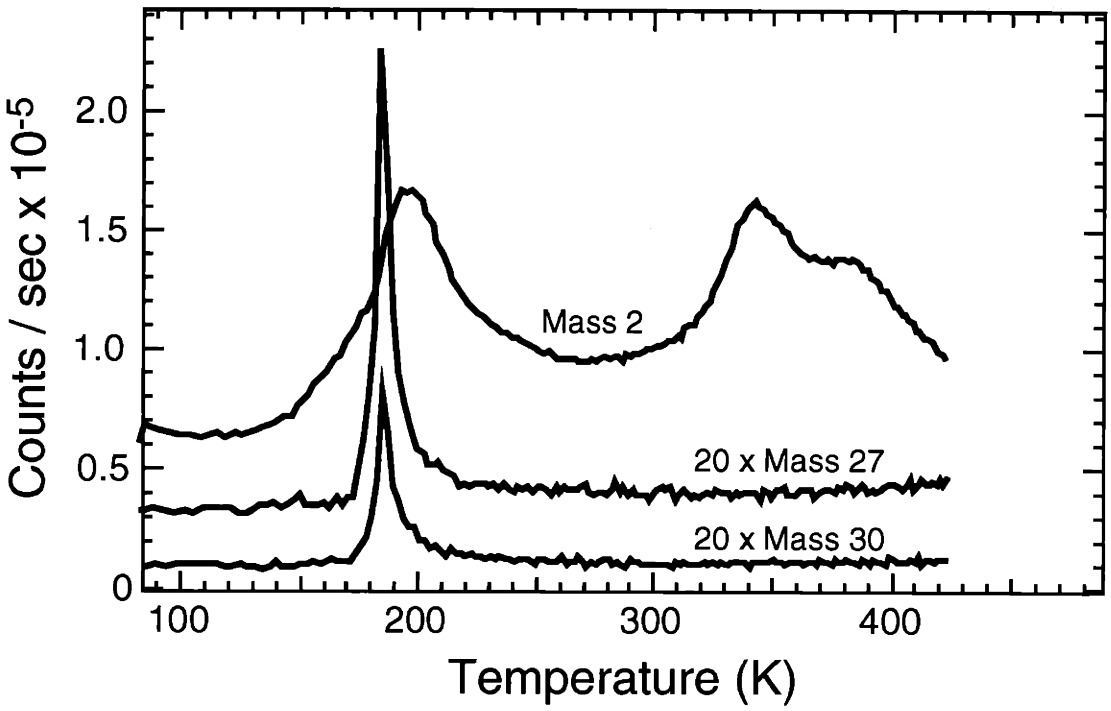

Figure 1.11. Thermal desorption spectrum measured from a crystal containing bulk H and covered with 0.05 ML adsorbed acetylene.

crystal can react with adsorbed acetylene to form ethylene and ethane. A clean crystal is exposed to H atoms which produces bulk hydrogen, but also produces hydrogen atoms adsorbed on the surface. The surface bound hydrogen is removed by exposure to a ~140 kcal/mol seeded beam of Xe atoms at an angle of incidence of 40° from the surface normal for 30 minutes. Acetylene is then exposed to the clean crystal surface to a coverage of 0.05 ML. The thermal desorption spectrum is shown in Figure 1.11.

A comparison of Figures 1.10 and 1.11 shows that the amount of bulk hydrogen in Figure 1.11 is less than that in Figure 1.10. But since all the hydrocarbon species desorb well before all the bulk hydrogen desorbs, the difference in the amount of bulk H does not affect the comparison between the hydrocarbon features. Several interesting observations can be made by comparing the mass 27 and mass 30 features of Figures 1.10 and 1.11. The features in the reaction of bulk hydrogen with adsorbed acetylene shown in Figure 1.11 are very narrow and

do not extend through the entire bulk hydrogen desorption feature (mass 2). The features observed in Figure 1.10 are much broader, although a close examination of the mass 27 and mass 30 signals reveals a sharp component followed by a tail lasting throughout the bulk hydrogen feature. The temperature at which the sharp component is observed matches well with that of the mass 27 and mass 30 desorption features from the reaction of bulk hydrogen with acetylene. Perhaps this sharp component is due to the reaction of the acetylene with bulk hydrogen, while the broader tail is due to the reaction of ethylidyne and bulk hydrogen. Assuming this is true, it can be seen that the reaction of ethylidyne with bulk hydrogen to form hydrogenation products is much slower than that of acetylene and bulk hydrogen.

Regardless of the assignment of the origin of the long tails in the mass 27 and mass 30 signals in Figure 1.10, the hydrogenation reaction which accounts for them is less efficient than that of bulk hydrogen and acetylene. This is seen not only in the desorption rate in the thermal desorption spectra, but also in the total amount of hydrocarbon desorbed. Table 1.2 shows the integrated desorption signals at mass 27 and mass 30 from Figures 1.8, 1.10 and 1.11. For comparable amounts of adsorbed hydrocarbon, the amount of desorbed ethylene and ethane is greater for the bulk hydrogen and acetylene reaction than for the bulk hydrogen and ethylidyne reaction. The difference in the efficiency of the hydrogenation reaction is even greater than indicated by the numbers because part of the signal seen in the reaction of bulk hydrogen and ethylidyne is due to the hydrogenation of the small amount of acetylene coadsorbed with ethylidyne. Ethylidyne hydrogenation by bulk hydrogen is a less efficient process than the hydrogenation of acetylene by bulk hydrogen.

	Reference Figure	Carbon Coverage Prior to TDS (ML)	Mass 2 Integral (millions)	Mass 27 Integral (thousands)	Mass 30 Integral (thousands)
Ethylidyne	Figure 1.8	0.25	5.7	38	16
Bulk H + Ethylidyne	Figure 1.10	0.25	14.5	74	36
Bulk H + Acetylene	Figure 1.11	0.10	8.0	77	31
Bulk H + Acetylene	Exp. not shown	0.28	7.5	190	51

Table 1.2. The integrated mass spectra signals measured in the thermal desorption spectra shown in Figures 1.8, 1.10, and 1.11.

III.A.2. Acetylene and Gas Phase Hydrogen Atoms

The reaction of adsorbed acetylene with gas phase hydrogen atoms has been investigated with Auger electron spectroscopy and electron energy loss spectroscopy. The following sections describe the results of these experiments and discuss their significance. The results will be compared to those from the reaction of adsorbed ethylene and hydrogen atoms when appropriate.

III.A.2.a. Carbon Auger measurements

Figure 1.12 shows C/Ni Auger ratios measured after 0.5 ML acetylene has been exposed to gas phase hydrogen atoms. The data are shown as function of the time of exposure to H atoms. The temperature of the crystal is 80 K prior to the H atom exposure, but increases to 120 K during the exposure. The Auger signals are measured at 80 K.

The results show that the carbon coverage decreases dramatically during the initial 30 seconds of H atom exposure. The carbon coverage continues to decrease after the first 30 seconds, but the rate is much slower. It appears that the adsorbed carbon is converted to a less reactive form than the initial form, acetylene.

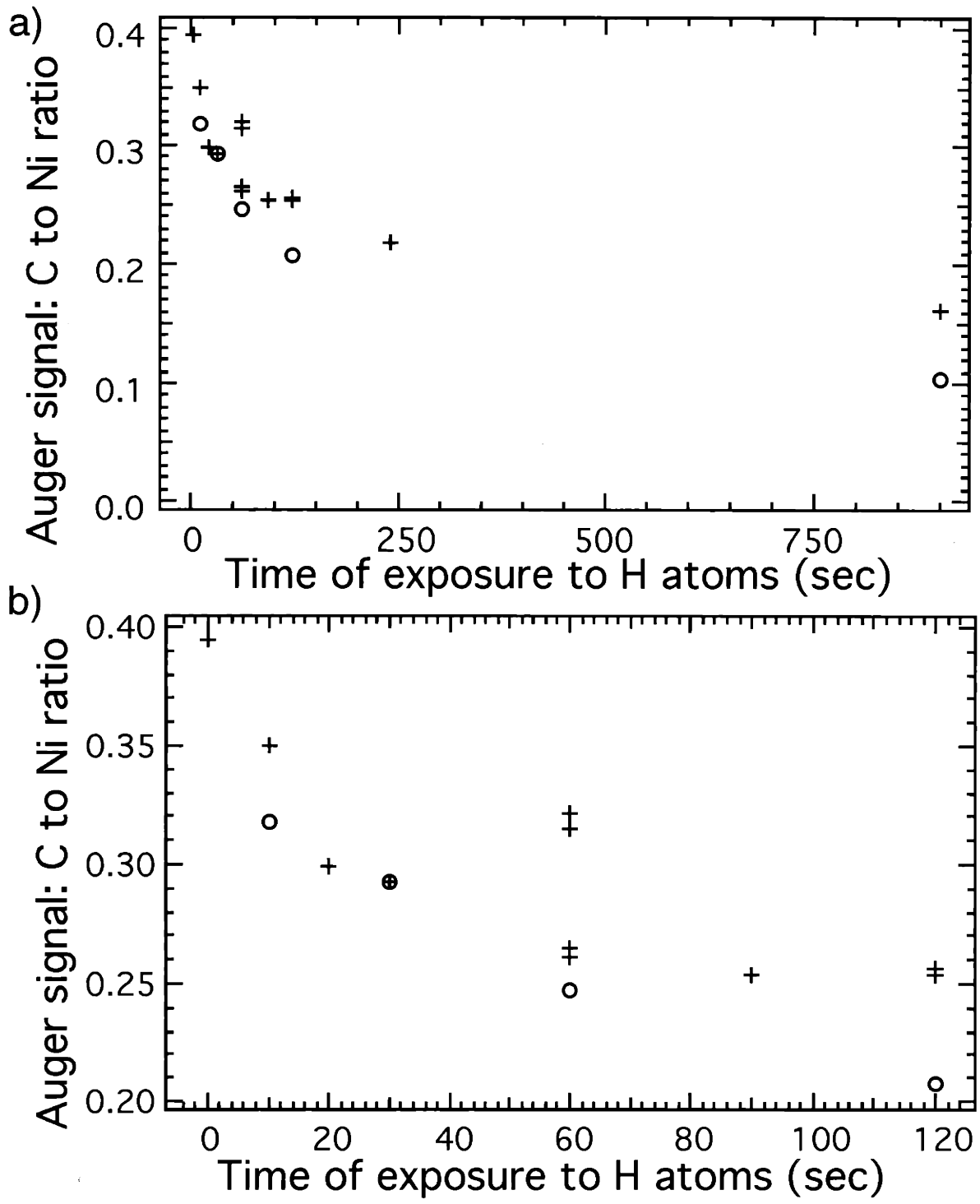

Figure 1.12. **a)** Carbon to nickel Auger signals after exposure of 0.5 ML adsorbed acetylene to H atoms. The +'s are after H atom exposure and O's are after H atom exposure and heating crystal to 300 K. **b)** Expanded view of a) showing initial drop in C/Ni ratio.

These results are similar to what is seen when ethylene is exposed to H atoms, but are not identical. In both cases, a dramatic decrease in the carbon coverage in the first 30 seconds of the H atom exposure is observed with a much slower carbon loss rate at longer exposures as shown in Figures 1.4 and 1.12. However, differences are seen in the transition between these two regimes: the transition from the initial high carbon loss rate to the later slow carbon loss rate is abrupt in the reaction of ethylene with H atoms while the transition is more gradual in the reaction of acetylene with H atoms. The difference in the transition between the two regimes may arise from the different initial carbon coverages in the two experiments. That is, the higher initial coverage of acetylene (0.5 ML) as compared to that of ethylene (0.25 ML) may give rise to the larger C/Ni ratio of 0.3 as compared to 0.1 after a 30 second reaction of H atoms with acetylene and ethylene, respectively. Nevertheless, the dramatic decrease in the carbon signal to approximately half of the initial carbon signal in the first 30 seconds of exposure to H atoms is similar the that observed for the reaction of H atoms with ethylene. As is observed for reaction of H atoms with ethylene, the next section will show that the less reactive form of carbon from the reaction of H atoms with acetylene is ethylidyne.

III.A.2.b. High resolution electron energy loss spectroscopy

The adsorbed reaction product of chemisorbed acetylene exposed to gas phase hydrogen atoms has been studied with electron energy loss spectroscopy. Figure 1.13 shows the electron energy loss spectra of 0.23 ML adsorbed acetylene after exposure to H atoms for two minutes. The surface temperature prior to the H atom exposure is 80 K, but increases to 120 K during the exposure. After the H atom exposure, the surface is heated to 300 K and immediately cooled to 80 K. Spectra of ethylene measured after exposure to H atoms, which has been previously assigned as ethylidyne, are included for comparison. Comparison of the two sets of spectra reveals that they are almost identical and demonstrates that acetylene and ethylene react with H atoms to produce the same adsorbate, ethylidyne. The detailed assignment of these

spectra to the ethylidyne species is discussed in Chapter II. Also observed in both sets of spectra are the 950 cm^{-1} and 860 cm^{-1} features. The 950 cm^{-1} feature is the antisymmetric Ni-H mode of surface hydrogen,[59] and the 860 cm^{-1} feature is shown later in this chapter to be the antisymmetric C-H bending mode of acetylene.

Electron energy loss spectra have also been measured after varied H atom exposure times. Figures 1.14 and 1.15 show the electron energy loss spectra of 0.5 ML acetylene after exposure to gas phase hydrogen atoms for different lengths of time. The surface temperature prior to the H atom exposure is 80 K, but increases to 120 K during the exposure. The vibrational spectra are measured at 80 K.

Ethylidyne features in the electron energy loss spectra are observed for hydrogen atom exposure times as short as 10 seconds. The strongest ethylidyne features, the C-C stretch and the CH_3 deformation modes are clearly visible at 1130 cm^{-1} and 1330 cm^{-1}. The 260 cm^{-1} and 1400 cm^{-1} features of ethylidyne, the symmetric C-Ni stretch and the antisymmetric CH_3 deformation modes, respectively, are also visible. The rest of the features are assigned to the vibrational modes of adsorbed acetylene, to overlapping modes of acetylene and ethylidyne or to a surface bound hydrogen vibrational mode. The 860 cm^{-1} and 1220 cm^{-1} are the antisymmetric C-H rocking mode and C-C stretching mode of acetylene, respectively. The 460 cm^{-1} and 2920 cm^{-1} features are overlapping C-Ni and C-H stretching modes, respectively, of both acetylene and ethylidyne. The 960 cm^{-1} feature is the antisymmetric Ni-H stretching mode. For exposure times of 30 seconds and longer, the ethylidyne and surface hydrogen vibrational features dominate the spectra. The only feature which cannot be assigned to ethylidyne or surface bound hydrogen is a weak feature at 860 cm^{-1}. The fact that ethylidyne continues to dominate the spectra even at high hydrogen atom exposures demonstrates the stability of ethylidyne in the presence of H atoms.

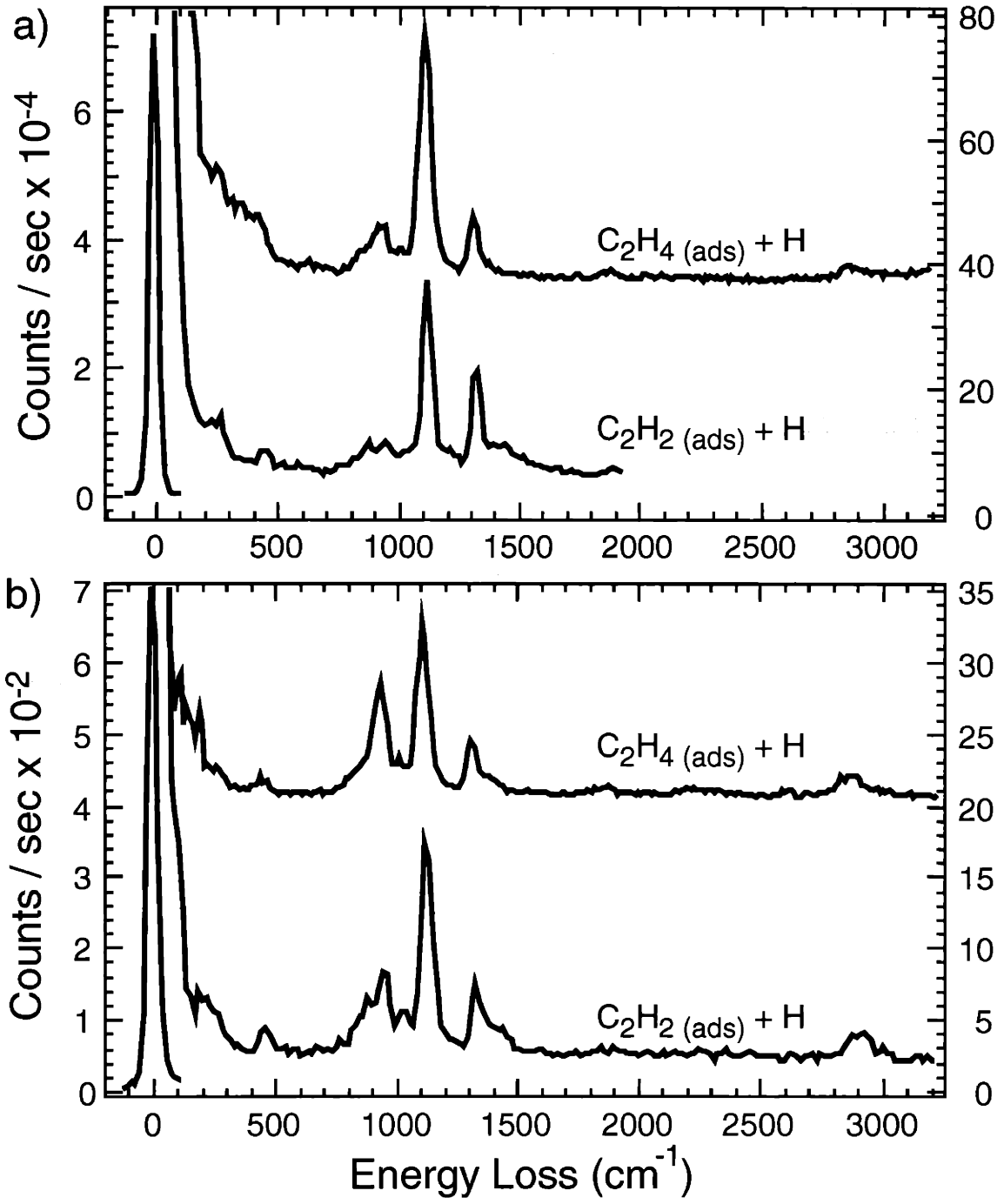

Figure 1.13. Electron energy loss spectra after a two minute exposure of 0.25 ML adsorbed ethylene or 0.23 ML acetylene to H atoms. The surface is heated to 300 K after H atom exposure and immediately cooled to 80 K, the temperature at which the spectra are measured. **a)** on-specular. **b)** 10° off-specular.

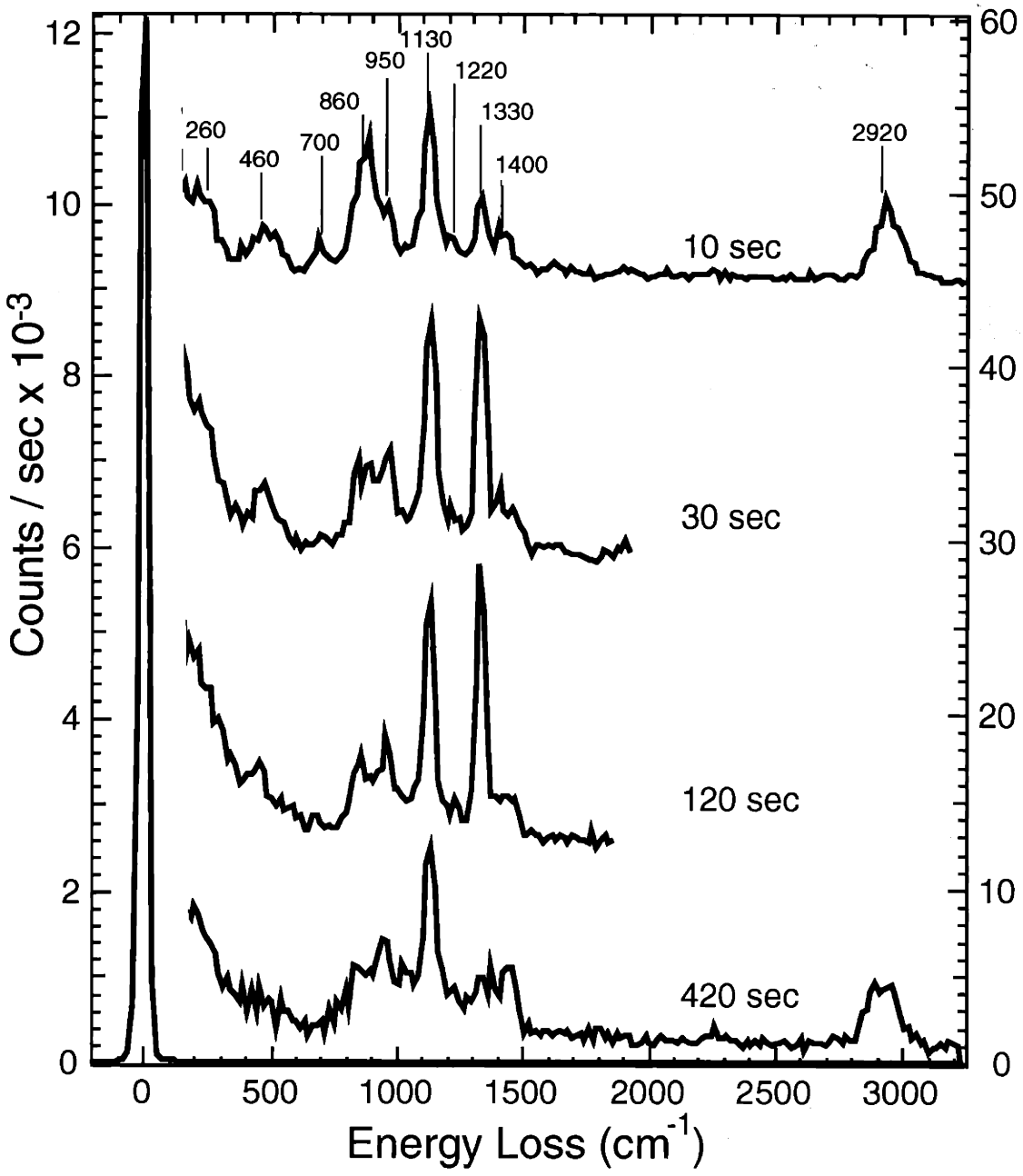

Figure 1.14. Electron energy loss spectra of 0.5 ML acetylene exposed to H atoms measured at the specular angle. The duration of the hydrogen atom exposure is indicated.

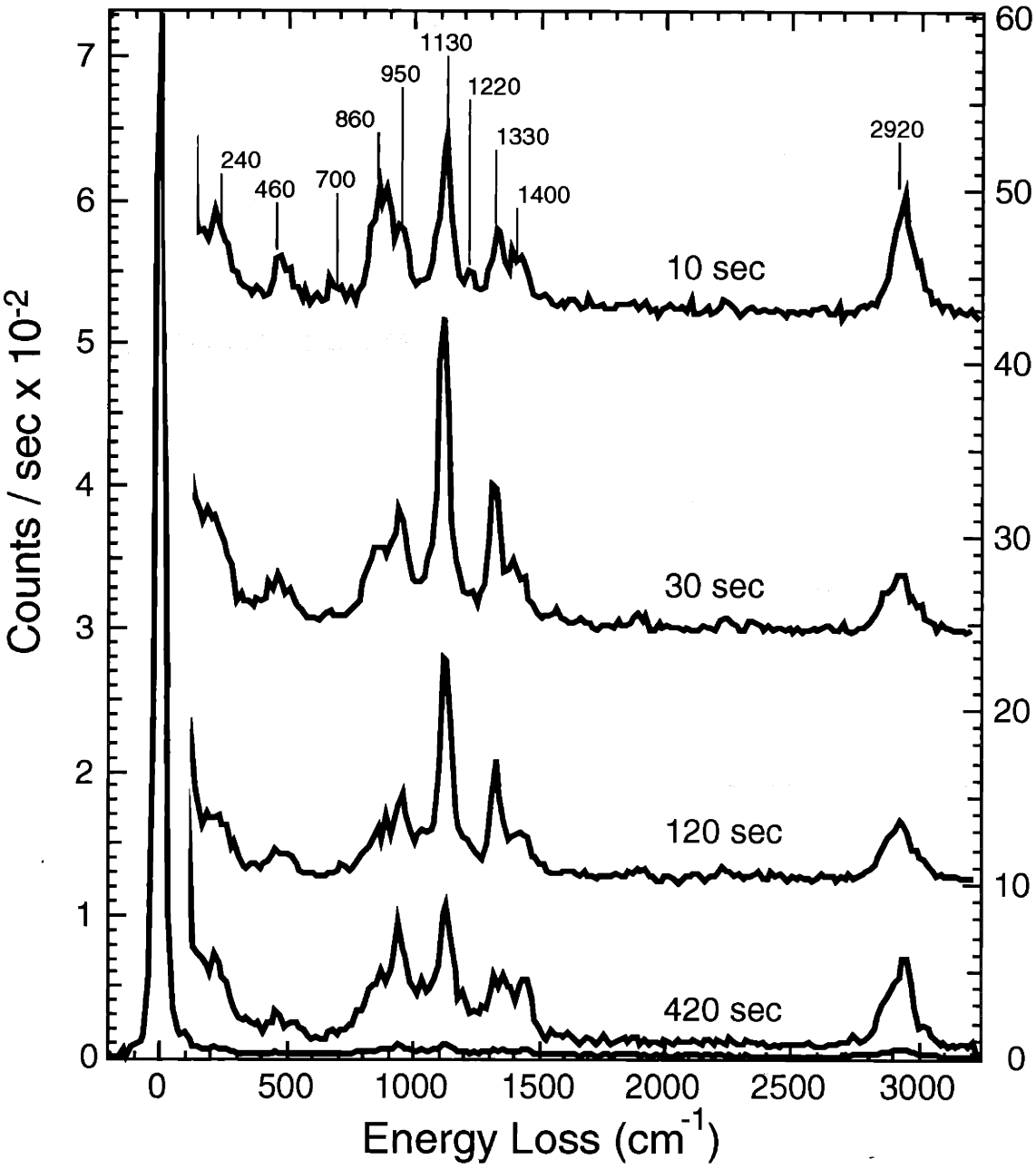

Figure 1.15. Electron energy loss spectra of 0.5 ML acetylene exposed to H atoms measured 10° off-specular. The duration of the hydrogen atom exposure is indicated.

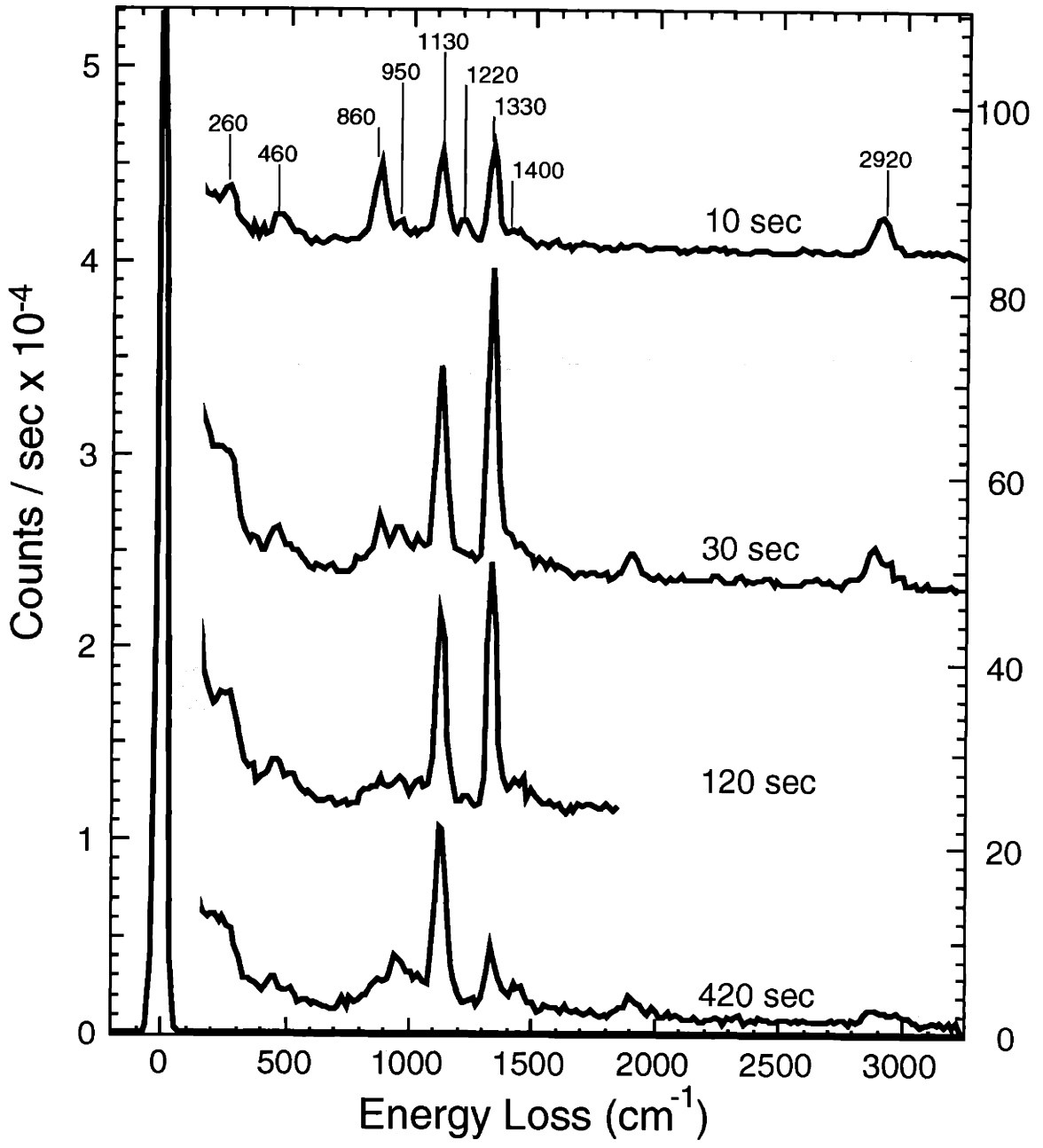

Figure 1.16. Electron energy loss spectra of 0.5 ML acetylene exposed to H atoms. Duration of H atom exposure is indicated. Crystal is heated to 300 K before spectra are measured on-specular at 80 K.

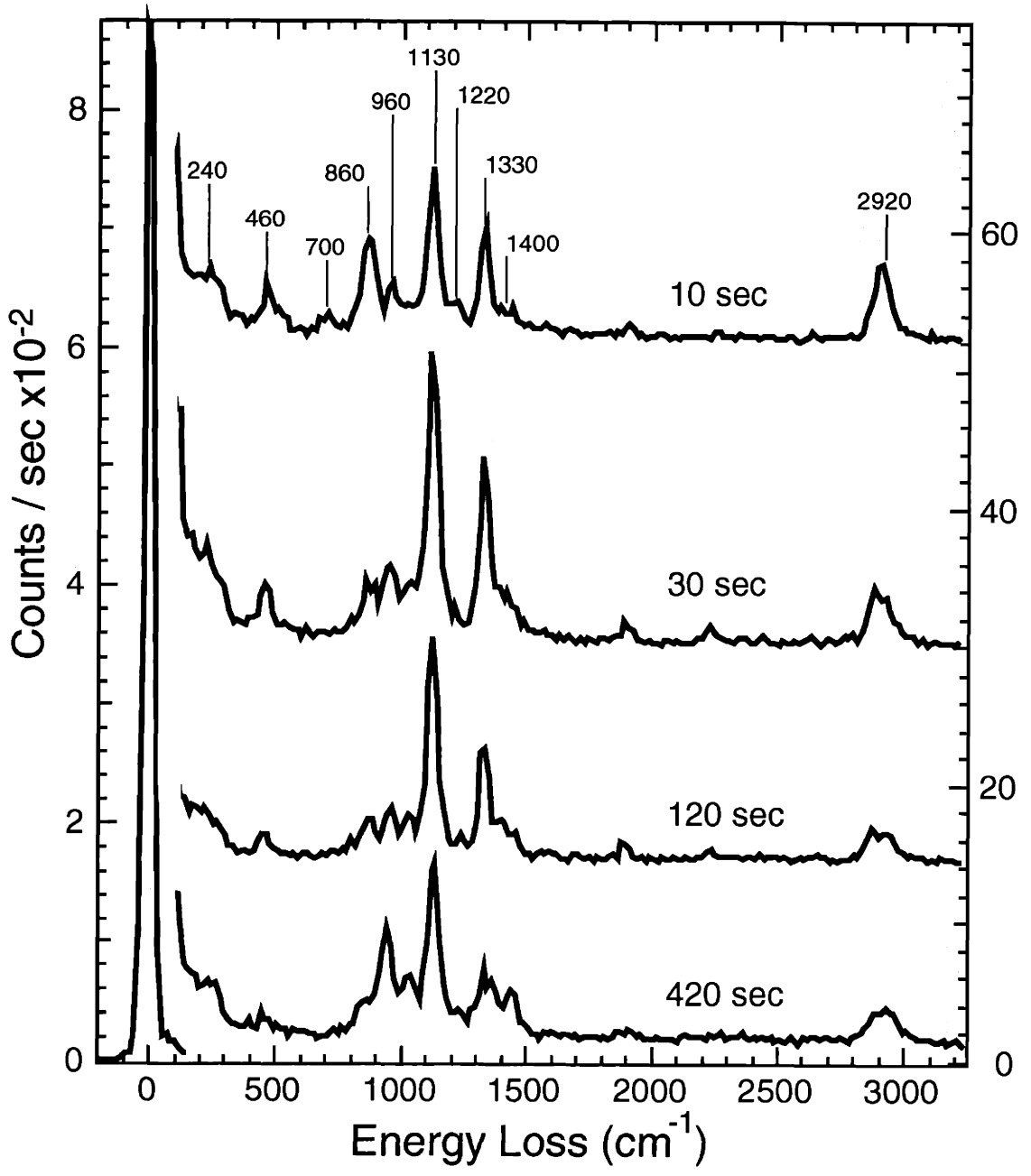

Figure 1.17. Electron energy loss spectra of 0.5 ML acetylene exposed to H atoms. Duration of H atom exposure is indicated. Crystal is heated to 300 K before spectra are measured 10° off-specular at 80 K.

The completion of the ethylidyne formation reaction after 30 seconds of H atom exposure is consistent with the Auger data in Figure 1.12 which shows the depletion rate of the carbon from the surface to decrease at approximately 30 seconds. The time for complete conversion of acetylene to ethylidyne will be used as a measure of the rate of this reaction. The rate of the reaction of acetylene with H atoms will be seen to be important in the discussion of the mechanism for ethylidyne formation later in this chapter in Section III.E.

Electron energy loss spectra have also been measured after heating the surface. Figures 1.16 and 1.17 show electron energy loss spectra of the same surface prepared as those shown in Figures 1.14 and 1.15 after heating the surface to 300 K. As is the case with the ethylidyne species formed from the reaction of adsorbed ethylene with H atoms, heating the crystal to 300 K after the H atom exposure affects the electron energy loss spectra only very slightly as shown in Figures 1.14, 1.15, 1.16, and 1.17. No new features are observed, but the on-specular intensity of the dipole active features, the symmetric C-Ni stretching , C-C stretching and the symmetric CH_3 deformation modes increase. The elastic feature also increases in intensity upon heating the crystal to 300 K. As discussed in Chapter II, the increase of the intensities of the dipole active features and the elastic feature is most likely due to ordering of the adsorbate that occurs at higher surface temperatures.

Heating the crystal to 300 K also causes a decrease in the intensity of the 860 cm^{-1} feature. Section III.D of this chapter will show the 860 cm^{-1} feature to be the C-H rocking mode of acetylene coadsorbed with ethylidyne. The explanation for the decrease in its intensity is the same as for the spectra measured after exposure of ethylene to H atoms. Gas phase hydrogen atoms produce bulk hydrogen in addition to reacting with the adsorbed hydrocarbon. Raising the crystal temperature causes the bulk hydrogen to emerge from the bulk to the surface. As it does, it hydrogenates some of the adsorbed acetylene to ethylene and ethane which desorb into the gas phase. The lower intensity of the 860 cm^{-1} vibrational feature reflects the removal of some of the adsorbed acetylene.

Comparing the spectra of ethylidyne produced from ethylene in Figure 1.6 to that from acetylene in Figure 1.16, a dramatic difference is seen in the intensity of the symmetric CH_3 deformation loss feature at 1330 cm^{-1} relative to the other features such as the C-C stretching feature at 1130 cm^{-1}. The symmetric CH_3 deformation mode is much more intense in the ethylidyne produced from the reaction of H atoms with 0.5 ML acetylene than it is for ethylidyne produced from 0.25 ML ethylene. The higher intensity of the symmetric CH_3 deformation mode is attributed to the higher ethylidyne coverage. Auger electron spectroscopy measurements in Figures 1.5 and 1.12 show that the carbon coverages after a two minute reaction of H atoms with 0.5 ML acetylene and with 0.25 ML ethylene are 0.63 ML and 0.25 ML, respectively. Recall that the coverage of carbon is double that of ethylene or acetylene since there are two carbon atoms per hydrocarbon molecule. Although some of the carbon is in the form of acetylene, most of it is in the form of ethylidyne.

Spectra of lower coverages of acetylene exposed to gas phase hydrogen atoms have been measured to confirm that the relative intensity of the symmetric CH_3 deformation feature is dependent on coverage and not on the form of the reactant carbon (acetylene vs. ethylene). Figure 1.18 shows the electron energy loss spectra of 0.23 ML of acetylene exposed to H atoms for two minutes. The spectra of 0.5 ML acetylene after identical exposure, reproduced from Figures 1.16 and 1.17, are shown for comparison. The relative intensity of the symmetric CH_3 deformation loss feature is observed to be lower in the spectra of the ethylidyne species at the lower coverage, and therefore it does not depend on the form of the reactant carbon.

The decrease in the intensity of the symmetric CH_3 deformation feature relative to the other features with decreasing coverage is also observed in Figures 1.14 and 1.16. The decay in the intensity as the exposure of 0.5 ML acetylene to H atoms is increased from 30 to 120 and to 420 seconds is consistent with the Auger electron spectroscopy measurements in Figure 1.12

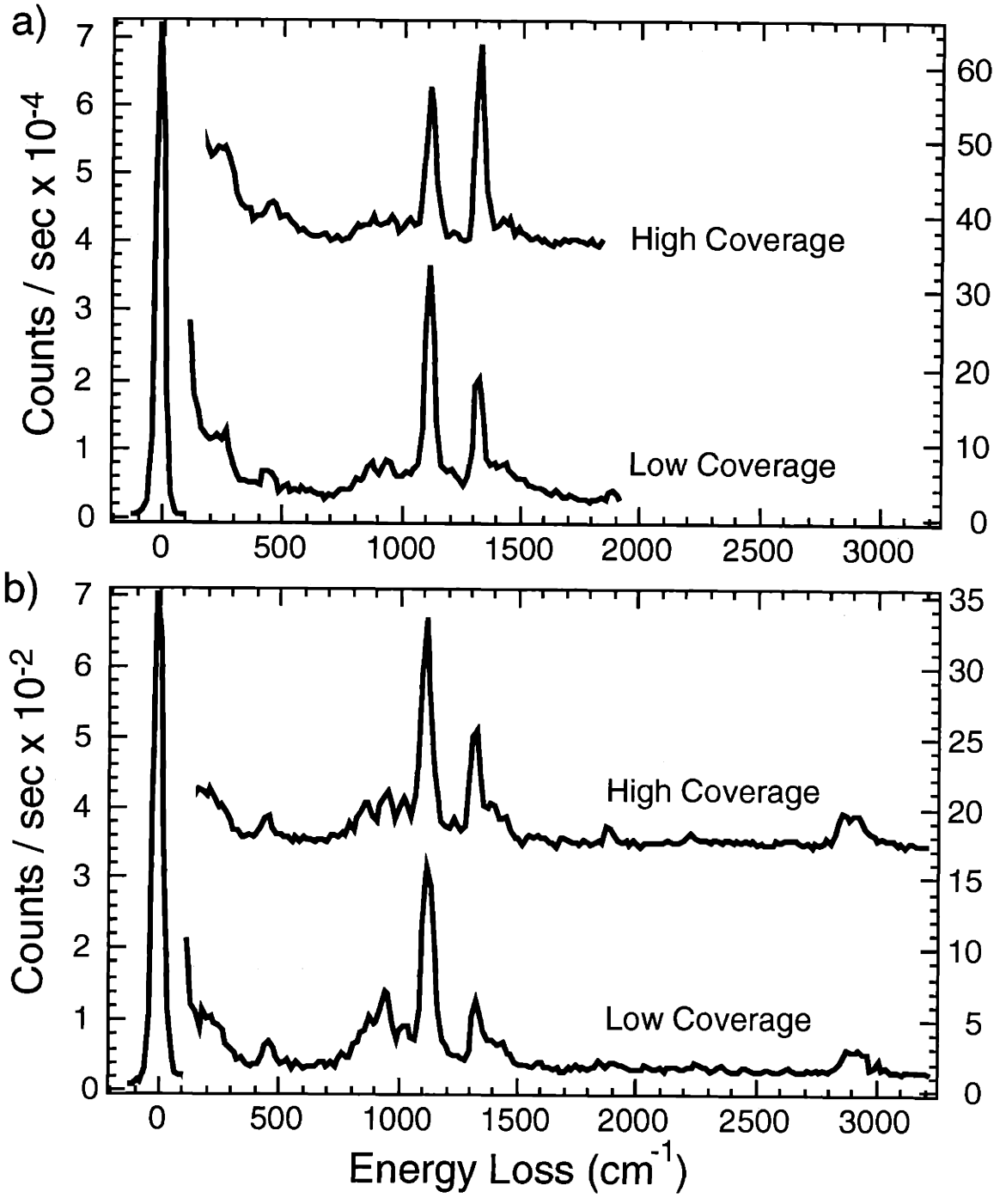

Figure 1.18. Electron energy loss spectra of 0.5 ML and 0.23 ML acetylene after exposure to two minutes of H atoms, labeled in the figure as high and low coverage, respectively. Crystal is heated to 300 K before spectra are measured. **a)** on-specular **b)** 10° off-specular

which shows that the carbon coverage decreases from 0.73 ML to 0.63 ML and to 0.53 ML, respectively. The carbon coverage after a 420 second H atom exposure is interpolated from the neighboring measurements in Figure 1.12. The same trend of the decrease in the relative intensity of the symmetric CH_3 deformation mode with decreasing carbon coverage is observed after heating the crystal to 300 K. Although the absolute coverage of ethylidyne cannot be determined because of the coadsorbed acetylene, the ethylidyne coverage is likely close to half the reported carbon coverage because the weak features attributed to acetylene in the electron energy loss spectra suggest that the acetylene coverage is very low. While the intensities of the symmetric CH_3 deformation feature depends on coverage, the dependence does not appear to be linear. The intensity of the ethylidyne symmetric CH_3 deformation feature in Figure 1.16 is 35, 30, and 9 counts/sec for the carbon coverages of 0.73, 0.63 and 0.53 ML respectively while the intensity of the C-C stretching feature remains more constant at 25, 24, and 22 counts/second, respectively.

III.A.3. Ethane and Gas Phase Hydrogen Atoms

The reaction of adsorbed ethane with gas phase hydrogen atoms has also been explored. Mass spectrometric measurements attempt to probe the products desorbing during exposure of ethane to H atoms. Thermal desorption, Auger electron spectroscopy and electron energy loss spectroscopy measurements after exposure of ethane to H atoms yield information on the adsorbed product of the reaction of ethane with H atoms.

Because ethane adsorption on Ni(111) has not been explored in previously, it is briefly addressed here before the reaction of adsorbed ethane and H atoms is discussed. Unlike ethylene[36,37] and acetylene[40], which chemisorb to a Ni(111) surface, ethane physisorbs to Ni(111) through a van der Waals interaction. An electron energy loss spectrum of adsorbed ethane is shown in Chapter II. The observed vibrational frequencies are identical to those of gas phase ethane indicating little chemical interaction between ethane and the surface. Thermal

desorption spectroscopy also suggests that ethane physisorbs to the Ni(111) surface. Figure 1.19 shows the thermal desorption spectra measured after exposure to 0.21 ML ethane. The maximum desorption rate of ethane occurs at 100 K with a heating rate of 2 K/sec. This temperature is much lower than observed for ethylene, 200 K.[37] Acetylene is so strongly bound to the surface that it dissociates completely before sufficiently high temperatures are reached for desorption to occur.[40] A maximum desorption rate at 100 K corresponds to a binding energy for ethane on Ni(111) of approximately 6 kcal/mol. The absence of thermal desorption features in the mass 2 signal at temperatures which correspond to recombinative desorption of H_2 from the surface, 300 - 400 K, indicates that the none of the ethane thermally decomposes on the surface.

Although the maximum desorption rate in the thermal desorption spectra is 100 K, a measurable desorption of ethane occurs at 80 K. Auger electron spectroscopy measurements of

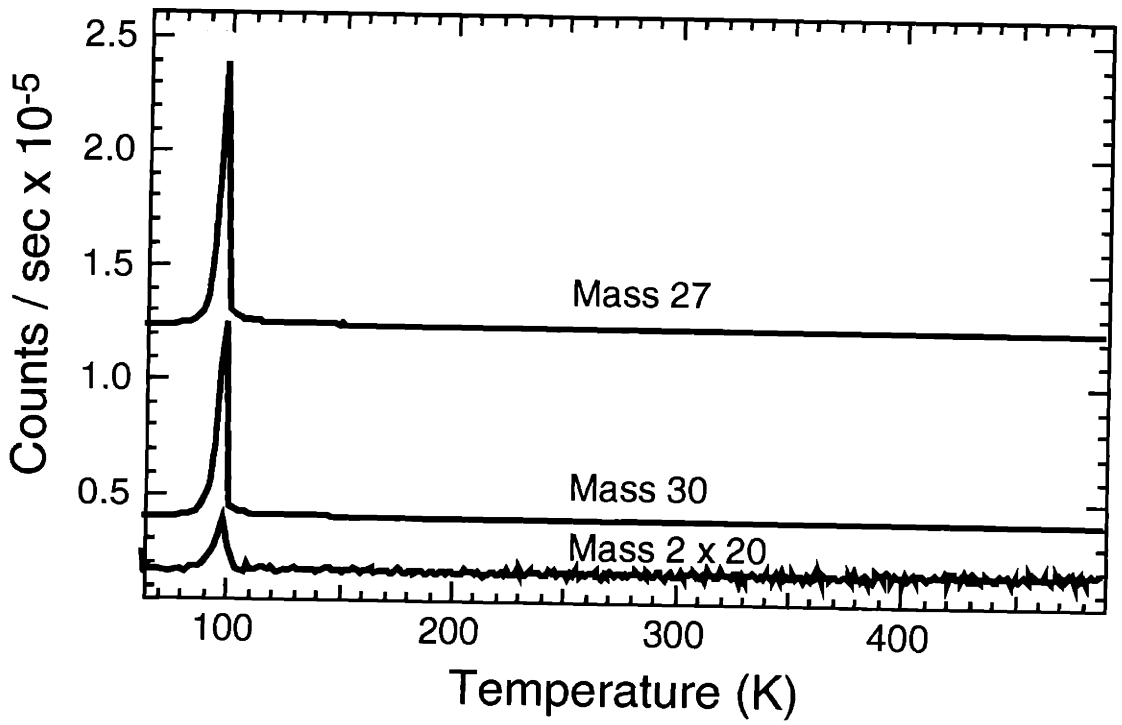

Figure 1.19. Thermal desorption spectrum after exposure of crystal to 0.21 ML ethane.

a surface initially covered with 0.21 ML ethane showed that approximately 0.02 ML ethane desorbs in 210 seconds from a crystal held at 80 K. No carbon is detected on the surface after 30 minutes. Lowering the crystal temperature decreases the ethane desorption rate. At a crystal temperature of 70 K, no loss of carbon signal is detected after 1 hour. Therefore, in the reactions of ethane with H atoms described in this section, the temperature of the crystal is kept below 80 K to minimize the desorption of ethane.

III.A.3.a. Mass spectrometric measurements

The evolution of gas phase hydrocarbons is monitored with a mass spectrometer during the exposure of 0.21 ML adsorbed ethane to H atoms. Figure 1.20 shows the mass spectrometer signals at mass 27 and mass 30 during the following sequence of exposure to H atoms. H_2 is leaked into the main chamber to maintain a pressure of $2x10^{-5}$ torr. Note that this H_2 pressure is higher than that employed during the exposures of ethylene and acetylene to H atoms. Then the hydrogen atom filament, positioned in front of the crystal, is turned on for a duration of three minutes. After the hydrogen atom filament is turned off, the H_2 leak into the chamber is shut off. The mass spectrometer is on throughout the experiment. The temperature of the crystal is approximately 10 K before the hydrogen atom filament is turned on. The temperature of the crystal increases to 50 K during the exposure to H atoms because of radiation from the hot filament.

The mass spectrometer signals at mass 27 and mass 30 increase dramatically as H_2 is leaked into the main chamber. As discussed earlier in Section III.A.1.a of this chapter, this increase in signal is most likely due to reactions in the mass spectrometer ionizer or displacement of hydrocarbons from the walls of the chamber. The small maxima in the mass 27 and mass 30 signals as the H_2 is initially leaked into the main chamber are due to an initial

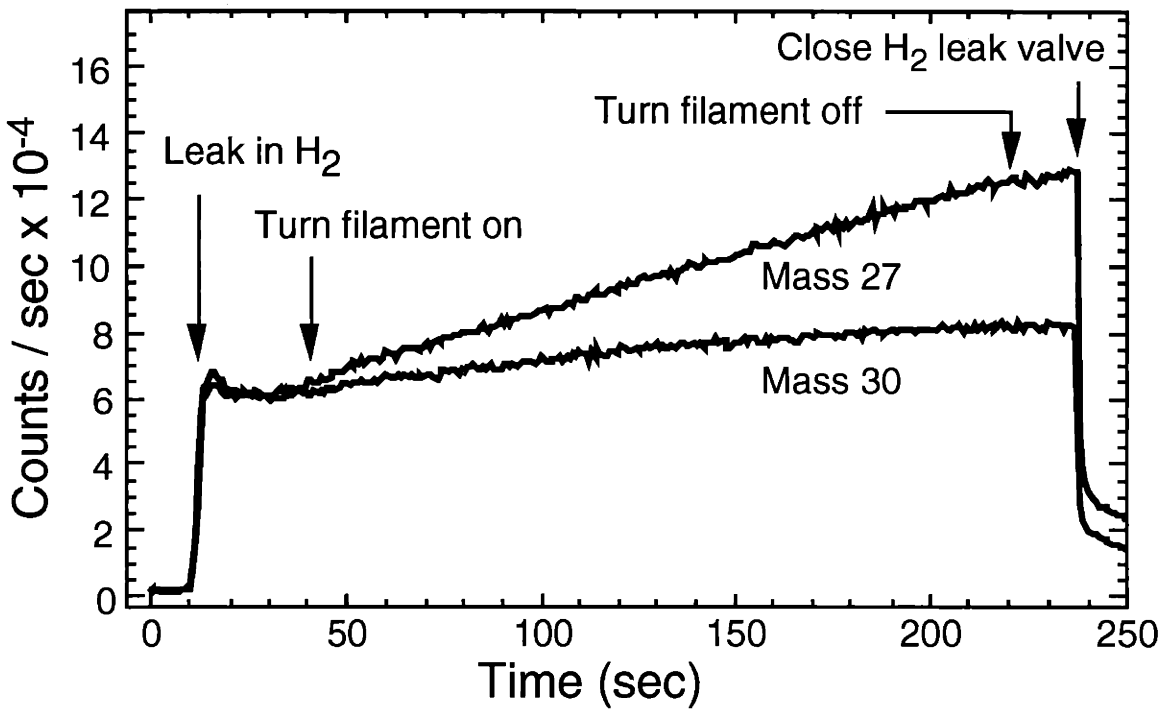

Figure 1.20. Mass spectrometer signal measured during exposure of 0.21 ML ethane to H atoms. The H_2 pressure is $2x10^{-5}$ torr.

overshoot in setting the hydrogen pressure. No detectable additional increase in the mass 27 and mass 30 signals are observed at the moment the filament is turned on. This observation is in contrast to that when exposing ethylene to H atoms. In that case, H atoms displace ethylene from the surface and hydrogenate ethylene to ethane which desorbs as shown in Figure 1.1. Although H atoms cannot hydrogenate ethane, it may have been anticipated that H atoms would displace ethane, especially considering ethane is physisorbed rather than chemisorbed. However, displacement of ethane by H atoms is not observed. The lower surface temperature, 50 K, used in the exposure of ethane to H atoms could possibly explain the observed difference. Monitoring the mass spectrometer signal during exposure of ethylene to H atoms at a crystal temperature of 50 K would be useful for comparison, but this experiment has not been carried out.

III.A.3.b. Thermal desorption spectrometry

Although displacement of ethane by H atoms is not observed as a measurable increase in the partial pressure of ethane at mass 30 during the H atom exposure, the depletion of ethane from the surface is detected in a different kind of experiment. Specifically, the amount of ethane which desorbs in a thermal desorption experiment after exposure to H atoms is used as a measure of the amount of ethane that remains after the H atom exposure. Figure 1.21 shows the integrated mass spectrometer signal at mass 30 during thermal desorption experiments subsequent to exposure of 0.21 ML ethane to H atoms as function of the length of H atom exposure. The crystal temperature prior to the H atom exposure is 10 K, but heats up to approximately 50 K due to radiation from the hot filament during the exposure. The H_2 pressure during the hydrogen atom exposure is $2x10^{-5}$ torr.

Figure 1.21 shows that the integrated mass 30 signal (ethane) decreases with longer exposures of ethane to H atoms. The integrated signal of mass 30 after no H atom exposure is, of course, equal to that of the thermal desorption experiment shown in Figure 1.19. The decrease in the ethane coverage with longer H atom exposures is likely due to displacement of ethane by H atoms. However, a reaction of adsorbed ethane with H atoms to form hydrocarbons other than ethane which desorb during the H atom exposure cannot be excluded because no hydrocarbon desorption could be detected as a result of the H atom exposure in the mass spectrometric measurement shown in Figure 1.20. Ethane may also be displaced by the H_2 present during the H atom exposure. Exposure of an ethane covered surface to H_2 could easily show this not to be the case, but that experiment has not been performed. However, because adsorption of H atoms is a much more exothermic process than adsorption of H_2, H atoms are expected to be more reactive than H_2 for the displacement of adsorbed ethane. Therefore, the favored explanation for the depletion of ethane is the displacement of ethane by H atoms, similar to the displacement of ethylene by H atoms observed in Figure 1.1.

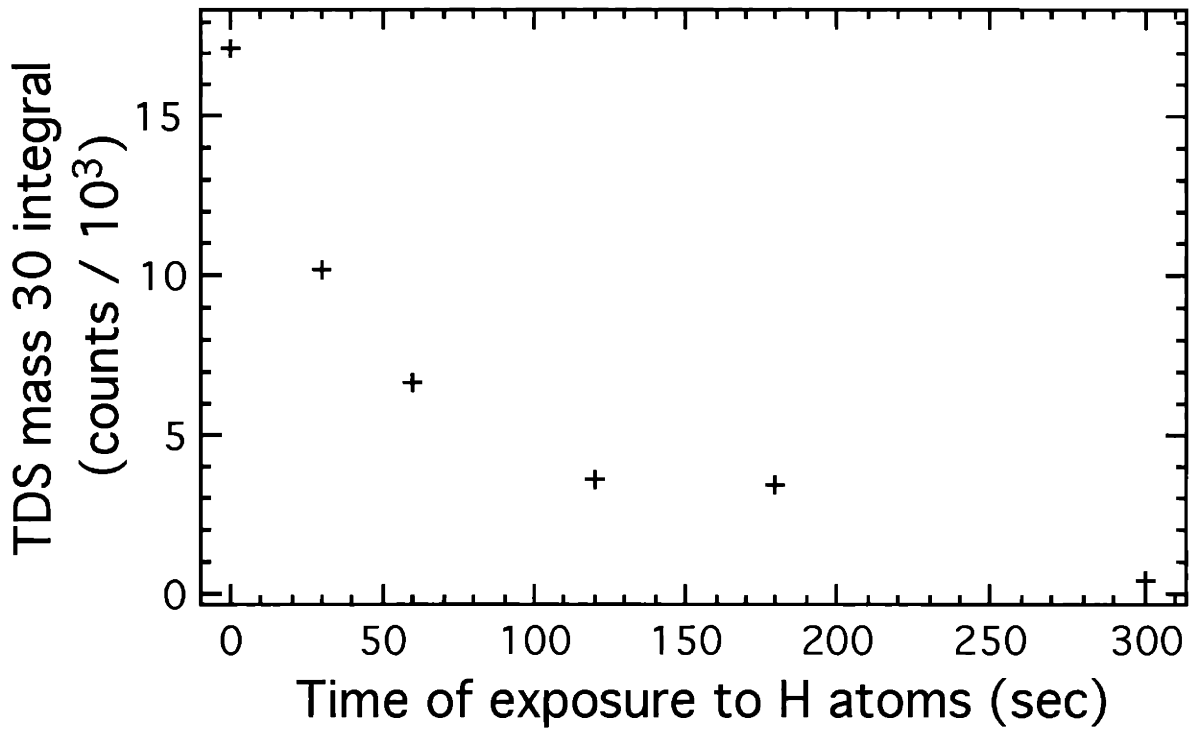

Figure 1.21. Integral of thermal desorption spectroscopy signal at mass 30 measured after exposures of 0.21 ML ethane to H atoms for the indicated time. The H_2 pressure is $2x10^{-5}$ torr.

The reason the displacement of ethane is not detected mass spectrometrically during the H atom exposure (Figure 1.20) is because the desorption rate for ethane is very low relative to the high background partial pressure of ethane during the measurement. Figure 1.21 shows that the integrated mass 30 signal is lowered by approximately 7000 counts in the first 30 seconds of exposure of ethane to H atoms. Assuming the decrease in the mass 30 signal is due to ethane desorption during the H atom exposure, an average 'desorption rate' at mass 30 is calculated to be 233 counts/second. This calculated desorption rate is an upper limit because a portion of the ethane may react with H atoms to form a species on the surface which does not desorb in the subsequent thermal desorption measurement. A 'desorption rate' of 233 counts/second is obscured by the noise in Figure 120 and therefore, the displacement of ethane upon H atom exposure is not detected.

III.A.3.c. Carbon Auger measurements

The exposure of ethane to H atoms has also been investigated by Auger electron spectroscopy. Figure 1.22 shows the C/Ni Auger signal after exposure of 0.21 ML ethane to H atoms at a H_2 pressure of $2x10^{-5}$ torr. The temperature of the crystal is 10 K prior to the H atom exposure, but warmed to approximately 50 K during it. The crystal is heated to 150 K prior to the Auger measurement to remove unreacted ethane. Because the crystal programmable temperature controller starting point does not go below 75 K, the temperature increase to 150 K is achieved in two stages: first the temperature is manually brought up to 80 K at an undefined rate and then the temperature is increased to 150 K at a rate of 2 K/s through use of the programmable temperature controller.

Figure 1.22 shows that indeed some of the adsorbed ethane reacts with the H atoms to form a hydrocarbon which is not removed by heating the crystal to 150 K. With no exposure to H atoms, the C/Ni Auger signal ratio is zero because all the ethane desorbs upon heating the crystal to 150 K. However, as the time of exposure is increased, the C/Ni Auger signal ratio increases, goes through a maximum and then decreases at longer exposure times. The next section describes the use of electron energy loss spectroscopy to identify the carbon on the surface to be that of ethylidyne. The dependence of ethylidyne coverage on H atom exposure time can be explained by the competition of two reactions involving H atoms: the reaction with ethane to produce ethylidyne and the reaction with ethylidyne to form a hydrocarbon which desorbs. After 30 seconds of H atom exposure, the ethylidyne depletion reaction dominates over the ethylidyne production reaction because the reactant of the ethylidyne production reaction, ethane, is consumed. This depletion of ethane coverage is observed in the thermal desorption measurements as the decreasing amount of ethane which desorbs at longer H atom exposures in Figure 1.21. Recall that the slow depletion of ethylidyne upon H atom exposure

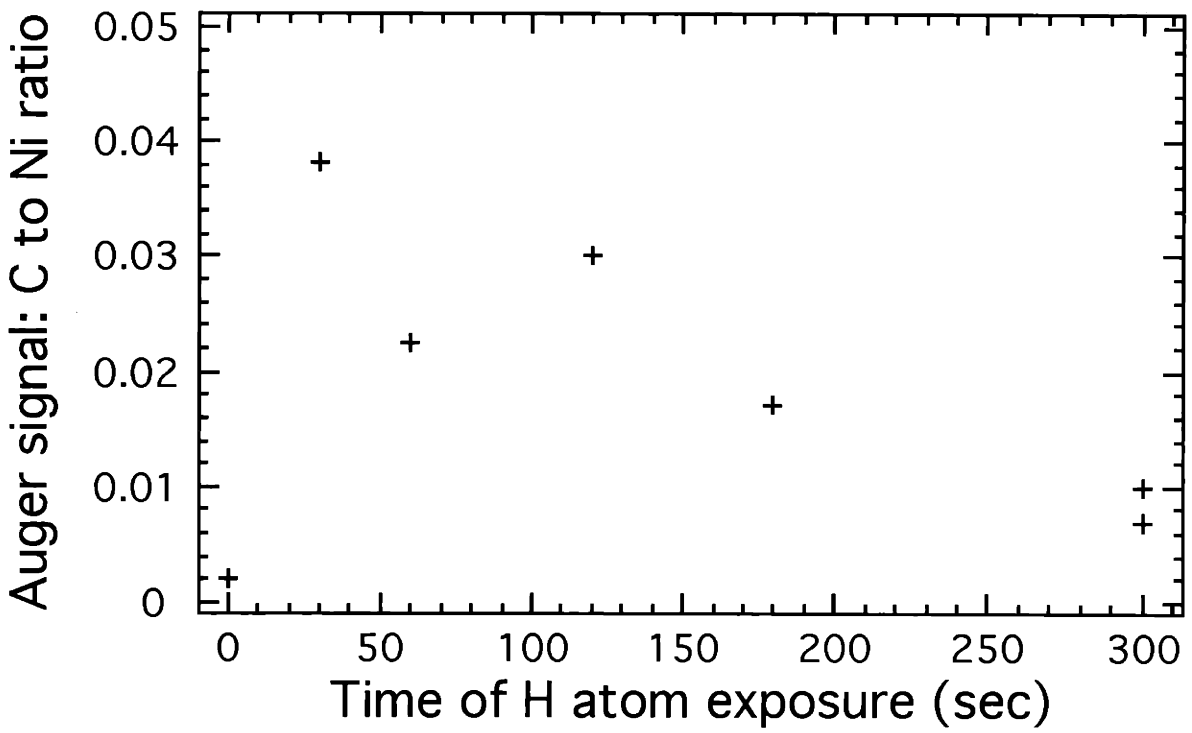

Figure 1.22. Carbon to nickel Auger signals after exposure of 0.21 ML ethane to H atoms and subsequent heating to 150 K to remove unreacted ethane. H_2 pressure during H atom exposure is $2x10^{-5}$ torr.

also is observed in the reactions of H atoms with ethylene and acetylene, Figures 1.5 and 1.12 respectively.

It should be again noted that a higher H_2 pressure, ($2x10^{-5}$ rather than $5x10^{-6}$ torr) is employed in all the experiments involving the reaction of ethane with H atoms so as to yield a higher flux of H atoms. A higher flux is used because the rate of the reaction of ethane with gas phase H atoms is lower than that with ethylene or acetylene. This difference in reaction rates is observed by comparing the time for complete conversion of the hydrocarbon to ethylidyne. In previous sections it is observed that the conversion of ethylene or acetylene to ethylidyne is complete after a 30 second H atom exposure. Figure 1.21 shows that ethane remains on the surface for H atom exposures as long as 300 seconds, ten times longer than ethylene or acetylene. Longer H atom exposures were not investigated and thus 300 seconds will be

considered a lower limit for the time of complete conversion of ethane to ethylidyne. Assuming the H atom flux to be linear with respect to the H_2 pressure, the flux of H atoms in the reactions of H atoms with ethane is four times greater than those in the reactions with ethylene or acetylene. Therefore, the reaction rate, defined as the inverse of the time for complete conversion of the initial hydrocarbon to ethylidyne, is at least 40 times slower for ethane than for ethylene or acetylene.

III.A.3.d. High resolution electron energy loss spectroscopy

The adsorbed product from the reaction of physisorbed ethane with gas phase hydrogen atoms has been explored with electron energy loss spectroscopy. Figure 1.23 shows electron energy loss spectra of 0.21 ML ethane after a five minute exposure to H atoms at a H_2 pressure of $2x10^{-5}$ torr. The temperature of the crystal prior to the H atom exposure is 70 K, but increased to 78 K during the exposure. The crystal is cooled to 70 K immediately after the H atom exposure, the temperature at which two of the electron energy loss spectra are measured. After the spectra are measured at 70 K, the crystal is warmed to 80 K. The crystal temperature is maintained at 80 K for 30 minutes prior to measuring electron energy loss spectra at this temperature.

The spectra in Figure 1.23 measured at 70 K are dominated by ethane features. The 260 cm^{-1}, 560 cm^{-1}, 820 cm^{-1}, 980 cm^{-1}, 1190 cm^{-1} 1390 cm^{-1}, and 1470 cm^{-1} features match very well with features of the electron energy loss spectra of adsorbed ethane shown in Figure 2.13 of Chapter II. The observation of ethane in the vibrational spectra measured at 70 K confirm the thermal desorption measurement in Figure 1.21 that after a 300 second exposure of ethane to H atoms, some ethane still remains unconverted to ethylidyne. As noted previously, ethane slowly desorbs at 80 K. No ethane features are present in the spectra measured after maintaining the crystal at 80 K for 30 minutes. Instead, vibrational features which are characteristic of ethylidyne are observed: the symmetric and antisymmetric C-Ni stretching

modes at 260 cm^{-1} and 440 cm^{-1}, the C-C stretching mode at 1130 cm^{-1} and the symmetric CH_3 deformation mode at 1330 cm^{-1}. In addition to the ethylidyne features, the antisymmetric Ni-H stretching mode is observed at 950 cm^{-1} along with a feature at 860 cm^{-1}.

Electron energy loss spectra of the product of the reaction of 0.21 ML ethane and H atoms after heating the crystal to 300 K have also been measured. Figure 1.24 shows the electron energy loss spectra of 0.21 ML of ethane after a ten minute exposure to gas phase H atoms at a H_2 pressure of $2x10^{-5}$ torr. Prior to the H atom exposure, the crystal temperature is 70 K, but increased to 78 K during the exposure. After the H atom exposure, the crystal is heated to 300 K and immediately cooled to 80 K prior to measuring the electron energy loss spectra. As will be discussed in Chapter II, better quality vibrational spectra are measured after heating the ethylidyne covered surface. Heating the crystal also removes the unreacted ethane by desorption. With the exception of the 860 cm^{-1} feature, the features observed in Figure 1.24 are characteristic of ethylidyne coadsorbed with hydrogen. The assignment of the vibrational features of ethylidyne are discussed in Chapter II.

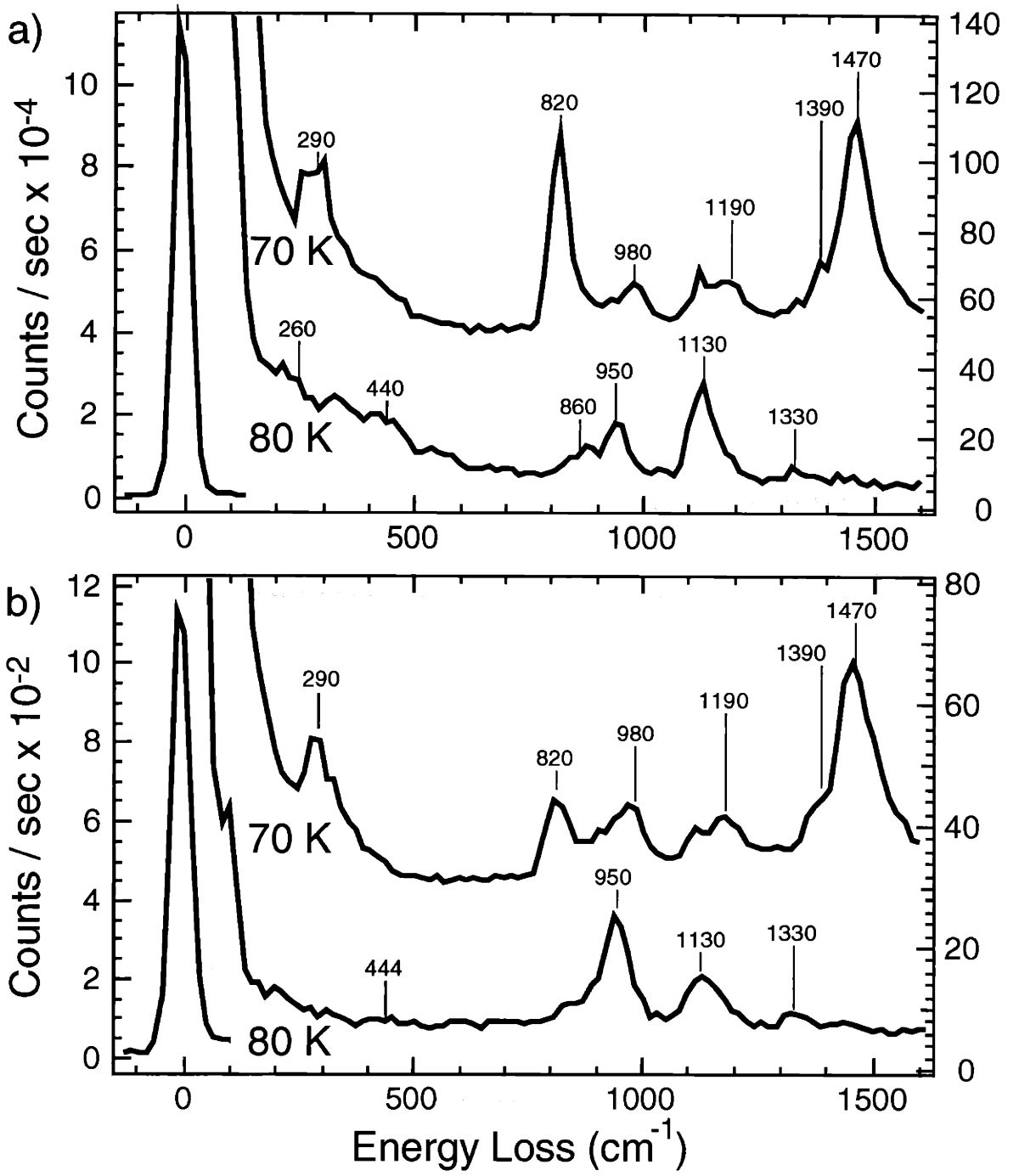

Figure 1.23. Electron energy loss spectra after a five minute exposure of 0.21 ML ethane to H atoms. H_2 pressure is $2x10^{-5}$ torr. Spectra are measured at 70 K and then crystal is warmed to 80 K and spectra are measured again. **a)** on-specular. **b)** 10° off-specular.

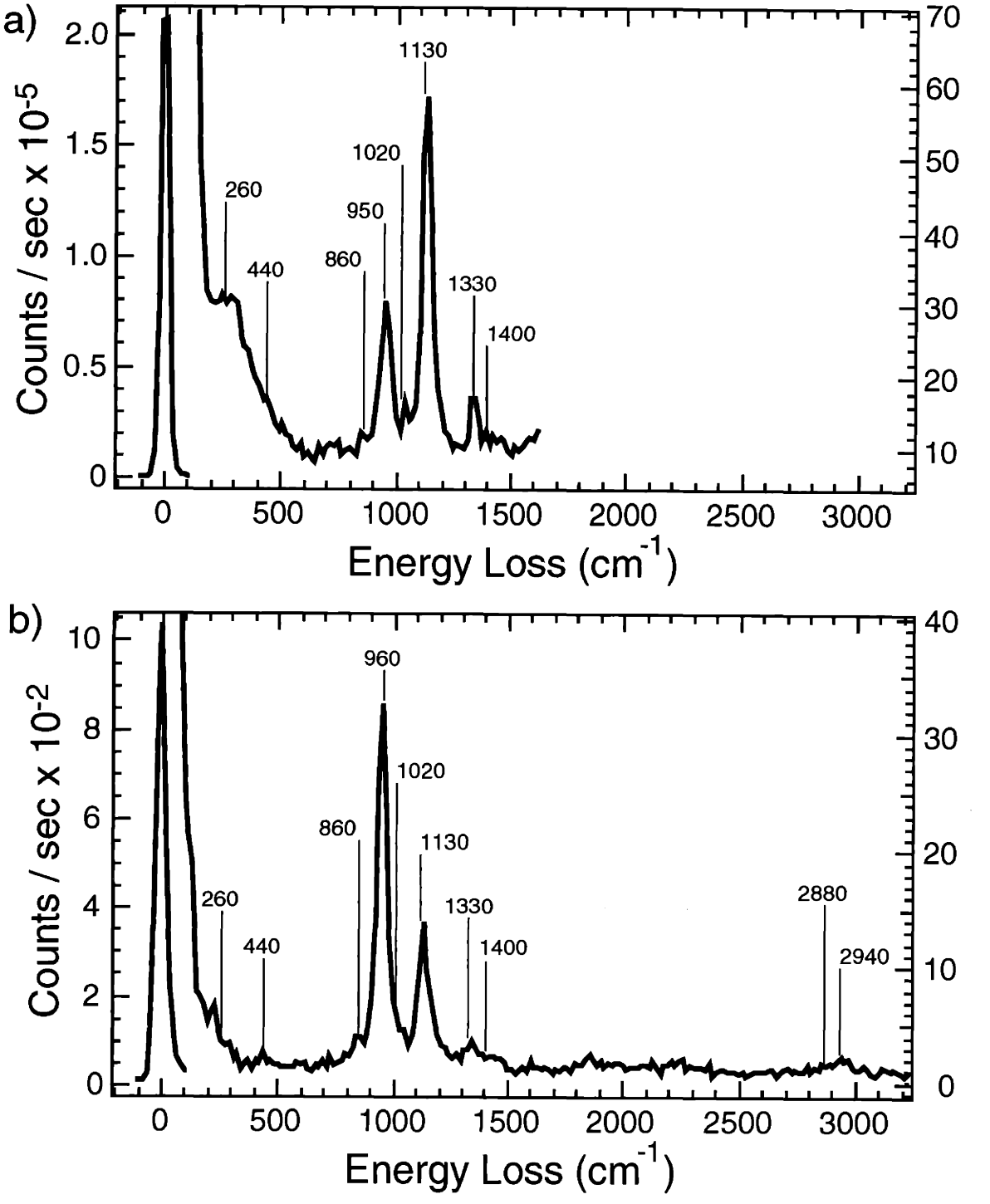

Figure 1.24. Electron energy loss spectra after a ten minute exposure of 0.21 ML ethane to H atoms. H_2 pressure is $2x10^{-5}$ torr. The crystal is heated to 300 K after H atom exposure. **a)** on-specular. **b)** 10° off-specular.

III.A.4. Adsorbed Reaction Product of Ethylene, Acetylene and Ethane

The electron energy loss spectra of the reaction products of ethylene, acetylene, or ethane with gas phase hydrogen atoms are almost identical. Gas phase hydrogen atom exposure to all three hydrocarbons produce the same adsorbed hydrocarbon species, ethylidyne. In addition to ethylidyne, a small amount acetylene is observed to be produced. Its production will be discussed in Section III.D of this chapter.

Because both the unsaturated and saturated C_2 hydrocarbons have been shown to react with gas phase hydrogen atoms to form ethylidyne, it is clear that both hydrogen addition to the adsorbed hydrocarbon and hydrogen abstraction from the adsorbed hydrocarbon are taking place. For example, a hydrogen atom must be added to the acetylene to produce ethylidyne. During the exposure of acetylene to H atoms, gas phase H atoms, surface bound H and bulk H are present. However, it is known that surface hydrogen does not react with adsorbed acetylene on Ni(111). While bulk H does hydrogenate acetylene at 180 K as shown in Figure 1.11, the temperature of the surface during the H atom exposure, 120 K, the temperature is too low for the bulk H to have sufficient mobility to emerge from the bulk to hydrogenate acetylene. Therefore, the addition of a H atoms to acetylene must be from the impinging gas phase H atoms.

Abstraction of H atoms from an adsorbed hydrocarbon has been demonstrated by the reaction of gas phase H atoms with ethane to form ethylidyne. Ethane must lose three H atoms to form ethylidyne. Adsorbed ethane does not thermally decompose on a Ni(111) surface as is evident by the lack of a H_2 desorption feature corresponding to desorption of surface bound hydrogen in the thermal desorption experiment shown in Figure 1.19. Some other mechanism must cause ethane to lose hydrogen atoms. That mechanism is H atom abstraction. Because the abstraction of a H atom from an adsorbed hydrocarbon by surface bound H and bulk H is not thermodynamically feasible as will be discussed in Section III.F of this chapter, H atoms impinging from the gas phase must abstract H atoms from adsorbed ethane.

Gas phase hydrogen atoms have also been observed to add to adsorbed ethylene to form ethane as demonstrated in Figure 1.1. Surface bound H and bulk H are also present during this H atom exposure, but surface H is known not to hydrogenate ethylene.[37] Bulk hydrogen can also be excluded because the temperature of the surface H atom exposure, 120 K, is too low for bulk hydrogen to emerge from the bulk. Therefore, only gas phase H atoms add to adsorbed ethylene during the exposure to H atoms.

These examples have provided evidenced that gas phase hydrogen atoms have the ability to both add to adsorbed hydrocarbons and to abstract H atoms from adsorbed hydrocarbons. Therefore, in determining the mechanism for ethylidyne formation in Section III.E of this chapter, both hydrogen addition and abstraction by gas phase hydrogen atoms will be considered. Although all three hydrocarbons react with H atoms to produce the same adsorbed reaction product, the rates of the reactions are all not equal. Section III.A.3.c of this chapter discussed the fact that the rate of the ethylidyne formation from ethane is observed to be at least 40 times slower than its formation from ethylene and acetylene. The mechanism of ethylidyne formation must also be able to account this difference in reaction rates.

III.A.5. Bulk Hydrogen and Adsorbed Acetylene: Ethylidyne Formation

The previous section demonstrated that ethylidyne is produced from the reaction of gas phase hydrogen atoms with all three C_2 hydrocarbons, ethylene, acetylene, and ethane. In this section, an ethylidyne formation reaction is described which does not require gas phase hydrogen atoms as a reactant. Specifically, ethylidyne has been observed as a product of the reaction of bulk hydrogen with adsorbed acetylene.

The dominant process in the reaction of bulk hydrogen with acetylene is hydrogenation of the acetylene to ethylene and ethane. These hydrogenation reactions are shown by the thermal desorption measurements in Figure 1.11. Production of both ethylene and ethane as indicated by the signals at mass 27 and mass 30 occurs at 180 K, the temperature at which bulk

hydrogen emerges from the surface. Bulk hydrogen hydrogenates the acetylene as it emerges from the bulk to the surface to form ethylene and ethane which desorb immediately

However, not all of the reaction products desorb. Figure 1.25 shows electron energy loss spectra measured after reaction of bulk hydrogen with adsorbed acetylene. The bulk hydrogen is prepared by a five minute exposure of a clean crystal to gas phase hydrogen atoms at a H_2 pressure of $2x10^{-5}$ torr. The surface hydrogen is then removed by a 30 minute exposure to a beam of 0.25% Xe/He expanded from a 1000 K nozzle and incident on the surface at 40° from the normal. This process is known to remove the surface hydrogen by recombinative desorption but it does not remove the bulk hydrogen.[52] A 0.14 ML of acetylene is adsorbed on the crystal which is then heated to 190 K. This temperature is just above that necessary for the hydrogen to emerge from the bulk and react with the adsorbed acetylene. The crystal is immediately cooled to 80 K and the electron energy loss spectra are measured. The vibrational features in the spectra are consistent with those of adsorbed ethylidyne as listed in Table 2.3 of Chapter II: symmetric and antisymmetric C-Ni stretching modes at 260 cm^{-1} and 440 cm^{-1}, CH_3 rocking mode at 1020 cm^{-1}, a C-C stretching mode at 1130 cm^{-1}, symmetric and antisymmetric CH_3 deformation modes at 1330 cm^{-1} and 1400 cm^{-1} and C-H stretches around 2900 cm^{-1}. Furthermore, the symmetric C-Ni stretch, C-C stretch and the symmetric CH_3 deformation modes are observed to be dipole active as is expected for ethylidyne. The 950 cm^{-1} feature is assigned to the antisymmetric stretching mode of surface bound hydrogen which results from the migration of hydrogen from the bulk to the surface. The unlabeled feature at 500 cm^{-1} is assigned to the librational mode of a small amount of adsorbed water. This contaminant was introduced to the surface during its exposure to the Xe beam. There were cooling water leaks in the molecular beam source chambers at the time of this experiment.

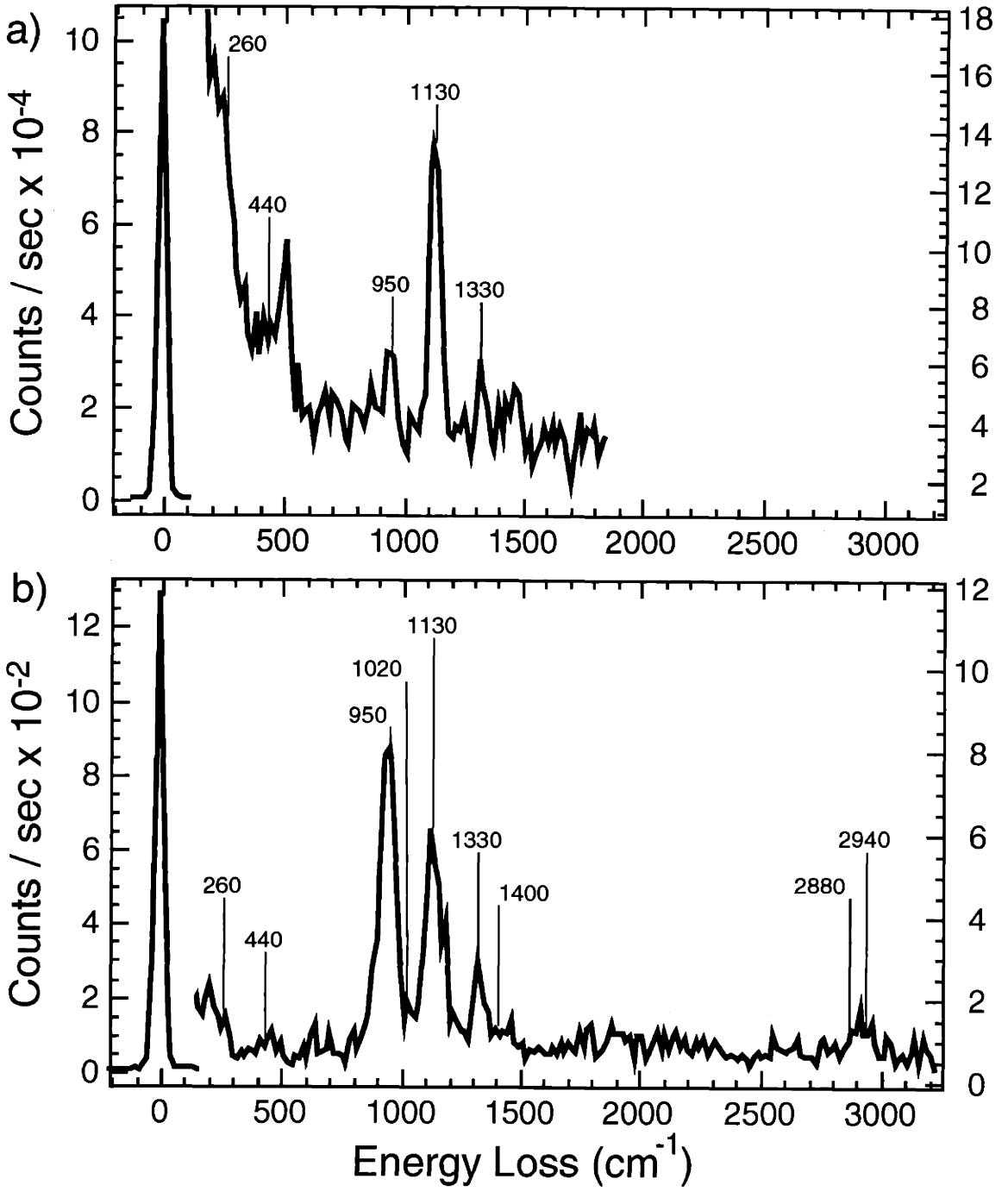

Figure 1.25. Electron energy loss spectra measured after the reaction of bulk hydrogen with adsorbed acetylene. **a)** Spectrum measured on-specular at a resolution of 39 cm^{-1}. **b)** Spectrum measured 10° off-specular at a resolution of 40 cm^{-1}.

The intensities of the ethylidyne features in Figure 1.25 are quite low. Although the carbon coverage was not measured by Auger electron spectroscopy, the low intensities of the ethylidyne features suggest that the coverage of ethylidyne is low and that the amount of ethylidyne produced by this reaction is small. It appears that the major products of the reaction of bulk H and acetylene are the hydrogenation products, ethylene and ethane, observed in Figure 1.11.

III.B. Ethylidyne Decomposition

This section discusses the thermal decomposition of ethylidyne. Ethylidyne will be shown to decompose to acetylene. Its thermal decomposition has been explored by measuring the electron energy loss spectra of both isotopically unlabeled ethylidyne and deuterated ethylidyne as a function of the crystal temperature.

Figures 1.26 and 1.27 shows electron energy loss spectra of 0.13 ML of ethylidyne heated to successively higher temperatures and then cooled to 80 K for the measurement of the spectra. The ethylidyne is prepared by a two minute exposure of 0.25 ML adsorbed ethylene to H atoms. The temperature to which the crystal is heated is indicated in the figure.

Upon heating the ethylidyne covered surface to 340 K, the feature at 950 cm^{-1} loses intensity and a new feature starts to grow in intensity at 760 cm^{-1}. The 950 cm^{-1} feature is assigned to the antisymmetric stretching mode of surface bound hydrogen as discussed in Chapter II. Hydrogen bound to the surface is known to recombinatively desorb in the temperature range of 300-400 K[52,64] as is observed in the thermal desorption measurement of ethylidyne coadsorbed with surface bound hydrogen in Figure 1.8. Previous studies have shown the frequency of the antisymmetric mode of surface bound hydrogen to be coverage dependent: at saturation coverage (1.0 ML), the frequency is 950 cm^{-1}, for hydrogen coverages up to 0.5 ML the frequency is approximately 770 cm^{-1}, and at hydrogen coverages between 0.5 ML and 1.0 ML both vibrational features, 770 cm^{-1} and 950 cm^{-1}, are observed

with neither feature being as intense as they are at the 0.5 ML or 1.0 ML coverages.[59] This trend is what is observed in the spectra of the ethylidyne and surface bound hydrogen that has been heated to 340 K; both the 770 cm^{-1} and the 950 cm^{-1} features are present with the 950 cm^{-1} feature having lost some intensity relative to the spectrum of the ethylidyne and surface bound hydrogen that has been heated to 300 K. Heating the surface to even higher temperatures, 350 - 370 K, causes the 950 cm^{-1} feature to lose more intensity while that of the 770 cm^{-1} feature gains. After ramping to 410 K, the surface bound hydrogen has completely desorbed, and therefore the 770 cm^{-1} feature is absent.

Heating the ethylidyne and hydrogen covered surface to above 340 K also causes the ethylidyne features to lose intensity: the antisymmetric C-Ni stretch at 440 cm^{-1}, the C-C stretch at 1130 cm^{-1}, the symmetric CH_3 deformation at 1330 cm^{-1}, and the antisymmetric CH_3 deformation modes at 1400 cm^{-1}. By 370 K, no features assigned to ethylidyne remain. Therefore, the ethylidyne adsorbate decomposes in the 340 to 360 K temperature range.

As the ethylidyne features decrease in intensity, other features at 480 cm^{-1}, 700 cm^{-1}, 860 cm^{-1}, 1090 cm^{-1}, 1200 cm^{-1} and 1380 cm^{-1} grow in intensity as the surface is heated. The most intense feature occurs at 860 cm^{-1}. The intensity of these features is a maximum when the ethylidyne features are no longer present, at 370 K. These feature are due to the ethylidyne decomposition product. After heating the crystal to 410 K, no electron energy loss features remain. The product of ethylidyne decomposition itself decomposes.

To help identify the ethylidyne decomposition product, electron energy loss spectra of deuterated ethylidyne are also measured as a function of surface temperature. Figure 1.28 shows the electron energy loss spectra of 0.13 ML deuterated ethylidyne heated to successively higher surface temperatures and immediately cooled to 80 K for the measurement of the spectra. Deuterated ethylidyne is prepared by a two minute exposure of 0.25 ML deuterated ethylene to D atoms. The temperature to which the crystal is heated is indicated in the figure.

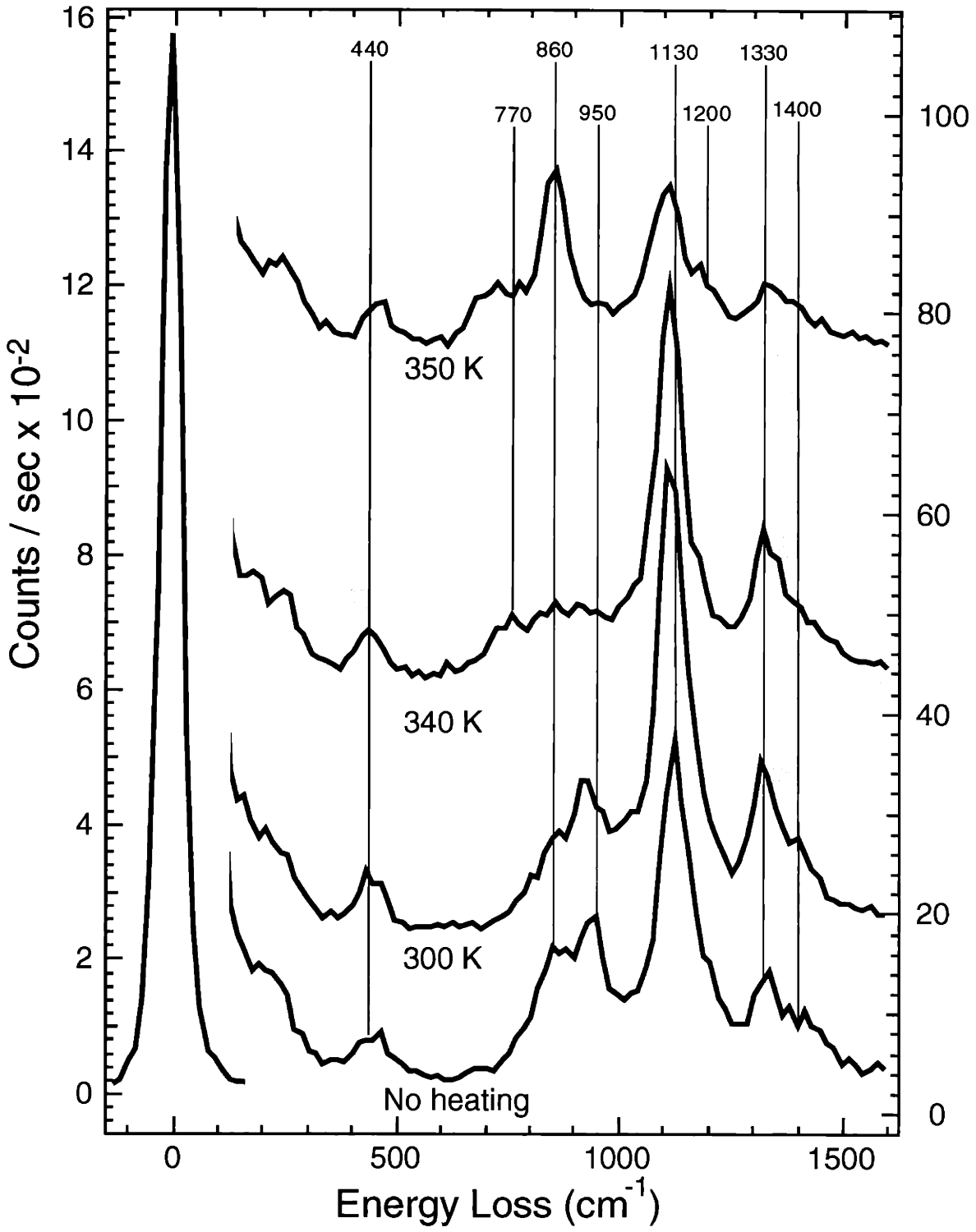

Figure 1.26. Electron energy loss spectra of 0.13 ML ethylidyne heated to the indicated temperatures and immediately cooled to 80 K. The spectra are measured 10° off-specular.

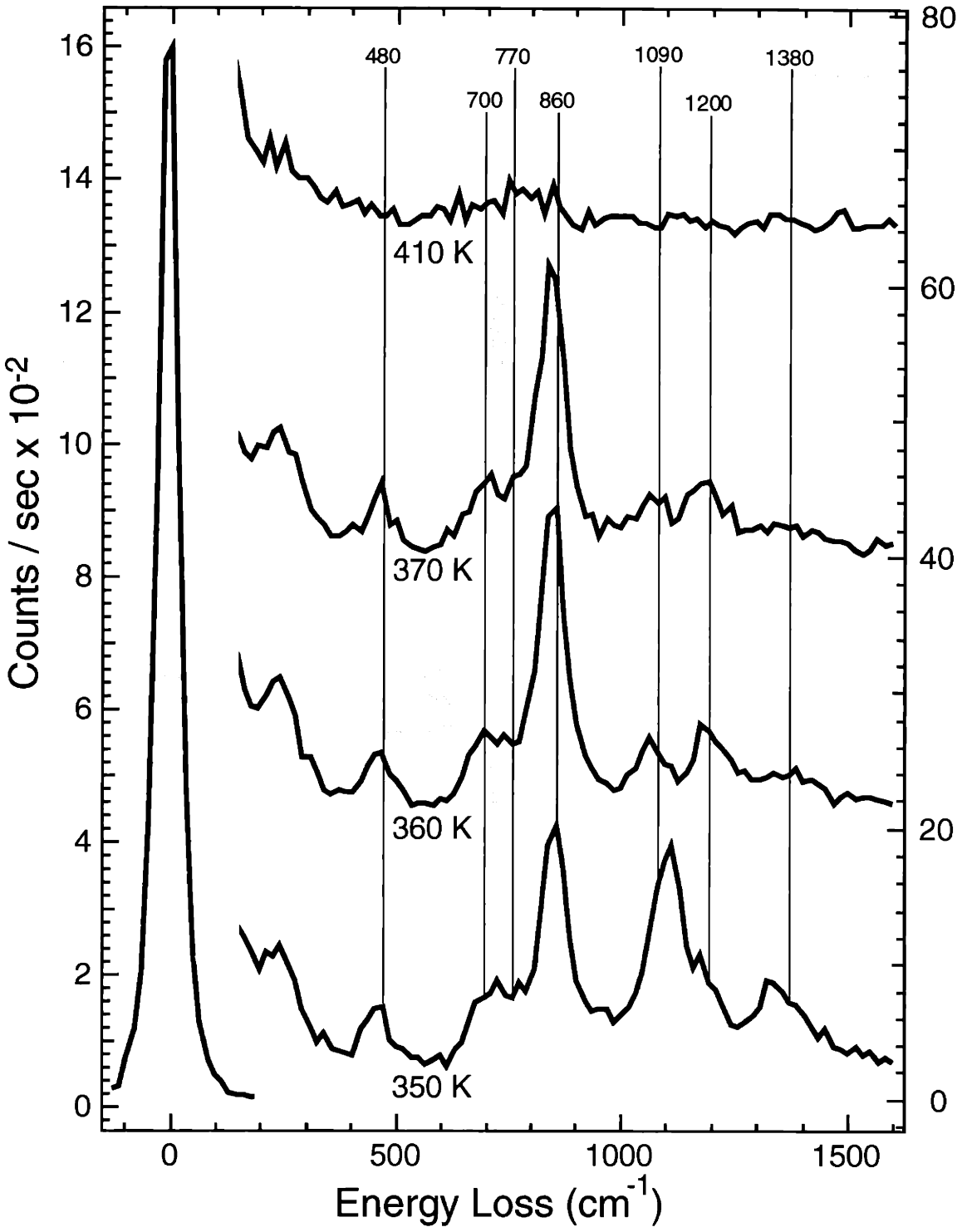

Figure 1.27. Electron energy loss spectra of 0.13 ML ethylidyne heated to the indicated temperatures and immediately cooled to 80 K. The spectra are measured 10° off-specular.

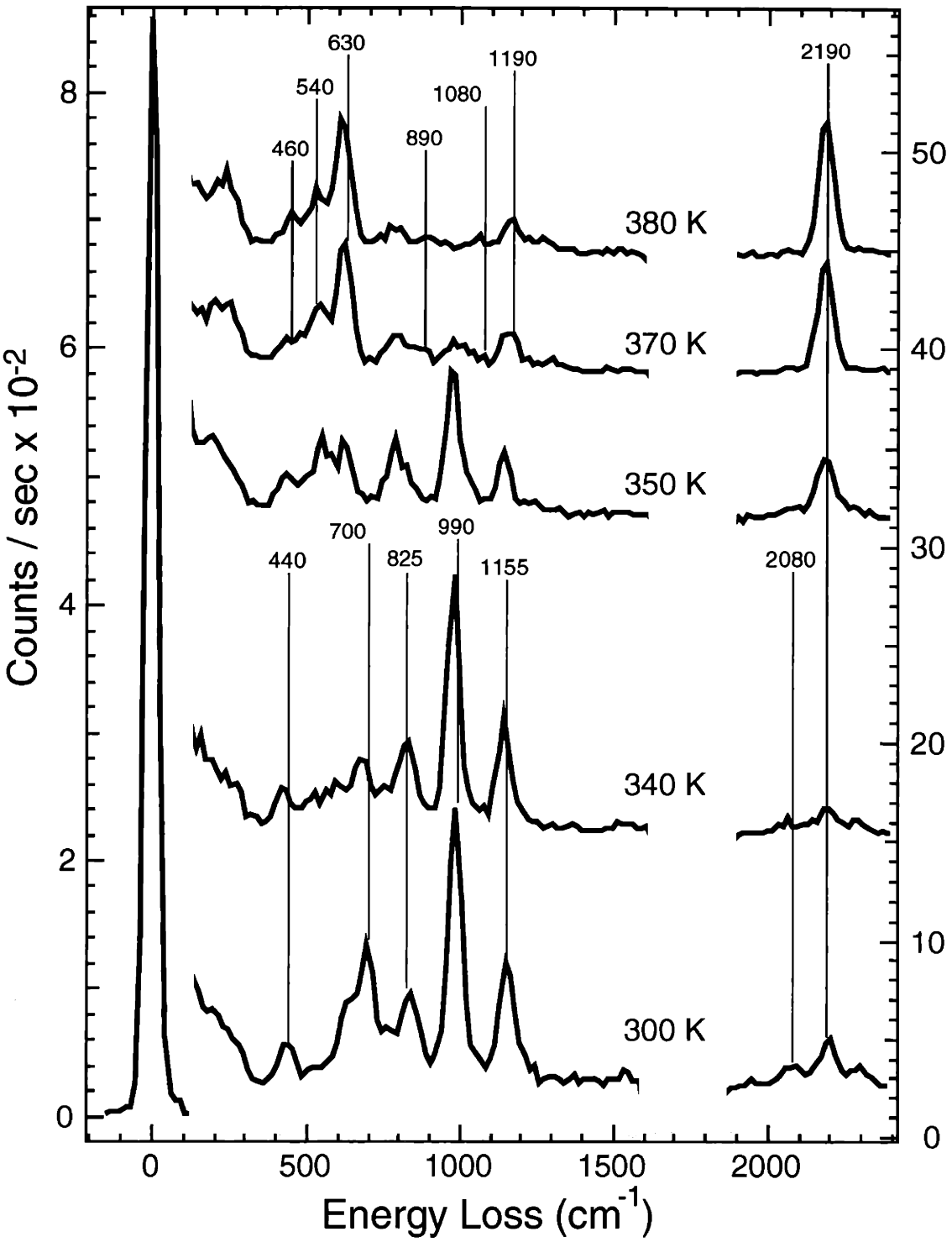

Figure 1.28. Electron energy loss spectra of 0.13 ML deuterated ethylidyne measured after heating to the indicated temperatures and immediately cooled to 80 K. The spectra are measured 10° off-specular.

As is observed for isotopically unlabeled surface hydrogen, the surface bound deuterium mode at 700 cm^{-1} decreases in intensity upon heating the crystal to higher temperatures while the surface deuterium feature at approximately 560 cm^{-1} grows in intensity. The 700 cm^{-1} and 560 cm^{-1} features have been assigned previously to the antisymmetric Ni-D stretching mode for 1.0 ML and 0.5 ML coverages, respectively. The decrease in the intensity of the 700 cm^{-1} feature and the increase in intensity of the 560 cm^{-1} feature are expected because the deuterium coverage is decreasing due to recombinative desorption in the 300 to 400 K temperature range.

The deuterated ethylidyne features, the antisymmetric C-Ni stretching mode at 440 cm^{-1}, the CD_3 rocking mode at 825 cm^{-1}, the symmetric CD_3 deformation mode at 990 cm^{-1}, the C-C stretching mode at 1155 cm^{-1} and the symmetric CD_3 stretching mode at 2080 cm^{-1}, lose intensity upon heating to higher temperatures. The feature at 2190 cm^{-1} (assigned to the antisymmetric CD3 stretching mode) initially loses intensity in going from 300 to 340 K, but then its intensity grows at higher temperatures. The frequency of this mode of ethylidyne is at the same frequency as the C-D stretch of the decomposition product and therefore, the intensity of the feature increases at higher temperatures. The decrease in the intensities of the deuterated ethylidyne vibrational features indicates its decomposition. As the deuterated ethylidyne features lose intensity, the decomposition product features at 460 cm^{-1}, 540 cm^{-1}, 630 cm^{-1}, 890 cm^{-1}, 1190 cm^{-1} and 2190 cm^{-1} grow in intensity. The small feature at 800 cm^{-1} is assigned to the symmetric Ni-D stretching mode. This frequency is indicative of lower coverages of surface bound deuterium.[59] After heating the crystal to 380 K, only features assigned to surface bound deuterium and the ethylidyne decomposition product are present; no ethylidyne features remain.

The frequencies observed for the ethylidyne decomposition product for both the unlabeled and the deuterated species match those observed for acetylene adsorbed on Ni(111).

Table 1.3 compares the frequencies of adsorbed acetylene[40] to those observed for the ethylidyne decomposition product.

The electron energy loss spectra of adsorbed acetylene has also been measured in this laboratory. These spectra are shown in Figure 2.14 of Chapter II. Comparison of these spectra to those of the ethylidyne decomposition product reveals a discrepancy. The spectrum of acetylene adsorbed on Ni(111) measured in the specular direction has a more intense 1200 cm^{-1} feature than is observed for the ethylidyne decomposition product. The difference in the intensity of the 1200 cm^{-1} feature is a result of the presence of surface bound hydrogen coadsorbed with the acetylene. It is produced by the adsorption of hydrogen atoms during the ethylidyne formation reaction and from the ethylidyne decomposition reaction. To demonstrate this effect, electron energy loss spectra of acetylene coadsorbed with surface hydrogen are measured and are shown in Figure 1.29. The surface is prepared by thermal decomposition of

	Adsorbed Acetylene		Ethylidyne Decomposition	
Mode	C_2H_2	C_2D_2	C_2H_2	C_2D_2
C-H str	2920	2190	2920	2190
asym C-H wag	1370	1090	1380	1080
C-C str	1220	1190	1200	1190
sym C-H wag	1080	890	1090	890
asym C-H rock	860	640	860	630
sym C-H rock	690	540	700	540
asym Ni-C str	560	-	-	-
sym Ni-C str	480	460	480	460

Table 1.3. Vibrational frequencies and assignments of adsorbed acetylene from reference 40 and observed vibrational frequencies of the ethylidyne decomposition product.

0.13 ML ethylene at 250 K. Ethylene is known to decompose on a Ni(111) surface to adsorbed acetylene and surface hydrogen at approximately 200 K.[36,37] In order to better emulate the composition of the surface upon ethylidyne decomposition, additional hydrogen is adsorbed by exposing the surface to $3x10^{-5}$ torr of H_2 while the crystal cools from 250 K to 80 K. The surface is lastly heated to 370 K, the same temperature to which ethylidyne covered surface is heated, and immediately cooled to 80 K, the temperature at which the electron energy loss spectra are measured.

As is seen in Figure 1.29, the vibrational spectra of the ethylidyne thermal decomposition product match very well with those of acetylene coadsorbed with hydrogen. In particular, the intensities of the C-C stretching mode at 1200 cm^{-1} measured in the specular direction are consistent. The features in the off-specular spectra are almost a perfect match both in frequency and intensity. Apparently, the coadsorption of surface hydrogen with the acetylene dramatically affects the on-specular intensity of the C-C stretching mode of acetylene. The reasons for this were not explored.

Additional confirmation of the identity of the ethylidyne decomposition product as acetylene is provided by the vibrational spectra of the deuterated ethylidyne decomposition product. Table 1.3 shows that the observed vibrational frequencies of the deuterated product match those previously assigned to deuterated acetylene adsorbed on Ni(111).[40] Also, the relative intensities of the features of the deuterated product are the same as those of the unlabeled product; the antisymmetric C-H rocking and C-H stretching modes are the stronger features while the other modes are weak in comparison.

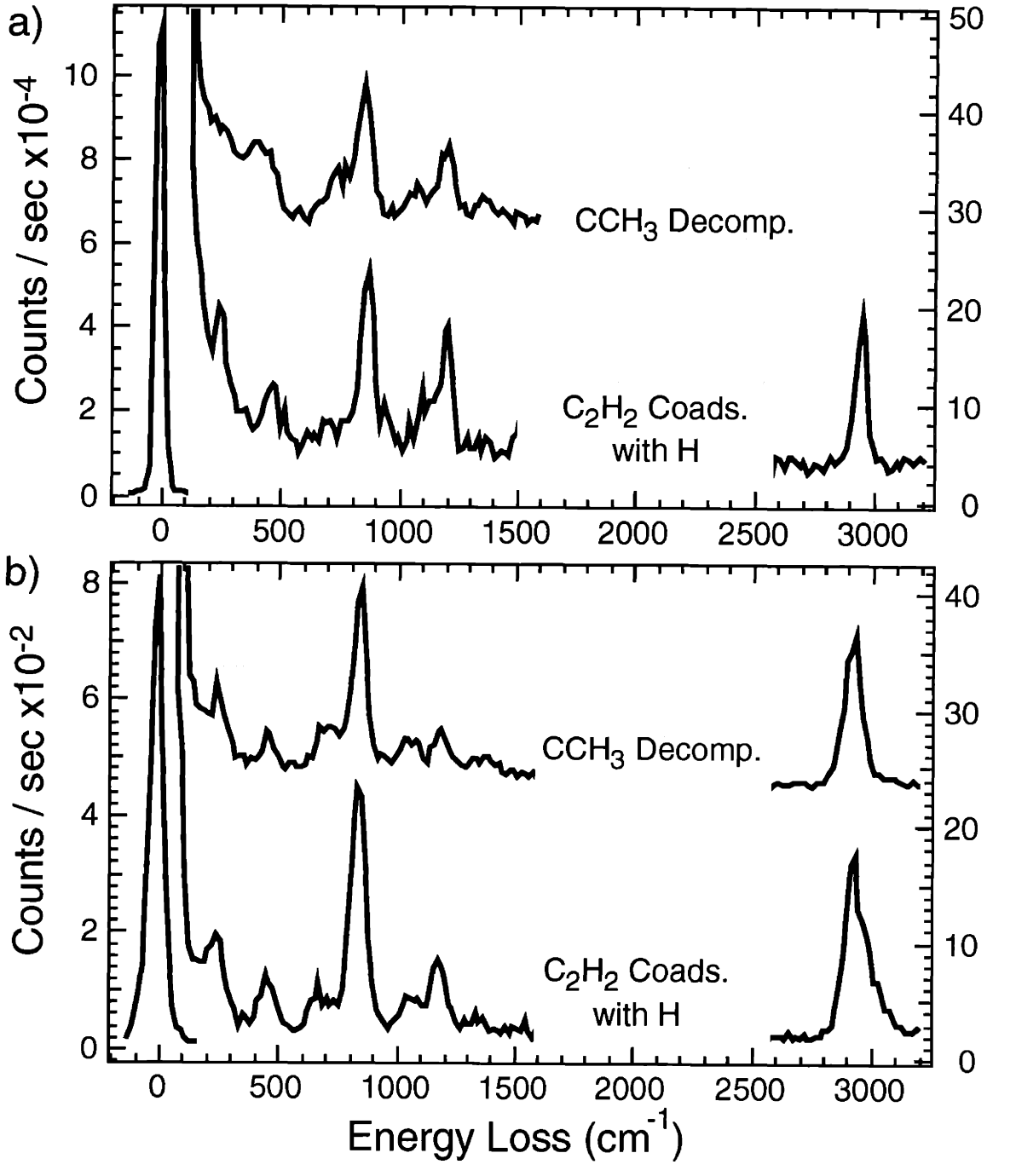

Figure 1.29. Electron energy loss spectra of ethylidyne after heating the crystal to 370 K and acetylene coadsorbed with hydrogen after heating the crystal to 370 K. All spectra are measured at 80 K. **a)** on-specular. **b)** 10° off-specular.

Ethylidyne coadsorbed with surface hydrogen decomposes on the Ni(111) surface in the 330 to 360 K temperature range which is the same temperature at which hydrogen desorbs. The simultaneous occurrence of these two processes suggests that the surface bound hydrogen stabilizes the ethylidyne species. That is, ethylidyne without coadsorbed hydrogen might decompose at lower temperatures. Stabilization of the ethylidyne by surface hydrogen is reasonable because the surface bound hydrogen might be blocking sites necessary for the C-H bond cleavage to occur. Coadsorbed hydrogen has been previously observed to stabilize an adsorbed hydrocarbon on Ni(111) relative to its thermal decomposition.[37] In particular, up to 0.16 ML of ethylene decomposes to acetylene, but when ethylene is coadsorbed with hydrogen, less ethylene decomposes, and desorption of ethylene successfully competes with decomposition.[37] Of course, the fact that ethylidyne decomposition takes place at the same temperature as hydrogen recombinative desorption could be a coincidence. In this case, ethylidyne in the absence of coadsorbed hydrogen would decompose at the same temperatures as it does in the presence of adsorbed hydrogen. Unfortunately, the stabilization effect of hydrogen cannot be tested because the only ethylidyne formation reactions available also produce coadsorbed hydrogen.

The decomposition of ethylidyne adsorbed on Pt(111) has been studied previously by electron energy loss spectroscopy and thermal desorption spectroscopy.[2] Ethylidyne bound to Pt(111) is found to be stable to approximately 500 K. The decomposition product was suggested to be methylidyne (-CH). Acetylene is not observed to be the decomposition product of ethylidyne adsorbed on Pt(111). It is probably not observed because acetylene is not stable on Pt(111) at the decomposition temperature of ethylidyne, 500 K.[2] Therefore, even if ethylidyne does decompose to acetylene, acetylene itself decomposes. Perhaps acetylene is an intermediate in the decomposition of ethylidyne on Pt(111). That is, ethylidyne first decomposes to acetylene which then further decomposes to methylidyne (-CH). An electron energy loss spectroscopy study has reported that acetylene does indeed thermally decompose to

methylidyne.[65] Further support for an acetylene intermediate in the thermal decomposition of ethylidyne on Pt(111) is given by a laser induced desorption experiment of ethylidyne on Pt(111) in which the dominant desorbing species is observed to be acetylene.[66] Decomposition of ethylidyne to acetylene is a result of the rapid heating of the surface by the laser pulse. Because the temperature rise is so fast due to heating by the short laser pulse, an acetylene species desorbs from the surface before it has time to decompose. These results suggest that the decomposition process of ethylidyne on Pt(111) is consistent with that observed here on Ni(111).

III.C. Hydrogen - Deuterium Exchange of Ethylidyne

The possibility of hydrogen - deuterium exchange between the hydrogen atoms on ethylidyne and gas phase H atoms has been explored. Figure 1.30 shows electron energy loss spectra of isotopically unlabeled ethylidyne after exposure to gas phase deuterium atoms. The ethylidyne species is prepared by a two minute exposure of 0.25 ML of ethylene to H atoms. Once prepared, the surface is heated to 300 K and immediately cooled to 80 K. The ethylidyne covered surface is then exposed to gas phase deuterium atoms at a molecular deuterium pressure of $5x10^{-6}$ torr. The times of exposure to deuterium atoms, 0 seconds, 30 seconds, 60 seconds and 240 seconds, are indicated in the figure.

The deuterium atoms are observed to exchange with the hydrogen atoms of the ethylidyne. This exchange is most obvious in the C-H stretch region (2800-3100 cm^{-1}) and C-D stretch region (2000 - 2200 cm^{-1}). As the intensity of the C-D stretching features increase with longer D atom exposure times, the C-H stretching features lose intensity. The small feature at 2200 cm^{-1} in the spectrum of normal ethylidyne is not a C-D stretching mode, but rather an overtone of the C-C stretching mode as will be discussed in Chapter II. The C-D bending features (990 cm^{-1}) also grow in intensity while the C-H bending features (1330 cm^{-1})

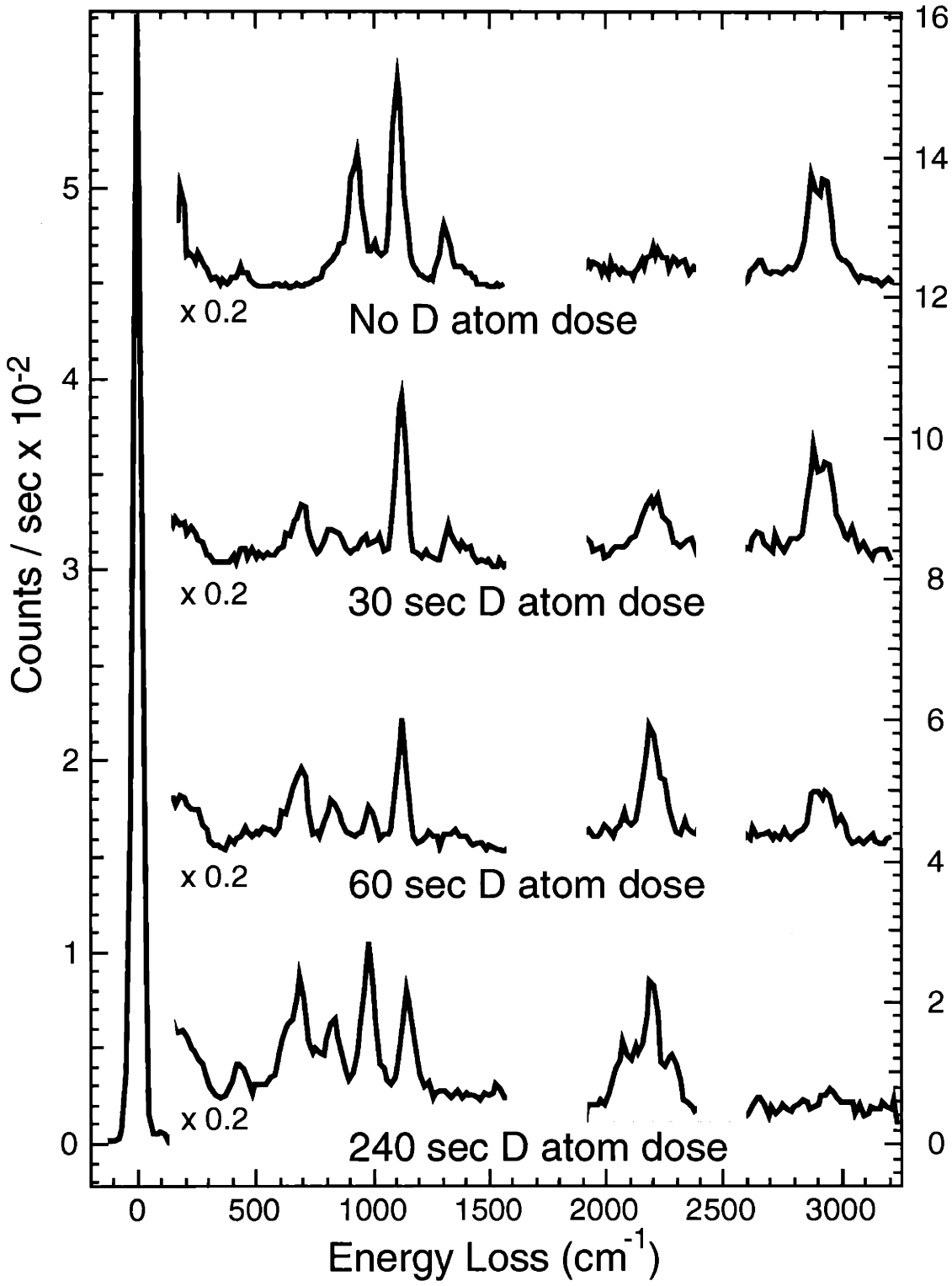

Figure 1.30. Electron energy loss spectra measured after exposure of isotopically unlabeled ethylidyne to D atoms. Spectra are measured 10° off-specular.

decrease in intensity with longer D atom exposures. The antisymmetric stretching feature of the surface bound deuterium at 700 cm^{-1} also increases in intensity as that of the surface bound hydrogen at 950 cm^{-1} decreases, indicating exchange of the surface bound hydrogen. After a 240 second deuterium atom exposure, all the hydrogen atoms on ethylidyne have been exchanged as is evident by the lack of C-H stretching and C-H bending modes. The spectrum obtained after the 240 second exposure is identical to that obtained from 120 second exposure of deuterated ethylene to D atoms as shown in Figure 2.3 of Chapter II.

This section has shown that exposure of deuterium atoms to adsorbed ethylidyne results in complete exchange of the hydrogen atoms on ethylidyne with deuterium atoms, and that the ethylidyne species remains intact. The next section proposes a mechanism for the exchange reaction.

III.D. Assignment of the 860 cm^{-1} Feature: Acetylene

Sections III.A.1, III.A.2 and III.A.3 showed that gas phase hydrogen atoms react with all C_2 hydrocarbons adsorbed on Ni(111) to produce adsorbed ethylidyne, adsorbed hydrogen and a product whose most intense vibrational feature occurs at 860 cm^{-1}. This section will show that this 860 cm^{-1} feature is a vibrational mode of adsorbed acetylene. Since acetylene has been shown earlier in this chapter to react itself with gas phase hydrogen atoms to produce ethylidyne, a plausible explanation for the coexistence of the acetylene and ethylidyne in the presence of gas phase hydrogen atoms naturally arises.

Figure 1.31 reproduces three spectra each previously shown in a different section of this chapter. The spectra are shown together here for ease of comparison. Shown in the figure are the electron energy loss spectra measured after exposure of 0.25 ML ethylene, 0.23 ML acetylene and 0.21 ML ethane to H atoms. The hydrogen atom exposures are two minutes at a H_2 pressure of $5x10^{-6}$ torr for the ethylene and acetylene reactions and five minutes at a H_2 pressure of $2x10^{-5}$ torr for the ethane reaction. Recall that a longer exposure time and higher

H_2 pressure is used for the ethane reaction because of its slower reaction rate with H atoms. The temperature of the surface during the H atom exposures are 120 K, 120 K and 77 K for the ethylene, acetylene and ethane reactions, respectively. The lower surface temperature for the ethane is necessary because it desorbs from the surface at temperatures of 80 K and above. Except for the intensity of the vibrational mode of surface hydrogen at 950 cm^{-1}, the spectra of the reaction products of gas phase hydrogen atoms with the three hydrocarbons are very similar. The 860 cm^{-1} feature is present independent of the adsorbed C_2 hydrocarbon reactant and its intensity relative to the ethylidyne features is similar in the three spectra.

While the 860 cm^{-1} feature is not present in the spectra of the reaction product of deuterated ethylene and D atoms, a mode at 640 cm^{-1} which cannot be assigned to deuterated ethylidyne or surface bound deuterium at 640 cm^{-1} is present as observed in Figures 2.3 and 2.5 of Chapter II. The 640 cm^{-1} feature has the same characteristics as the 860 cm^{-1} feature. That is, it is slightly dipole active, it decreases in intensity after ramping the crystal to 300 K and it is present in the spectra measured after the reaction of D atoms with both ethylene and acetylene. These observations suggest that the 640 cm^{-1} feature is the isotopic equivalent of the 860 cm^{-1} feature. The ratio of the frequencies of these features is 1.34. As discussed in Chapter II, modes involving primarily hydrogen bending or stretching motions of hydrocarbons are expected to exhibit frequency shifts of a factor of 1.34 upon deuteration. Since a frequency of 860 cm^{-1} is too low for a C-H stretching mode, the 860 cm^{-1} (640 cm^{-1}) is assigned to a hydrocarbon C-H bending mode.

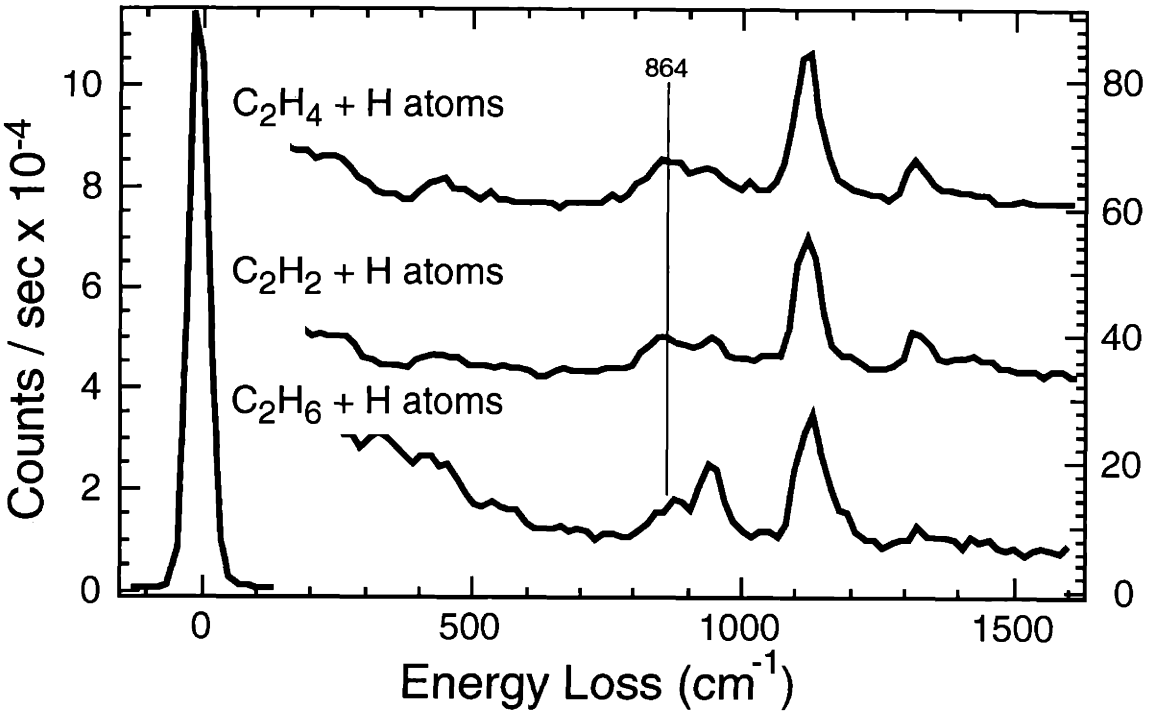

Figure 1.31. Electron energy loss spectra measured after exposure of ethylene, acetylene and ethane to gas phase H atoms. The spectra are measured on-specular.

An additional feature at 700 cm^{-1} is observed in the spectra when the 860 cm^{-1} feature is very intense. The spectrum in Figure 1.6, measured prior to heating the crystal to 300 K, shows one of the most intense 860 cm^{-1} features observed after exposure of ethylene to H atoms along with a very weak feature at 700 cm^{-1}. After heating the surface to 300 K, the 860 cm^{-1} feature loses intensity and the 700 cm^{-1} feature is absent. This observation suggests that the 700 cm^{-1} feature arises from the same adsorbate that gives rise to the 860 cm^{-1} feature. Other modes of the hydrocarbon species which gives rise to the 860 cm^{-1} feature should also be observed. However, these other modes are likely masked by the vibrational features of the adsorbed ethylidyne species. Because the ethylidyne species is probably the major species on the surface, its masking of the other modes of an additional hydrocarbon adsorbate is not

unreasonable, provided that the 860 cm^{-1} feature is the most intense vibrational feature of the adsorbate.

Acetylene has a very intense vibrational feature at 860 cm^{-1}, and when it is coadsorbed with hydrogen, the 860 cm^{-1} feature is the strongest feature observed as shown in Figure 1.29. The 860 cm^{-1} feature in the spectra of acetylene is also known to be dipole active and to shift to 640 cm^{-1} upon deuteration[40]. Adsorbed acetylene also has a weak vibrational feature at 700 cm^{-1}. The similarity of the vibrational spectra of acetylene to that of the reaction product and the properties of the 860 cm^{-1} vibrational mode of acetylene to the 860 cm^{-1} vibrational mode of the reaction product of C_2 hydrocarbons with H atoms strongly suggests that the 860 cm^{-1} feature is the antisymmetric C-H rocking mode of acetylene coadsorbed with ethylidyne.

Additional support for this conclusion comes from the comparison, shown in Figure 1.32, of the spectrum of the reaction product of ethylene exposed to H atoms from Figure 1.6 to the spectrum of acetylene coadsorbed with surface hydrogen from Figure 1.29. The scales for the intensities of the loss features for the acetylene spectra have been adjusted so that the intensities of its 860 cm^{-1} feature matches that of the 860 cm^{-1} feature in the spectra of the reaction product of ethylene exposed to H atoms. This comparison demonstrates that the vibrational features of ethylidyne can easily obscure the observation of acetylene features other than the 860 cm^{-1} feature because their intensities are very low. Perhaps one possible exception should be noted. The intensity of the 1200 cm^{-1} feature measured in the specular direction is much larger in the acetylene spectrum than the spectrum of the ethylene and H atom reaction product. The dependence of the intensity of the 1200 cm^{-1} feature upon coadsorption of hydrogen has been discussed in Section III.B of this chapter. The 1200 cm^{-1} feature of acetylene is much less intense when acetylene is coadsorbed with hydrogen than without coadsorbed hydrogen. It is suggested that the high concentration of ethylidyne coadsorbed with the acetylene could also attenuate the intensity of the 1200 cm^{-1} feature of acetylene just as presence of coadsorbed hydrogen attenuated it.

Confirmation of this proposal is found in the spectra measured after a 10 second exposure of acetylene to gas phase H atoms shown in Figure 1.14. Intense features assigned to ethylidyne are present in the spectra, but it is clear that not all the acetylene has reacted to form ethylidyne because the 860 cm^{-1} feature is still one of the most intense features. The presence of features at 460 cm^{-1}, 700 cm^{-1}, and 1200 cm^{-1} also confirms the presence of a significant amount of acetylene. Now, in looking at the intensities of the 860 cm^{-1} feature and the 1200 cm^{-1} feature measured in the specular direction in Figure 1.14, it is seen that the latter is very small relative to the former. It appears that the presence of ethylidyne dramatically affects the intensity of the 1200 cm^{-1} feature of acetylene, even more so than surface hydrogen. Therefore, the absence of a more intense 1200 cm^{-1} feature in the reaction product spectrum measured in the specular direction in Figure 1.32 does not change the conclusion that a small amount of acetylene is coadsorbed with ethylidyne.

Thermal desorption spectrometry also suggests that the 860 cm^{-1} feature arises from coadsorbed acetylene. As discussed earlier, the 860 cm^{-1} feature is most intense prior to heating the surface to 300 K. In monitoring the thermal desorption products during heating of the crystal, ethylene and ethane are observed to desorb from the surface at 180 K (Figure 1.8). These are the same desorption products observed in the reaction of bulk hydrogen and adsorbed acetylene in which bulk hydrogen hydrogenates acetylene as it emerges from the bulk to the surface at 180 K (Figure 1.11). Because hydrogenation of the adsorbed acetylene by bulk hydrogen is more efficient than hydrogenation of the adsorbed ethylidyne by bulk hydrogen as discussed in Section III.A.1.d of this chapter, more acetylene than ethylidyne is removed from the surface resulting in a decrease in the intensity of the 860 cm^{-1} feature relative to the ethylidyne features. Therefore, thermal desorption measurements support the assignment of the 860 cm^{-1} feature to a vibrational mode of acetylene coadsorbed with the ethylidyne species.

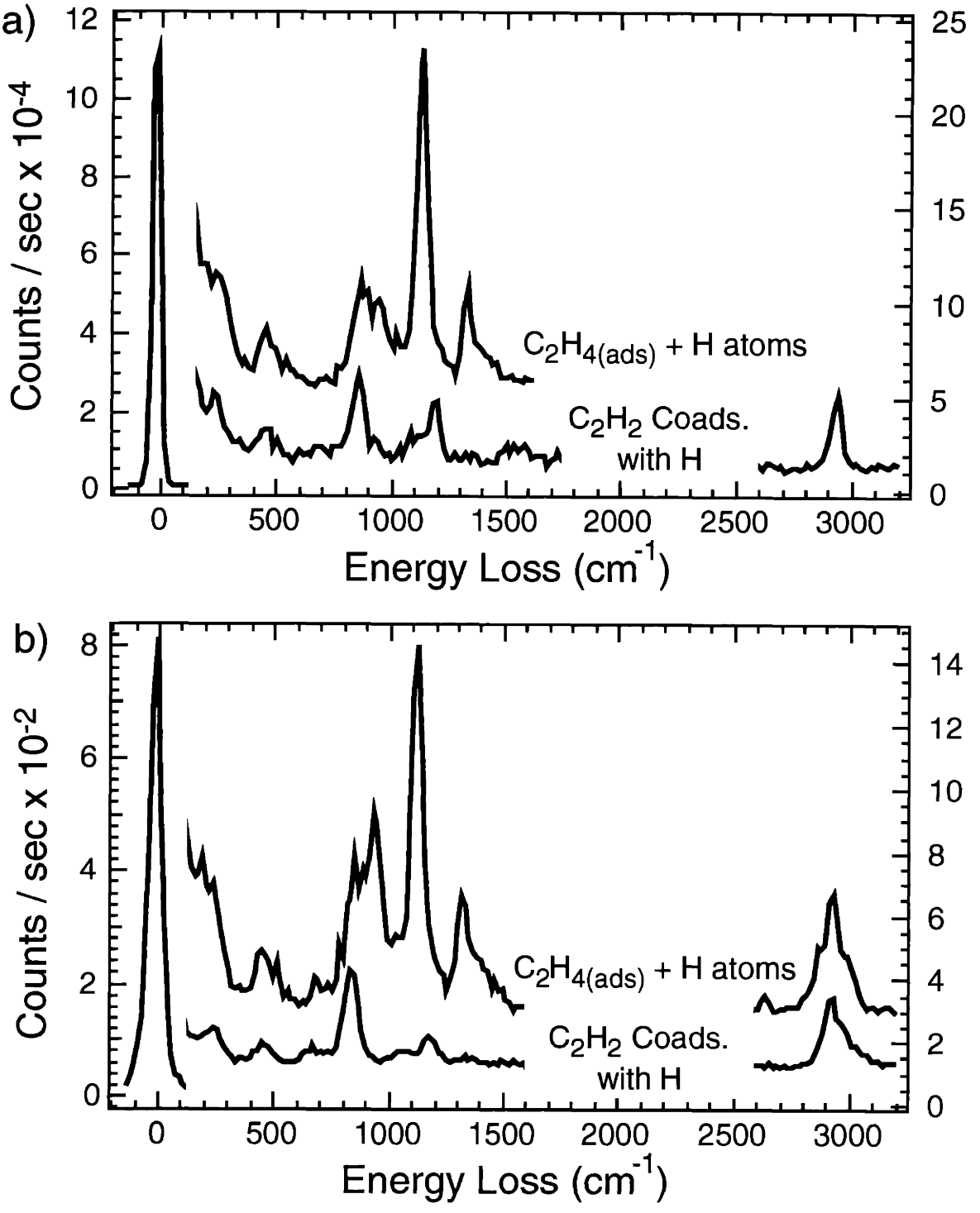

Figure 1.32. Electron energy loss spectra of the reaction product of ethylene exposed to H atoms (taken from Figure 1.6) and acetylene coadsorbed with hydrogen (taken from Figure 1.29). **a)** on-specular. **b)** 10° off-specular.

Earlier in this chapter, it was shown that gas phase hydrogen atoms react with adsorbed acetylene. This observation would suggest that acetylene cannot be coadsorbed with ethylidyne after exposure to H atoms because it would react with H atoms to form ethylidyne. However, it is possible for a dynamic equilibrium between acetylene and ethylidyne to exist in the presence of gas phase hydrogen atoms. While the reaction of adsorbed acetylene with H atoms to form adsorbed ethylidyne has been verified, an equilibrium requires the reverse reaction to also take place. That is, gas phase hydrogen atoms must also react with adsorbed ethylidyne to form adsorbed acetylene as shown in Figure 1.33. This competition between the two reactions will be referred to as the dynamic equilibrium in further discussion. Because the ethylidyne features in the vibrational spectra are much stronger than those of acetylene, the dynamic equilibrium appears to favor ethylidyne.

Several observations are consistent with this dynamic equilibrium between acetylene and ethylidyne in the presence of gas phase hydrogen atoms. First, acetylene, identified by the 860 cm^{-1} feature, is observed to be coadsorbed with the ethylidyne produced from the reaction of H atoms with all three C_2 hydrocarbons, ethylene, acetylene or ethane. Second, the thermal decomposition product of ethylidyne is acetylene. Third, gas phase hydrogen atoms are known

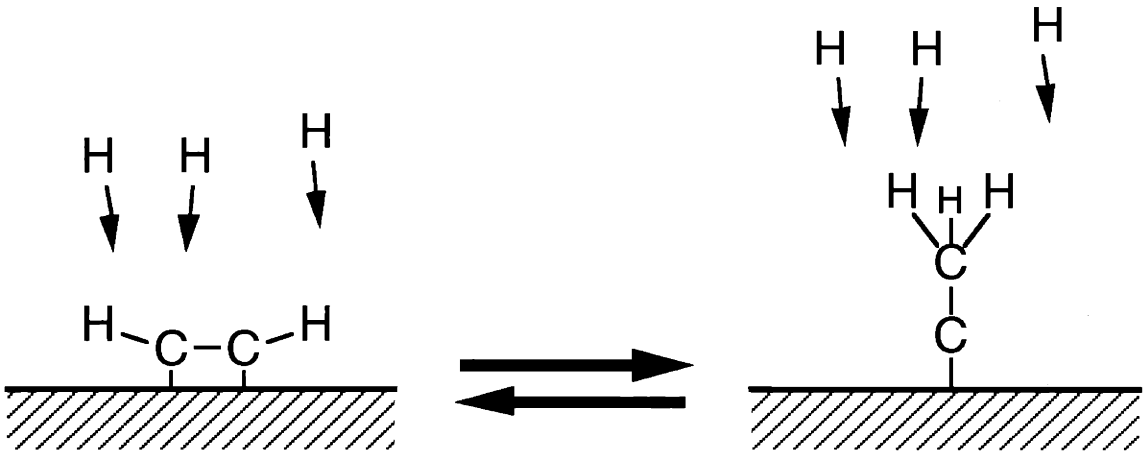

Figure 1.33. Pictorial representation of the dynamic equilibrium of acetylene and ethylidyne in the presence of gas phase hydrogen atoms.

to abstract hydrogen atoms from adsorbed hydrocarbons. Fourth, hydrogen/deuterium exchange occurs between gas phase H atoms and the H atoms on ethylidyne. Lastly, the electron energy loss spectra of ethylidyne formed from bulk hydrogen and acetylene does not show the presence of acetylene. Each of these points is now described in more detail.

Probably the strongest evidence for a dynamic equilibrium is the independence of the relative acetylene coverage on the reactant C_2 hydrocarbon, ethylene, acetylene or ethane. Had the acetylene been formed by a branching or side reaction of the adsorbed C_2 hydrocarbons with the H atoms, it would be expected that the acetylene coverage relative to that of ethylidyne would be dependent on the starting reactant. On the other hand, if a dynamic equilibrium exists between acetylene and ethylidyne in the presence of gas phase H atoms, the amount of acetylene is expected to be constant relative to ethylidyne because its amount is dictated by the rates of the forward and reverse reactions. The acetylene coverage relative to that of ethylidyne can be judged from the vibrational spectra by comparison of the intensity of the 860 cm^{-1} feature, assigned to acetylene, to the intensity of the ethylidyne features. The ratios of the intensity of the 860 cm^{-1} feature of acetylene to that of the 1130 cm^{-1} vibrational feature of ethylidyne formed by the reaction of H atoms with ethylene, acetylene and ethane are 3.5, 4.1, and 3.8, respectively. Although these ratios are not exactly equal, they are quite close and the noise in the vibrational spectra can explain their differences. Therefore, the independence of the relative coverage of acetylene to ethylidyne on the reactant hydrocarbon supports the notion of a dynamic equilibrium between acetylene and ethylidyne in the presence of H atoms.

The observation of the thermal decomposition of ethylidyne to acetylene also gives support to the dynamic equilibrium because it shows that the ethylidyne to acetylene conversion is a viable reaction. While cleavage of a C-H bond of ethylidyne is probably the first step in its thermal decomposition, a reasonable first step in the mechanism for the reaction of ethylidyne with H atoms to produce acetylene is cleavage of a C-H bond by abstraction of one of the H atoms from ethylidyne by a gas phase H atom. A comparison of the two processes is shown in

Figure 1.34. Provided that H atom abstraction from an adsorbed hydrocarbon by a gas phase H atom occurs, the decomposition of ethylidyne to acetylene is a viable reaction which allows the dynamic equilibrium to be present. Indeed, gas phase hydrogen atoms have been observed previously to abstract hydrogen atoms from gaseous hydrocarbons[46-48]. The abstraction of a surface bound hydrogen by a gas phase H atom has also been directly observed.[67] Abstraction of a H atom from an adsorbed hydrocarbon has been observed indirectly in previous work[43,44] and this work. Section III.F of this chapter discusses the abstraction of H atoms from an adsorbed hydrocarbon by gas phase H atoms.

The isotopic exchange between the hydrogen atoms on ethylidyne and gas phase D atoms demonstrated in the vibrational spectra measured after exposure of ethylidyne to D atoms

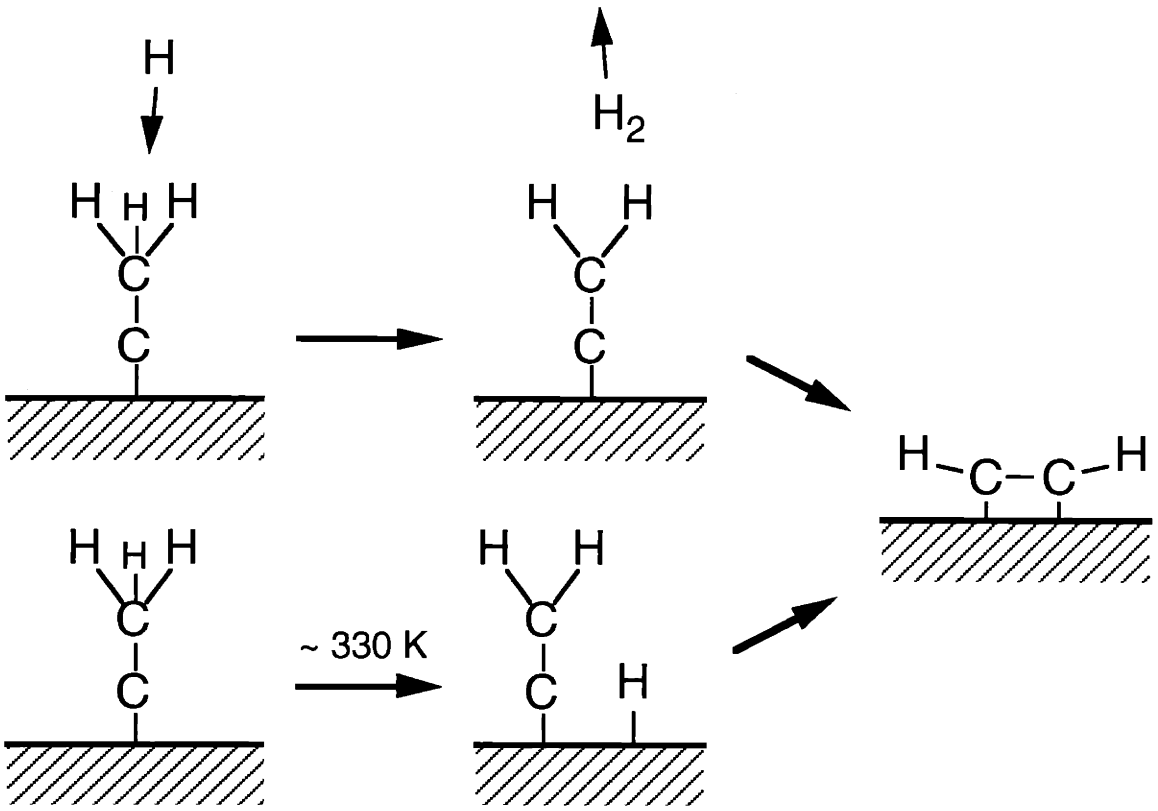

Figure 1.34. Pictorial representation comparing the breaking a C-H bond of ethylidyne by hydrogen abstraction and a thermal process.

shown in Figure 1.30 also supports the presence of a dynamic equilibrium. The dynamic equilibrium between ethylidyne and acetylene is expected to yield H/D exchange of the H atoms on the hydrocarbons upon exposure of an acetylene and ethylidyne covered surface to D atoms. Figure 1.35 pictures a schematic of the exchange reactions. The figure shows the exchange of one H atom on the ethylidyne and acetylene with a D atom. All the H atoms of the ethylidyne and acetylene can be exchanged by repeating the pictured reaction sequence several times.

Additional support for the dynamic equilibrium is provided by the absence of adsorbed acetylene in the reaction of bulk hydrogen with adsorbed acetylene to produce ethylidyne. The vibrational spectra measured after the reaction of bulk hydrogen with adsorbed acetylene in

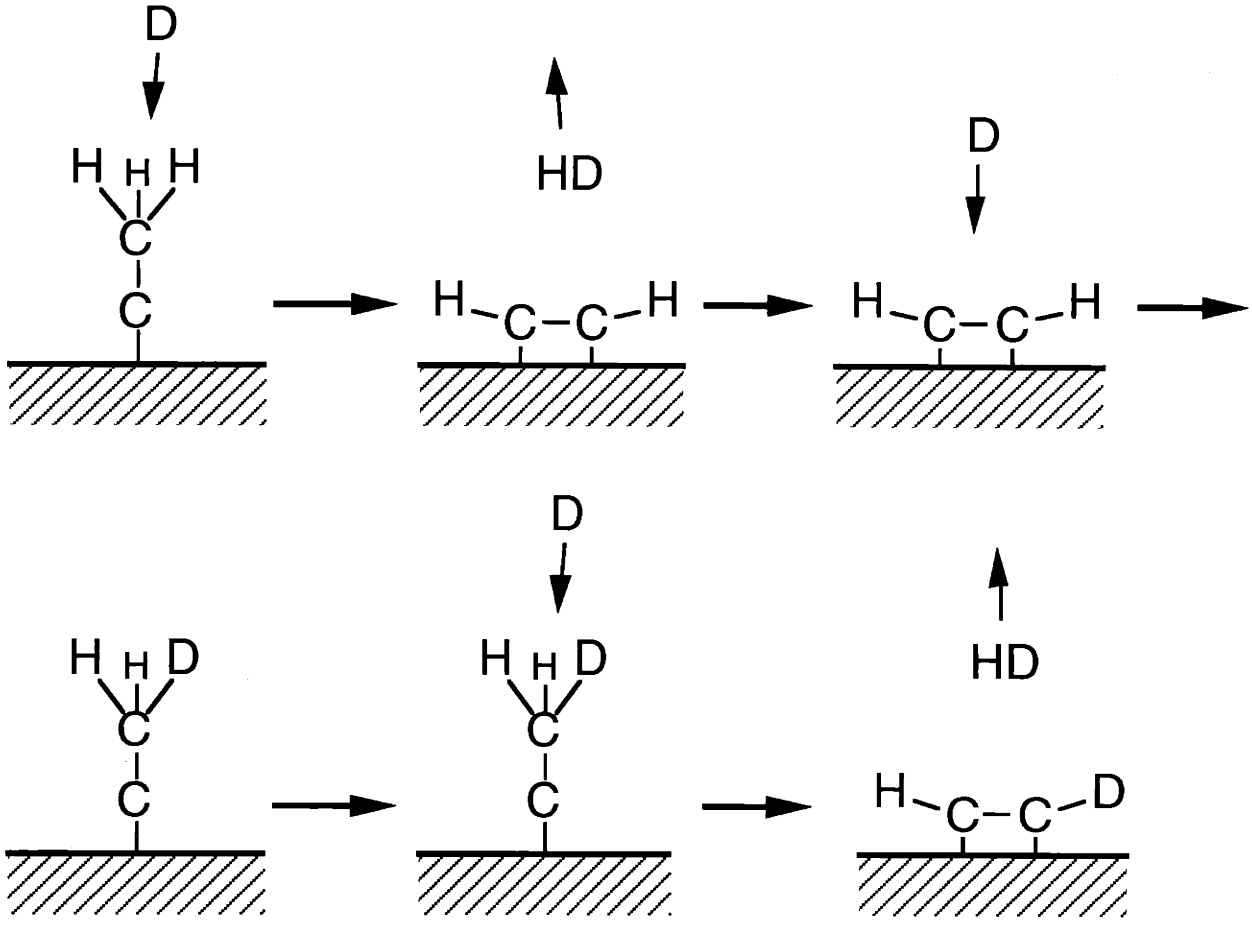

Figure 1.35. Pictorial representation of hydrogen - deuterium exchange expected during the dynamic equilibrium of acetylene and ethylidyne in the presence of deuterium atoms.

Figure 1.25 shows features of ethylidyne only. The lack of an 860 cm^{-1} feature indicates that no acetylene is coadsorbed with ethylidyne. The absence of adsorbed acetylene lends strong support to the presence of a dynamic equilibrium between acetylene and ethylidyne and gas phase H atoms, but not between the hydrocarbons and bulk H. The dynamic equilibrium cannot be achieved with bulk H because bulk hydrogen does not have enough energy to abstract H atoms from ethylidyne as discussed in Section III.F of this chapter. Because bulk hydrogen cannot abstract hydrogen atoms from adsorbed hydrocarbons, the ethylidyne to acetylene reaction cannot take place and therefore, no acetylene is coadsorbed with ethylidyne when ethylidyne is formed from the reaction of acetylene with bulk hydrogen.

In summary, the 860 cm^{-1} feature observed in the spectra of adsorbed ethylene, acetylene or ethane after exposure to H atoms is assigned to the antisymmetric C-H rocking mode of acetylene. Support for this assignment includes the electron energy loss spectra and thermal desorption measurements. Although acetylene has been shown to react with gas phase atoms to form ethylidyne, a dynamic equilibrium between ethylidyne and acetylene in the presence of gas phase H atoms explains their coexistence.

III.E. Mechanism of Ethylidyne Formation

The formation of ethylidyne from the reaction of gas phase hydrogen atoms with adsorbed hydrocarbons could proceed through a variety of mechanisms. This section discusses these possible mechanisms.

The first approach to the determination of the ethylidyne formation mechanism was stopping the reaction of the H atoms with the adsorbed hydrocarbons before completion and attempting to identify reaction intermediates through electron energy loss spectroscopy. Unfortunately, no reaction intermediates were identified. The electron energy loss spectra show only the reactant hydrocarbons, ethylidyne or a combination of the two. It is likely that the

intermediates are not sufficiently stable at the surface temperatures at which the reactions are carried out for them to be detected once the H atom exposure is halted.

Because no intermediates have been isolated and identified, many different mechanisms must be evaluated for their plausibility. Figure 1.36 shows many possible mechanisms for ethylidyne formation involving many different intermediates. However, the intermediates, reactants and products differ only in the number or positions of the hydrogen atoms on the C_2 backbone. Therefore, each step of the reaction involves either an addition of a H atom to, loss of a H atom from, or migration of a H atom along the C_2 backbone.

In the presence of gas phase H atoms, the possible mechanisms are compounded by the multiple ways in which each intermediate can be formed because three different types of H atoms are present: gas phase H atoms, surface bound H, and bulk H. That is, an adsorbed C_2 hydrocarbon can in principle add a H atom by reaction with a gas phase H atom, a surface bound H atom or a bulk H atom. However, the addition of a H atom to the hydrocarbon by a bulk H can be excluded because the temperatures at which the ethylidyne formation reaction are carried out, below 120 K, is too low for a bulk H atom to be mobile enough to emerge from the bulk.[52,60,63] Therefore, there are two ways to add a H atom to an adsorbed hydrocarbon: from a surface bound H atom or a gas phase H atom. Likewise, an adsorbed C_2 hydrocarbon can lose a H atom by multiple mechanisms. Both thermal dissociation of the hydrocarbon resulting in a H atom bound to the surface or H atom abstraction by a gas phase H atom resulting in gas phase H_2 will lead to a loss of a H atom from the adsorbed hydrocarbon. Abstraction of a H atom from an adsorbed hydrocarbon by a surface bound H or bulk H is not thermodynamically viable under the reaction condition as discussed in the next section. Therefore, there are two ways for an adsorbed hydrocarbon to lose a H atom: thermal dissociation of the hydrocarbon adsorbate or H atom abstraction by a gas phase H atom.

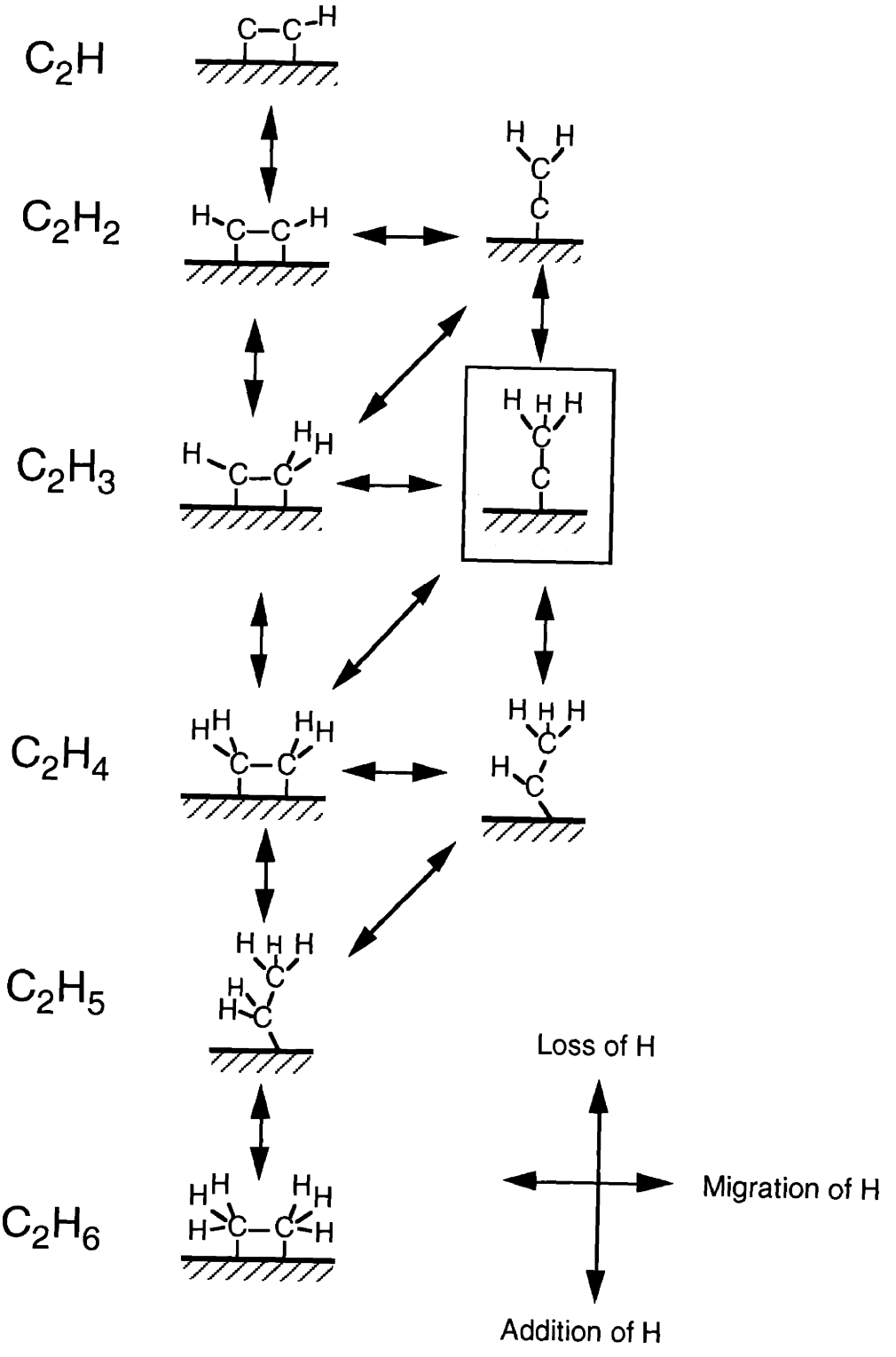

Figure 1.36. Possible reaction mechanisms for ethylidyne formation.

Because the number of possible mechanisms for ethylidyne formation is very large, a discussion of these possibilities must be approached in a systematic way. The discussion will start with the last step of the formation of ethylidyne. Only intermediates which can form ethylidyne in a single step will be considered. The combination of previous knowledge of the chemistry of C_2 hydrocarbons adsorbed on Ni(111) with the present observations allows some of these possible ethylidyne formation intermediates to be excluded. The single step mechanisms for formation of the intermediates that cannot be excluded are then explored, as was done for the intermediates that yield ethylidyne in a single step. The combination of previous knowledge of the chemistry of C_2 hydrocarbons on Ni(111) with present observations may again allow some of these intermediates to be excluded. The discussion will proceed in this manner until the initial steps involving the reactants of the ethylidyne formation reaction are reached.

In considering the final step of ethylidyne formation, three intermediates can form ethylidyne in a single step as shown in Figure 1.37: vinylidene ($-CCH_2$), by addition of a H atom; vinyl ($-CHCH_2$), by migration of H on the C_2 backbone; or ethylidene ($-CHCH_3$), by loss of a hydrogen atom. The labels shown in the figure, addition of H, migration of H and loss of H, refer to the hydrocarbon species itself. For example, a hydrogen atom transferring from the hydrocarbon to the surface is referred to as a loss of hydrogen and not a hydrogen migration.

Recall that although there are only three intermediates that can form ethylidyne in one step, there are more than three possible mechanisms for the final step in the ethylidyne formation. For example, surface bound H atoms can add to vinylidene ($-CCH_2$) in a thermally activated step to form ethylidyne or a gas phase H atom can add directly to vinylidene to form ethylidyne. Also, ethylidene ($-CHCH_3$) can lose a H atom to the surface by thermal dissociation or to a gas phase H atom by hydrogen abstraction. Therefore, there are five possible mechanisms for the final step of ethylidyne formation.

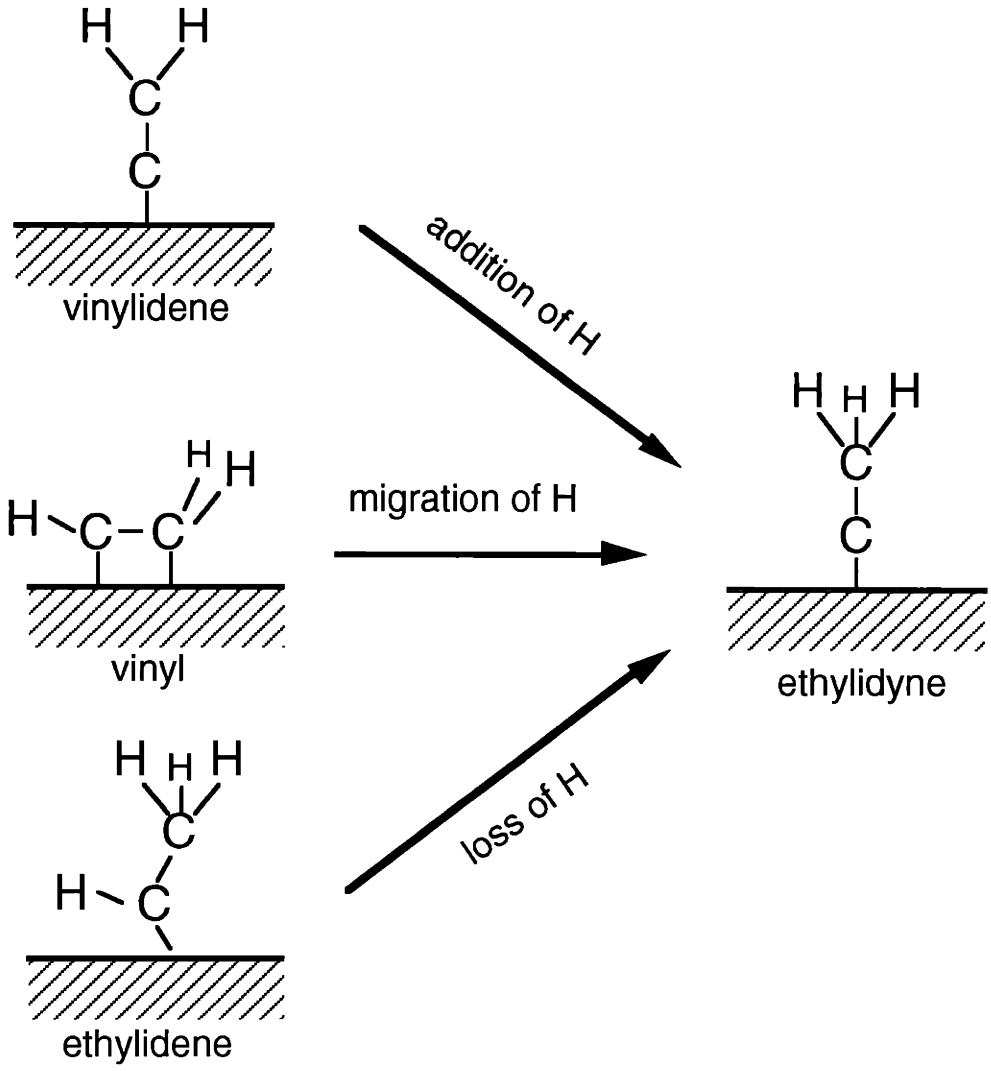

Figure 1.37. The only possible mechanistic steps to form ethylidyne in one step.

One of these possibilities, the migration of H on vinyl (-$CHCH_2$) to produce ethylidyne can be excluded. The argument is as follows. Ethylene is known to decompose to acetylene on a Ni(111) surface at a temperature of approximately 200 K.[37] Unless the loss of the two hydrogen atoms is a concerted process, the reaction must go through a vinyl intermediate. Previous evidence suggests that the dissociation of ethylene is not concerted. That is, when deuterium is coadsorbed with isotopically unlabeled ethylene and subsequently heated, deuterium atoms are observed to exchange with the hydrogen atoms on the ethylene in the same

temperature range that the ethylene decomposes (200 K).[37] Simultaneous occurrence of exchange with decomposition suggests that the ethylene decomposition does not proceed by a concerted loss of two H atoms, but rather proceeds through a vinyl intermediate. Since no ethylidyne is formed in the decomposition of ethylene, the migration of a H atom on a vinyl intermediate at 200 K can be excluded.

The previous argument concluded that vinyl does not thermally convert to ethylidyne at 200 K. However, because the temperature of the surface during the ethylidyne formation reactions is below 120 K, it would be useful to be able to break a C-H bond of ethylene at 120 K and determine what happens to the resulting vinyl intermediate at this temperature. Previous work has shown that C-H bonds can be activated by low energy electrons.[68-71] In fact, vinyl is reported to be formed on the Ag(111) surface by exposure of adsorbed ethylene to electrons with an energy of 10 to 60 eV.[69] In an effort to synthesize a vinyl species on Ni(111), ethylene has been exposed to electrons. Figure 1.38 shows the electron energy loss spectra measured after a 30 minute exposure of 0.25 ML ethylene to 40 eV electrons at a current to the crystal of $7x10^{-5}$ amps. The temperature of the surface prior to the electron exposure is 80 K, but increased to 120 K during the electron exposure. The spectra of acetylene coadsorbed with hydrogen from Figure 1.29 are included in the figure for comparison.

Comparison of the two sets of spectra in Figure 1.38 shows the product of the exposure of ethylene to electrons to be acetylene. All the frequencies of the electron energy loss features match as well as the dipole activity of the features. Similar to the thermal decomposition of ethylene to acetylene on Ni(111), the electron stimulated dissociation of ethylene to acetylene at 120 K likely proceeds through a vinyl intermediate. The same experiment has been performed at 50 K, and the results are same. Acetylene is produced from the exposure of ethylene to electrons. No ethylidyne is observed in either experiment. Therefore, the migration of a H atom on a vinyl intermediate to form ethylidyne is excluded from the ethylidyne formation mechanism.

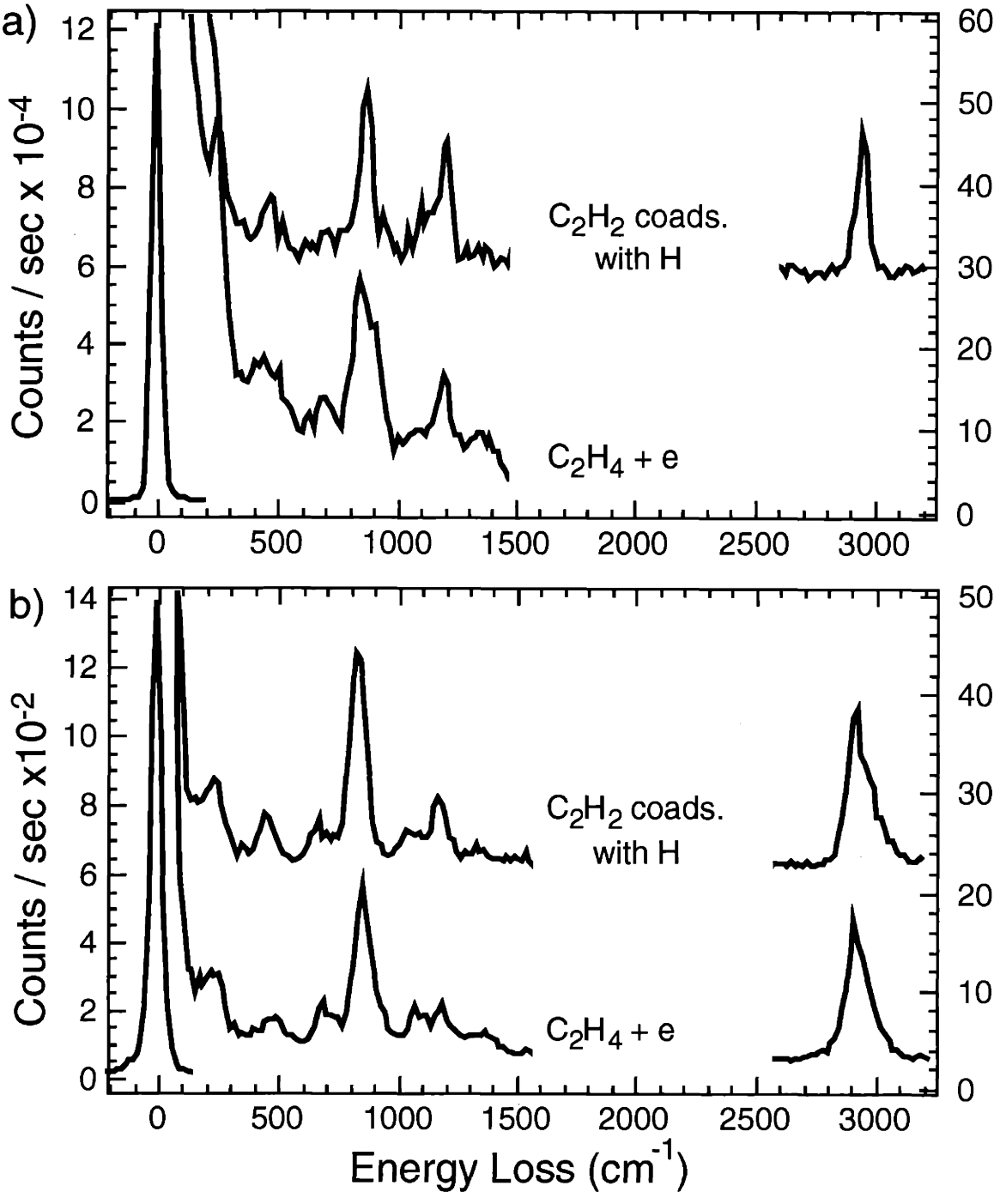

Figure 1.38. Electron energy loss spectra measured after exposure of ethylene to electrons and spectra of acetylene coadsorbed with hydrogen (taken from Figure 1.29). **a)** on-specular. **b)** 10° off-specular.

With the elimination of H atom migration on vinyl to form ethylidyne, only two other possible hydrocarbon species can be involved in the final step of the ethylidyne formation mechanism, vinylidene ($-CCH_2$) and ethylidene ($-CHCH_3$). Since there is no experimental evidence that can exclude either from the final step, the mechanisms for formation of both vinylidene ($-CCH_2$) and ethylidene ($-CHCH_3$) will be considered.

Three hydrocarbon species, acetylide (-CCH), acetylene (HCCH) and vinyl ($-CHCH_2$), can react to form the vinylidene intermediate in a single step as shown in Figure 1.39. While there are only three hydrocarbon structures that are possible intermediates for the formation of vinylidene, there are five possible reactions that can produce vinylidene in a single step. They are migration of a H atom on acetylene, loss of a H atom on vinyl by thermal dissociation or by abstraction by gas phase H atom or addition of a H atom to acetylide from the surface or from the gas phase.

One of the possible reactions to form vinylidene in a single step can be excluded: hydrogen atom migration on acetylene to produce vinylidene. Previous electron energy loss spectroscopy and thermal desorption work has shown that acetylene adsorbed on Ni(111) is stable to temperatures above 360 K.[41,72] Even when adsorbed acetylene is heated to higher temperatures, it is not observed to form vinylidene.[41] Therefore, H migration on acetylene to form vinylidene is excluded from the possible vinylidene formation mechanisms.

With the elimination of H atom migration on acetylene to form vinylidene, only two other possible hydrocarbon species can be involved in a vinylidene formation mechanism, acetylide (-CCH) and vinyl ($-CHCH_2$). Neither intermediate can be excluded on the basis of either present or previous spectroscopic evidence. However, when considering the observed rate of formation of ethylidyne from acetylene and ethylene, the vinyl intermediate is favored. The argument is as follows. Ethylene and acetylene are shown to react to form ethylidyne at approximately the same rate. Their conversion to ethylidyne is complete after 30 seconds. In

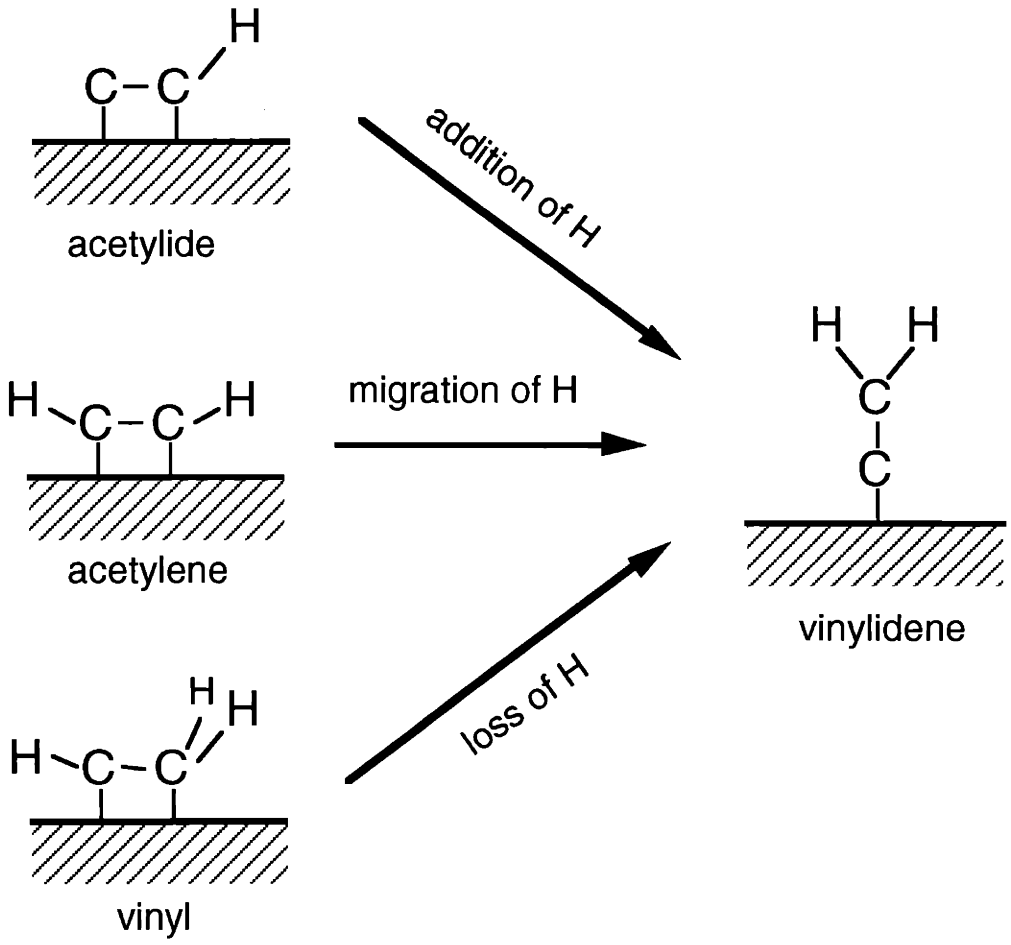

Figure 1.39. The possible mechanisms which form the vinylidene intermediate in one step.

the conversion of acetylene to acetylide, only one step is necessary, the loss of one H atom. Ethylene, on the other hand, must lose three hydrogen atoms to form acetylide. It must first lose a hydrogen atom to produce vinyl, lose another to produce acetylene and then another to produce the acetylide species. The first and last of these steps, ethylene to vinyl and acetylene to acetylide, must involve abstraction by gas phase H atoms because the C-H bonds of ethylene and acetylene do not cleave at the temperatures at which the exposure to H atoms is carried out.[37,41,72] The intermediate step, vinyl to acetylene is a thermal process as has been discussed previously. Because of the additional steps required by ethylene to form a acetylide intermediate, the ethylene reaction with gas phase H atoms to form ethylidyne would

presumably take longer than the acetylene reaction if the mechanism involved an acetylide intermediate. In addition, ethylene must lose its H atoms while competing with the process of H atom addition. Gas phase hydrogen atoms add readily to adsorbed hydrocarbons as discussed in Section III.A.4 of this chapter. Unfortunately, the relative rates of addition versus abstraction are not known. On the assumption that the rate of H atom addition is comparable to that of H atom abstraction, it seems difficult for ethylene to convert to acetylide at approximately the same rate as acetylene converts to acetylide.

In contrast, ethylene and acetylene are both a single step away from producing the vinyl intermediate by H atom addition and abstraction, respectively. If the rates of addition and abstraction are approximately equal, then both ethylene and acetylene would produce vinyl, and hence ethylidyne, at approximately the same rate. Therefore, the observation that acetylene and ethylene produce ethylidyne at approximately the same rate favors the vinyl species over the acetylide species as the intermediate in the ethylidyne formation reaction.

The preceding arguments favoring the vinyl over the acetylide intermediate assume that the subsequent vinylidene reaction to form ethylidyne is not the rate determining step in the ethylidyne formation reaction. If this were the case, then the rate at which the acetylide or vinyl intermediates are formed would not be significant in the overall ethylidyne formation reaction. It is probably a good assumption that the conversion of vinylidene to ethylidyne is not the rate determining step because if it were, the vinylidene concentration would have been large enough to be observed in the electron energy loss spectra of the reactions which are stopped before completion. However, no evidence of vinylidene is observed in these spectra. Therefore, the approximately equal rates of ethylidyne formation from ethylene and acetylene favor the vinyl over the acetylide intermediate.

Vinylidene to ethylidyne is one possibility for the final step in the ethylidyne formation. Ethylidene ($-CHCH_3$) to ethylidyne is the other possible final step. There are three hydrocarbons, vinyl ($-CHCH_2$), ethylene (CH2CH2) and ethyl (-CH2CH3), in five possible

reactions that can produce ethylidene in one step. Figure 1.40 shows the possible ethylidene formation mechanisms and intermediates. Again, the hydrogen migration reaction can again be eliminated because ethylene is a stable adsorbate at 120 K and below, the surface temperatures during gas phase H atom exposures. At 200 K, ethylene decomposes to acetylene but even at this temperature it does not rearrange to form ethylidene.[37]

The exclusion of the conversion of ethylene to ethylidene leave two possible intermediates which can react to form ethylidene in a single step, vinyl and ethyl. The relative rates of ethylidyne formation from the three different C_2 hydrocarbon reactants can again be used as an argument to favor the vinyl intermediate over the ethyl intermediate. Acetylene and ethylene react with gas phase H atoms to form ethylidyne at approximately the same rate. While ethylene can form ethyl in a single reaction step by the addition of a gas phase H atom, acetylene must add three hydrogen atoms to form the ethyl intermediate. Two of these three additions must be H atoms from the gas phase, because surface bound H does not add to acetylene and ethylene.[37] The conversion of acetylene to the ethyl intermediate would be expected to be a slower process, considering the greater number of steps. Therefore, if the ethyl species were an intermediate in the ethylidyne formation reaction, the acetylene reaction to form ethylidyne would be expected to be slower than the ethylene reaction. In contrast, both ethylene and acetylene can form the vinyl intermediate in one step. Since the relative rates of ethylidyne formation from ethylene and acetylene are similar, a vinyl intermediate is favored over an ethyl intermediate.

The fact that ethane reacts to form ethylidyne more slowly than ethylene and acetylene also favors the vinyl intermediate. Recall that ethane forms ethylidyne at a rate estimated to be 40 times slower than ethylidyne formation from ethylene or acetylene. While ethylene and acetylene are only one H addition or one H abstraction away from the vinyl intermediate, ethane must lose three hydrogen atoms to form the vinyl intermediate. Two of these steps are dependent on gas phase H atoms. The loss of the first H atom must occur by H atom

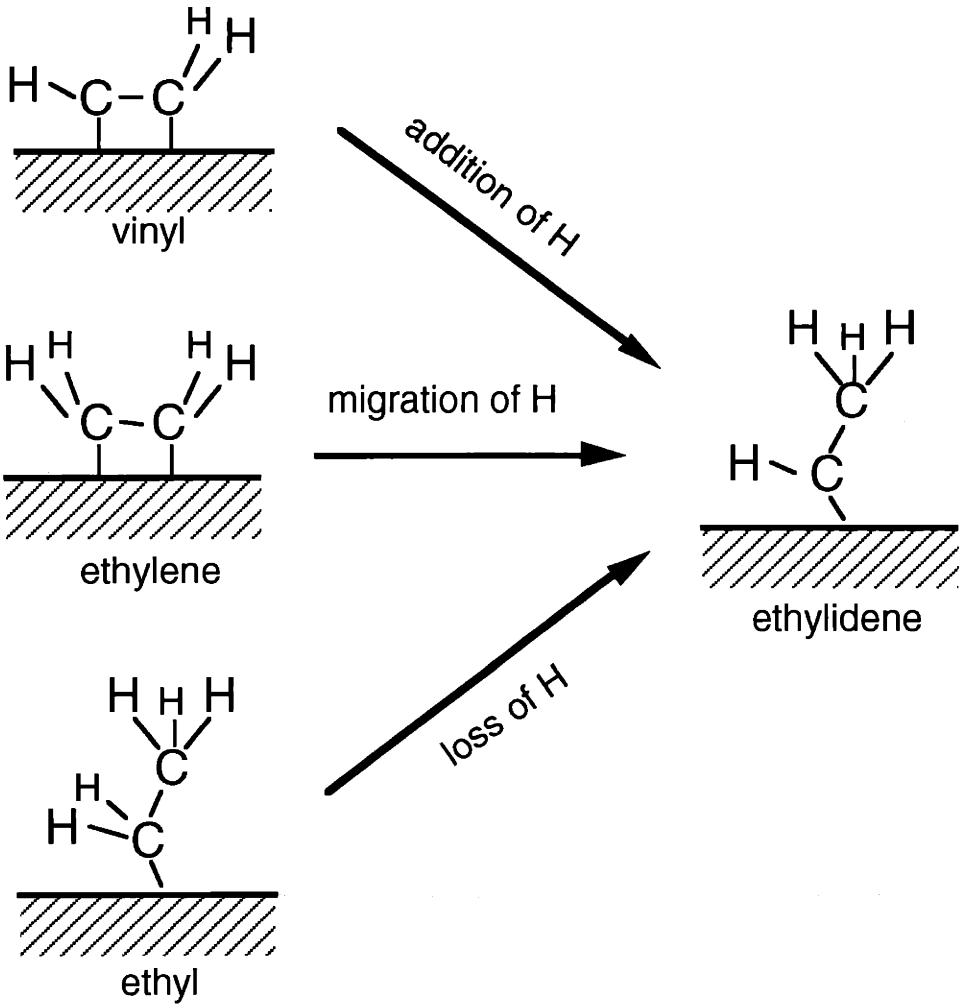

Figure 1.40. The possible mechanisms which form ethylidene intermediate in a single step.

abstraction because ethane does not dissociate thermally on Ni(111). Once one H atom is removed, the adsorbed ethyl intermediate thermally dissociates on the surface to form ethylene and surface bound H. This process will be discussed further in Chapter III. The next step, conversion of ethylene to the vinyl intermediate, must occur by H atom abstraction because ethylene does not thermally dissociate at surface temperatures of 120 K or below, the temperatures of the ethylidyne formation reaction. The process of converting ethane to the vinyl intermediate and subsequently to ethylidyne would be expected to be slower than that of ethylene or acetylene to the vinyl intermediate and then to ethylidyne. Therefore, the slower rate

of ethylidyne formation exhibited by ethane is consistent with the greater number of steps to form the vinyl intermediate. These arguments do assume that the final step of ethylidyne formation from ethylidene is not the rate determining step. This assumption is reasonable because no ethylidene is observed in the electron energy loss spectra of the reactions of gas phase hydrogen atoms with adsorbed hydrocarbons in which the reaction is stopped before completion.

The choice of the vinyl intermediate over the ethyl intermediate based on the reaction rate observed for ethane is not conclusive since the difference in the ethylidyne formation rates could also be explained by a slower rate of abstraction of a H atom from ethane than the rate for addition of a hydrogen atom to ethylene to form the ethyl intermediate. Unfortunately, no information about the relative rates of addition versus abstraction for these adsorbed hydrocarbons is available. However, assuming the two rate to be comparable, the observed slower rate of ethylidyne formation from ethane than that from ethylene and acetylene gives additional support for the vinyl over the ethyl intermediate.

Figure 1.41 summarizes the discussion of the ethylidyne formation mechanism. The arrows with crosses through them indicate the mechanistic steps which are not supported by the available data. Also indicated in the figure are the two reactions which have been argued to be not as favorable as the competing reactions. As seen, a good portion of the possible reaction mechanism steps have been eliminated or at least shown to be less favorable. Figure 1.42 shows the same reaction mechanisms but with the invalidated and less favored intermediates removed.

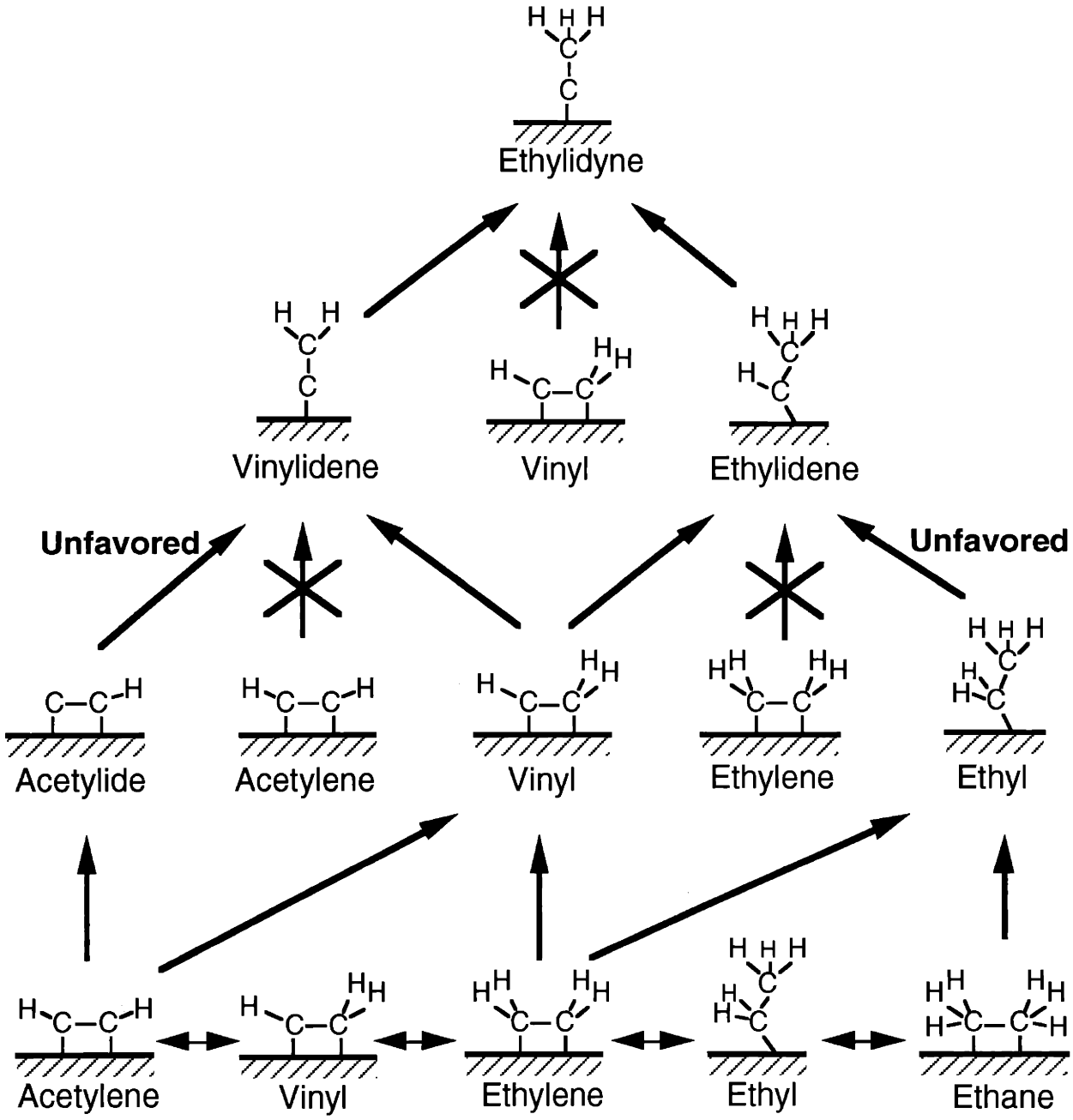

Figure 1.41. Possible mechanisms of ethylidyne formation. Steps which have been excluded are crossed out and the less favored steps are indicated.

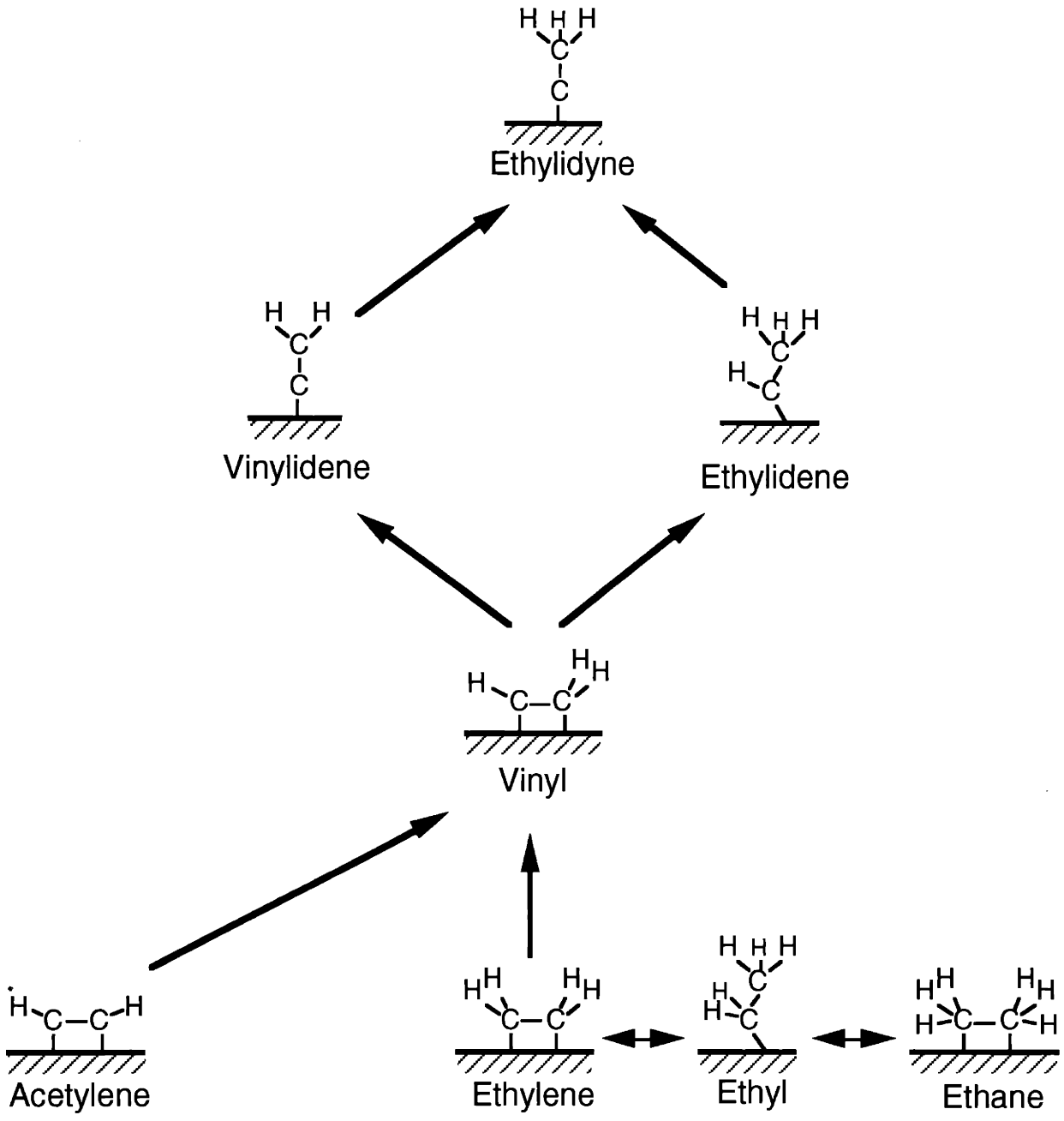

Figure 1.42. Possible mechanisms of ethylidyne formation with the excluded and unfavored steps removed.

With the assumption that the unfavored mechanistic steps involving acetylide and ethyl intermediates do not occur, the possible ethylidyne formation mechanism has been greatly simplified. Only two different reaction pathways remain as shown in Figure 1.42. In the reaction of all three C_2 hydrocarbons with H atoms, the initial step is conversion of the hydrocarbon to a vinyl intermediate. From the starting reactants acetylene and ethylene, this conversion is a single step process involving addition of a gas phase H atom to acetylene and abstraction of a H atom from ethylene by a gas phase H atom. The conversion of ethane to the vinyl intermediate is a three step process: 1) abstraction of a H atom from ethane to form the ethyl intermediate, 2) thermal dissociation of the ethyl intermediate to ethylene and 3) abstraction of a H atom from ethylene to form the vinyl intermediate. The second step, conversion of the ethyl intermediate to ethylene could also involve H abstraction from ethyl by a gas phase H atom in addition to thermal decomposition.

The next step in the ethylidyne formation reaction is the conversion of the vinyl intermediate to either the vinylidene intermediate or the ethylidene intermediate. Neither mechanistic step can be excluded using the experimental results discussed so far. In both cases the vinyl conversion requires a gas phase H atom: hydrogen abstraction to form vinylidene and hydrogen addition to form ethylidene. Thermally, vinyl reacts to form acetylene, and therefore the conversion to neither vinylidene nor ethylidyne is a thermal process.

The last step in the ethylidyne formation mechanism is the conversion of the vinylidene intermediate or the ethylidene intermediate to ethylidyne. This step could proceed either thermally or by reaction with a gas phase H atom. No proof of either process is available since neither intermediate has been directly synthesized and isolated on the surface. Also, no previous experimental evidence of vinylidene or ethylidene adsorbed on Ni(111) is available. Without further evidence, neither vinylidene nor ethylidene can be excluded from the ethylidyne reaction mechanism and each intermediate's conversion to ethylidyne could be either a thermal reaction or reaction with a gas phase H atom.

Up to this point, the analysis of the ethylidyne formation reaction mechanism which is summarized in Figure 1.41 has not included the knowledge that ethylidyne can also be synthesized by the reaction of bulk H with adsorbed acetylene. This information is important because unlike an impinging gas phase H atom, hydrogen emerging from the bulk cannot abstract hydrogen atoms from an adsorbed hydrocarbon as will be discussed in detail in Section III.F of this chapter. If it assumed that the intermediates involved in the reaction of bulk H with acetylene are the same as those in the reaction of adsorbed hydrocarbons with H atoms then the steps which involve abstraction of H atoms from hydrocarbon intermediates can be eliminated from the ethylidyne formation reaction.

Discussion of the ethylidyne formation reaction from bulk hydrogen and adsorbed acetylene will start with two intermediates which are involved in the reactions labeled unfavored in Figure 1.41, acetylide and ethyl. Acetylene must lose a hydrogen atom to form the acetylide intermediate. Although this process could occur in the presence of gas phase H atoms, bulk hydrogen cannot abstract a H atom from acetylene to form acetylide. Therefore, the acetylide intermediate can be eliminated from the possible ethylidyne formation mechanism.

The ethyl intermediate conversion to ethylidene intermediate step can also be excluded. Bulk hydrogen can add to the adsorbed acetylene to form ethyl as evident by the formation of ethane in Figure 1.1, but it cannot react with ethyl to form ethylidene. Ethyl to ethylidyne conversion involves abstraction of a H atom, and bulk hydrogen cannot abstract H atoms. This argument that the ethyl to ethylidyne conversion is a H atom abstraction event relies on the fact that the conversion is not a thermal process. The thermal decomposition product of ethyl will be shown in Chapter III to be ethylene. The fact that ethyl does not thermally dissociate to ethylidene, coupled with the knowledge that it is not thermodynamically feasible for bulk hydrogen to abstract H atoms from adsorbed hydrocarbons, excludes the ethyl intermediate from the mechanism for the formation of ethylidyne.

The observation that acetylene reacts with bulk hydrogen can be used to invalidate one more possible step in the ethylidyne formation mechanism, the vinyl to vinylidene conversion. Again, this step can be excluded because bulk hydrogen cannot abstract hydrogen atoms from a vinyl intermediate to form the vinylidene intermediate. Also, this process is known not to take place thermally, as discussed previously. Because the vinyl to vinylidene conversion cannot take place thermally nor can bulk hydrogen induce the transition, the vinylidene intermediate is eliminated as an intermediate in the ethylidyne formation reaction.

The elimination of the vinyl to vinylidene conversion results in only one remaining possible intermediate for the last step in this mechanism of ethylidyne formation, ethylidene. The final step involves loss of a H atom from the ethylidene intermediate to form ethylidyne. The inability of a bulk hydrogen to abstract the hydrogen atom distinguishes the last step as a thermal dissociation process of ethylidene to ethylidyne.

Provided the reaction of bulk hydrogen with adsorbed acetylene to form ethylidyne proceeds via the same intermediates as that of gas phase H atoms with adsorbed C_2 hydrocarbons, the mechanism for ethylidyne is known. The mechanism is shown in Figure 1.43. In the reaction of all three C_2 hydrocarbons with H atoms to form ethylidyne, the initial step is conversion of the hydrocarbon to a vinyl intermediate. From the starting reactants acetylene and ethylene, this conversion is a single step process involving addition of a gas phase H atom to acetylene and abstraction of a H atom from ethylene by a gas phase H atom. The conversion of ethane to the vinyl intermediate is a three step process: 1) abstraction of a H atom from ethane to form the ethyl intermediate, 2) thermal dissociation of the ethyl intermediate to ethylene and 3) abstraction of a H atom from ethylene to form the vinyl intermediate. The second step, conversion of the ethyl intermediate to ethylene could also involve H abstraction from ethyl by a gas phase H atom. In the reaction of bulk hydrogen with acetylene the vinyl intermediate is formed by addition of bulk hydrogen to adsorbed acetylene.

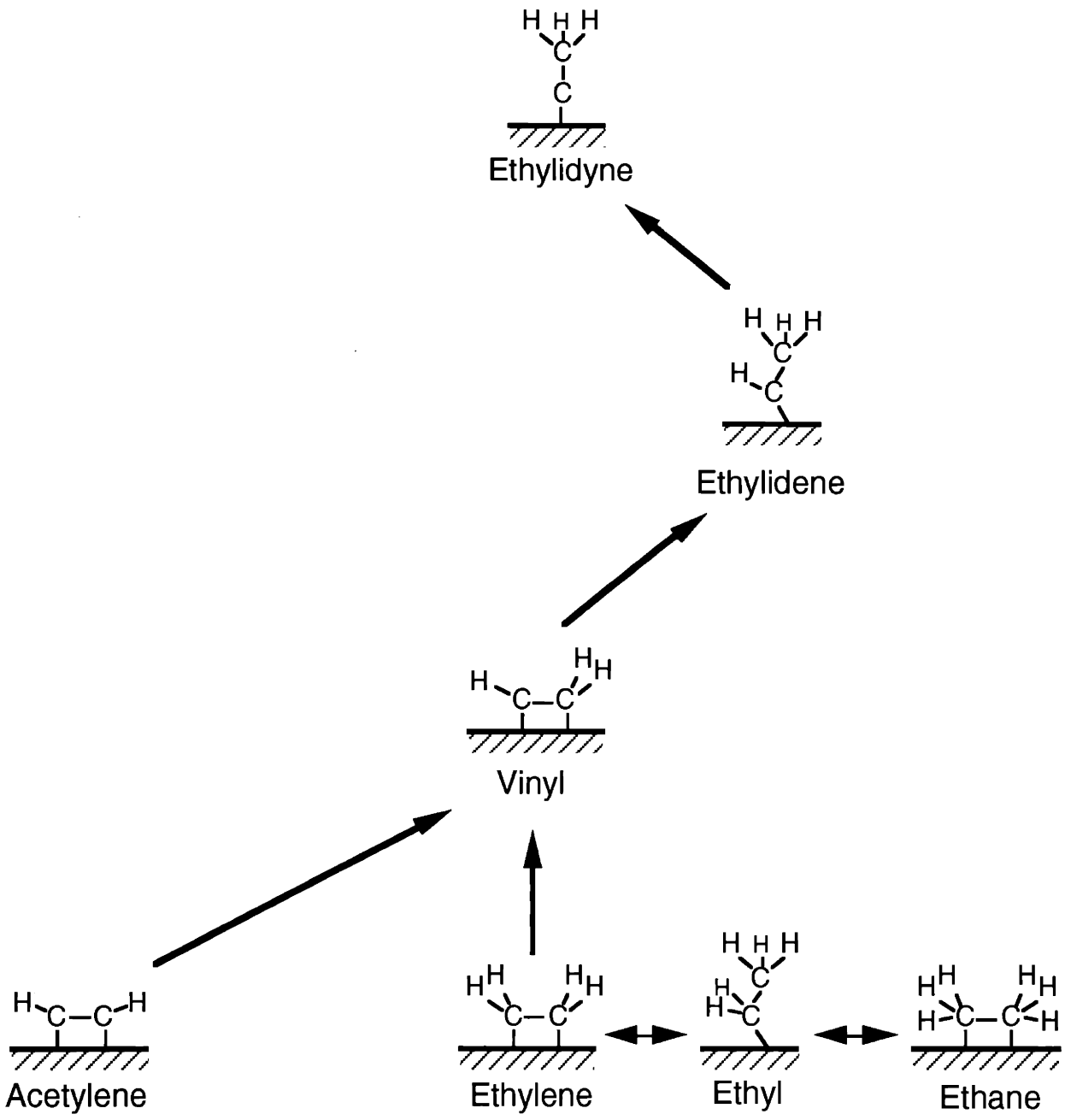

Figure 1.43. The mechanism of ethylidyne formation.

The second step in the ethylidyne formation reaction is the conversion of the vinyl intermediate to the ethylidene intermediate. The conversion to ethylidene requires a gas phase H atom or a bulk H atom because a surface bound H does not add to vinyl to produce ethylidyne.

The last step in the ethylidyne formation mechanism is the conversion of the ethylidene intermediate to ethylidyne. The reaction of bulk H with acetylene showed this conversion is a thermal process, but this step could also proceed by abstraction by a gas phase H atom.

It should be noted that the reaction of bulk hydrogen with adsorbed ethylene has also been explored with electron energy loss spectroscopy. No ethylidyne formation is observed. The only reactions observed are hydrogenation of ethylene to form ethane and displacement of ethylene by bulk H. Auger measurements show that no carbon remains on the surface.[37] Looking at Figure 1.43, it is easy to explain why no ethylidyne is formed. The initial conversion of ethylene to the vinyl intermediate requires loss of a hydrogen atom. This process does not take place thermally at the temperature at which H emerges from the bulk, nor can it occur through an abstraction reaction with bulk hydrogen. Therefore, no ethylidyne formed. The inability of bulk hydrogen to react with ethylene to form ethylidyne further supports the mechanism for ethylidyne formation shown in Figure 1.43.

III.F. Comparison of the Reactivity of Surface Hydrogen, Bulk Hydrogen and Gas Phase Hydrogen Atoms

The reaction of ethylene with surface hydrogen and bulk hydrogen has been studied extensively.[37] The results of these experiments will be summarized here and then compared to the results of the reaction of gas phase H atoms with ethylene.

Hydrogen coadsorbed with ethylene on a Ni(111) surface does not react to form ethane. This observation is very interesting since the most widely accepted mechanism for hydrogenation of unsaturated hydrocarbons, the Horiuti-Polanyi mechanism, is stepwise addition of the surface bound H atoms to the adsorbed olefin. The chemistry of ethylene

coadsorbed with surface bound hydrogen on Ni(111) is the same as that observed in the absence of surface bound hydrogen: competition between desorption of ethylene and decomposition of ethylene to adsorbed acetylene. Reaction of surface deuterium coadsorbed with ethylene yielding exchange with the H atoms of ethylene shows that the lack of hydrogenation is not due to a lack of mobility of the reactants, and therefore the lack of hydrogenation must be due to other considerations.

Bulk hydrogen, on the other hand, is observed to hydrogenate ethylene. As hydrogen emerges from the bulk to the surface onto which ethylene is adsorbed, two processes are observed, hydrogenation of ethylene to ethane and displacement of ethylene. After hydrogen emerges from the bulk to the surface, no carbon remains on the surface.

One possible explanation for the reactivity of bulk H is that its direction of approach is a favorable geometry for hydrogenation. The lowest energy barrier for addition in the gas phase is predicted to be a perpendicular approach to the molecular plane of ethylene.[73] This prediction intuitively makes sense, since the H atom is adding to the π bond of ethylene which is directed out of the molecular plane. Figure 1.44 shows the two situations pictorially. Because surface bound hydrogen must approach adsorbed ethylene in the molecular plane, the hydrogen atoms on the ethylene molecule sterically hinder the approach to the π orbital and therefore, the barrier to the addition is higher. Bulk hydrogen, on the other hand, approaches adsorbed ethylene perpendicular to the molecule plane. The hydrogen atoms on the ethylene molecule do not hinder the approach to the π orbital of ethylene and therefore the barrier is lower. Figure 1.45 shows the two different situations.

It should be noted that the adsorbed ethylene molecules shown in Figure 1.45 are different than those pictured in Figure 1.44 for gas phase ethylene. The hydrogen atoms of the adsorbed ethylene are bent slightly out of the molecular plane. They are portrayed this way because the observed C-C stretching frequency of adsorbed ethylene is 1200 cm^{-1} in contrast to the gas phase value of 1624 cm^{-1}. The interaction of ethylene with the Ni(111) surface partially

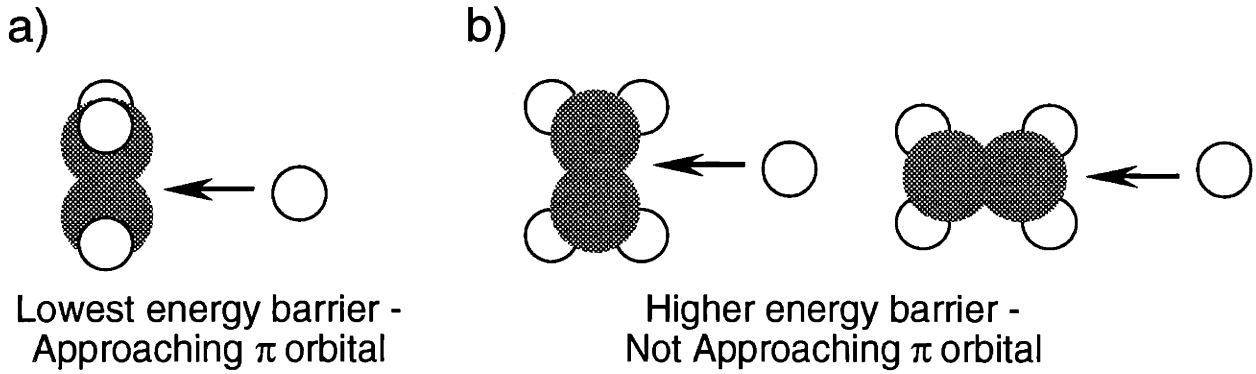

Figure 1.44. Pictorial representation of the approach of a gas phase hydrogen atom to gas phase ethylene molecule. **a)** Approach perpendicular to the molecular plane of ethylene. **b)** Approach in the molecular plane of ethylene.

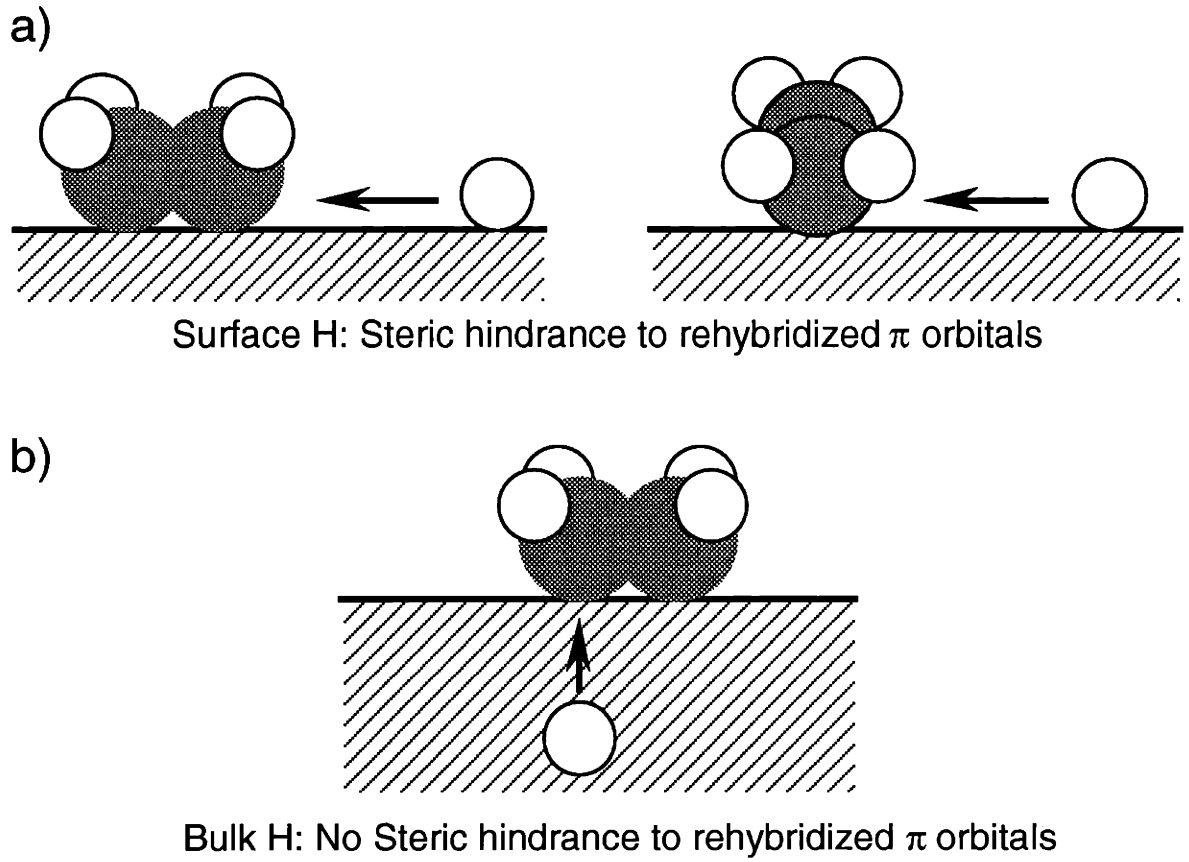

Figure 1.45. Pictorial representation of the approach of surface and bulk hydrogen atoms to an adsorbed ethylene molecule. **a)** Surface hydrogen must approach in the molecular plane of ethylene. **b)** Bulk hydrogen approaches perpendicular to the molecular plane of ethylene.

breaks the π bond of the ethylene molecule, resulting in a lower C-C stretching frequency. Typical single C-C bond frequencies are approximately 950 cm^{-1}. The observed frequency, 1200 cm^{-1}, is between the single and double bond values, suggesting a bond order of approximately 1.5 and reflecting a carbon hybridization somewhere between sp^2 and sp^3. Therefore, the hydrogen atoms on adsorbed ethylene are expected to be slightly tilted out of the molecular plane, as shown in the pictures of Figure 1.45. Even with the slight tilting of the hydrogen atoms, they would still be expected to inhibit the approach of a surface hydrogen atom. Therefore, the variance in the geometries could explain the difference in the reactivity observed for surface and bulk hydrogen. However, geometry alone cannot account for the observed difference in the reactivity. No hydrogenation of ethylene to ethane is observed in the reaction of ethylene adsorbed on top surface hydrogen, even though the surface hydrogen has the most favorable direction of approach when ethylene is bound on top of it. Therefore, another difference must account for the difference in reactivity of bulk and surface hydrogen.

A major difference between bulk and surface bound H is their energetics, as shown by the one dimensional potential energy diagram of the interaction of hydrogen with a nickel crystal in Figure 1.46.[52] The vertical axis of the potential energy diagram is energy per hydrogen atom and the horizontal axis is the distance perpendicular to the surface, z. The zero of energy is defined at the infinite separation of a hydrogen molecule and the surface. The zero value of z is loosely defined as the position of the nickel surface. Therefore, negative values of z are positions inside the bulk of the crystal and positive values are positions at the surface or extending into the vacuum. Three types of potential wells are seen in the potential energy diagram corresponding to bulk hydrogen absorption, surface hydrogen chemisorption, and molecular hydrogen physisorption.

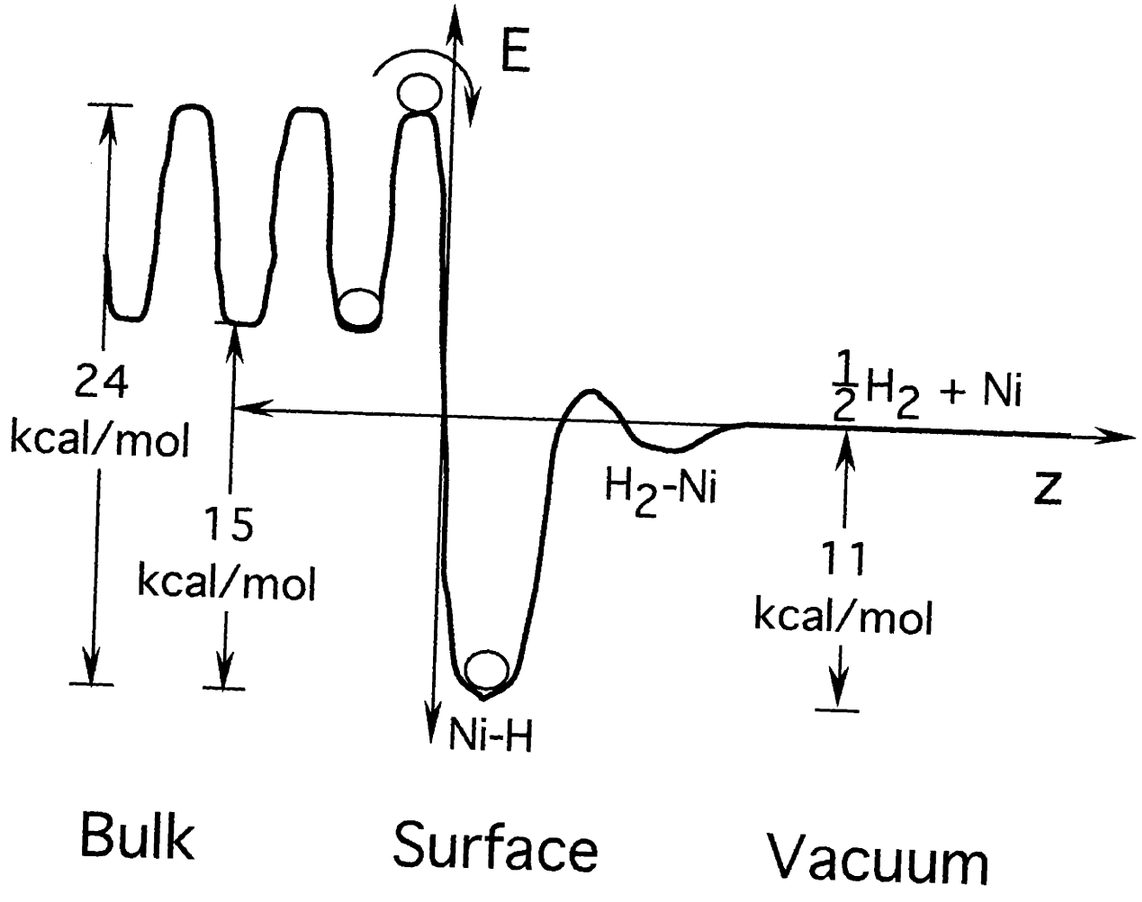

Figure 1.46. Potential energy diagram of the interaction of hydrogen with a Ni(111) surface.

As is seen in the potential energy diagram, hydrogen migration from the bulk to the surface is an exothermic process by 15 kcal/mol. But, in migrating from the bulk to the surface, the hydrogen atom must overcome a 9 kcal/mol barrier. Therefore, a hydrogen atom emerging from the bulk has up to 24 kcal/mol more energy than a hydrogen atom adsorbed on the surface. This energy can be channeled into the reaction coordinate for addition of a hydrogen atom to an adsorbed ethylene molecule. Surface hydrogen, on the other hand, has only thermal energy, characterized by the surface temperature, which is evidently not enough to overcome the barrier for addition of a H atom to adsorbed ethylene. Because bulk hydrogen is

a more energetic species, it can overcome the barrier to addition to adsorbed ethylene and thus, hydrogenates it.

Geometry and energy considerations account for the differences observed in the reactivity of surface and bulk hydrogen. They can also explain the unique reactivity of gas phase hydrogen atoms. Figure 1.47 shows the geometry of a hydrogen atom approaching an adsorbed ethylene molecule and the energetics of a gas phase H atom compared to that of a H atom emerging from the bulk. The geometry of approach of a gas phase hydrogen atom to adsorbed ethylene is similar to that of a bulk hydrogen atom. That is, a gas phase H atom and a bulk H atom both approach adsorbed ethylene perpendicular to the molecular plane. Gas phase H atoms are even a more energetic species than bulk H atoms, and therefore should also have enough energy to overcome the barrier to hydrogenation of adsorbed ethylene. Indeed, gas phase hydrogen atoms do react with adsorbed ethylene in a similar manner to bulk hydrogen with both hydrogenation of ethylene to ethane and displacement of ethylene reaction channels observed. However, there is a major difference in the observed reactivity: gas phase H atoms react with ethylene to produce ethylidyne, but bulk hydrogen does not.

The difference in reactivity of bulk hydrogen and gas phase hydrogen atoms is a consequence of energetics. Unlike bulk H atoms, gas phase H atoms are sufficiently energetic to abstract hydrogen atoms from adsorbed hydrocarbons. The abstraction reaction by gas phase H atoms is exothermic by approximately 5 kcal/mol, given an average C-H bond strength of 99 kcal/mol and a H-H bond strength of 104 kcal/mol. Of course, exothermicity alone does not determine the feasibility of a reaction. There might be barriers associated with the abstraction reaction. However, we have indirectly observed hydrogen atom abstraction from adsorbed hydrocarbons by gas phase H atoms in the reaction of gas phase H atoms with ethane to form ethylidyne. The first step in this reaction must be loss of a H atom from ethane. Adsorbed ethane does not thermally decompose on a Ni(111) surface as is evident by the lack of H_2

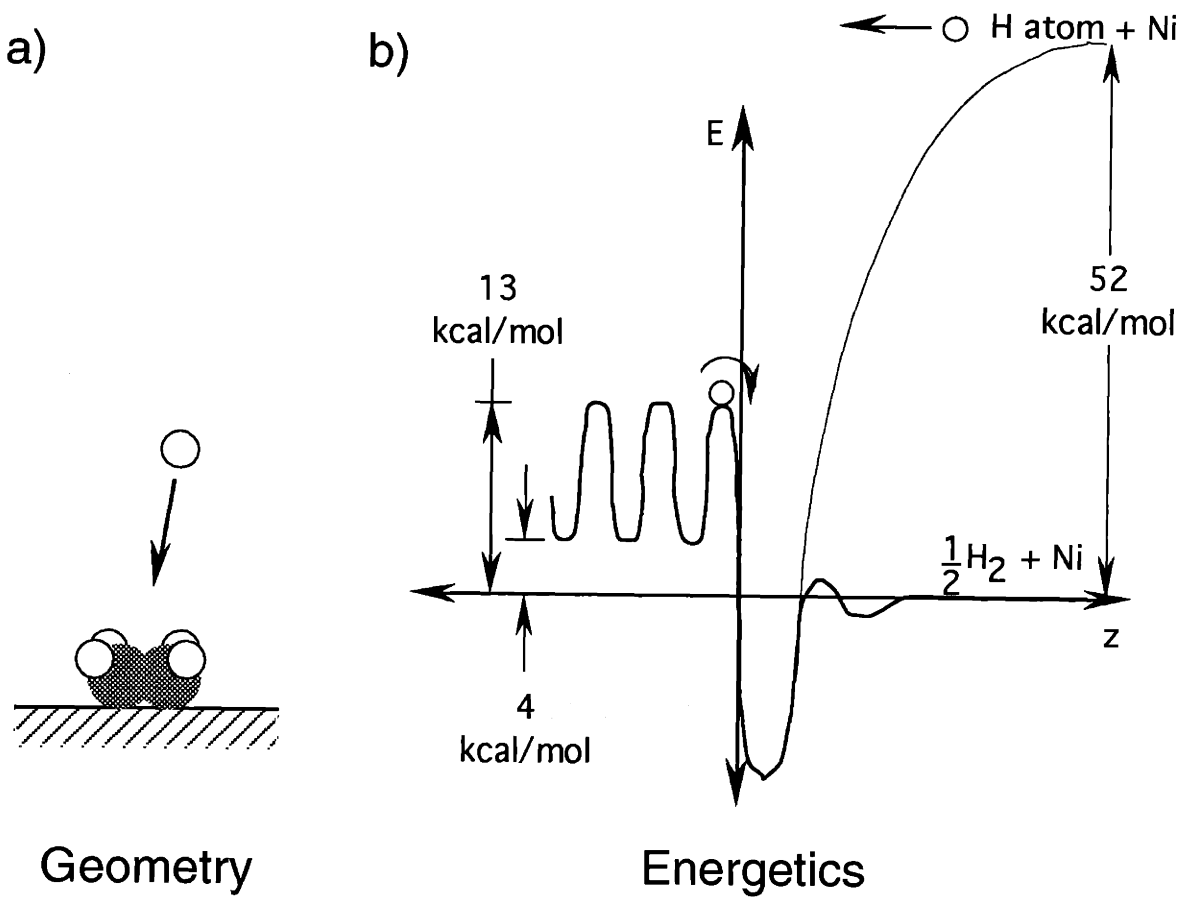

Figure 1.47. **a)** Pictorial representation of approach of a gas phase hydrogen atom to adsorbed ethylene. **b)** Potential energy diagram of the interaction of hydrogen with a Ni(111) surface which includes the gas phase hydrogen atoms energy level.

desorbing from the surface in the thermal desorption experiment shown in Figure 1.19. Therefore, the only possible mechanism for the loss of a H atom from ethane is abstraction by a gas phase H atom. This observation demonstrates that any barrier to hydrogen abstraction is not insurmountable by the potential energy and thermal energy of the gas phase H atom.

A hydrogen atom emerging from the bulk to the surface does not have enough energy to abstract a hydrogen atom from a surface adsorbate. The process is endothermic by 43 kcal/mol because a bulk hydrogen atom has 48 kcal/mol less potential energy less than a gas phase hydrogen atom. Therefore, the different reactivities of gas phase and bulk hydrogen atoms is due to the energetics: gas phase hydrogen atoms have enough energy to abstract hydrogen

atoms, while bulk hydrogen atoms do not. The observation that bulk H reacts with acetylene but not ethylene to produce ethylidyne is explained by the inability of bulk H to abstract H atoms from adsorbed hydrocarbons. Section III.E of this chapter shows that the first step in the ethylidyne formation reaction is conversion of the adsorbed hydrocarbon to the vinyl intermediate. The conversion of acetylene to vinyl is H atom addition, which bulk H is known to do. However, conversion of ethylene to vinyl is H atom abstraction and bulk H does not have enough energy to abstract H atoms from adsorbed hydrocarbons, and therefore no ethylidyne is formed in the reaction of bulk H with adsorbed ethylene.

The conversion of ethylene to ethylidyne shows the ability of gas phase hydrogen atoms to both add to and abstract hydrogen atoms from adsorbed hydrocarbons. As discussed earlier, the mechanism for ethylidyne formation is conversion of the adsorbed hydrocarbon to vinyl, then to ethylidene, and finally to ethylidyne. The first step in the reaction of ethylene with gas phase H atoms is its conversion to vinyl by loss of a hydrogen atom. Because this process does not take place thermally it must occur by abstraction by a gas phase H atom. The next step, vinyl to ethylidyne, involves addition of a hydrogen atom. Again this process does not take place thermally and must result from addition of the gas phase H atom to the vinyl species. The last step, ethylidene to ethylidyne, could be also be an abstraction event, but this process can take place thermally as shown by the formation of ethylidyne from the reaction of bulk H with acetylene. Therefore, in the reaction of gas phase H atoms with adsorbed ethylene to from ethylidyne, both H atom abstraction from and H atom addition to adsorbed hydrocarbons by gas phase H atoms takes place.

IV. Conclusions

Gas phase hydrogen atom reactions with ethylene, acetylene and ethane have all been shown to produce adsorbed ethylidyne which competes with displacement and/or

hydrogenation of the adsorbed hydrocarbon. Hydrogen emerging from the bulk to the surface of the crystal to which acetylene is adsorbed has also been shown to produce ethylidyne in competition with hydrogenation. The experimental results of this work demonstrate for first time the synthesis and spectroscopic identification of ethylidyne on a nickel single crystal.

Assuming that the four reactions observed to produce ethylidyne proceed via the same intermediates, the mechanism for ethylidyne formation is determined. In the first step, the adsorbed hydrocarbon reacts to form vinyl. This step is initiated by a gas phase H atom since the production of vinyl is not a thermal process at the temperatures employed in the ethylidyne formation reaction. The vinyl intermediate then reacts to form ethylidene. Again, this process is initiated by a gas phase H atom since vinyl does not thermally react to form ethylidene. The last step in the ethylidyne formation mechanism is the conversion of ethylidene to ethylidyne. This process could be initiated by a gas phase hydrogen atom, but not need be, since this process also takes place thermally.

It is noted that ethylidyne has previously been observed on alumina supported Ni when the supported Ni is first exposed to hydrogen and then to ethylene.[29] The mechanism for the ethylidyne formed in this study may involve bulk H because these experiments are carried out under 'high' pressure conditions (0.1 to 10 torr).

Ethylidyne and hydrogen are not the only adsorbates present after a gas phase hydrogen atom exposure to adsorbed hydrocarbons. A feature present in the electron energy loss spectra at 860 cm^{-1} is assigned to acetylene. Although acetylene has been shown to react with gas phase hydrogen atoms, a dynamic equilibrium exists between ethylidyne and acetylene in the presence of gas phase hydrogen atoms.

Ethylidyne thermally decomposes in the 340 - 360 K surface temperature range. Electron energy loss spectroscopy shows that the ethylidyne features start to lose intensity after heating to 340 K and are no longer present after heating the surface to 370 K. A small kinetic isotope effect is observed. Deuterated ethylidyne must be heated to 380 K to remove all the

ethylidyne features. Electron energy loss spectroscopy reveals the thermal decomposition product to be acetylene.

As mentioned in Section I of this chapter, ethylidyne has been previously proposed as an intermediate in the hydrogenation of ethylene to ethane on a Pt(111) surface. However, the results of this work show that ethylidyne is less reactive with gas phase hydrogen atoms and bulk hydrogen toward hydrogenation than ethylene on Ni(111) which suggests that ethylidyne is not an intermediate in the hydrogenation of ethylene to ethane.

Surface hydrogen, bulk hydrogen and gas phase hydrogen atoms have very different reactivity with adsorbed hydrocarbons on Ni(111). Surface hydrogen does not hydrogenate adsorbed unsaturated hydrocarbons. Bulk hydrogen does hydrogenate adsorbed unsaturated hydrocarbons. Gas phase hydrogen atoms also hydrogenate unsaturated adsorbed hydrocarbons, but an additional process is observed, hydrogen abstraction. These differences in reactivities can be understood in terms of the geometry and energetics of the different forms of hydrogen.

V. References

1. H. Ibach, H. Hopster and B. Sexton, Appl. Phys. **14**, 21 (1977).
2. A. M. Boro and H. Ibach, J. Chem. Phys. **74**, 4194 (1981).
3. L. L. Kesmodel, L. H. Dubois and G. A. Somorjai, J. Chem. Phys. **70**, 2180, (1979).
4. H. Steininger, H. Ibach and S. Lehwald, Surf. Sci. **117**, 685 (1982).
5. J. R. Creighton and J. M. White, Surf. Sci. **129**, 327 (1983).
6. K. M. Ogle, J. R. Creighton, S. Akhter and J. M. White, Surf. Sci. **169**, 246 (1986).
7. M. A. Chesters and E. M. McCash, Surf. Sci. **187**, L639 (1987).
8. J. L. Gland, F. Zaera, D. A. Fischer, R. G. Gland and E. B. Kollin, Chem. Phys. Lett. **151**, 277 (1988).

9. S. B. Mohsin and M. Trenary, Chem. Phys. Lett. **154**, 511 (1989).

10. F. Zaera, J. Am. Chem. Soc. **111**, 4240, (1989).

11. W. G. Johnson, V. Buch and M. Trenary, J. Chem. Phys. **93**, 9167 (1990).

12. C. L. Pettiette-Hall, D. P. Land, R. T. McIver and J. C. Hemminger, J. Phys. Chem. **94**, 1948 (1990).

13. T. A. Land, T. Michely, R. J. Behm, J. C. Hemminger and G. Comsa, J. Chem. Phys. **97**, 6774 (1992).

14. U. Starke, A. Barbieri, N. Materer, M. A. Van Hove and G. A. Somorjai, Surf. Sci. **286**, 1 (1993).

15. W. Erley, Y. Li, D. P. Land and J. C. Hemminger, Surf. Sci. **301**, 177 (1994).

16. M. Yata and R. J. Madix, Surf. Sci. **328**, 171 (1995).

17. F. Zaera, Langmuir **12**, 88 (1996).

18. L. L. Kesmodel and J. A. Gates, Surf. Sci **111**, L747 (1981).

19. L. L. Kesmodel and J. A. Gates, J. Electron Spectrosc. Related Phenom. **29**, 307 (1983).

20. M. A. Barteau, J. Q. Broughton and D. Menzel, Appl. Surf. Sci. **19**, 92 (1984).

21. C. M. Greenlief, P. L. Radloff, X. L. Zhou and J. M. White, Surf. Sci. **191**, 93 (1987).

22. L. H. Dubois, D. G. Castner and G. A. Somorjai, J. Chem. Phys., **72**, 5234 (1980).

23. B. E. Koel, B. E. Bent and G. A. Somorjai, Surf. Sci. **146**, 211 (1984).

24. G. A. Somorjai, *Introduction to Surface Chemistry and Catalysis*, New York: Wiley, 1994.

25. T. S. Marinova and K. L. Kostov, Surf. Sci. **181**, 573 (1987).

26. F. Zaera and G. A. Somorjai, J. Am. Chem. Soc. **106**, 2288 (1984).

27. T. P. Beebe and J. T. Yates, J. Am. Chem. Soc. **108**, 663 (1986).

28. T. P. Beebe and J. T. Yates, J. Phys. Chem. **91**, 254 (1987).

29. M. P. Lapinski and J. G. Ekerdt, J. Phys. Chem. **96**, 5069 (1992).

30. D. K. Paul, T. P. Beebe, K. J. Uram and J. T. Yates, J. Am. Chem. Soc. **114**, 1949 (1992).

31. P. Cremer, C. Stanners, J. W. Niemantsverdriet, Y. R. Shen and G. A. Somorjai, Surf. Sci. **328**, 111 (1995).

32. D. Kang and A. Anderson, Surf. Sci. **155**, 639 (1985).

33. Z. Liu, X. Zhou, D. A. Buchanan, J. Kiss and J. White, J. Am. Chem. Soc. **114**, 2031 (1992).

34. R. G. Windham and B. E. Koel, J. Phys. Chem. **94**, 1489 (1990).

35. E. A. Carter and B. E. Koel, Surf. Sci. **226**, 339 (1990).

36. J. C. Bertolini and J. Rousseau, Surf Sci. **83**, 531 (1979).

37. S. P. Daley, Ph. D. Thesis, Massachusetts Institute of Technology, 1994.

38. S. Bao, P. Hofmann, K. M. Schindler, V. Fritzsche, A. M. Bradshaw, D. P. Woodruff, C. Casado and M. C. Asenio, Surf. Sci. **323**, 19 (1995).

39. T. Shimanouchi, Tables of Molecular Vibrational Frequencies, Natl. Std. Ref. Data Ser., Natl. Bur. Std. (US) **39** (1962).

40. H. Ibach and S. Lehwald, J. Vac. Sci. Technol. **18**, 625 (1981).

41. Q. Y. Yang, A. D. Johnson, K. J. Maynard and S. T. Ceyer, J. Am. Chem. Soc. **111**, 8748 (1989).

42. X. Y. Zhu and J. M. White, Catal. Lett. **1**, 247 (1988).

43. M. Xi and B. E. Bent, J. Phys. Chem. **97**, 4167 (1993).

44. C. Lutterloh, A. Schenk, J. Biener, B. Winter and J. Kuppers, Surf. Sci. **316**, L1039 (1994).

45. M. Xi and B. E. Bent, J. Vac. Sci. Technol. B **10**, 2440 (1992).

46. W. E. Jones, S. D. Macknight and L. Teng, Chemical Reviews **73**, 407 (1973).

47. P. D. Lightfoot and M. J. Pilling, J. Phys. Chem. **91**, 3373 (1987).

48. P. S. Monks, F. L. Nesbitt, W. A. Payne, M. Scanlon, L. J. Stief and D. E. Shallcross, J. Phys. Chem. **99**, 17151 (1995).

49. C. U. Morgan and K. J. White, J. Am. Chem. Soc. **92**, 3309 (1970).

50. K. Hiraoka, K. Matsunaga, T. Shoda and H. Takimoto, Chem. Phys. Lett. **197**, 292 (1992).

51. M. Iwasaki, K. Toriyama, H. Muto and K. Nunome, Chem. Phys. Lett. **56**, 494 (1978).

52. A. D. Johnson, Ph. D. Thesis, Massachusetts Institute of Technology, 1991.

53. S. L. Tang, Ph. D. Thesis, Massachusetts Institute of Technology, 1985.

54. M. B. Lee, Ph. D. Thesis, Massachusetts Institute of Technology, 1987.

55. J. D. Beckerle, Ph. D. Thesis, Massachusetts Institute of Technology, 1988.

56. E. Stenhagen, S Abrahamsson and F. W. McLafferty, *Atlas of Mass Spectral Data*, New York: Interscience Publishers, 1969.

57. A. Zangwill, *Physics at Surfaces*, Cambridge: University Press, 1988.

58. J. Xu, H. J. Jänsch and J. T. Yates, J. Vac. Sci. Technol. A **11**, 726 (1993).

59. Q. Y. Yang, Ph. D. Thesis, Massachusetts Institute of Technology, 1989.

60. A. D. Johnson, K. J. Maynard, S. P. Daley, Q. Y. Yang and S. T. Ceyer, Phys. Rev. Lett. **67**, 927 (1991).

61. A. D. Johnson, S. P. Daley, A. L. Utz and S. T. Ceyer, Science **257**, 223, (1992).

62. S. P. Daley, A. L. Utz, T. R. Trautman and S. T. Ceyer, J. Am. Chem. Soc. **116**, 6001, (1994).

63. K. J. Maynard, A. D. Johnson, S. P. Daley and S. T. Ceyer, Faraday Discuss. Chem. Soc. **91**, 437 (1991).

64. H. P. Steinruck, A. Winkler and K. D. Rendulic, Surf. Sci. **152/153**, 323 (1985).

65. J. E. Demuth, Surf. Sci. **69**, 365 (1977).

66. M. G. Sherman, D. P. Land, J. C. Hemminger and R. T. McIver, Chem. Phys. Lett. **137**, 298 (1987).

67. C. T. Rettmer, Phys. Rev. Lett. **69**, 383 (1992).

68. X. L. Zhou, M. E. Castro and J. M. White, Surf. Sci. **238**, 215 (1990).

69. X. L. Zhou and J. M. White, J. Phys. Chem. **96**, 7703 (1992).

70. C. Xu and B. E. Koel, Surf. Sci. Lett. **292**, L803 (1993).

71. X. L. Zhou, A. L. Schwaner and J. M. White, J. Am. Chem. Soc. **115**, 4309 (1993).

72. S. Lewald and H. Ibach, Surf. Sci. **89**, 425 (1979).

73. H. B. Schlegel, J. Phys. Chem. **86**, 4878 (1982).

CHAPTER II:
VIBRATIONAL IDENTIFICATION OF ETHYLIDYNE ON Ni(111)

I. Introduction

The previous chapter described four reactions which lead to ethylidyne ($-CCH_3$) formation on a Ni(111) surface: adsorbed ethylene, acetylene, and ethane with gas phase hydrogen atoms and adsorbed acetylene with hydrogen emerging from the bulk to the surface. This chapter focuses on the vibrational assignment of the electron energy loss spectral features to those of adsorbed ethylidyne. Four different isotopomers of adsorbed ethylidyne, $-CCH_3$, $-CCD_3$, $-^{13}C^{13}CH_3$, and $-^{13}C^{13}CD_3$, have been synthesized and their electron energy loss spectra have been measured and analyzed.

Several approaches are used in the assignment of the spectra to ethylidyne. First, each vibrational feature is compared to a list of characteristic vibrational frequencies, known as group frequencies. An extensive library of group frequencies exists for hydrocarbons.[1] Second, the observed frequencies of the electron energy loss features are directly compared to those of vibrational spectra of gas phase and organometallic molecules which contain an ethylidyne moiety and whose structures have been determined by other techniques such as NMR or x-ray crystallography. Third, the shifts in frequency of the vibrational features upon isotopic substitution have been carefully examined for each mode. Spectroscopists use this technique extensively to assign vibrational modes to spectral features because isotopic substitution changes the reduced mass without affecting the force constant and therefore, the frequency of the mode shifts in a predictable way. Finally, a computational normal modes analysis of the spectra using a reasonable geometry for ethylidyne has been carried out. The calculated frequencies have been compared directly to the observed vibrational features, and the force constants in the calculation which yield the best fit for the frequencies of the vibrational features are compared to previous normal mode calculations of molecules with an ethylidyne moiety.

In the discussion of the assignment of the electron energy loss spectral features to the modes of ethylidyne, this chapter directly addresses two interesting aspects observed in the

assignment of the spectral features to ethylidyne. The first is an unusual shift of the carbon-carbon bond stretching frequency upon isotopic labeling of the hydrogen atoms. Counter to expectation, this mode is observed to shift upward in frequency upon deuteration. The second interesting phenomenon is the intensity of the symmetric CH_3 deformation. While the symmetric CH_3 deformation mode is dipole active in hydrogen unlabeled ethylidyne, it is not dipole active in deuterated ethylidyne. These peculiarities have also been observed previously in vibrational spectra of ethylidyne adsorbed on other metal surfaces[2,3] and in vibrational spectra of an organometallic ethylidyne species.[4]

After the assignment of each of the vibrational features, the discussion addresses the symmetry of adsorbed ethylidyne. The symmetry of ethylidyne adsorbed on Ni(111) is revealed through analysis of the dipole activity of the electron energy loss features. The symmetry of ethylidyne in turn leads to determination of its adsorption site on the Ni(111) surface. The adsorption site is shown to be identical to that previously reported for ethylidyne bound to Rh(111) and Pt(111) surfaces.[5,6]

To confirm further the assignment of the spectra to an adsorbed ethylidyne species, the observed vibrational spectra are shown to be inconsistent with any other adsorbed C_2 hydrocarbon. Special attention has been given to the ethylidene ($-CHCH_3$) hydrocarbon fragment. Its structure is very similar to that of ethylidyne and therefore, their vibrational spectra should be similar. Ethylidyne and ethylidene adsorbed on Pt(111) have been confused in earlier work.[7-9]

II. Experimental

The apparatus utilized in the experiments has been described in detail elsewhere.[10-12] A brief overview of the apparatus is presented in Chapter I.

II.A. High resolution electron energy loss spectroscopy

High resolution electron energy loss spectroscopy is a vibrational spectroscopy that utilizes the interaction of low energy electrons (less than 10 eV incident energy) with a surface. A monoenergetic beam of electrons is directed at the surface while the number of electrons scattering from the surface is measured as a function of the scattered electron's energy. Most of the electron scatter elastically, but some of the electrons scatter inelastically. The electrons that scatter inelastically lose their energy to vibrational modes of adsorbates at the surface. A plot of the number of scattered electrons versus the difference between their energy and that of the incident electrons results in a vibrational spectrum of the adsorbate.

The electron energy loss spectrometer consists of two 127° cylindrical deflectors for the incident electron monochromater and scattered electron energy analyzer. When measuring the electrons scattered in the specular direction, the incident and scattered electron beams are 60° from the normal angle to the surface. Electrons which are scattered away from the specular direction are detected by rotating the crystal about an axis which is perpendicular to the scattering plane. Rotation of the crystal not only affects the detection angle, but also affects the incident angle. The incident electron beam if formed by the electron gun of the spectrometer. The bias between the filament of the electron gun and the crystal defines the impact energy of the incident electrons. For all the spectra shown in this thesis, the electron gun filament has been held at ground potential and the crystal has been held at 6.5 V. The typical step size used for the analyzer pass energy is 2 mV, but in some spectra a step size of 1 mV has been used so as to better resolve some features and to better define the energy of the features.

The vibrational frequencies of the features indicated in the spectra and tables shown in this chapter represent the average value of the observed frequencies from 9 to 42 separate spectra. However, only the frequencies of the vibrational features which have been resolved are included into the average and therefore, because some of the features are not always

resolved, a few of the averages only include 2 to 4 observations. The uncertainties of the frequencies indicated in Tables 2.3 and 2.5 represent the 90% confidence limits. The modes which have not been resolved in more nine separate measurements are indicated. The resolution reported in the electron energy loss spectra in this work are measured as the full width of energy of the elastic feature at half its maximum intensity.

II.B. Chemisorbed Ethylene

Ethylene chemisorbed on Ni(111) is produced by exposure of the surface to a molecular beam of 2% ethylene in argon. Argon is used as a diluent so that the time of exposure can be more precisely controlled (typical exposure times of tens of seconds rather than tenths of seconds). The temperature of the crystal during exposure is maintained at 80 K. Argon does not adsorb to the surface at this temperature.[12] In all experiments described in this chapter the saturation coverage of ethylene, 0.25 ML,[13] was employed. Saturation coverage was determined by an ethylene exposure above which no increase in the carbon Auger signal was observed.

Isotopically unlabeled ethylene was obtained from MG Industries at a purity of 99.95%. C_2D_4 and $^{13}C_2H_4$ were obtained from Cambridge Isotope Laboratories at purities of 98% and 99% respectively, with partially unlabeled ethylene as the major impurity.

II.C. Gas Phase Hydrogen Atoms

Hydrogen atoms are formed by dissociation of H_2 over a hot tungsten filament as discussed in Chapter I. In all experiments described in this chapter, the H_2 pressure was held at 5×10^{-6} torr during the H atom exposure.

III. Results and Discussion

In this section, ethylidyne is identified as the adsorbed product of the reaction of chemisorbed ethylene and gas phase hydrogen atoms by analysis of its vibrational spectrum measured by high resolution electron energy loss spectroscopy. The analysis involves a combination of several approaches for assigning the electron energy loss features to the vibrational modes of ethylidyne. The section begins with a brief description of these approaches and is followed by a presentation of the spectral data and the results of a normal modes analysis. Then, the assignment of each vibrational feature will be discussed in terms of the ethylidyne interpretation. After each vibrational feature has been assigned to a mode of ethylidyne, the adsorption symmetry of ethylidyne is discussed and is followed by a discussion of the adsorption site. Finally, as further support for the identity of the reaction product as ethylidyne, the assignment of the spectra to other possible reaction products will be considered. This discussion will conclude that these hydrocarbon and hydrocarbon fragments cannot yield the observed vibrational spectra.

III.A. Interpreting Electron Energy Loss Spectra

Several approaches enable the assignment of adsorbed hydrocarbon vibrational features measured by electron energy loss spectroscopy: 1) comparison of the observed frequencies to group frequencies, 2) comparison of the spectra to vibrational spectra of similar compounds, 3) determination of the frequency shifts due to isotopic labeling of adsorbates, 4) identification of the dipole active modes and, 5) comparison of the observed frequencies to calculated normal modes frequencies. All of the above approaches have been used to assign vibrational features of the spectra in this chapter, so a brief description of each is appropriate.

III.A.1. Group frequencies

Empirically, it has been observed that certain parts of molecules often have characteristic vibrational frequencies. A reasonable first step in making spectral assignments is to assign the observed vibrational features using these characteristic vibrational frequencies, referred to as group frequencies. Almost all organic chemistry books have a table listing group frequencies in the IR assignment section. Table 2.1 summarizes group frequencies observed for hydrocarbon groups. The observed frequencies will not always exactly match group frequencies because coupling of the mode with other modes of the molecule can significantly alter the observed frequency. Therefore, comparison of the observed frequency to a group frequencies alone cannot establish an assignment of a spectral features to a specific mode, but it can provide a reasonable hypothesis for the identity of the observed feature.

Mode	Frequency Range
C-H stretches	
Acetylinic C-H	3310 - 3350
Ethylenic or Aromatic C-H	3000 - 3120
Saturated C-H	2850 - 3030
C-H bends	
asym. CH_3 def.	1380 - 1460
sym. CH_3 def.	1280 - 1420
CH_3 rock	900 - 1100
CH_2 sciss	1420 - 1470
CH_2 rock	750 - 1050
CH_2 wag	1070 - 1350
C-C stretches	
C-C triple bond	2100 - 2200
C-C double bond	1620 - 1680
C-C single bond	880 - 1000

Table 2.1. Characteristic frequencies in cm^{-1} of hydrocarbon groups.

III.A.2. Vibrational spectra of similar compounds

Another means of assigning vibrational features of adsorbed species is direct comparison of their spectra to those of structurally similar gas phase or organometallic molecules whose structures can be additionally supported by the results of x-ray crystallography or NMR. Table 2.2 lists the vibrational frequencies for a few molecules which have an ethylidyne moiety: $HC\text{-}CCH_3$, $Cl_3\text{-}CCH_3$, $Br_3\text{-}CCH_3$, and $(CO)_9Co_3(\text{-}CCH_3)$.[1,4,14]

Mode	$HC\text{-}CCH_3$	$Cl_3\text{-}CCH_3$	$Br_3\text{-}CCH_3$	$(CO)_9Co_3\text{-}CCH_3$
asym CH_3 str	3008 (2235)	3009 (2259)	2993 (2241)	2930 (2192)
sym CH_3 str	2918 (2110)	2943 (2130)	2938 (2116)	2888
asym CH_3 def	1452 (1048)	1444 (1050)	1432 (1038)	1420 (1031)
sym CH_3 def	1382 (1115)	1384 (1142)	1373 (1110)	1356 (1002)
C-C str	931 (830)	1071 (975)	1045 (953)	1163 (1182)
CH_3 rock	1053 (835)	1079 (914)	1064 (883)	1004 (828)
asym C-X str		711 (654)	628 (583)	555 (536)
sym. C-X str		525 (504)	408 (388)	401 (393)
	Ref. 1	Ref. 14	Ref. 14	Ref. 4

Table 2.2. Observed frequencies in cm^{-1} for molecules with an ethylidyne moiety. Numbers in parentheses are values for the deuterated species.

III.A.3. Frequency shifts upon isotopic labeling

Frequency shifts upon isotopic labeling also help to assign vibrational features. Using the harmonic oscillator approximation, the frequency of a vibration is given by the equation

$$\upsilon = \sqrt{\frac{k}{\mu}}, \qquad (2.1)$$

where υ is the frequency of the vibration, k is the force constant, and μ is the reduced mass. Because isotopic substitution changes the reduced mass but not the force constant, the frequency of the mode changes in a predictable way. By observing this frequency shift in a vibrational mode upon isotopic substitution, one can determine whether the isotopically labeled atom is involved in that mode. For example, if a vibrational frequency shifts upon isotopic labeling of the hydrogen atoms, then the vibrational mode involves hydrogen atom displacement.

Since carbon is much more massive than hydrogen, a good approximation for the change in the reduced mass of a vibration involving a C-H motion is to consider only the change in the mass of the hydrogen atom. Ratios of the vibrational frequencies of hydrogen bending and stretching modes upon deuteration are then given by the equation

$$\frac{\upsilon_{C-H}}{\upsilon_{C-D}} = \sqrt{\frac{k/1}{k/2}} = \sqrt{\frac{2}{1}} = 1.41. \qquad (2.2)$$

However, ratios of the frequencies of the C-H versus C-D vibrations are rarely observed to be as large as 1.41. Shifts in frequencies upon deuteration are usually smaller because of the anharmonicity of the vibrational mode and because the approximation used in Equation 2.2 is that of a motionless carbon atom. Observed shifts in frequencies upon deuteration are typically closer to a ratio of 1.35.[15]

Another caveat must be noted. The preceding discussion has assumed that isotopic substitution does not affect the normal modes of the molecule or adsorbate. However, a change in the mass of the atoms of the molecule or adsorbate may also change the normal modes of the molecule and therefore, the expected or calculated shifts in frequencies upon isotopic labeling are sometimes not observed. Therefore, some care must be exercised when interpreting shifts upon isotopic substitution. However, more often than not, the observed shifts in the frequencies upon isotopic labeling occur as expected and therefore, determination of these shifts in frequency is helpful in assigning the vibrational features to vibrational modes.

III.A.4. Dipole activity of the features

4) Determination of dipole activity is also helpful in assigning vibrational features measured by high resolution electron energy loss spectroscopy because only totally symmetric modes are dipole allowed. A detailed discussion of dipole activity appears in Ibach,[15] but a brief overview follows.

Dipole interaction involves the interaction of the electron with a dynamic dipole moment of an adsorbate. Only transitions to totally symmetric modes are dipole allowed as illustrated by the following equation:

$$I \propto \left\langle \Psi_{fin} \middle| \mu_z \middle| \Psi_{init} \right\rangle , \qquad (2.3)$$

where I is the dipole intensity of the transition, Ψ_{init} and Ψ_{fin} are the wavefunctions of the initial and final states respectively, and μ_z is component of the dynamic dipole operator perpendicular to the surface. Note that only the perpendicular component of the dynamic dipole moment operator contributes to the dipole activity. The parallel components do not contribute because any dipole moment parallel to the surface is effectively canceled by its image charge in the metal crystal and therefore, an impinging electron does not see a net dipole in the parallel direction. The perpendicular dipole moment operator μ_z has the same symmetry as translation in the z direction. Inspection of character tables shows that in all possible point group symmetries for adsorbates, z translation is totally symmetric, and thus μ_z is totally symmetric. The wave function, Ψ_{init}, is also totally symmetric assuming that it is the ground vibrational state. Practically all adsorbates are in the ground vibrational state due to the low temperatures at which electron energy loss spectra are measured. Therefore, unless Ψ_{fin} is totally symmetric, the integrand in Equation 2.3 is odd and the integral equals zero. The absence of any dipole transition intensity for antisymmetric modes is what is referred to as the 'surface selection rule' - only totally symmetric transitions are dipole allowed. Loss features which result from a dipolar interaction are said to be dipole active. Since only totally symmetric modes are dipole allowed, observation of dipole activity can be used to determine whether the mode is symmetric. Determination of the symmetry of the mode which gives rise to a loss feature assists in the assignment of the feature.

Not all electron energy loss features result from dipolar interaction. Impact scattering is another energy loss mechanism. The impact scattering mechanism does not have a strict selection rule allowing only transitions to symmetric modes. Transitions to antisymmetric

modes are also observed with the electron impact mechanism. Therefore, in order to use dipole activity for the assignment of symmetric modes, one must be able to differentiate between loss features which arise from a dipolar mechanism and those which arise from an impact scattering mechanism.

The dipole activity of a loss feature is identified by comparison of spectra measured in the specular direction to those measured away from the specular direction. Modes which decrease dramatically in intensity as the angle of detection is moved away from the specular direction are the dipole active modes. The decrease in intensity results from the long range nature of a dipolar interaction. While the electrostatic potential of a surface is corrugated very near the surface, it smoothes out rapidly with increasing distance from the surface. Electrons which scatter from the surface at long range encounter a smooth potential surface and therefore, are favored to scatter in the specular direction. Electrons which penetrate closer to the surface as they must for the short range electron impact energy loss mechanism, sample a much more corrugated electrostatic potential which causes them to scatter in all directions. Therefore, while electron energy loss features arising from a dipolar interaction are most intense in spectra measured at the specular angle and dramatically lose intensity as the detection angle is moved away from the specular angle, the intensities of the loss features arising from an impact scattering mechanism do not have a large dependence on the detection angle.

Although all dipole active features are totally symmetric, the converse in not true. All totally symmetric features are not dipole active. While symmetry arguments can show that the integral in Equation 2.3, which is proportional to the intensity of a mode excited by a dipolar interaction, is zero by inspection, they cannot determine the magnitude of a non-zero integral. A mode which is dipole allowed is not necessarily dipole active because the magnitude of the integral may be very small. Although we can assign dipole active modes as symmetric features, we cannot use the lack of dipole activity to assign features as

antisymmetric modes. Further information about the dynamic dipole moment of the mode would be necessary to do this.

III.A.5. Normal modes analysis

5) The last technique used in assigning vibrational features to modes of an adsorbate is comparison of the observed frequencies to those calculated in a normal modes analysis. A computational normal modes analysis of the vibrational features has been carried out using a ethylidyne geometry and potential. In the calculation, the potential of the molecule is defined in terms of force constants within an internal coordinate system. Internal coordinates are defined as each bond stretch and bond bend of the molecule. Internal coordinates are used because force constants are often reported in the literature as internal force constants. The potential consists of harmonic force constants for each internal coordinate as well as harmonic coupling between the internal coordinates that are significantly coupled. Equation 2.4 defines the potential energy:

$$V = \sum_{i}^{3N} f_{ii}(\Delta x_i)^2 + \sum_{i \neq j}^{3N} \frac{f_{ij}}{2} \Delta x_i \Delta x_j , \qquad (2.4)$$

where V is the potential energy, f_{ii} is the harmonic force constant and Δx is the displacement from equilibrium for coordinate i, and f_{ij} is the harmonic coupling term for internal coordinates i and j. Many f_{ij} are set equal to zero because the coupling of the modes is not expected to be significant. It should be noted that the units of the force constant are dependent on the type of coordinate. For example, a force constant for a bond stretching mode is in units of energy/displacement squared, but a force constant for a bending mode is in units of energy/radians squared (or simply energy since radians are unitless). Some conventions divide the bending force constants by the bond lengths of the two adjacent bonds so that stretching and bending force constants have the same units.[16] This convention is not

used here because the literature values for the force constants to which the calculated force constants are compared did not use this convention.[4,17,18]

With the potential energy so defined, the force constant matrix is generated numerically in cartesian coordinates.

$$f^{cc}_{ij} = \frac{\partial^2 V}{\partial x_i \partial x_j}, \qquad (2.5)$$

where f^{cc}_{ij} is the matrix element, V is the potential, x_i is the cartesian coordinate (x, y, or z).

The mass weighted force constant matrix is calculated from the force constant matrix by dividing each matrix element by the square root of the mass of the atoms corresponding to that matrix element:

$$f^{mw}_{ij} = \frac{f^{cc}_{ij}}{\sqrt{m_i m_j}}, \qquad (2.6)$$

where f_{ij} is the cartesian coordinate force constant matrix element, f^{mw}_{ij} is the mass weighted cartesian coordinate force constant matrix element, and m_i and m_j are the masses of the atoms associated with cartesian coordinates i and j.

The eigenvalues and eigenvectors are then calculated by diagonalization of the mass weighted force constant matrix[19] using the Householder method.[20] The diagonal elements of the diagonalized matrix are the eigenvalues (harmonic frequencies). The normal coordinates are the coordinate system for which the mass weighted force constant matrix is diagonal and therefore, are equal to the eigenvectors.

The normal mode frequencies are also calculated for the isotopically labeled species. Since isotopic labeling does not affect the force constants, the normal mode frequencies can be calculated by simply changing the mass of the atoms. Inclusion of the isotopically labeled species in the analysis helps to better determine the force constants of the molecule because

the number of observed frequencies used to fit the force constants increases but the number of force constants remains the same.

The force constants initially entered into the calculation are reasonable guesses, but then they are varied by use of a nonlinear least squares fitting routine[20] to make the calculated frequencies better fit the observed frequencies. The derivative of the difference between the calculated frequencies and the observed frequencies with respect to each force constant utilized in the normal modes calculation is numerically calculated. The least squares fitting routine uses these derivatives to decide how to vary the force constants such that the differences between the calculated frequencies and the observed frequencies is lowered. The force constants are sequentially varied until the difference between the calculated frequencies and the observed frequencies decreases by less than 0.1%. With twelve force constants as fitting parameters and only 21 observed vibrational frequencies as data points, a close fit could probably be made independent of the assignment of the modes. However, the calculated force constants must also make physical sense. For example, a negative value for a bond stretching or bending force constant is not realistic, nor is a bond stretching force constant which is double the typical values for force constants. Therefore, the true test of the assignment of the features is to compare the best fit force constants to literature values for force constants of molecules with similar geometry and bonding.

III.B. Electron Energy Loss Spectra

Products of the reaction of gas phase atomic hydrogen with chemisorbed ethylene are characterized by high resolution electron energy loss spectroscopy. Figure 2.1 shows spectra measured after a two minute exposure of 0.25 ML C_2H_4 to H atoms. The temperature prior to the H atom exposure was 80 K. The temperature of the crystal increased to 120 K during the H atom exposure, but immediately cooled to 80 K upon completion of the exposure. The electron energy loss spectra were measured at a crystal temperature of 80 K.

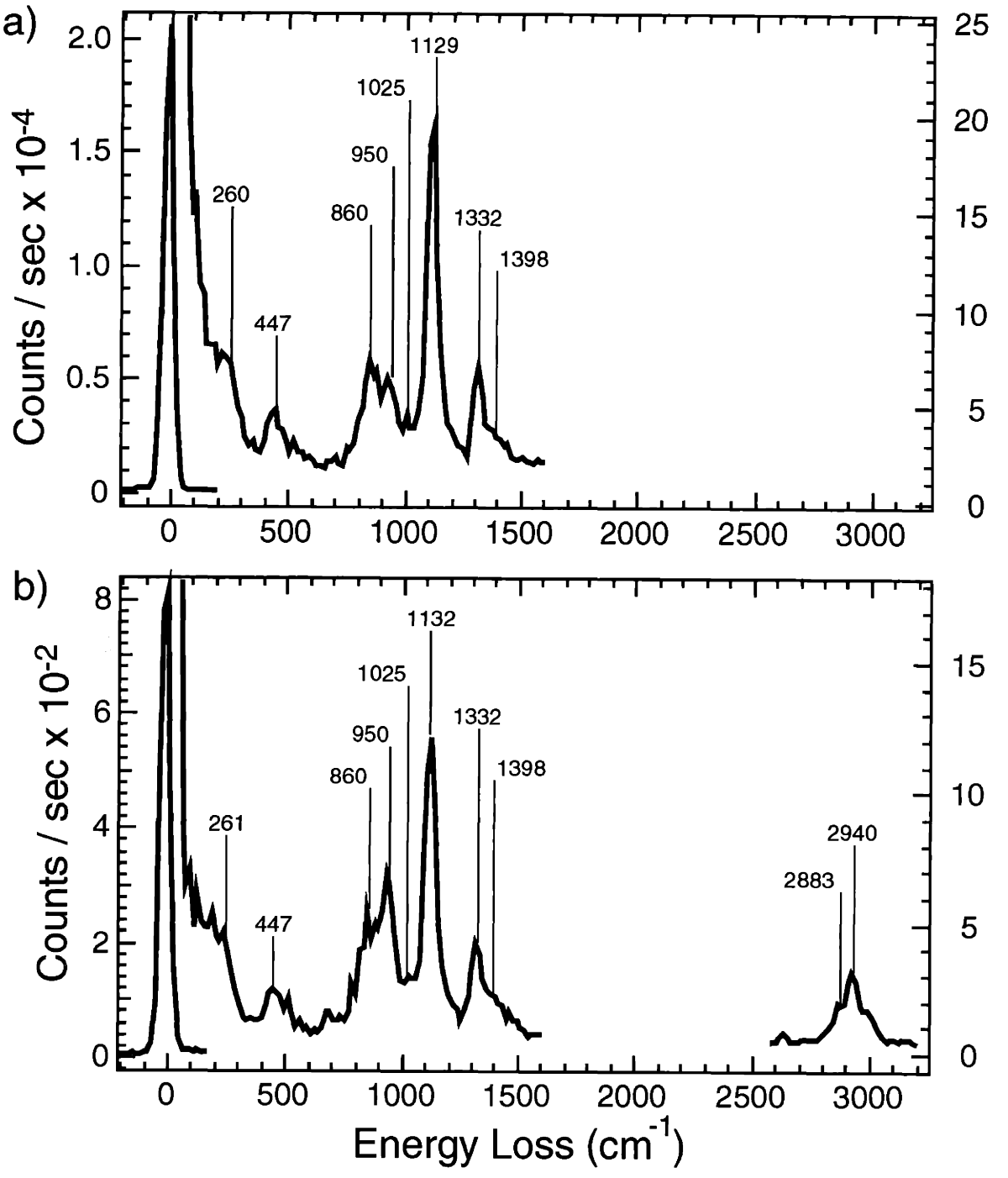

Figure 2.1. Electron energy loss spectra measured after a two minute exposure of 0.25 ML ethylene to H atoms. **a)** Spectrum measured on specular with a resolution of 47 cm^{-1} **b)** Spectrum measured 10° off specular with a resolution of 44 cm^{-1}.

Figure 2.2 shows electron energy loss spectra of the same experiment as shown in Figure 2.1, except that the crystal is heated to 300 K immediately after the H atom exposure in order to remove the bulk hydrogen which is produced by exposure to H atoms,[21,22] as discussed in Chapter I. The removal of bulk H aids in the identification of the hydrocarbon adsorbate features by ensuring that a bulk hydrogen vibrational feature does not mask some of the adsorbate features. Chapter I shows that the adsorbed hydrocarbon reaction product is stable during heating to 300 K. No new features are seen in the spectra after heating the surface to 300 K, but the elastic feature and some of the loss features, ones which will be shown to be dipole active, have increased in intensity in the spectra measured in the specular direction. Therefore, heating the crystal to 300 K aids the assignment process by making the dipole active features easier to identify. The increase in intensities can be understood in terms of ordering of the adsorbates. At higher temperatures, the adsorbate can more easily relax into the lowest energy configuration, which may involve lateral migration to produce an ordered overlayer. The electrostatic potential of an ordered surface is smoother than that of an unordered surface and therefore, the electrons are favored to scatter in directions closer to the specular direction. Higher intensity features from more ordered systems have been observed previously in this lab. For example, the electron energy loss spectra of chemisorbed ethylene exhibit much more intense elastic and dipole active features at saturation coverage which yields a well ordered overlayer than coverages slightly below saturation which are less ordered. Because of the enhanced intensities of the dipole active loss features and the absence of complications from bulk hydrogen features, this chapter concentrates on the analysis of the reaction product spectra measured after heating the surface temperature to 300 K.

As mentioned previously, isotopic substitution helps in assigning the vibrational spectral features. To obtain a completely deuterated reaction product (C_xD_y), deuterated chemisorbed ethylene (C_2D_4) is exposed to gas phase deuterium atoms. Figure 2.3 shows high resolution electron energy loss spectra measured after a two minute exposure of 0.25 ML

C_2D_4 to D atoms. The crystal is heated to 300 K after the D atom exposure and before the electron energy loss spectra are measured at a crystal temperature of 80 K.

^{13}C-ethylene is utilized as a reactant to yield a product with labeled carbon atoms ($^{13}C_xH_y$). Figure 2.4 shows spectra measured after a two minute exposure of 0.25 ML $^{13}C_2H_4$ to H atoms. The crystal is subsequently heated to 300 K and immediately cooled to 80 K, the temperature at which the electron energy loss spectra are measured.

Ideally, one would expose $^{13}C_2D_4$ to deuterium atoms to obtain a reaction product with isotopic labels on both carbon and hydrogen atoms. Unfortunately, the cost of this isotopically labeled ethylene is prohibitively high. However, as discussed in Chapter I, reaction of C_2H_4 with deuterium atoms can yield a completely deuterated reaction product through hydrogen-deuterium exchange. Therefore, a doubly labeled reaction product ($^{13}C_xD_y$) is obtained from the reaction of isotopically carbon labeled ethylene ($^{13}C_2H_4$) with gas phase deuterium atoms. Figure 2.5 shows the electron energy loss spectra measured after a four minute exposure of 0.25 ML $^{13}C_2H_4$ to D atoms. The crystal was heated to 300 K after the D atom exposure and subsequently cooled to 80 K, the temperature at which the spectra are measured. A longer D atom exposure is employed to ensure complete hydrogen/deuterium exchange, yielding a reaction product with no unlabeled hydrogen atoms. Complete exchange is confirmed by the absence of any C-H stretching or bending modes. The results in Chapter I show that a four minute exposure to H (D) atoms does not significantly alter the coverage of the reaction product relative to a two minute exposure. Therefore, these spectra can be directly compared to the spectra of the other isotopomers of the reaction product shown in Figures 2.2, 2.3, and 2.4.

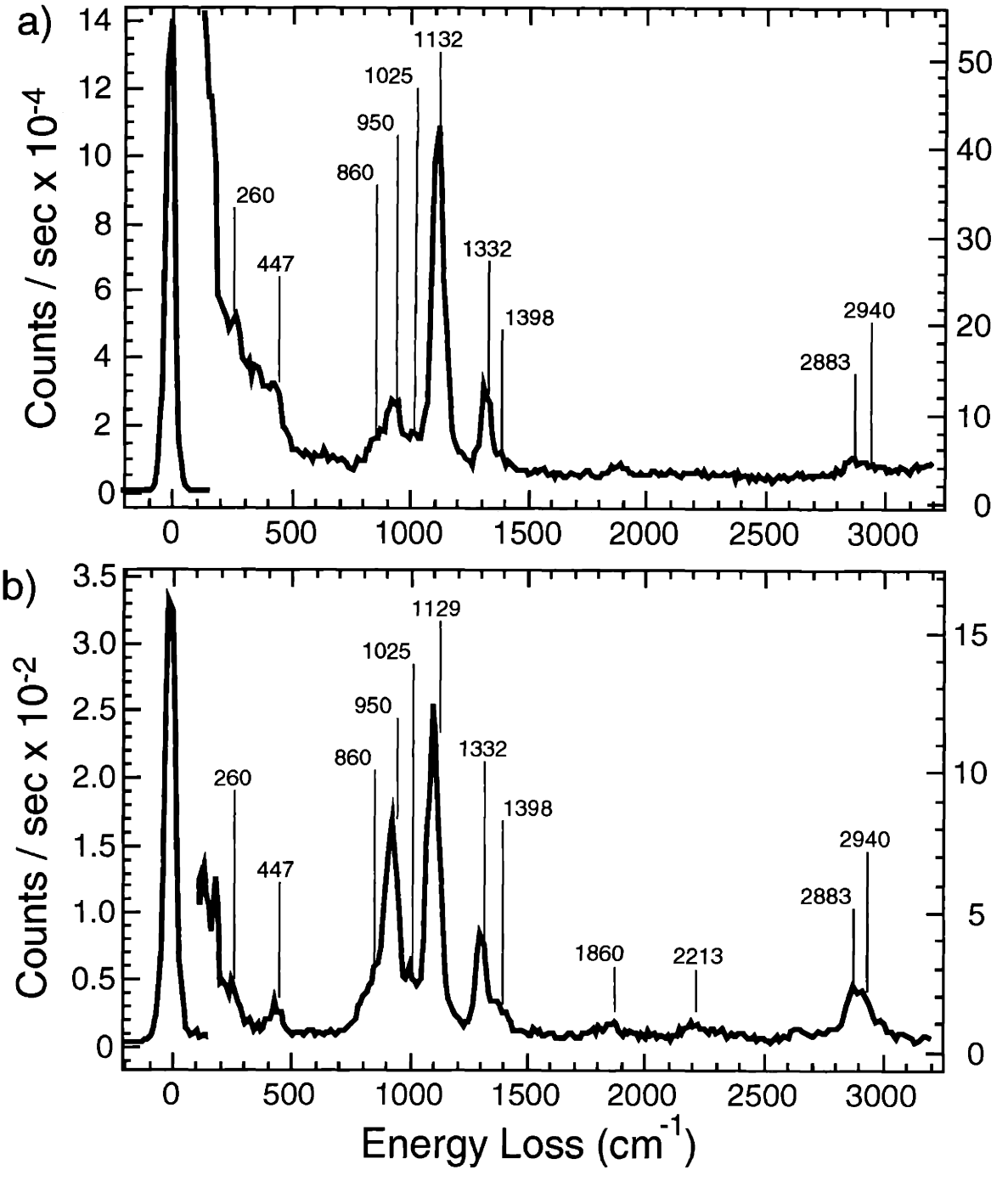

Figure 2.2. Electron energy loss spectra measured after a two minute exposure of 0.25 ML ethylene to H atoms and heating the crystal to 300 K following H atom exposure. **a)** Spectrum measured on specular with a resolution of 44 cm^{-1} **b)** Spectrum measured 10° off specular with a resolution of 50 cm^{-1}.

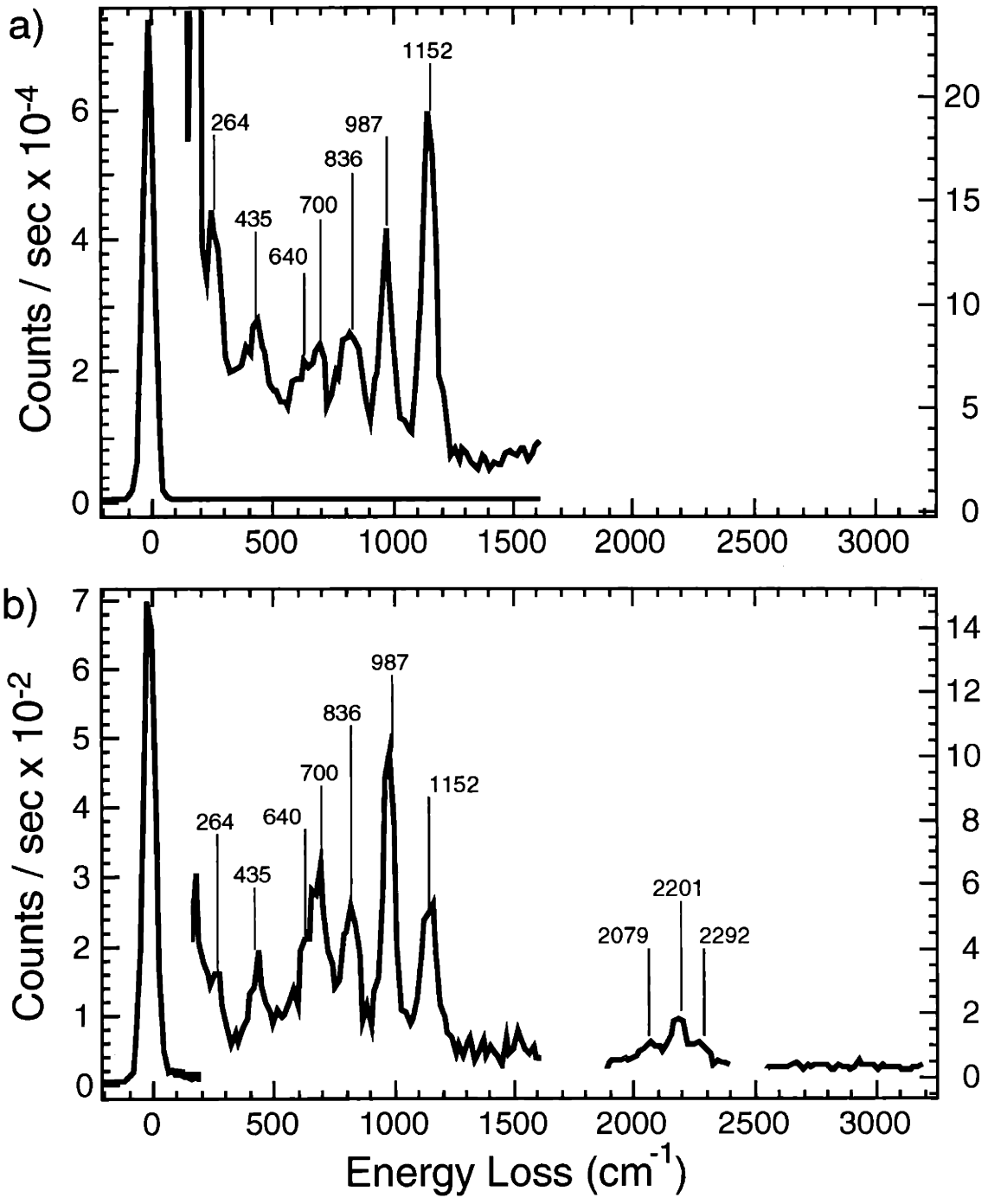

Figure 2.3. Electron energy loss spectra measured after a two minute exposure of 0.25 ML deuterated ethylene to D atoms and heating the crystal to 300 K following H atom exposure. **a)** Spectrum measured on specular with a resolution of 51 cm^{-1} **b)** Spectrum measured 10° off specular with a resolution of 55 cm^{-1}.

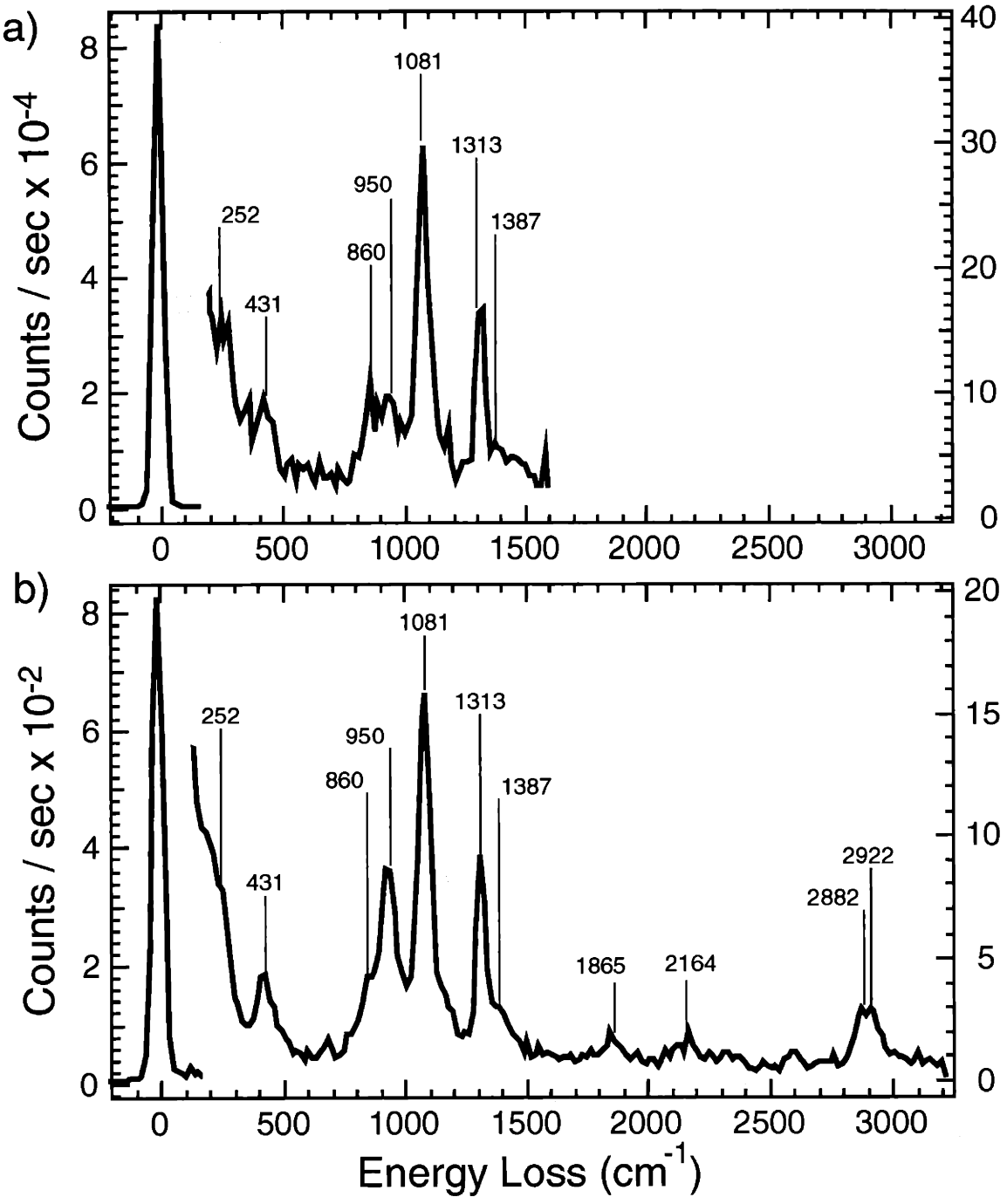

Figure 2.4. Electron energy loss spectra measured after a two minute exposure of 0.25 ML $^{13}C_2H_4$ to H atoms and heating the crystal to 300 K following H atom exposure. **a)** Spectrum measured on specular with a resolution of 46 cm^{-1} **b)** Spectrum measured 10° off specular with a resolution of 49 cm^{-1}.

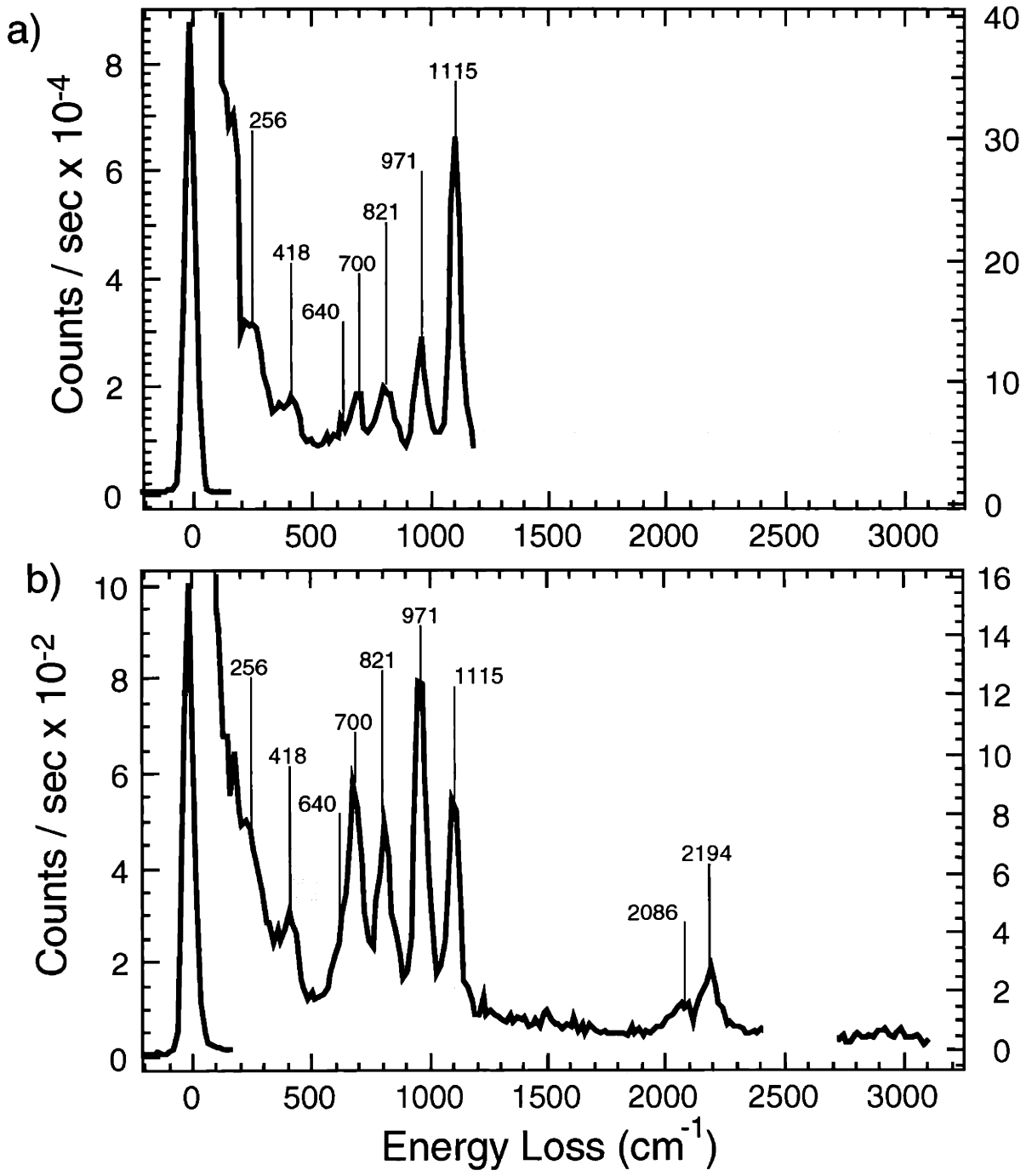

Figure 2.5. Electron energy loss spectra measured after a four minute exposure of 0.25 ML $^{13}C_2H_4$ to D atoms and heating the crystal to 300 K following H atom exposure. **a)** Spectrum measured on specular with a resolution of 47 cm^{-1}. **b)** Spectrum measured 10° off specular with a resolution of 48 cm^{-1}.

The atomic hydrogen exposures in these experiments also produce surface bound hydrogen in addition to bulk hydrogen.[21,22] Some of the features in Figures 2.2, 2.3, 2.4 and 2.5 are possibly vibrational modes of adsorbed surface hydrogen, because heating the surface to 300 K does not remove all of the surface bound hydrogen.[22,23] Figure 2.6 shows the vibrational spectrum of 1 ML surface bound hydrogen. The spectrum shows vibrational features at 950 cm^{-1} and 1160 cm^{-1} which are similar in frequency to the 950 cm^{-1} and 1129 cm^{-1} features observed in Figure 2.2 and to the 950 cm^{-1} and 1081 cm^{-1} features in Figure 2.4. The 950 cm^{-1} and 1160 cm^{-1} features in the surface hydrogen spectra are the antisymmetric and symmetric vibrational modes of surface bound hydrogen respectively.[24] Neither feature is dipole active. The modes at 1129 cm^{-1} and 1081 cm^{-1} in the spectra of the reaction product shown in Figures 2.2 and 2.4, respectively, are dipole active which suggests that these features are not a surface hydrogen mode. Furthermore, the intensity of the

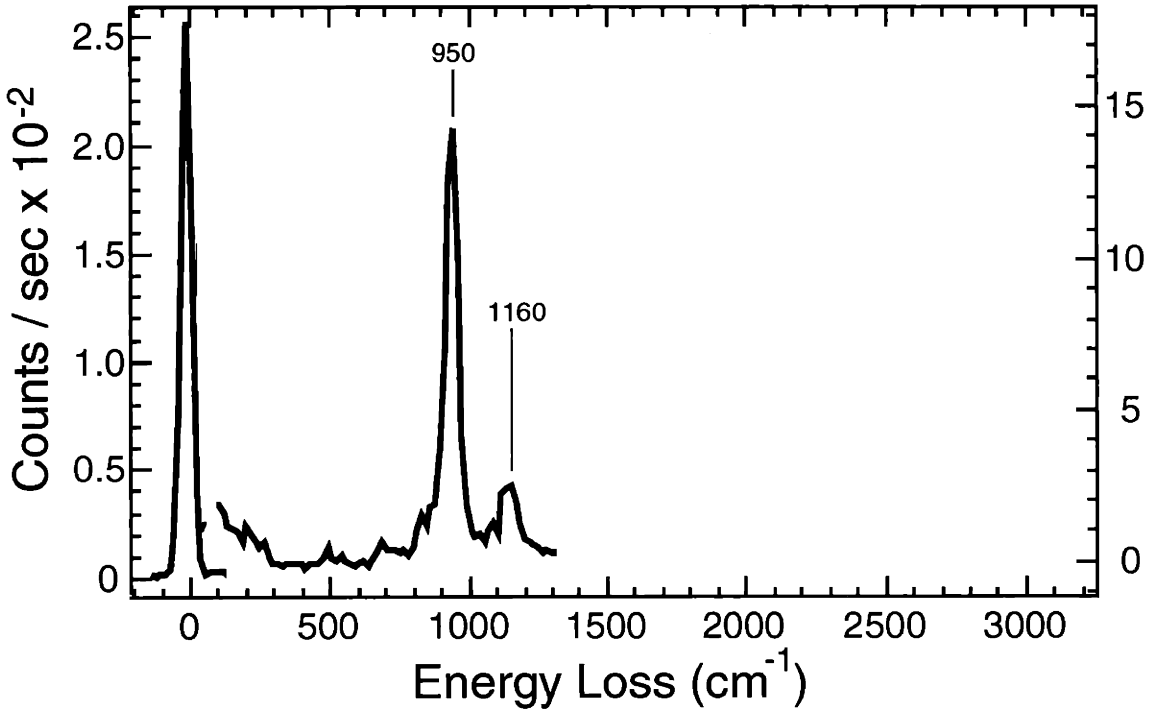

Figure 2.6. Electron energy loss spectra of 1.0 ML surface bound hydrogen measured 10° off specular with a resolution of 43 cm^{-1} .

symmetric mode of surface bound hydrogen is much lower than that of the antisymmetric mode at an incident electron energy of 6.5 eV. The features at 1129 cm^{-1} and 1081 cm^{-1} in the reaction product spectra are very intense. Therefore, the feature at 950 cm^{-1} in the spectra of the reaction product is assigned as a vibrational mode of surface bound hydrogen, while the features at 1129 cm^{-1} and 1081 cm^{-1} are not. These feature must arise from vibrational modes of the adsorbed hydrocarbon product of the reaction of adsorbed ethylene and H atoms.

Following similar logic, the 700 cm^{-1} feature in the deuterated reaction product species in Figures 2.3 and 2.5 is assigned to the antisymmetric stretching mode of surface bound deuterium. Figure 2.7 shows the spectrum of 1 ML surface bound deuterium. The antisymmetric and symmetric modes of surface deuterium are observed at 700 and 840 cm^{-1} respectively.[24] The feature seen at approximately 840 cm^{-1} in Figures 2.3 and 2.5 is too

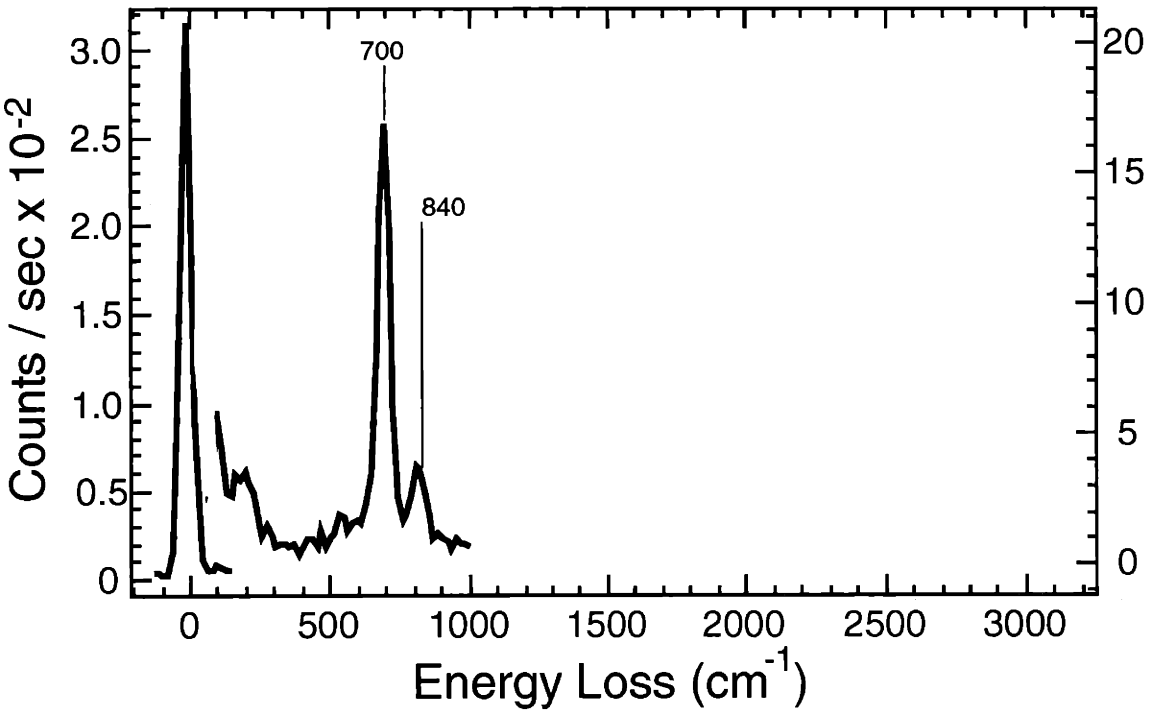

Figure 2.7. Electron energy loss spectra of 1.0 ML surface bound deuterium measured 10° off specular with a resolution of 44 cm^{-1} .

intense relative to the 700 cm^{-1} feature to be assigned solely to the Ni-D symmetric vibrational mode. This feature must also be a vibrational mode of the adsorbed hydrocarbon reaction product.

Table 2.3 summarizes the observed vibrational frequencies of the adsorbed reaction product of H atoms and adsorbed ethylene. This table includes almost every feature observed in the vibrational spectra of the four different isotopomers. Only features assigned to surface hydrogen or deuterium and a low intensity feature seen at approximately 860 cm^{-1} in Figures 2.2 and 2.4 (unlabeled hydrogen species) and 640 cm^{-1} in Figures 2.3 and 2.5 (deuterated species) have been omitted. The 860 cm^{-1} and 640 cm^{-1} features have been accounted for in Section III.D of Chapter I. The following section will show that all of the frequencies of the features listed in Table 2.3 are consistent with the vibrational modes of ethylidyne.

Mode	C_2H_3	$^{13}C_2H_3$	C_2D_3	$^{13}C_2D_3$
sym C-Ni str	260 ± 16	252 ± 34‡	264 ± 37	256 ± 25‡
asym C-Ni str	447 ± 13	431 ± 16	435 ± 39	418 ± 12
CH_3 rock	1025 ± 16	obscured	836 ± 34	821 ± 12
C-C str	1129 ± 21	1081 ± 21	1152 ± 34	1115 ± 7
sym CH_3 def	1332 ± 19	1313 ± 25	987 ± 26	971 ± 5
asym CH_3 def	1398 ± 22	1387 ± 22	obscured	obscured
C-C str overtone	2213 ± 27‡	2164 ± 49‡	2292 ± 30	obscured
sym CH_3 str	2883 ± 6‡	2882 ± 40‡	2079 ± 20	2086 ± 58‡
asym CH_3 str	2940 ± 17‡	2922 ± 31‡	2201 ± 13	2194 ± 15‡

Table 2.3. Compilation of the observed vibrational frequencies in cm^{-1} for the four isotopomers of ethylidyne. Frequency values represent averages from 9 to 42 separate spectra except where otherwise noted and uncertainties indicate 90% confidence limits. ‡ indicates the mode was resolved in four or less measurements.

III.C. Normal Modes Analysis

A normal modes analysis of the frequencies of the vibrational features listed in Table 2.3 has been carried out using an ethylidyne geometry and force constants. The geometry used for the calculation is shown in Fig 2.8. The values for the C-C and the C-Ni bond lengths of 1.5 Å and 1.9 Å, respectively, are equal to the C-C and C-Pt bond lengths measured previously in a low energy electron diffraction tensor study for ethylidyne bound to Pt(111),[6] and are close to the C-C and C-Co bond lengths of 1.5 Å and 1.80 Å, respectively, measured by x-ray crystallography for $(CO)_9Co_3(\text{-}CCH_3)$.[4] The C-C-Ni angle of 126° was selected so as to leave the Ni-Ni separation equal to the bulk value of 2.7 Å.[25] Because no C-H bond lengths were measured in these two studies, a C-H bond length of 1.07 Å was picked to be intermittent to the values used in previous ethylidyne normal modes calculations of 1.06[18] and 1.09[17]. Although the geometry was not optimized to yield the best fit to the observed vibrational frequencies, different geometries were explored. The normal modes analysis using different equilibrium geometries showed that the precise equilibrium geometry was not critical in the calculation. The equilibrium geometry was varied by changing the bond angles and bond lengths: all bond angles were varied ±15°, bond lengths were varied ± 0.5 Å for the C-C bond, ± 0.5 Å for the C-Ni bonds and ± 0.2 Å for the C-H bonds. A smaller bond length range was explored for the C-H bonds because most known C-H bond lengths fall into this range. The normal mode frequencies calculated using different equilibrium geometries were equal to those reported in Table 2.3 within the experimental uncertainties, and best fit force constants employed in the calculations were comparable to those obtained using the geometry shown in Figure 2.8.

Table 2.4 lists the force constants used in the normal modes analysis which yield calculated frequencies which best fit the observed frequencies. Also included in the table are force constants used in comparable normal mode analyses of the ethylidyne moiety of $(CO)_9Co_3(\text{-}CCH_3)$, methyl acetylene $(HC\text{-}CCH_3)$, and ethylidyne adsorbed on Pt(111).[4,17,18]

The values for the C-C bond and C-H bond force constants used in this study are very similar to those used in these previous studies. However, the force constants used for the carbon-metal bonds are not as close in value. The discrepancies in these force constants will be discussed in the section describing the individual mode assignments.

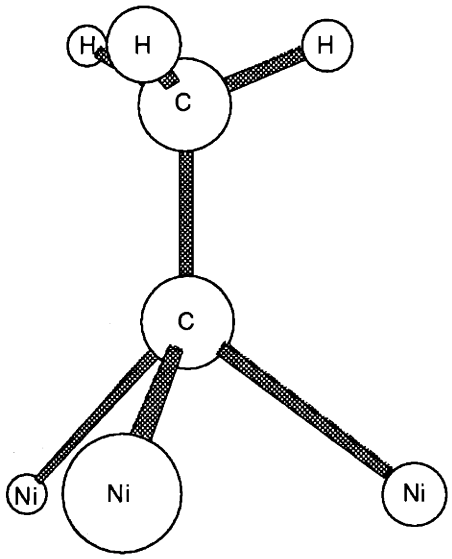

Bond Lengths (Å)		Bond Angles (degrees)	
C-H	1.07	H-C-H	109
C-C	1.5	H-C-C	111
C-Ni	1.9	C-C-Ni	126
		Ni-C-Ni	89

Figure 2.8. Geometry used in the normal modes calculation of ethylidyne.

Table 2.5 lists the frequencies calculated by the normal modes analysis along with the observed frequencies. The frequencies calculated for Ni-Ni vibrations are not included for two reasons. First, the simplified geometry is not expected to accurately reproduce lattice vibrations. Second, these modes are not observed because they are very low in frequency and

are masked by overlap with the intense elastic peak in the electron energy loss spectra. The calculated frequencies are also shown overlaid on the vibrational spectra of the four isotopomers of ethylidyne in Figure 2.9.

Force Constants	Ni(111) -CCH_3	$Co_3(CO)_9$ -CCH_3	Pt(111)* -CCH_3	HC* -CCH_3
C-H str.	4.63	4.65	4.9	4.86
C-C str.	4.67	4.63	3.54	4.45
C-M str.	0.97	1.51	2.45	
M-M str.	0.30	1.10	0.20	
H-C-H bend	0.45	0.52	0.48	0.55
H-C-C bend	0.61	0.62	0.59	0.64
C-C-M bend	0.23	0.59	1.50	
C-H / C-H	0.03	0.08	0.11	0.04
C-C / H-C-H	-0.28	-0.30	-0.27	0
M-M / C-C-M	-0.12	-0.38	-0.1	
M-M / M-M	0	-0.13	0	
H-C-H / H-C-H	-0.03	0	0	0
Reference	This work	Ref. 4	Ref. 18	Ref. 17

Table 2.4. Force constants used in the normal modes calculation of ethylidyne in this work and in previous work. The last five force constants shown are coupling constants between the two modes shown. Units are in mdyne/Å for bond stretches and stretch/stretch coupling terms, mdyne Å for bond bends and bend/bend coupling terms, and mdyne for stretch/bend coupling terms. M = Ni, Co, or Pt. * additional force constants beyond those listed in the table are used in these studies.

$-C_2H_3$		$-^{13}C_2H_3$		$-C_2D_3$		$-^{13}C_2D_3$	
obs.	calc.	obs.	calc.	obs.	calc.	obs.	calc.
260 ± 16	263	252 ± 34‡	257	264 ± 37	250	256 ± 25‡	246
447 ± 13	446	431 ± 16	433	435 ± 39	422	418 ± 12	412
1025 ± 16	1025	obscured	1014	836 ± 34	816	821 ± 12	803
1129 ± 21	1135	1081 ± 21	1094	1152 ± 34	1145	1115 ± 7	1105
1332 ± 19	1337	1313 ± 25	1329	987 ± 26	973	971 ± 5	964
1398 ± 22	1409	1387 ± 22	1408	obscured	1008	obscured	1006
2883 ± 6‡	2896	2882 ± 40‡	2892	2079 ± 20	2094	2086 ± 58‡	2086
2940 ± 17‡	2947	2922 ± 31‡	2935	2201 ± 13	2194	2194 ± 15‡	2177

Table 2.5. Comparison of observed vibrational frequencies in cm^{-1} to those calculated for the four isotopomers of ethylidyne. Observed frequency values represent averages from 9 to 42 separate spectra except where otherwise noted and uncertainties indicate 90% confidence limits. ‡ indicates the mode was resolved in four or less measurements.

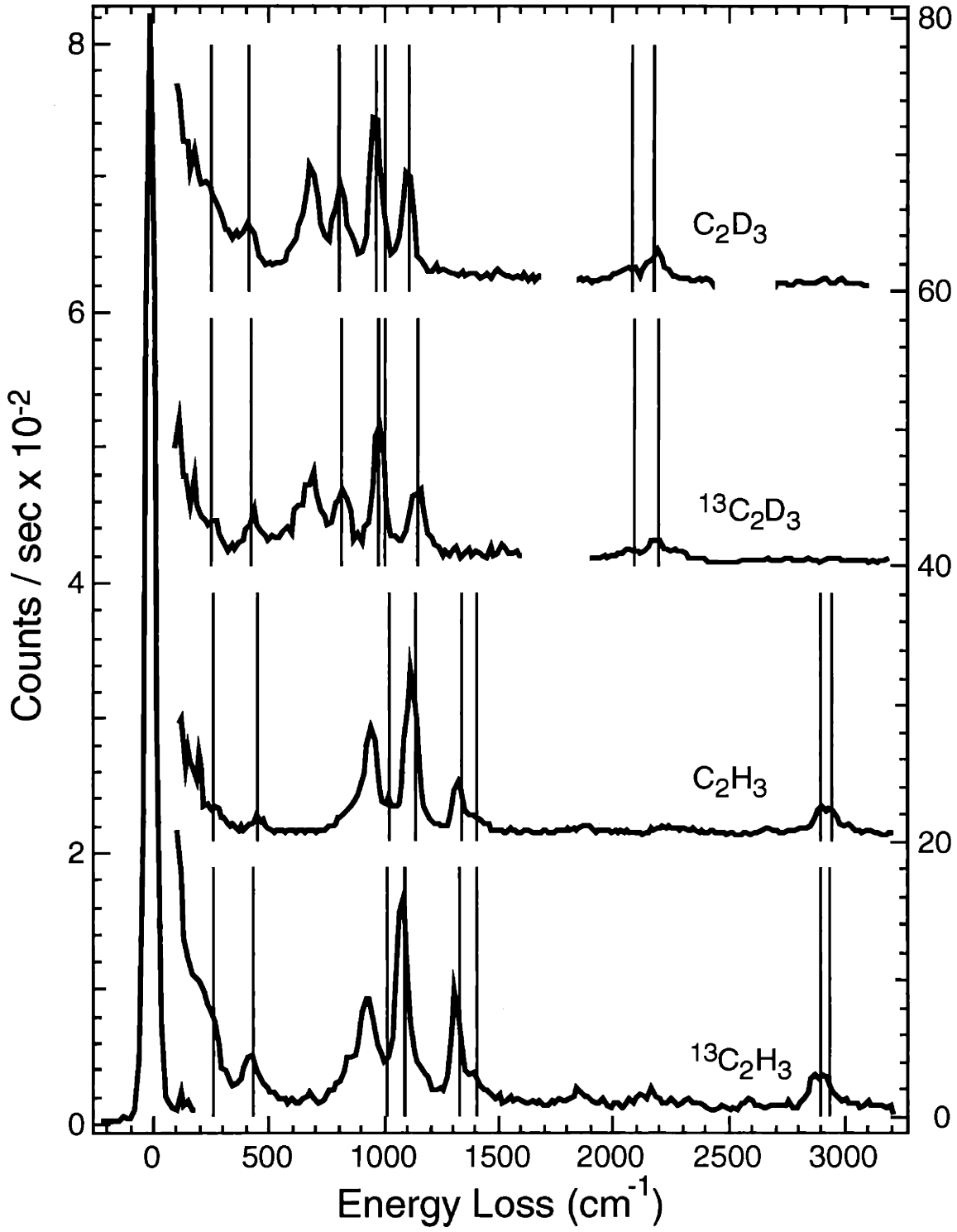

Figure 2.9. Calculated vibrational frequencies of the four isotopomers of ethylidyne overlaid on the electron energy loss spectra of the four isotopomers of ethylidyne measured 10° off specular from Figures 2.2, 2.3, 2.4 and 2.5.

III.D. Assignment of the Spectra as Ethylidyne

III.D.1. Symmetric and Antisymmetric CH_3 stretching modes

Assignment of the high frequency features at 2883 cm^{-1} and 2940 cm^{-1} in Figure 2.2 is straightforward. The two features are assigned to the symmetric and antisymmetric CH_3 stretching modes. Only C-H stretches have group frequencies in this range as seen in Table 2.1. Table 2.2 shows that the observed frequencies of the C-H stretching modes are also very close in frequency to those of $(CO)_9Co_3(\text{-}CCH_3)$ at 2888 cm^{-1} and 2930 cm^{-1}.

The C-H stretching mode assignment is supported by the deuterated ethylidyne spectra in Figure 2.3, as there are no modes in the 3000 cm^{-1} range. Instead, new features are present in the C-D stretching region, 2000 - 2300 cm^{-1}. Only two features are observed in the C-H stretching region of the spectra of the isotopically unlabeled hydrogen ethylidyne species, while three modes at 2079 cm^{-1}, 2201 cm^{-1} and 2280 cm^{-1} are observed in the C-D stretch region of the spectra of the deuterated ethylidyne. The symmetric and antisymmetric CD_3 stretch are assigned to the features at 2079 cm^{-1} and 2201 cm^{-1}, respectively, while the additional feature at 2292 cm^{-1} is assigned to the overtone of the C-C stretch as discussed in Section III.D.2 of this chapter. The C-C stretching overtone of deuterated ethylidyne is more intense than that of unlabeled ethylidyne ($\text{-}CCH_3$) because of a Fermi resonance of the overtone with the symmetric CD_3 stretch. Fermi resonance is a mixing of a fundamental and an overtone that are close in energy and have the same symmetry representation.[26] The Fermi interaction has two effects. One effect of a Fermi interaction is that the mixing of the two states causes the states to split apart in energy. In this case, the mixing causes a downward shift in the symmetric CD_3 stretching fundamental mode and an upward shift in the C-C stretching overtone. The second effect of a Fermi interaction is 'intensity borrowing'. Since the wave functions of the two modes are mixed, the overtone has some fundamental character and therefore, it is observed to be more intense than typical overtone transitions.

Both effects, frequency shifting and intensity borrowing, are observed. Most apparent is the increased intensity of the C-C stretching overtone feature. It is much more intense in the spectrum of deuterated ethylidyne at 2292 cm^{-1} than in the spectrum of the hydrogen unlabeled ethylidyne at 2213 cm^{-1}. Splitting of the levels is also observed. In unlabeled ethylidyne, the frequency of the C-C stretching overtone mode at 2213 cm^{-1} is 45 cm^{-1} less than twice that of the fundamental at 1129 cm^{-1}, but in deuterated ethylidyne the frequency of the C-C stretching overtone at 2292 cm^{-1} is only 12 cm^{-1} less than twice that of the fundamental at 1152 cm^{-1}. Therefore, the C-C stretching overtone mode is shifted in frequency due to the Fermi resonance. A downward shift in the symmetric CD_3 stretching frequency is observed by comparing the ratio of frequencies for the symmetric and the antisymmetric CH_3 (CD_3) stretches. The antisymmetric CH_3 stretch shifts downward by a factor of 1.34 upon deuteration. If the symmetric CH_3 stretch frequency shifted by the same factor upon deuteration, the symmetric CD_3 stretch frequency would be 2159 cm^{-1}. Instead, it is observed at a lower frequency, 2079 cm^{-1}, shifted downward due its Fermi resonance with the C-C stretching overtone.

Neither the feature assigned to the symmetric CH_3 stretch nor the feature assigned to the antisymmetric CH_3 stretch is observed to be dipole active. This further confirms the assignment of these features because C-H stretching modes are rarely dipole active because their dynamic dipole moments are very small.[15]

The normal modes analysis also verifies the assignment of the symmetric and antisymmetric CH_3 stretches. Table 2.5 shows that the calculated frequencies equal the observed frequencies for all four isotopomers of ethylidyne within experimental uncertainty. The C-H stretching force constant utilized in the normal modes calculation of ethylidyne in this work differs by less than 6% from the C-H stretching force constants utilized in all the other normal modes calculations of ethylidyne shown in Table 2.4.

III.D.2. C-C stretching mode

The intense feature at 1129 cm^{-1} in Figure 2.2 is assigned to the C-C stretching mode of ethylidyne. This assignment is based on several factors: no downward shift in frequency of this feature upon deuteration, a downward shift in the frequency of this feature upon isotopic labeling of the carbon atoms, comparison of the frequency of the feature to those of other ethylidyne moieties, dipole activity of the feature, and the normal modes analysis.

The feature assigned to the C-C stretching mode does not shift downward in frequency upon deuteration as it should if it were a mode involving mostly H atom motion. However, there is an upward shift in the frequency of the C-C stretching mode from 1129 cm^{-1} to 1152 cm^{-1} upon deuteration as is seen in Table 2.3. Increasing the mass of the H atoms is expected to shift the frequency of the mode downward, if at all. A similar upward shift of the frequency of the C-C stretching mode upon deuteration has been observed in the vibrational spectra of ethylidyne bound to other hexagonal metal surfaces and in the vibrational spectra of $(CO)_9Co_3(\text{-}CCH_3)$.[2-4] Explanation of this unexpected isotope shift is deferred until the remaining evidence for the C-C stretch assignment has been discussed.

Upon isotopic labeling of the carbon atoms, the mode which exhibits the largest shift in frequency is the C-C stretching mode. The frequency of the C-C stretching mode shifts downward upon increasing the mass of the carbon atoms from 1129 cm^{-1} to 1081 cm^{-1} in going from $\text{-}CCH_3$ to $\text{-}^{13}C^{13}CH_3$ and from 1152 cm^{-1} to 1115 cm^{-1} in going from $\text{-}CCD_3$ to $\text{-}^{13}C^{13}CD_3$. The ratios of the C-C stretching frequencies of the carbon unlabeled versus carbon labeled ethylidyne species, 1.04 and 1.03, are very close to that calculated by Equation 2.7.

$$\frac{\nu_{C^{12}-C^{12}}}{\nu_{C^{13}-C^{13}}} = \sqrt{\frac{13}{12}} = 1.04 . \qquad (2.7)$$

The dipole activity of the feature also supports its assignment to the C-C stretching mode. As discussed previously, a mode has to be symmetric and have a dynamic dipole

moment perpendicular to the surface for it to be dipole active. The C-C stretching mode is symmetric in all adsorption geometries. Also, motion of carbon atoms perpendicular to the surface is expected to yield a significant perpendicular dynamic dipole moment. Therefore, the C-C stretching mode of ethylidyne is expected to be a dipole active feature. For all four isotopomers of ethylidyne, the spectral feature assigned to the C-C stretching mode is indeed dipole active.

Comparison of the frequency of the C-C stretch to those of the C-C stretches of other ethylidyne species also lends support for this assignment. Typical C-C single bond group frequencies are in the range of 880-1000 cm^{-1}, but the C-C stretch of ethylidyne is not observed in this frequency range. For example, the observed frequency of the C-C stretching mode of $(CO)_9Co_3(-CCH_3)$ is 1160 cm^{-1},[4] and the frequency of the C-C stretching mode observed for ethylidyne bound to Pt(111), Rh(111) and Ru(001) is 1130 cm^{-1}, 1120 cm^{-1} and 1120 cm^{-1} , respectively.[2,3,27] These frequencies observed for the C-C stretches agree well with that of the feature assigned to the C-C stretch of ethylidyne bound to Ni(111), 1129 cm^{-1}.

The normal mode calculation also supports the C-C stretch assignment. Table 2.5 shows that the frequency of the C-C stretching mode calculated by the normal modes analysis equals the observed frequency within experimental error. The C-C stretching force constant used in the calculation of this work, 4.67 mdyne/Å, is similar in value to those used in previous normal modes analyses of $(CO)_9Co_3(-CCH_3)$ and $HC-CCH_3$, 4.63 and 4.45 mdyne/Å, respectively, as shown in Table 2.4. In addition to fitting the frequency of the C-C stretching mode of $-CCH_3$, the frequencies calculated by the normal modes analysis for the C-C stretches of the other three isomers of ethylidyne match those observed within experimental error. The normal mode analysis correctly predicts the downward shift upon isotopic labeling of the carbon atoms, as well as the unexpected upward shift of the frequency of the C-C stretching mode upon deuteration.

The explanation for the upward shift of the frequency of the C-C stretching mode upon deuteration comes to light through the normal modes analysis. Although this mode has been labeled a C-C stretch, it is not exclusively a C-C stretch. A C-C stretch is a local mode representation and is not a normal mode. The normal mode, as seen by the displacement vectors calculated by the normal mode analysis program, is a combination of two local modes, the C-C stretch and the symmetric CH_3 deformation. Figure 2.10 displays exaggerated calculated normal mode vectors for the mode labeled as the C-C stretch in $-CCH_3$ and $-CCD_3$. The amount of mixing is seen by comparing the displacement vector of the carbon atom of the CH_3 unit with the displacement vectors of the hydrogen atoms. If no mixing occurred, the two vectors would be equal and the hydrogen atom motion would be exactly vertical. The mixing is more apparent for the case of deuterated ethylidyne. The displacement vectors are dramatically different because the motions of the carbon atom and hydrogen atoms are out of phase. The difference is not as easily seen in hydrogen unlabeled ethylidyne, but close examination reveals a small difference in the displacement vectors. Therefore, mixing of the C-C stretch and symmetric CH_3 deformation occurs in both $-CCH_3$ and $-CCD_3$, but it is more extensive for deuterated ethylidyne.

The mixing of two modes causes the two modes to shift to frequencies different from what their values would be if no mixing occurred. The higher frequency mode shifts to a higher frequency, and the lower frequency mode shifts to a lower frequency. Mixing of the C-C stretch and symmetric CH_3 deformation of ethylidyne causes the frequency of the C-C stretch to shift downward in the ethylidyne isotopomers with hydrogen ($-CCH_3$ and $-^{13}C^{13}CH_3$) because the symmetric CH_3 deformation mode is higher in frequency than the C-C stretch. In deuterated isotopomers of ethylidyne ($-CCD_3$ and $-^{13}C^{13}CD_3$), the symmetric deformation mode is lower in frequency than the C-C stretch and the mixing of the two causes the frequency of the C-C stretch to shift upward. Therefore, an upward shift in the frequency of the feature assigned to the C-C stretching mode is observed upon deuteration.

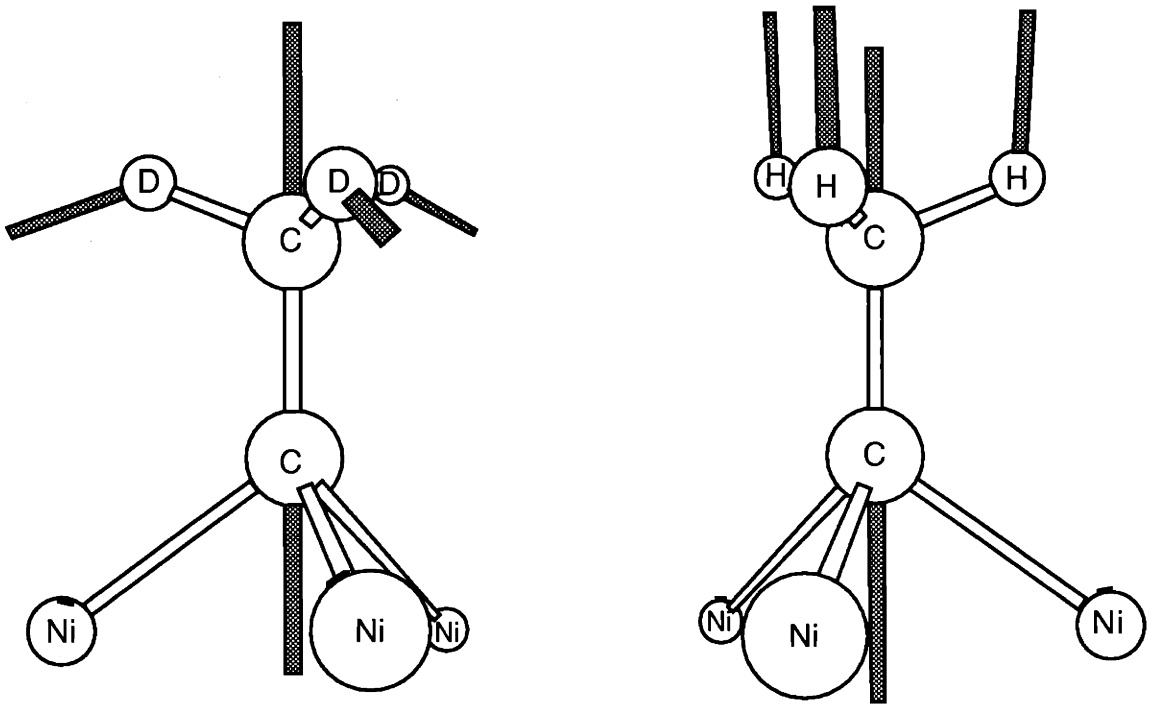

Figure 2.10. Pictoral representation of the normal mode displacement vectors for the C-C stretch of $-CCH_3$ and $-CCD_3$. The absolute displacements are exaggerated in length, but the relative displacements are constant.

The feature at 2213 cm^{-1} is assigned to the overtone of the C-C stretching mode. As is expected, the frequency of this overtone, 2213 cm^{-1}, is slightly less than double the frequency of the fundamental which is observed at 1129 cm^{-1}. Frequencies of overtones are not exactly double the those of the fundamentals because of anharmonicity.[15] The low intensity of this feature is also consistent with its assignment to an overtone because the features of overtones are typically low in intensity.[15] Perhaps the most convincing evidence for the assignment of the feature at 2213 cm^{-1} to the overtone to the C-C stretching mode is its shift downward in frequency to 2164 cm^{-1} upon isotopic labeling of the carbon atoms. Labeling of the carbon atoms is expected to shift the frequency of the overtone of the C-C stretching mode as it does the frequency of the fundamental of the C-C stretching mode.

III.D.3. Symmetric and antisymmetric CH_3 deformation Modes

The intense electron energy loss feature at 1332 cm^{-1} in Figure 2.2 is assigned to the symmetric CH_3 deformation mode. Close inspection of the spectra reveal a small shoulder on the intense 1332 cm^{-1} feature at 1398 cm^{-1} which is assigned to the antisymmetric deformation mode.

These modes cannot be assigned to a CH_3 rocking mode of ethylidyne because the frequency is too high. Table 2.1 shows the frequency of CH_3 rocking modes to be in the range of 900 - 1100 cm^{-1}. The assignment of either of these features to a C-C stretch can also be discounted because these modes shift significantly downward in frequency upon deuteration. Furthermore, the frequencies are too low for C-H stretches and too high for C-Ni stretches, leaving only C-H bending modes as possibilities. The two C-H bending modes of ethylidyne are the symmetric and antisymmetric CH_3 deformations. Table 2.1 shows that a frequency of 1332 cm^{-1} is within the typical frequency range for symmetric CH_3 deformations, 1280 - 1420 cm^{-1}, as is a frequency of 1398 cm^{-1} for antisymmetric CH_3 deformations, 1380 - 1460 cm^{-1}. Table 2.2 shows that the frequencies of 1332 cm^{-1} and 1398 cm^{-1} are close to those observed for symmetric and antisymmetric CH_3 deformations of the ethylidyne moiety of $HC\text{-}CCH_3$, $Cl_3\text{-}CCH_3$, $Br_3\text{-}CCH_3$, and $(CO)_9Co_3(\text{-}CCH_3)$ at 1382 cm^{-1} and 1452 cm^{-1}, 1384 cm^{-1} and 1444 cm^{-1}, 1373 cm^{-1} and 1432 cm^{-1}, and 1356 cm^{-1} and 1420 cm^{-1}, respectively.

Upon deuteration, the symmetric deformation mode shifts down in frequency from 1332 cm^{-1} to 987 cm^{-1}. The ratio of these two frequencies is 1.35. Analysis of the shift in frequency of the antisymmetric deformation mode upon deuteration is not possible in this study. The antisymmetric CD_3 deformation mode is not resolved in the corresponding deuterated ethylidyne spectra and therefore, both its frequency and its shift in frequency upon deuteration are unknown.

The dipole activity of the symmetric CH_3 deformation mode of the hydrogen unlabeled ethylidyne species (-$^{13}C^{13}CH_3$ and -CCH_3) also helps to verify its assignment. In all adsorption geometries, the symmetric CH_3 deformation mode is dipole allowed. Furthermore, the symmetric CH_3 deformation involves motion of the atoms perpendicular to the surface, which in turn leads to an expectation of a dynamic dipole perpendicular to the surface arising from the vibration. Thus, the symmetric CH_3 deformation mode is expected to be dipole active as is observed. The antisymmetric CH_3 deformation mode is not dipole allowed in some adsorption geometries and therefore, its lack of dipole activity is further evidence that this mode has been properly assigned.

Finally, the normal modes analysis confirms the assignment of the symmetric and antisymmetric CH_3 deformation modes. Table 2.5 shows that the calculated frequencies are equal to the observed frequencies for all four isotopomers of ethylidyne within experimental error. The three force constants which most dramatically affect the calculated frequencies of the symmetric and asymmetric CH_3 deformations are the H-C-H bending force constant, the H-C-C bending force constant and the C-C stretch/C-C-H bend coupling constant. As shown in Table 2.4, the H-C-H bending force constant of 0.45 mdyne Å is close to the range used in previous normal modes calculations, 0.48 to 0.55 mdyne Å, and the H-C-C bending force constant of 0.61 mdyne Å and the C-C stretch/C-C-H bend coupling constant of -0.28 mdyne fall within the range of force constants used in previous normal modes calculations, 0.59 to 0.64 mdyne Å and -0.3 to -0.27 mdyne, respectively.

One aspect of the assignment of the symmetric CH_3 deformation which is difficult to interpret is the dipole activity of this mode. The symmetric CH_3 deformation is dipole active for the hydrogen unlabeled ethylidyne species (-$^{13}C^{13}CH_3$ and -CCH_3), but dipole inactive for the deuterated ethylidyne species (-CCD_3 and -$^{13}C^{13}CD_3$). A possibility which can explain the dipole activity in hydrogen unlabeled ethylidyne and lack of it in deuterated ethylidyne is the extent of the hydrogen atom motion. Relative to the hydrogen atoms, the

more massive deuterium atoms have smaller displacements in similar modes. Larger amplitude motion in the hydrogen atoms could give rise to a larger dynamic dipole moment, explaining the observed dipole activity.

The intensities of IR absorption features of deuterated gas phase molecules have been previously shown to be lower than that of the corresponding non-hydrogen labeled molecules.[28] Equation 2.7 shows that ratios of the intensity of a mode to its frequency squared, summed over all modes of the same symmetry is constant, independent of isotopic substitution.

$$\sum_k \frac{I_k}{\nu_k{}^2} = \text{constant} \qquad (2.8)$$

In equation 2.8 where I_k is the intensity of the IR absorbence of mode k, ν_k is the frequency of mode k, and k is the modes of the molecule that are of the same symmetry. The molecule must not have a permanent dipole moment or the symmetry of the modes over which the sum is carried out must not be the same as that of any rotation of the molecule which moves the permanent dipole moment for Equation 2.8 to hold. Because the frequencies of deuterated molecules are lower, the sum of the intensities of its modes are therefore lower. Application of Equation 2.8 to the observed intensities of the ethylidyne symmetric modes is not enlightening because the intensity of the symmetric C-Ni stretching mode, which contributes the most to the sum because it is lowest in frequency, has a large uncertainty because of its overlap with the elastic feature. However, the observed lower intensity of the symmetric CD_3 deformation mode as compared to that of the symmetric CH_3 deformation mode is consistent with the prediction of Equation 2.8 that modes involving C-D motion rather than C-H motion have lower intensities when excited by a dipolar interaction.

III.D.4. CH_3 rocking mode

The feature at 1025 cm^{-1} observed in the spectra shown in Figure 2.2 is assigned to the methyl rocking mode. A frequency of 1025 cm^{-1} falls in the frequency range expected for CH_3 rocking modes shown in Table 2.1, 900 - 1100 cm^{-1}. Table 2.2 shows that a frequency of 1025 cm^{-1} also closely matches the frequencies of the CH_3 rocking modes observed for the ethylidyne moieties of HC-CCH_3 and $(CO)_9Co_3(-CCH_3)$, 1053 cm^{-1} and 1004 cm^{-1}, respectively.

The feature at 836 cm^{-1} in the spectra of -CCD_3 shown in Figure 2.3 is assigned to the CD_3 rocking mode. The observed frequency of 836 cm^{-1} is consistent with the expected downward shift in frequency of this mode upon deuteration, a factor of 1.23 lower than the frequency of the CH_3 rocking mode of -CCH_3, 1025 cm^{-1}. A factor of 1.23 is less than the factor of 1.3 to 1.4 expected for modes involving mostly motion of hydrogen atoms upon deuteration. However, there is significant motion of the carbon atom in the CH_3 rocking mode, decreasing the relative change in the reduced mass of the mode upon deuteration and therefore, lowering the factor by which the frequency of the mode is shifted upon deuteration. Ethylidyne moieties in Table 2.2 exhibit a range of 1.1 to 1.26 for the factor by which the frequency of the CH_3 rocking mode shifts upon deuteration which is consistent with the observed factor of 1.23 in this study. Further validation of the CH_3 rocking mode assignment is provided by the -$^{13}C^{13}CD_3$ spectra. The frequency of the rocking mode of this ethylidyne isotopomer is even lower, 821 cm^{-1}, in the ^{13}C substituted and deuterated product. Isotopic labeling of the carbon atoms is expected to shift the frequency of the CH_3 rocking mode because of the significant motion of the carbon atom in this mode.

The absence of dipole activity of the features assigned to methyl rocking modes in the four isotopomers of ethylidyne also lends support for the assignment. Rocking modes have motions that are largely parallel to the surface, so they are unlikely to give rise to a

perpendicular dynamic dipole. Therefore, even if this mode were dipole allowed it would be unlikely to be dipole active.

Finally, the normal modes analysis confirms the assignment of the CH_3 rocking mode. Table 2.5 shows that the calculated frequencies are equal to the observed frequencies of the four isotopomers of ethylidyne within experimental error. The force constants which most dramatically affect the CH_3 rocking mode are the H-C-C bend and the C-C stretch/C-C-H bend coupling constant. The previous section discussed that the values of these force constants used in this study fall within the range of values of the force constants used previously in normal modes calculations of an ethylidyne moiety.

III.D.5. Symmetric and antisymmetric C-Ni stretching modes

Two low frequency features at approximately 260 cm^{-1} and 440 cm^{-1} remain to be assigned. Because of their low frequency, it is reasonable that these modes involve motion of heavy atoms such as C-Ni stretching modes. Table 2.1 does not present any group frequencies for C-Ni stretches because none are available. Typical hydrocarbons do not contain Ni atoms. However, we can compare the observed frequencies for C-Ni stretching modes to those of C-X stretching modes, where X is a heavy atom. For example, Table 2.2 shows the frequencies of the symmetric and antisymmetric C-Br stretching modes of Br_3CCH_3 to be 408 cm^{-1} and 628 cm^{-1}, respectively. Also, low C-Ni stretching frequencies have been measured for other hydrocarbon adsorbates on Ni(111). Ethylene,[29] acetylene[30] and methyl[31] adsorbed on Ni(111) have C-Ni stretching frequencies equaling 440 cm^{-1}, 480 cm^{-1} and 385 cm^{-1} respectively. Therefore, the features at 260 cm^{-1} and 447 cm^{-1} are assigned to the C-Ni stretching modes of ethylidyne.

The lower frequency feature at 260 cm^{-1} is dipole active, indicating that it is a totally symmetric mode. The feature at 447 cm^{-1} is not dipole active. Therefore, the feature at 260 cm^{-1} is assigned as the symmetric C-Ni stretch and the feature at 447 cm^{-1} is assigned as the

antisymmetric C-Ni stretch. This assignment is consistent with the fact that symmetric modes are generally lower in frequency than antisymmetric modes.

The frequency of the antisymmetric C-Ni stretching mode shifts downward to 431 cm^{-1} upon increasing the mass of the carbon atoms, 435 cm^{-1} upon deuteration and 418 cm^{-1} upon isotopic labeling of the both the carbon and hydrogen atoms. In these isotopically labeled ethylidyne species the mass of the ethylidyne unit increases and therefore, the frequencies of the C-Ni stretching modes are expected to decrease upon isotopic labeling. The 260 cm^{-1} feature is a shoulder on the elastic feature making it difficult to observe any shift upon isotopic labeling of the carbon or hydrogen atoms .

Comparison of the observed vibrational frequencies to those of the ethylidyne moiety of $(CO)_9Co_3(-CCH_3)$ has been useful throughout this section. However, the carbon-metal stretch frequencies of ethylidyne bound to Ni(111) are lower than those observed for $(CO)_9Co_3(-CCH_3)$, 401 cm^{-1} and 555 cm^{-1}. However, this discrepancy is reasonable because the comparison being made is between ethylidyne species in which the carbon is bonded to different metal atoms.

As shown in Table 2.5, the frequencies calculated by the normal modes analysis equal the observed symmetric and antisymmetric C-Ni stretching frequencies of the four isotopomers of ethylidyne within experimental error. However, it is difficult to judge the quality of the force constants employed in the calculation. No force constants for C-Ni bending and stretching are available in the literature for comparison. As shown in Table 2.4, comparison of the C-Ni force constants to the C-M force constants, where M= Co or Pt, yields some discrepancy between the values employed. The C-M stretching force constant is 0.97, 1.51, and 2.45 mdyne/Å for M = Ni, Co, or Pt, respectively, and the C-C-M bending force constant is 0.23, 0.59, and 1.5 mdyne Å, respectively. There are a couple possible explanations for this discrepancy. One explanation is the fact that the observed vibrational frequencies for the carbon-metal stretching modes have dissimilar values. It is reasonable

that modes with different frequencies would yield different best fit force constants. Another potential reason the carbon-metal force constants differ is the simplified geometry used in the calculations. The ethylidyne geometry used in this calculation includes only three metal atoms. Obviously, the Ni(111) surface contains many more than that. The normal modes calculation of ethylidyne on Pt(111) includes the next nearest neighbor metal atoms in addition to the three metal atoms to which the ethylidyne is bound. In addition to including more metal atoms, force constants are used for the metal-metal interactions and cross terms between the metal atoms are included in this calculation. These additional force constants increase the number of fitting parameters in the ethylidyne on Pt(111) calculation. Adding more atoms and force constants to the calculation of ethylidyne on Ni(111) would likely result in different best fit force constants for the carbon-metal bond. However, because only two vibrational modes involving the metal atoms are observed, adding more fitting parameters is not justified and does not yield additional information. The normal modes calculation for the ethylidyne moiety of $(CO)_9Co_3(\text{-}CCH_3)$ has also used a simplified geometry by ignoring the nine carbonyl groups bound to the Co trimer. The ethylidyne C-Co bond stretching modes could be extensively mixed with the carbonyl C-Co bond stretching modes. The simplification of the geometry likely results in different C-Co stretching and bending force constants. Therefore, considering the difference in the metal atoms to which the ethylidyne moiety is bound and the simplification of the geometries used in the normal modes calculations, the discrepancy between the carbon-metal stretching and bending force constants shown in Table 2.4 is not surprising.

III.E. Symmetry of Ethylidyne Adsorbed on Ni(111)

In this section, the symmetry of ethylidyne is determined through analysis of the dipole activity of its electron energy loss features. In the discussion that follows, only the

nickel atoms at the surface are included in the symmetry considerations. Deeper lying nickel atoms are not included in the symmetry arguments.

The symmetry of an unbound ethylidyne species is C_{3v}. The symmetry elements present are a three-fold axis of rotation, three mirror planes and, of course, the identity relation. The symmetry axis of rotation is aligned with the C-C bond, and each mirror plane cuts through the C-C bond and one of the C-H bonds.

The symmetry of an adsorbed species can only be equal to or lower than that of the species without the surface present. The symmetry of the adsorbate is lowered if the presence of the surface atoms breaks the symmetry of the adsorbate. Ethylidyne can bind to a Ni(111) surface with C_{3v} point group symmetry if its binding site is such that neither the three-fold axis of rotation nor the three mirror planes are broken by the presence of the surface atoms. A C_3 adsorption symmetry is realized if the binding site of ethylidyne is such that the Ni surface atoms do not line up with the mirror planes, while still maintaining the three-fold axis of rotation. Even lower symmetry, C_s or C_1, can be attained by breaking the symmetry of the three-fold axis of rotation. This three-fold axis of rotation can be broken by ethylidyne binding to a site which does not have three-fold symmetry or by tilting of the ethylidyne with respect to the surface. C_s symmetry is achieved if a mirror plane which cuts through one of the hydrogen atoms, both of the carbon atoms and some of the surface Ni atoms is present. If no mirror plane or three-fold axis of rotation is present, the adsorption symmetry is C_1, with no symmetry operations other than the identity operation. Some examples of binding sites for ethylidyne that result in C_{3v}, C_3, and C_s symmetries are shown in Figure 2.11.

Table 2.6 shows the symmetry representation of the modes of ethylidyne for the C_{3v}, C_3, C_s and C_1 point groups. Of particular interest are the totally symmetric modes because they are the modes that are dipole allowed. Totally symmetric modes are defined as modes which are symmetric with respect to every symmetry element within the point group. The

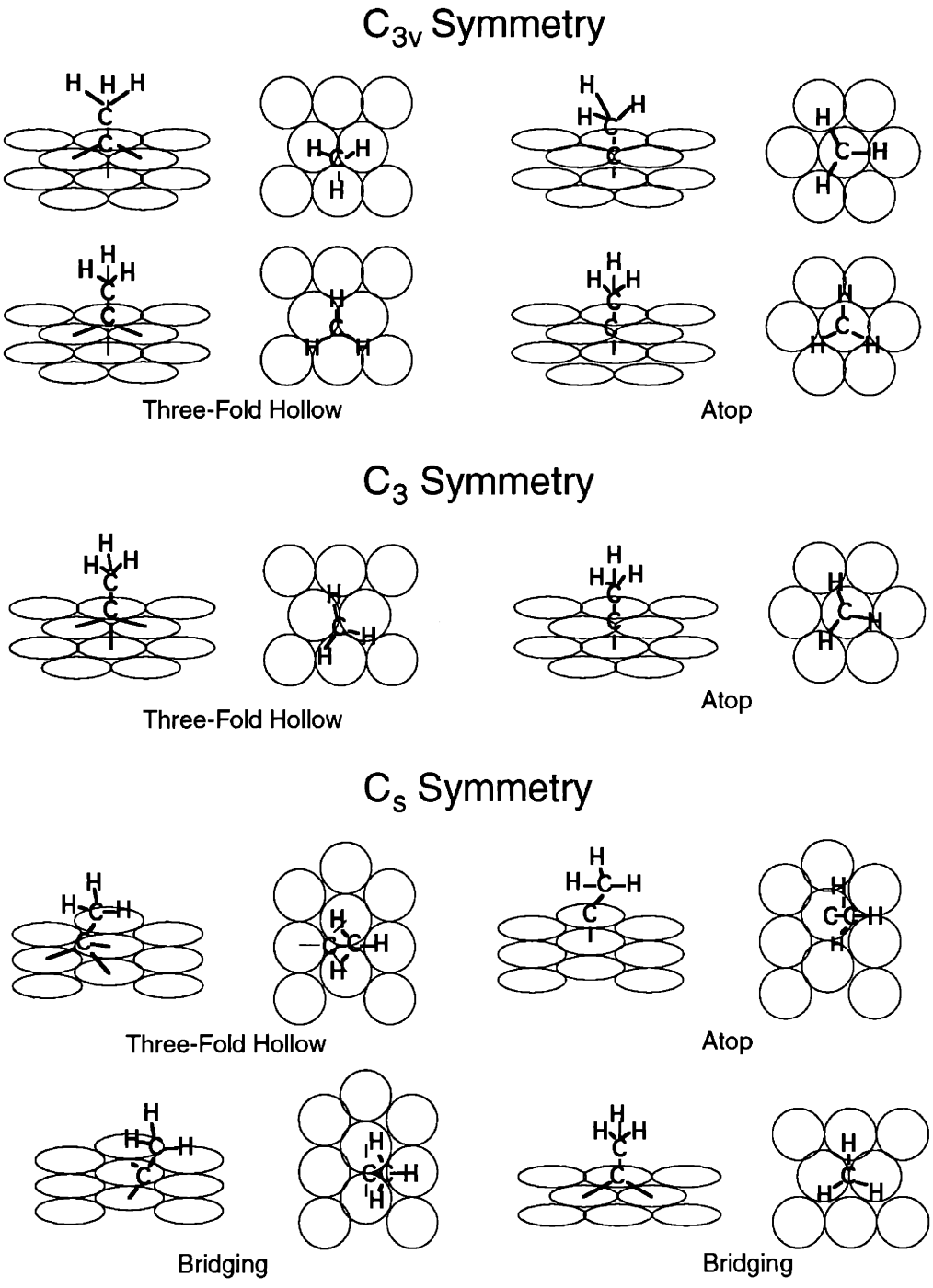

Figure 2.11. Examples of possible ethylidyne binding sites and resulting symmetries.

totally symmetrical representations are A_1 in the C_{3v} point group, A' in the C_s point group, and A in C_3 and C_1 point groups. It is seen in Table 2.6 that in going from high to low symmetry, more modes become totally symmetric, and thus are dipole allowed. Adsorbed ethylidyne in the C_{3v} symmetry point group has four dipole allowed modes: the symmetric CH_3 stretch, the symmetric CH_3 deformation, the C-C stretch, and the symmetric C-Ni stretch. In the C_3 point group, the three mirror planes of the C_{3v} point group are no longer present, and one more mode, the internal rotation, becomes dipole allowed. In C_s symmetry, the inequivalency of the hydrogen atoms breaks the degeneracy of the modes which have an E representation in the C_{3v} and C_3 symmetry point groups: the antisymmetric C-H stretches, the antisymmetric CH_3 deformations, the methyl rocking modes, and the antisymmetric C-Ni stretches. These doubly degenerate antisymmetric modes in C_{3v} and C_3 symmetry are split into two singly degenerate modes in C_s symmetry, a symmetric, A', and an antisymmetric, A". The A' modes, with mirror plane symmetry, become dipole allowed, while the A" modes are not dipole allowed. In the C_1 point group, no symmetry elements other than the identity element remain. All of the modes are totally symmetric and therefore, all modes are dipole allowed.

In principle, the symmetry of adsorbed ethylidyne can be readily determined from both the total number of features observed in its spectrum and the number of dipole active features. For example, Table 2.6 shows ethylidyne with a C_1 symmetry should exhibit a total of 15 modes with all of them being dipole active, C_s symmetry should exhibit a total of 15 modes with 8 of them being dipole active, C_3 symmetry should exhibit 10 modes with 5 of them being dipole active, and adsorbed ethylidyne with C_{3v} symmetry should exhibit 10 modes with 4 being dipole active. In practice, assigning a symmetry by counting the total number of modes and the number of dipole active modes requires great consideration for two reasons. First, as discussed previously, dipole activity depends not only on a mode being

	Symmetry			
Vibrational Mode	C_{3v}	C_3	C_s	C_1
asym CH_3 str	E	E	A'	A
			A"	A
sym CH_3 str	A_1	A	A'	A
asym CH_3 def	E	E	A'	A
			A"	A
sym CH_3 def	A_1	A	A'	A
C-C str	A_1	A	A'	A
CH_3 rock	E	E	A'	A
			A"	A
asym C-Ni str (R_x, R_y)	E	E	A'	A
			A"	A
sym C-Ni str (T_z)	A_1	A	A'	A
internal rot. (R_z)	A_2	A	A"	A
hindered trans. (T_x, T_y)	E	E	A'	A
			A"	A

Table 2.6. Symmetry representations of the vibrational modes of adsorbed ethylidyne within the four possible symmetry point groups.

totally symmetric, but also on the magnitude of its dynamic dipole moment perpendicular to the surface. If the dynamic dipole moment of a mode is small then the mode will not be detected as dipole active even though it is a totally symmetric mode. The absence of dipole activity for any of the C-H stretches is an excellent case in point. At least one of the C-H stretches is dipole allowed in all symmetry point groups, but none of the C-H stretches are

experimentally observed to be dipole active. Lack of dipole activity of C-H stretches is not surprising given that C-H stretches of hydrocarbon adsorbates are rarely observed to be dipole active because they have very small dynamic dipole moments.[15] Little information about the ethylidyne symmetry is gained by examination of the dipole activity of the C-H stretches. Secondly, while lowering the symmetry removes the degeneracy of some of the modes, these modes could still be very close in frequency, and because of electron energy loss spectroscopy's limited resolution, two modes close in frequency may be observed as one feature. Thirdly, some of the modes are too low in frequency to be observed with electron energy loss spectroscopy because they overlap with the intense elastic feature.

With these caveats noted, the C_1 and C_s symmetry point groups for adsorbed ethylidyne can be discounted. The total number of modes of adsorbed ethylidyne with a C_1 or C_s symmetry should be 15, but only 8 modes are observed in the vibrational spectra. Furthermore, ethylidyne in C_1 or C_s symmetry should yield a larger number of dipole active modes than is observed. With the acceptance that none of the C-H stretches are dipole active, 11 modes of ethylidyne should be dipole active in C_1 symmetry and 7 modes should be dipole active in C_s symmetry. However, only 3 modes are observed to be dipole active and therefore, the C_1 and C_s symmetry point groups for adsorbed ethylidyne are eliminated.

Further evidence which discounts the C_1 and C_s point groups for the symmetry of adsorbed ethylidyne is provided by the Fermi resonance observed between the symmetric CD_3 stretch at 2079 cm^{-1} and the overtone of the C-C stretch at 2195 cm^{-1} in the spectrum of $-CCD_3$ shown in Figure 2.3. Two observations show that the C-C stretching overtone is in Fermi resonance with the symmetric CD_3 stretch but is not in resonance with the antisymmetric CD_3 stretch. The first observation is the intensity borrowing from the symmetric CD_3 stretch by the C-C stretching overtone. In the vibrational spectrum of $-CCH_3$ shown in Figure 2.2, the symmetric and antisymmetric CH_3 stretching modes are equal in intensity while in the vibrational spectrum of $-CCD_3$ shown in Figure 2.3, the intensity of the

symmetric CD_3 stretch is half that of the antisymmetric CD_3 stretch due to the intensity 'borrowed' by the C-C stretch overtone as a result of the Fermi resonance. Secondly, the shift from the expected frequency of the symmetric CD_3 stretching mode, as discussed in Section III.D.1 of this chapter, shows that the C-C stretching overtone is in Fermi resonance with the symmetric CD_3 stretch but not in resonance with the antisymmetric CD_3 stretch. A Fermi interaction is allowed for modes of the same symmetry only.[26] The C-C stretch is a totally symmetric mode in all adsorption geometries, and its overtone is also totally symmetric because the cross product of a symmetric representation with another symmetric representation yields a symmetric representation. Therefore, the Fermi interaction of the overtone must be with a totally symmetric mode. The Fermi interaction is observed between the C-C stretching overtone and the symmetric CD_3 stretch and not the antisymmetric CD_3 stretch, even though the antisymmetric CD_3 stretch is closer in energy to the C-C stretching overtone. Because the antisymmetric CD_3 stretching mode is symmetric in the C_1 and C_s point group symmetries, the observed C-C stretching overtone's Fermi resonance with the symmetric CD_3 stretch but not with the antisymmetric CD_3 stretch is further evidence against the C_1 and C_s point group symmetries for ethylidyne bound to Ni(111) .

Elimination of the C_1 and C_s point groups leaves only the C_{3v} and C_3 point groups for adsorbed ethylidyne. From the vibrational spectra, differentiation between C_{3v} and C_3 is not possible because the internal rotation mode is not observed. This mode is expected to be very low in frequency and is probably masked by the large elastic feature in the electron energy loss spectra. For example, the comparable rotational mode for tribromoethane (Br_3-CCH_3) has been previously observed at 145 cm^{-1},[14] and the internal rotation of ethylidyne bound to Pt clusters supported on alumina is believed to be a free rotor.[32] Therefore, it is not surprising that the internal rotation mode of ethylidyne bound to Ni(111) is not observed in the electron energy loss spectra. Without observation of the internal rotation mode, differentiation between C_{3v} and C_3 symmetry is not possible with electron energy loss data alone.

The available spectroscopic evidence strongly suggests a C_{3v} or C_3 point group adsorption symmetry. The evidence includes: 1) only 8 vibrational modes of ethylidyne are observed; 2) of the 8 vibrational modes observed, only 3 are dipole active; and 3) a Fermi resonance is observed between the C-C stretching overtone and the symmetric CD_3 stretch but not with the antisymmetric CD_3 stretch. Ethylidyne has been reported to have C_{3v} point group geometry on two other hexagonal close packed metal surfaces, Pt(111) and Rh(111). Evidence for the geometry includes low energy electron diffraction data[5,6] in addition to a symmetry analysis of electron energy loss and IR spectroscopy data.[2,33] The symmetry for ethylidyne bound to a Co_3 cluster compound has also been determined by x-ray crystallography to be C_{3v}.[34]

Now that the symmetry of adsorbed ethylidyne has been deduced to be C_{3v} or C_3, the symmetry can be used to determine an adsorption site. Ethylidyne can bind to the Ni(111) surface with C_{3v} or C_3 symmetry at only two different adsorption sites: binding on top of one Ni atom on an atop site, or binding to three Ni atoms in a three-fold hollow site. Elimination of the atop binding site is straightforward because two C-Ni stretches are observed. Only one C-Ni stretch would be present if ethylidyne were bound to one Ni atom at the atop site. Therefore, ethylidyne adsorbed on Ni(111) is bound at a three-fold hollow site with either the C_3 or C_{3v} point group symmetry. The three-fold hollow adsorption site is not surprising considering the tetravalent bonding nature of carbon.

III.F. Assigning the Spectra to Other Two-Carbon Hydrocarbons or Hydrocarbon Fragments

To further substantiate the assignment of ethylidyne as the adsorbed reaction product of gas phase hydrogen atoms with ethylene chemisorbed on Ni(111), the assignment of the spectral features shown in Figure 2.2 to other possible adsorbed products such as ethylene, ethane, acetylene, ethyl, vinyl, acetylide, vinylidene, and ethylidene is considered. In each

case, it is demonstrated that the observed vibrational features are inconsistent with those expected for these hydrocarbons or hydrocarbon fragments.

As discussed in Chapter I, the evolution of gas phase ethylene and ethane is observed upon exposure of adsorbed ethylene to H atoms. Therefore, it is appropriate to consider ethylene and ethane in the assignment of the reaction product spectra since some of the ethylene or ethane may remain bound to the surface. The high resolution electron energy loss spectra of ethylene has been measured in this lab. Figure 2.12 shows the spectra of 0.25 ML ethylene on Ni(111). Comparison of these spectra to those of the reaction product show major differences. For example, a larger number of vibrational features are observed for adsorbed ethylene than are observed for the reaction product. Adsorbed ethylene exhibits features at approximately 2600 cm^{-1} that correspond to 'soft C-H stretches' while no comparable features are seen in the spectra of the reaction product. Another striking difference is that the three features at 400 cm^{-1}, 1200 cm^{-1} and 1440 cm^{-1} in the vibrational spectra of ethylene are dipole active while the reaction product spectra do not have dipole active features at these frequencies. Therefore, the reaction product cannot be assigned as ethylene.

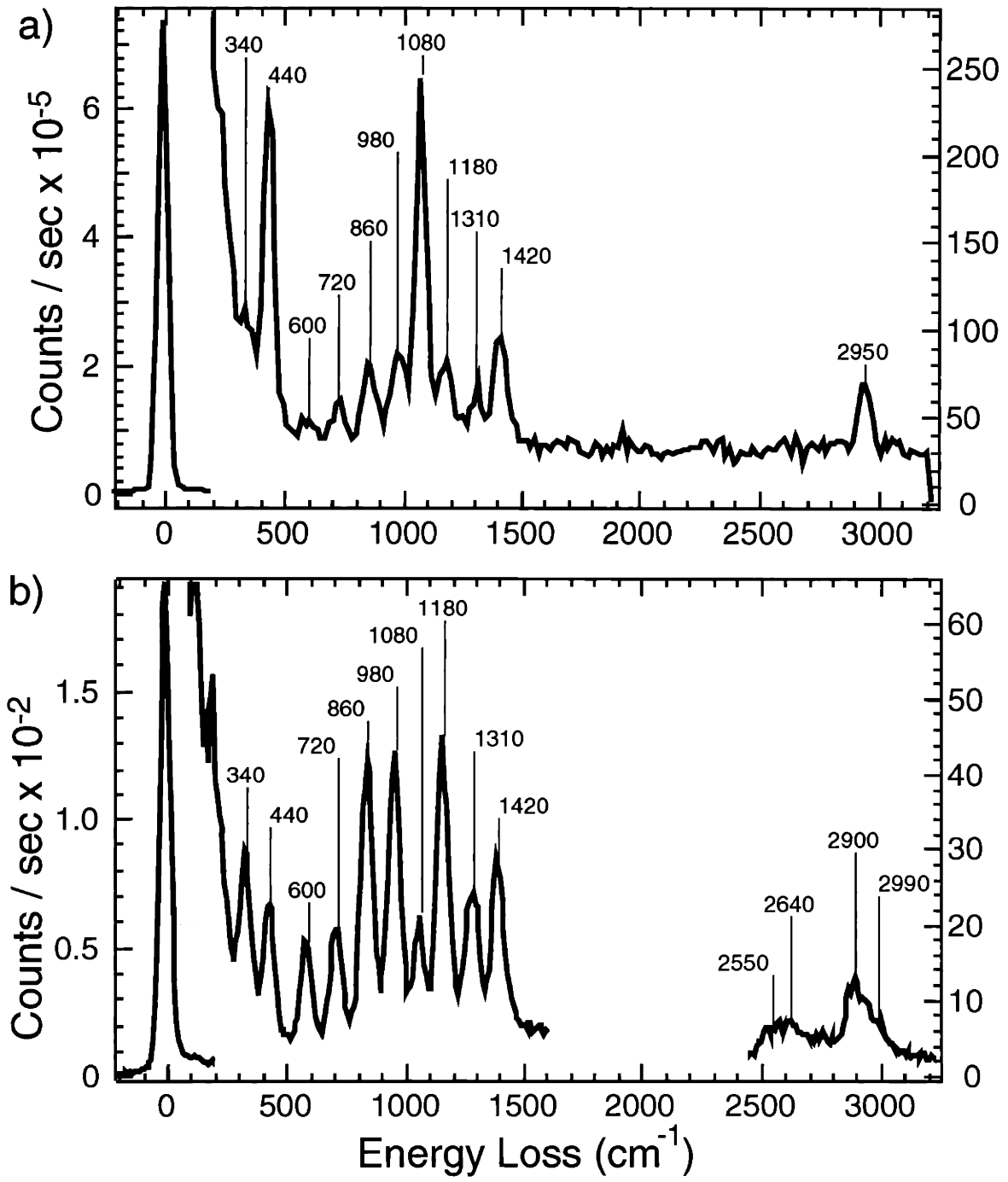

Figure 2.12. Electron energy loss spectra of 0.25 ML ethylene. **a)** Spectrum measured on specular with a resolution of 46 cm^{-1} **b)** Spectrum measured 10° off specular with a resolution of 42 cm^{-1}.

The possibility that the reaction product is adsorbed ethane can also be discounted. As discussed in Chapter I, molecular ethane desorbs from Ni(111) at temperatures as low as 80 K. Because the nickel crystal temperature is 120 K during exposure to H atoms, any ethane formed during the reaction should desorb from the surface. As mentioned previously, this gas phase evolution of ethane is exactly what is observed. Additional evidence which excludes ethane as the adsorbed reaction product is provided by the vibrational spectra of ethane. The high resolution electron energy loss spectra of 0.25 ML ethane adsorbed on Ni(111) are shown in Figure 2.13. The spectra are measured at 10 K, ensuring that the ethane does not desorb during the measurement. These spectra are very different from those observed for the reaction product. A dramatic difference between the spectra is the presence of a very intense dipole active feature at 810 cm^{-1}, the methyl rocking mode, in the spectra of adsorbed ethane while no intense features are observed in the spectra of the reaction product at this frequency. The symmetric and antisymmetric CH_3 deformation features also show differences. In the spectra of adsorbed ethane, the stronger of the two features is the antisymmetric CH_3 deformation at 1460 cm^{-1} while the symmetric CH_3 deformation feature is a shoulder on the low frequency side at approximately 1380 cm^{-1}. In contrast, the symmetric CH_3 deformation mode in the spectra of the reaction product is much more intense than the antisymmetric deformation mode. Differences also exist in the low frequency region of the spectra: modes are present at 290 cm^{-1} and 560 cm^{-1} in the spectra of adsorbed ethane while modes are present at 260 cm^{-1} and 447 cm^{-1} in the spectra of the reaction product. The vibrational spectra of the reaction product shown in Figures 2.2 are clearly not those of adsorbed ethane.

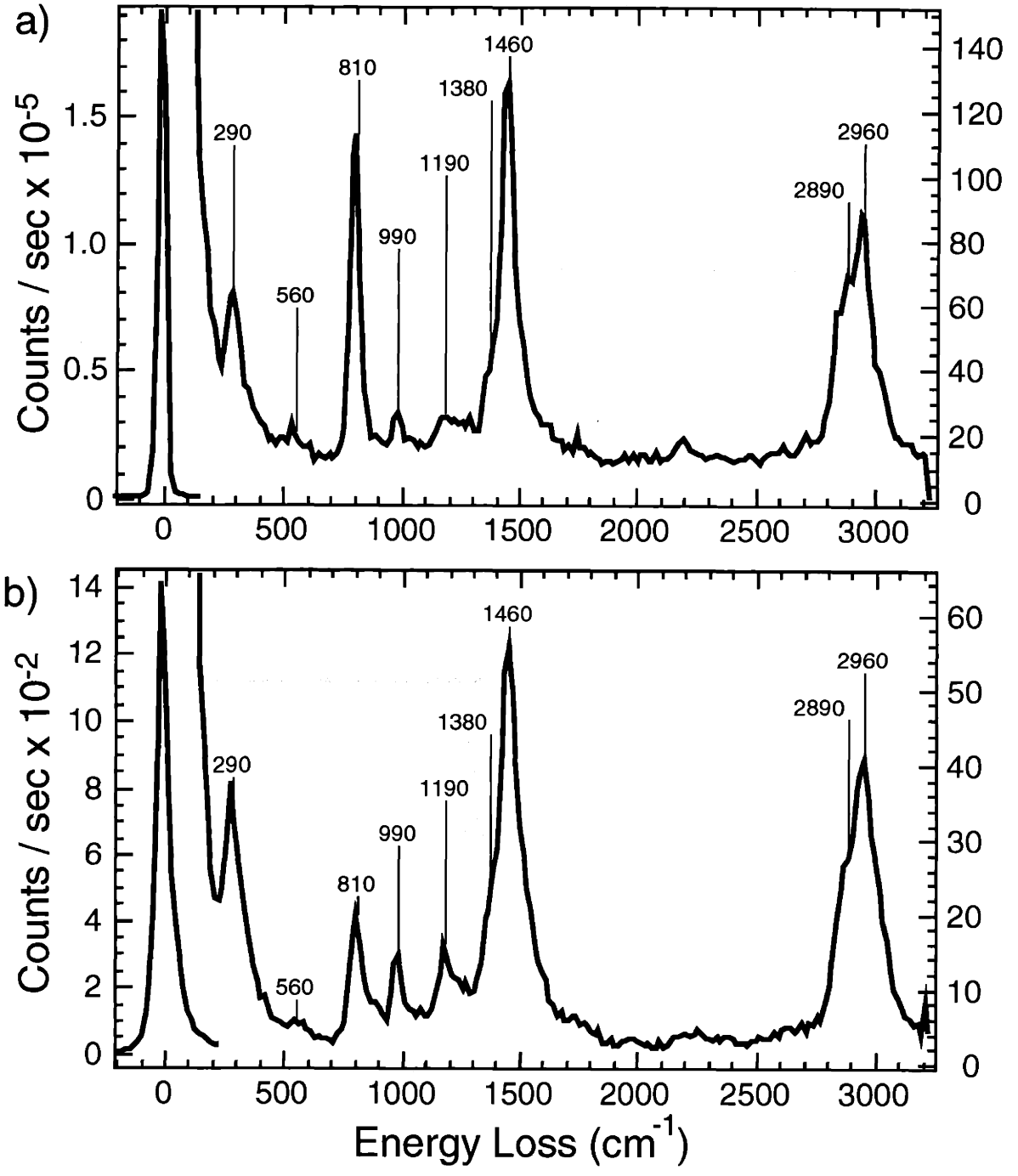

Figure 2.13. Electron energy loss spectra of 0.21 ML ethane. **a)** Spectrum measured on specular with a resolution of 40 cm^{-1} **b)** Spectrum measured 10° off specular with a resolution of 67 cm^{-1}.

Another possible reaction product is acetylene. As discussed in Chapter I, acetylene also reacts with gas phase hydrogen atoms to yield the same reaction product as the reaction of H atoms with adsorbed ethylene. This fact suggests that the reaction product is not acetylene. However, the most compelling evidence comes from a comparison between the vibrational spectra of adsorbed acetylene with those of the reaction product. Figure 2.14 shows the electron energy loss spectra of acetylene adsorbed on Ni(111). The most striking difference is the presence of a very intense dipole active feature at 1220 cm^{-1} in the spectra of adsorbed acetylene which is not observed in the spectra the reaction product. Also, the C-H stretch of acetylene is more intense than those of the reaction product. Another difference is the number of C-H stretches observed; one C-H stretch in the spectra of acetylene and two in the spectra of the reaction product. Finally, no features are observed at 500 cm^{-1} and 690 cm^{-1} in the spectra of the reaction product, but are observed in those of adsorbed acetylene. As discussed in Chapter I, one reaction product feature which does correlate well with acetylene is the 860 cm^{-1} feature. While it is clear that a small amount of acetylene is coadsorbed with ethylidyne, the features of the spectra of the reaction product cannot be assigned solely to acetylene.

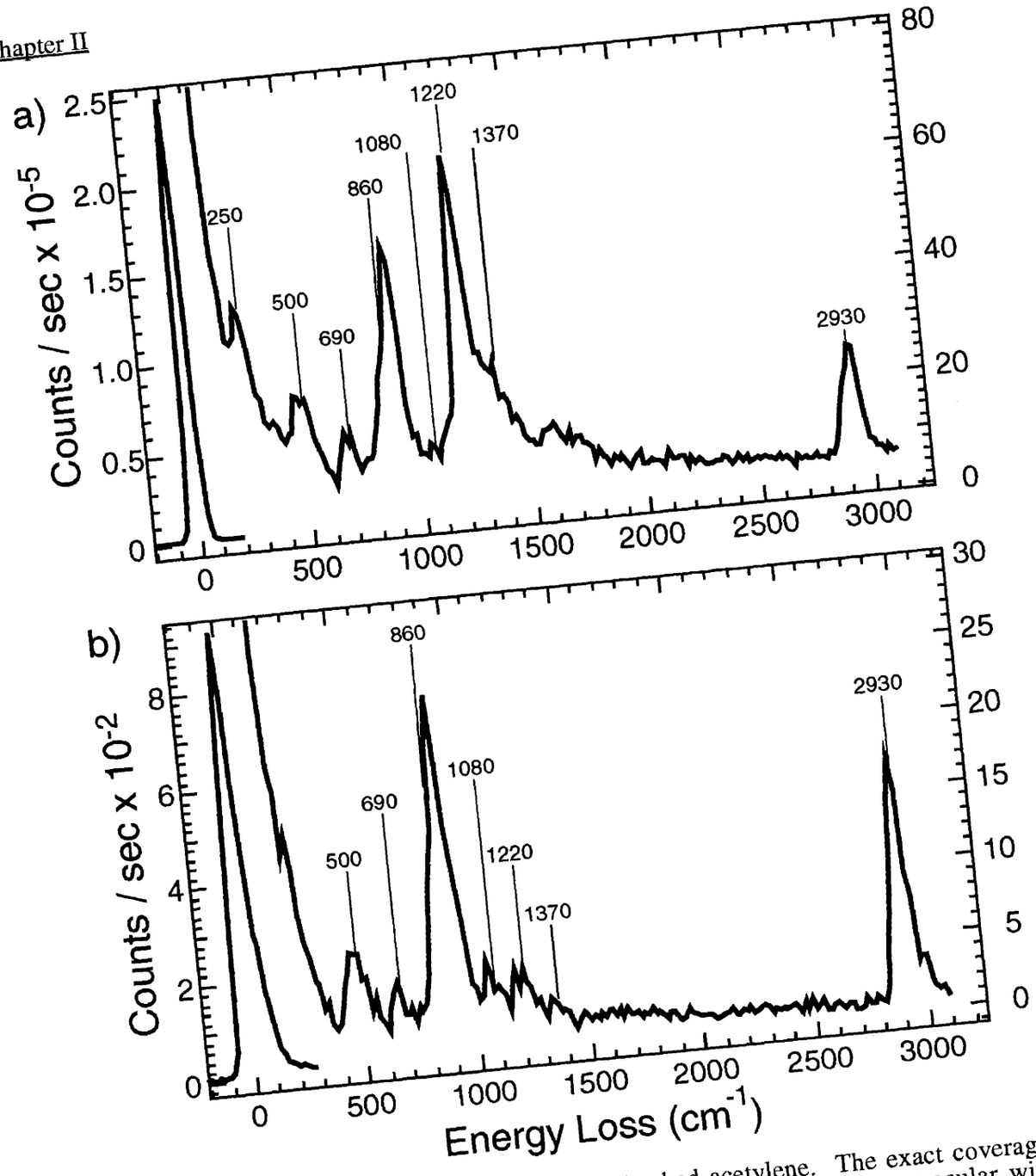

Figure 2.14. Electron energy loss spectra of adsorbed acetylene. The exact coverage is unknown, but it is likely close to 0.25 ML **a)** Spectrum measured on specular with a resolution of 42 cm^{-1} **b)** Spectrum measured 10° off specular with a resolution of 72 cm^{-1}.

Elimination of adsorbed ethylene, ethane and acetylene as possible reaction products is readily accomplished by comparison of their spectra measured after exposure of the Ni surface to gas phase ethylene, ethane and acetylene. Unlike these hydrocarbons, other possible hydrocarbon reaction products, ethyl, vinyl, acetylide, vinylidene, and ethylidene, are not 'available in a bottle'. Therefore, the surface cannot be directly exposed to these hydrocarbon fragment species, and their spectra cannot be readily measured for the purpose of serving as reference spectra. Instead, these species must be synthesized on the metal surface before their vibrational spectra can be measured. Unfortunately the synthesis and positive identification of these species can be quite difficult. For this reason, the vibrational spectra of the hydrocarbon fragments adsorbed on Ni(111) that are considered here as the possible reaction product are not available. Although none of the remaining possibilities have been spectroscopically identified on Ni(111), the vibrational spectra of these species bound to other metal surfaces have been reported. However, caution must be used when using these results as a reference because some of these studies are not always extensive as is possible or as is necessary for compelling identification of the hydrocarbon adsorbate. For example, the spectra of the isotopically labeled species are not always measured, and the resolution of the electron energy loss spectra are sometimes poor. It is also possible that the same hydrocarbon species adsorbed on a different metal surface exhibits slightly different vibrational spectra. Although not ideal, the spectra of these synthesized adsorbates combined with the vibrational spectra of gas phase and organometallic molecules with similar structure provide a reasonable data set for comparison with the reaction product spectra. Frequencies of the features observed in the vibrational spectra of hydrocarbon fragment adsorbates of ethyl, vinyl, acetylide, vinylidene, and ethylidene have been compiled and are shown in Tables 2.7, 2.8, 2.9, 2.10 and 2.13 respectively. Vibrational frequency data for molecules and organometallic compounds with similar structures are also included in the tables.

The possibility of adsorbed ethyl ($-CH_2CH_3$) as the reaction product has been explored. Table 2.7 shows vibrational frequencies for molecules with an ethyl moiety.[1,35] Included in the table are vibrational frequencies for molecular ethyl bromide adsorbed to Ni(111). This vibrational spectrum has been measured in this lab and is shown in Figure 2.15. One major difference between the ethyl species and the reaction product is the frequency of the C-C stretching mode. In all the examples of ethyl given in Table 2.7, the frequency of the C-C stretching mode of the ethyl moiety is below 1000 cm^{-1}, far from that observed for the frequency of the C-C stretching mode of the reaction product at 1130 cm^{-1}. Other differences involve the vibrational features of the CH_2 group: the CH_2 rocking mode at 1050 cm^{-1}, the CH_2 wagging mode at 1240 cm^{-1} and the CH_2 scissors mode at 1450 cm^{-1}. These features are seen in spectra of ethyl but not in that of the reaction product. The CH_2 wagging and CH_2 scissors modes are symmetric modes of an ethyl species in all adsorption symmetries and therefore, are expected to be intense in the spectra of ethyl measured in the specular direction as has been observed for ethyl adsorbed on Pt(111)[35] and is observed for molecular ethyl bromide on Ni(111) shown in Figure 2.15. The above evidence demonstrates that the spectral features of the reaction product do not match those of an adsorbed ethyl species.

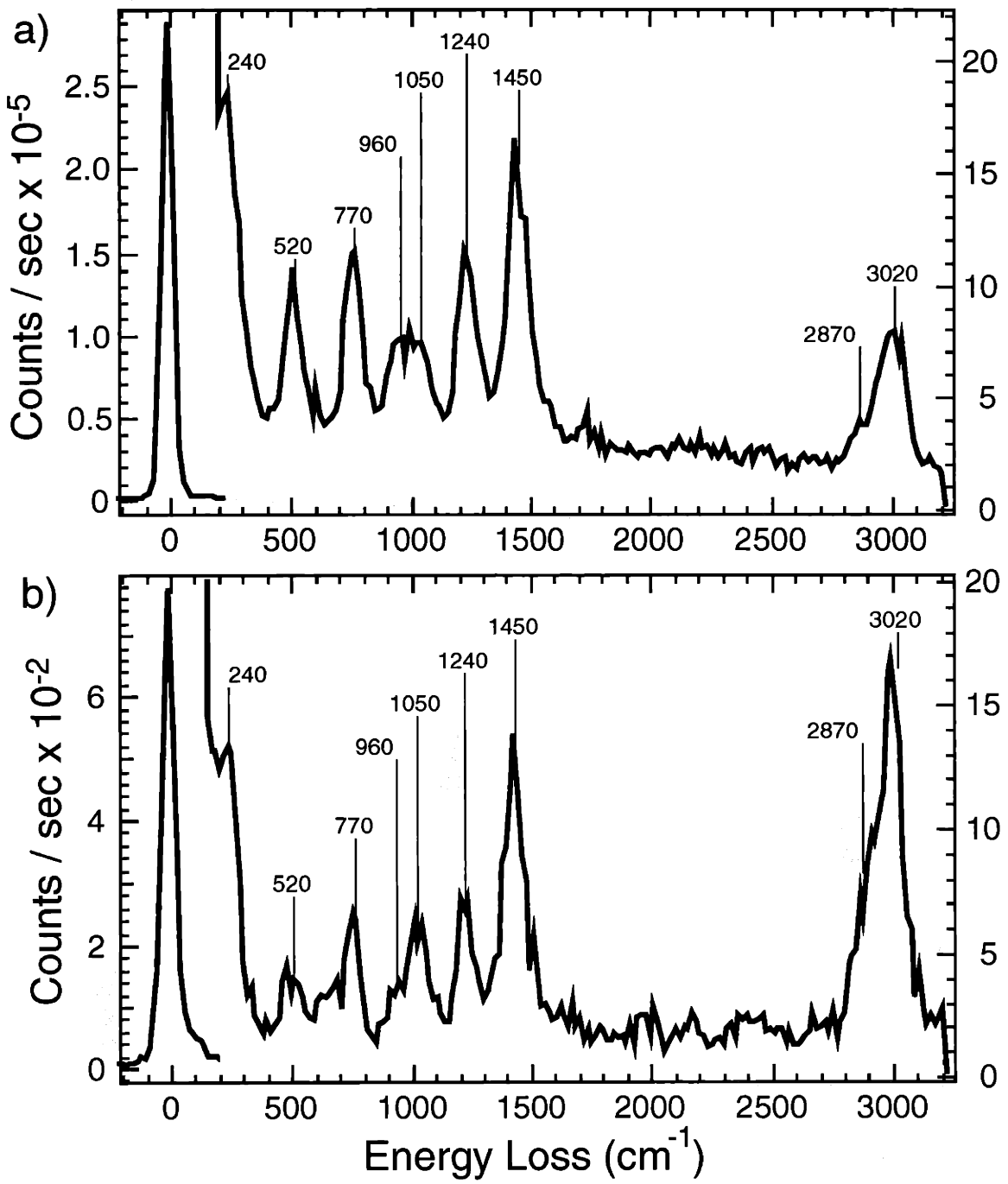

Figure 2.15. Electron energy loss spectra of ethyl bromide at less than saturation coverage. **a)** Spectrum measured on specular with a resolution of 44 cm^{-1} **b)** Spectrum measured 10° off specular with a resolution of 46 cm^{-1}.

Mode	Sym.	F $-CH_2CH_3$	Cl $-CH_2CH_3$	Br $-CH_2CH_3$	Pt(111) $-CH_2CH_3$	Ni(111)-Br $-CH_2CH_3$
asym CH_2 str	A"	3003	3012	3018		3020
asym CH_3 str	A'	3003	2983	2988	2918	3020
asym CH_3 str	A"	3003	2983	2988		
sym CH_2 str	A'	2941	2946	2937	2918	2870
sym CH_3 str	A'	2915	2890	2880	2918	2870
CH_2 sciss	A'	1479	1452	1451	1450	1450
asym CH_3 def	A'	1449	1452	1451	1430	1450
asym CH_3 def	A"	1449	1452	1451		
sym CH_3 def	A'	1395	1389	1386	1376	1400
CH_2 wag	A'	1365	1287	1252	1173	1240
CH_2 twist	A"	1277	1244	1248		
C-C str	A'	1048	972	964	1022	960
CH_3 rock	A'	1108	1080	1061	941	1050
CH_3 rock	A"	1048	972	964		
CH_2 rock	A"	810	785	770		770
C-X str	A'	880	676	583	484	520
C-C-X def	A'	415	336	290		240
Torsion	A"	243	243	247		
Reference		Ref. 1	Ref. 1	Ref. 1	Ref. 35	Figure 2.15

Table 2.7. Observed vibrational frequencies in cm^{-1} for molecules with an ethyl moiety.

Another possibility for the reaction product, vinyl (-$CHCH_2$), has also been explored. Several studies have reported the vibrational spectrum of adsorbed vinyl.[36-41] The most complete and compelling of these studies is one in which a vinyl species is produced from ethylene decomposition on Ni(100) at 175 K.[36] The reported vibrational frequencies are reproduced in Table 2.8 along with those of other molecules with vinyl moieties. The most striking difference in the vibrational features of vinyl compared to those of the reaction product is the frequency of the C-C stretching mode. Excluding organometallic complexes, the frequency of the C-C stretching mode of a vinyl moiety occurs in the 1550-1610 cm^{-1} range, but no feature is observed in this frequency range in the spectra of the reaction product. The frequency of the C-C stretching mode of the organometallic vinyl species is observed at lower frequencies, approximately 1300 cm^{-1}, because of interaction of the π electrons of the C-C double bond with the metal atoms of the complex, lowering the C-C bond strength. The spectra of the reaction product in Figure 2.2 show features at 1329 cm^{-1}, but they cannot be assigned to the C-C stretching mode because their frequency shifts downward upon deuteration. Another difference between the vibrational spectra of a vinyl species and that of the reaction product is the intense CH_2 scissors mode in the frequency range of 1370-1480 cm^{-1} observed for the vinyl species. Although an intense feature is observed at 1332 cm^{-1} in the reaction product spectra to which a CH_2 scissors mode of vinyl could be assigned, the vinyl moiety can not account for the 1398 cm^{-1} feature observed in the spectra of the reaction product. The intensity of the 1398 cm^{-1} feature in the spectra of the reaction product in Figure 2.2 is too low for this features to be assigned to the CH_2 scissors mode because this mode is one of the most intense features of the electron energy loss spectra of a vinyl species bound to a metal surface.[36-38] A final difference between the spectra of vinyl and those of the reaction product is that vinyl has a CH rocking mode between 1220-1270 cm^{-1} which is not observed in the spectrum of the reaction product. This evidence eliminates adsorbed vinyl as the reaction product of hydrogen atoms with ethylene adsorbed on Ni(111).

Mode	Br-$CHCH_2$	M-$(CHCH_2)_4$, M=Si, Ge, Sn, and Pb	Ni(100)-$CHCH_2$	Pt(111)-$CHCH_2$	$(CO)_9Os_3H$-$CHCH_2$	$(C_5H_5)_2Ru_2$-$CHCH_2$
C-X str	611	420-530	420			
CH wag	583	450-580	760	690	786	780
CH_2 wag	942	920-950	915	955	1009	970
CH_2 twist		900-1020	1160			
CH_2 rock	1006	900-1020	1160		990	865
CH rock	1256	1220-1265	1280	1255	1266	1286
CH_2 sciss	1373	1370-1400	1405	1380	1475	1469
C=C str	1604	1565-1610	1555	1600	1311	1301
CH str	3086	2930-3080	2920	2920	2997	2981
sym CH_2 str		2900-3030	2920	2920	2920	2904
asym CH_2 str		3000-3110	3090	2920	3062	3041
Ref.	Ref. 42	Ref. 41	Ref. 36	Ref. 37	Ref. 40	Ref. 40

Table 2.8. Observed vibrational frequencies in cm^{-1} for molecules with a vinyl moiety.

Similarly, the spectrum of the reaction product can be shown to be inconsistent with that of adsorbed acetylide (-CCH). Acetylide has been proposed as a decomposition product of acetylene,[43-48] ethylene[44,47,49,50-52] and benzene[53] on a variety of metal surfaces. The observed frequencies of the vibrational features from some of these studies are reproduced in Table 2.9 along with the vibrational frequencies of an organometallic acetylide species.[54] There are difficulties in assigning the spectra of the reaction product to that of acetylide. First, 8 modes are observed in the spectra of the reaction product while only 6 modes which have been identified in the spectra of acetylide. The frequency of the C-C stretching mode of

acetylide is also different from that observed for the reaction product. The observed frequencies for a the C-C stretch of acetylide occur between 1260 - 1540 cm^{-1}, but the frequency of the C-C stretching mode of the reaction product is 1130 cm^{-1}. Finally, the observed C-H bending mode frequencies of acetylide are all below 930 cm^{-1}, while the reaction product has two C-H bending modes at 1332 cm^{-1} and 1398 cm^{-1}. Clearly, the reaction product cannot be assigned as adsorbed acetylide.

Mode	Br-CCH	$Os_3H(CO)_9$ -CCH	Ni(110)- CCH	Ru(001)- CCH	Ru(111)- CCH	Pd(110)- CCH
sym C-M str	618		380		325	400
asym C-M str			465	435	475	460
C-H rock		760			800	650
C-H wag	618	860	890	750	850	925
C-C str	2085	1534	1290	1290	1365	1260
C-H str	3325	3157	2990	2960	3008	2960
Reference	Ref. 1	Ref. 54	Ref. 44	Ref. 49	Ref. 53	Ref. 51

Table 2.9. Observed vibrational frequencies in cm^{-1} for molecules with an acetylide moiety.

Vinylidene (-CCH2) has also been considered as the reaction product. Vinylidene has been proposed as a decomposition product of both ethylene and vinyl iodide on a few different metal surfaces.[39,55-57] However, in two of these studies,[55,56] no C-H bending modes have been resolved so these studies have not been included in the compilation of the vibrational frequencies for vinylidene species shown in Table 2.10. The frequencies of the CH_2 rocking mode observed in the remaining studies are very scattered, 960 - 1320 cm^{-1}, making comparison to this mode difficult. Observation of the CH_2 wagging mode of vinylidene could be obscured by the Ni-H feature in the spectra of the reaction product

because the frequency of the antisymmetric Ni-H stretching mode, 950 cm^{-1}, is close to the range of frequencies observed for the CH_2 wagging mode, 890 - 970 cm^{-1}. Also, the CH_2 twisting mode is observed only in two of the studies listed in Table 2.10 and neither of these studies are of a vinylidene moiety that is bound to a metal surface. Therefore, it is difficult to exclude vinylidene as a possible reaction product using the frequencies of the CH_2 twisting, CH_2 wagging, and CH_2 rocking modes of vinylidene for comparison with the spectral features of the reaction product. However, the C-C stretching mode and the CH_2 scissors mode of vinylidene can be shown to be inconsistent with the spectral features of the reaction product. In vinylidene, the frequencies of the C-C stretching mode are reported to range from 1300 cm^{-1} to 1660 cm^{-1}, which are very different from the frequency observed for the C-C stretch of the reaction product, 1129 cm^{-1}. The CH_2 scissors mode of vinylidene is also inconsistent with the observed vibrational features of the reaction product. Although the feature at 1398 cm^{-1} in the spectra of the reaction product matches the frequency range expected for a CH_2 scissors mode of vinylidene, 1400 - 1470 cm^{-1}, the feature is too low in intensity to be assigned as such. The CH_2 scissors mode is a symmetric mode in all adsorption symmetries and therefore, is expected to be an intense mode. It has indeed been observed to be one of the more intense features in the electron energy loss spectra of vinylidene bound to a metal surface.[57] The vibrational features of vinylidene do not match those of the reaction product, and therefore, it can be excluded as a possibility.

Mode	Hydrocarbon -CCH_2	Cl_2 -CCH_2	$Os_3H_2(CO)_9$ -CCH_2	$Ru_2(CO)_3(C_5H_5)_2$ -CCH_2	Pt(111) -CCH_2	Ru(001)/O -CCH_2
X-C str		603,800	255,311			455
CH_2 twist		686	811			
CH_2wag	885-895	857	963	973	921	895
CH_2 rock	1290-1320	1095	1051	988	1071	965
CH_2 sciss	1420-1410	1400	1470		1440	1435
C=C str	1620-1660	1627	1331	1582	1306	1435
sym CH_2 str	2970-2985	3035	2987	3028		2985
asym CH_2 str	3075-3095	3130	3047	3095		3050
Reference	Ref. 58	Ref. 1	Ref. 59	Ref. 59	Ref. 39	Ref. 57

Table 2.10. Observed vibrational frequencies in cm^{-1} for molecules with an vinylidene moiety.

The last structure considered in assigning the vibrational spectra of the reaction product is an ethylidene structure (-$CHCH_3$). The possibility of ethylidene as the reaction product is considered extensively because the similarity of its structure to that of ethylidyne could result in nearly identical vibrational spectra. Ethylidene might also explain the feature observed at 860 cm^{-1} in Figure 2.2 which cannot be assigned as a ethylidyne mode. Included in the examination of ethylidene as the reaction product is a normal modes analysis of the spectral features of the reaction product with an ethylidene geometry which is shown in Figure 2.16. The force constants that yield the calculated frequencies which best fit the observed frequencies are given in Table 2.12 along with force constants employed in previous normal modes calculations for molecules with ethylidene moieties.[60,61] The calculated

frequencies are listed in Table 2.11 and are shown in Figure 2.17 overlaid on the vibrational spectra of the reaction product.

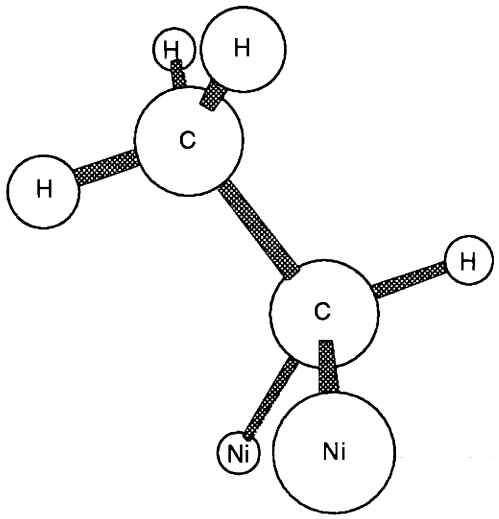

Bond Angles (degrees)		Bond Lengths (Å)	
H_3-C-H_3	107	C-H_3	1.09
H_3-C-C	111	C-C	1.52
C-C-Ni	111	C-Ni	1.57
Ni-C-Ni	112	C-H	1.09
C-C-H	110		

Figure 2.16. Geometry used in the normal modes calculation of ethylidene.

Mode	Sym	Ni_2-$CHCH_3$
CH str	A'	2951
asym CH_3 str	A'	2945
asym CH_3 str	A"	2947
sym CH_3 str	A'	2882
asym CH_3 def	A'	1405
asym CH_3 def	A"	1404
CH_3 def	A'	1375
sym CH def	A'	1305
asym CH def	A"	876
CH_3 rock	A'	1052
CH_3 rock	A"	1024
CC str	A'	1129
asym CX_2 str	A"	265
sym CX_2 str	A'	437

Table 2.11. Calculated vibrational frequencies in cm^{-1} for ethylidene.

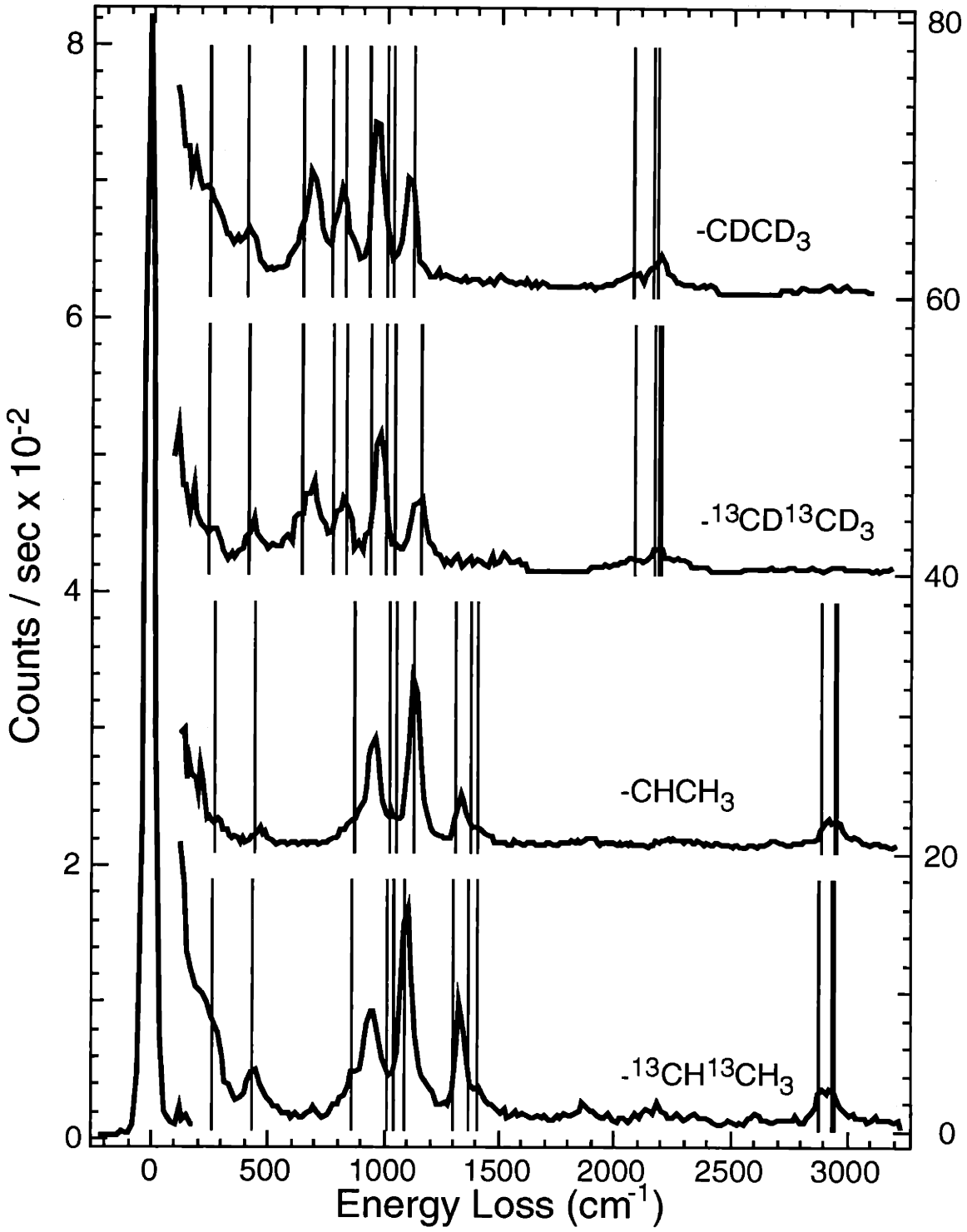

Figure 2.17. Electron energy loss spectra of the four isotopomers of the reaction product with the calculated normal mode frequencies of ethylidene included and shown as vertical lines.

Force Constant	Cl_2-$CHCH_3$	Br_2-$CHCH_3$	Ni_2-$CHCH_3$
C-H_3 str	4.86	4.84	4.64
C-C str	4.28	4.33	5.1
H_3-C-H_3 bend	0.53	0.52	0.45
H_3-C-C bend	0.64	0.69	0.71
C-H_3 / C-H_3	0.07	0.08	0.04
C-C / H_3-C-C	0.25	0.25	0.04
H_3-C-C / H_3-C-C	-0.02	-0.02	0
C-H str	4.99	5.01	4.71
C-C-H bend	0.64	0.57	0.86
H-C-X bend	0.61	0.58	0.34
C-C-X bend	1.46	1.4	0.18
X-C-X bend	1.05	1.21	0
CH_3 tors.	0.016	0.13	0
C-X str	2.5	1.81	0.89
C-X / C-X	0.67	0.38	0.6
C-X / X-C-X	0.25	0.25	0
C-C / C-X	0.4	0.4	0
C-X / H-C-X	0.2	0.2	0
Ni-Ni str			0.3
C-C / H_3-C-H_3			-0.35
H_3-C-H_3 / H_3-C-H_3			-0.04
Reference	This work	Ref. 61	Ref. 60

Table 2.12. Force constants used in the normal modes calculation of ethylidene in this work and previous work. Units are in units of mdyne/Å for stretching and stretch/stretch coupling constants, mdyne Å for bending and bend/bend coupling constants and mdyne for stretch/bend coupling constants. X = Cl, Br or Ni.

Mode	Sym in C_s point group	Cl_2 -$CHCH_3$	Br_2 -$CHCH_3$	$Os_2(CO)_8$ -$CHCH_3$	$Ru_2(CO)_3(C_5H_5)_2$ -$CHCH_3$	Pt(111)/K-$CHCH_3$
CH str	A'	3017	3023	2918	2903	2955
asym CH_3 str	A'	2997	2996	2950	2947	
asym CH_3 str	A"		2985			
sym CH_3 str	A'	2947	2937	2849	2835	2855
asym CH_3 def	A'	1448	1443	1449	1445	1435
asym CH_3 def	A"					
CH_3 def	A'	1387	1383	1369		
sym CH def	A'	1284	1260	1302	1264	1210
asym CH def	A"	1232	1172	945	968	
CH_3 rock	A'	1089	1070	1053		1110
CH_3 rock	A"	1067	1045	1030	968	
CC str	A'	984	966	989		900
asym CX_2 str	A"	707	620	545		415
sym CX_2 str	A'	652	545	448		
Reference		Ref. 60	Ref. 61	Ref. 63	Ref. 63	Ref. 62

Table 2.13. Observed vibrational frequencies in cm^{-1} for molecules with an ethylidene moiety.

Ethylidene has been reported to be the decomposition product of ethylene on a potassium covered Pt(111) surface.[62] The vibrational frequencies observed for ethylidene adsorbed on a potassium covered Pt(111) surface are shown in Table 2.13 along with observed frequencies of gas phase and organometallic molecules with an ethylidene moiety.[60,61,63] The most striking difference between the vibrational spectra reported for

ethylidene and those of the reaction product is the C-C stretching frequency. Table 2.13 shows the C-C stretching mode of ethylidene to be in the 960 - 990 cm^{-1} frequency range in contrast to the C-C stretching mode of the reaction product observed at 1130 cm^{-1}.

In principle, ethylidene can be distinguished from ethylidyne by the total number of vibrational modes. Because it has one more hydrogen atom than ethylidyne, ethylidene has three more modes than ethylidyne, one C-H stretching and two C-H deformation modes. Another difference between the two which results in more modes expected for ethylidene than ethylidyne is the symmetry of the two adsorbates. Since adsorbed ethylidene cannot attain the C_3 or C_{3v} symmetry that adsorbed ethylidyne has been shown to attain in Section III.E, the degeneracy of the doubly degenerate modes, the antisymmetric CH_3 stretching modes, the antisymmetric CH_3 deformation modes and the CH_3 rocking modes is lifted, and each should yield two modes in the vibrational spectra. Therefore, ethylidene should have six more modes than ethylidyne.

If spectra of the reaction product were those of ethylidene these modes must be accounted for. Table 2.1 shows typical frequencies for the C-H stretch of ethylidene to occur at 2900 - 3020 cm^{-1}. A mode in this frequency range could be obscured from observation by overlap with the symmetric and antisymmetric CH_3 stretching modes. The additional two deformation modes of ethylidene due to the extra H atom must still be accounted for in the vibrational spectra. Table 2.13 shows that the frequency of the antisymmetric CH deformation mode of ethylidene is expected to be lower in frequency than the symmetric CH deformation mode. The low intensity, slightly dipole active, 860 cm^{-1} feature observed in the reaction product spectra in Figure 2.2 could possibly be assigned to the antisymmetric CH deformation of ethylidene. As discussed previously in this chapter a mode must have a significant perpendicular dynamic dipole moment for it to be dipole active. Movement of a hydrogen atom parallel to the surface, as is the case for the antisymmetric CH deformation of ethylidene, is not expected to create a large dynamic dipole perpendicular to the surface.

Because it is observed to be dipole active, assignment of the 860 cm^{-1} feature to the antisymmetric CH deformation mode of ethylidene is inconsistent.

If the reaction product was ethylidene, its symmetric CH deformation mode must also be accounted for in the vibrational spectra. Vibration of this mode is perpendicular to the surface, and is expected to be dipole active. Therefore, the symmetric CH deformation should be quite intense in the spectra measured in the specular direction of ethylidene bound to a surface. The symmetric CH deformation mode has been reported to be the second most intense mode in the spectra of ethylidene bound to a Pt(111) surface.[62] Table 2.13 shows the frequency of the symmetric CH deformation mode of ethylidene to be in the 1210 - 1310 cm^{-1} range. No feature in the spectra of the reaction product is seen in this frequency range. Perhaps the symmetric CH deformation mode is superimposed with the symmetric CH_3 deformation at 1332 cm^{-1} in the spectra of the reaction product. Attempts to fit these two modes to the same frequency, 1332 cm^{-1}, with the normal modes analysis have failed as the frequency of neither mode is fit to 1332 cm^{-1}. Table 2.11 shows that the resulting calculated frequencies are 1375 and 1305 cm^{-1} for the symmetric CH_3 and the symmetric CH deformation modes, respectively. Examination of the normal mode displacement vectors offers an explanation: the two modes are efficiently mixed and therefore, repel each other with neither mode being fit to the 1332 cm^{-1} frequency. The fact that the normal modes analysis is unable to fit both the symmetric CH_3 and the symmetric CH deformation modes to the same frequency suggests that the 1332 cm^{-1} feature is not a superposition of these two modes. The resolution of the electron energy loss spectra is such that two modes separated by 70 cm^{-1} should be resolvable. Therefore, no symmetric CH deformation mode of ethylidene can be assigned to an observed feature in the reaction product spectra.

The modes in which the degeneracy is lifted in the lower symmetry of ethylidene are the antisymmetric CH_3 deformation mode, the antisymmetric CH_3 stretching mode and the CH_3 rocking mode. Only one feature is observe for each pair of these modes in the spectra of

the reaction product. However, the detection of only one feature could be a result of the limited resolution of the electron energy loss spectra. The observed feature might be a superposition of the two modes. Table 2.11 shows that, unlike the symmetric CH_3 and the symmetric CH deformation modes, the normal modes calculation is able to fit each pair of antisymmetric CH_3 deformation modes, antisymmetric CH_3 stretching modes and CH_3 rocking modes to frequencies that are within the resolution of the electron energy loss spectra. Therefore, the observation of only one feature for each pair of these modes is not inconsistent with an ethylidene species. However, the observed lack of dipole activity of features arising from the CH_3 rocking and the antisymmetric CH_3 deformation modes is inconsistent with assigning these features to those of ethylidene because these modes are dipole allowed in C_s or lower symmetry. Also, because surface bound ethylidene is expected to be tilted with respect to the surface, the CH_3 rocking mode and the antisymmetric CH_3 deformation mode are expected to have a dynamic dipole moment perpendicular to the surface. A dynamic dipole moment perpendicular to the surface would result in these dipole allowed CH_3 rocking mode and antisymmetric CH_3 deformation mode to be dipole active features. The fact that neither the antisymmetric CH_3 deformation nor the CH_3 rocking modes are observed to be dipole active in the reaction product spectra provides further evidence that the spectra of the reaction product is not that of ethylidene.

Assignment of the spectra of the reaction product to vibrational modes of ethylidene is inconsistent for several reasons: 1) The frequency of the C-C stretching mode observed in the spectrum of the reaction product is higher than that expected for an ethylidene species. 2) The antisymmetric CH deformation mode is not expected to be dipole active, in contrast to the dipole active 860 cm^{-1} feature observed in the reaction product spectrum. 3) The total number of modes observed in the vibrational spectrum is inconsistent with an ethylidene structure because no symmetric CH deformation mode is observed, and 4) The lack of dipole

activity of the CH_3 rocking and the antisymmetric CH_3 deformation modes observed in the reaction product spectra is inconsistent with the low symmetry of an ethylidene structure.

In summary, the spectra of the adsorbed reaction product from exposure of adsorbed ethylene to gas phase hydrogen atoms have been shown to be inconsistent with that of ethylene, ethane, acetylene, ethyl, vinyl, vinylidene, acetylide, or ethylidene. Elimination of these possible hydrocarbon and hydrocarbon fragment species further validates the adsorbed reaction product assignment to adsorbed ethylidyne.

IV. Conclusions

The adsorbed reaction product of gas phase hydrogen atoms with adsorbed ethylene has been identified as ethylidyne. The evidence has come from the assignment of the electron energy loss spectra of four ethylidyne isotopomers. Several different approaches to the assignment have been employed: comparison of the observed vibrational frequencies to group frequencies, comparison of the vibrational features to those of other molecules with ethylidyne moieties, determination of the shift in the mode frequencies upon isotopic labeling, and determination of the dipole activity of the feature.

The assignment has been confirmed by a normal modes analysis calculation. The force constants employed in the calculation have been shown to be appropriate by comparison to force constants used in other normal modes calculation. The observed frequencies match the frequencies calculated by the normal modes analysis within experimental error. The normal modes calculations showed the upward shift in the C-C stretching frequency upon deuteration to be due to mixing of this mode with the symmetric CH_3 deformation mode.

The assignment of the spectral features of the reaction product to those of ethylidyne has been further confirmed by showing that the electron energy loss spectra are inconsistent with every other two-carbon hydrocarbon or hydrocarbon fragment.

The symmetry of ethylidyne adsorbed on the Ni(111) surface has been determined to be C_{3v} or C_3 through the analysis of the dipole activity of the electron energy loss spectra. Using the adsorption symmetry, the adsorption site has been determined to be the three-fold hollow site. The three-fold hollow site for ethylidyne adsorption on Ni(111) is consistent with the ethylidyne adsorption site previously determined on two other hexagonal close packed surfaces: Pt(111) and Rh(111).

V. References

1. T. Shimanouchi, Tables of Molecular Vibrational Frequencies, Natl. Std. Ref. Data Ser., Natl. Bur. Std. (US) **39** (1962).
2. H. Steininger, H. Ibach and S. Lehwald, Surf. Sci. **117**, 685 (1982).
3. B. E. Koel, B. E. Bent and G. A. Somorjai, Surf. Sci. **146**, 211 (1984).
4. P. Skinner, M. W. Howard, I. A. Oxton, S. F. Kettle, D. B. Powell and N. Sheppard, J. Chem. Soc., Faraday Trans. **77**, 1203 (1981).
5. L. H. Dubois, D. G. Castner and G. A. Somorjai, J. Chem. Phys. **72**, 5234 (1980).
6. U. Starke, A. Barbieri, N. Materer, M. A. Van Hove and G. A. Somorjai, Surf. Sci. **286**, 1 (1993).
7. H. Ibach and S. Lewald, J. Vac. Sci. Technol. **15**, 407 (1978)
8. L. L. Kesmodel, L. H. Dubois and G. A. Somorjai, J. Chem. Phys. **70**, 2180, (1979).
9. H. Steininger, H. Ibach and S. Lehwald, Surf. Sci. **117**, 685 (1982).
10. S. L. Tang, Ph. D. Thesis, Massachusetts Institute of Technology, 1985.
11. M. B. Lee, Ph. D. Thesis, Massachusetts Institute of Technology, 1987.
12. J. D. Beckerle, Ph. D. Thesis, Massachusetts Institute of Technology, 1988.

13. L. Hammer, T. Hertlein and K. Muller, Surf. Sci. **178**, 693 (1986).

14. T.R. Stengle and R. C. Taylor, J. Mol. Spec. **34**, 33 (1970).

15. H. Ibach and D. L. Mills, *Electron Energy Loss Spectroscopy and Surface Vibrations*, New York: Academic Press, 1982.

16. G. Hertzberg, *Molecular Spectra and Molecular Structure, Vol. 2*, Malabar: Krieger Publishing, 1991.

17. J. L. Duncan, Spectrochim. Acta **20**, 1197, (1964).

18. W. G. Johnson, V. Buch and M. Trenary, J. Chem. Phys. **93**, 9167 (1990).

19. S. Califano, *Vibrational States*, New York: John Wiley & Sons, 1976.

20. W. H. Press, *Numerical Recipes in FORTRAN: The Art of Scientific Computing*, New York: Cambridge Universiy Press, 1992.

21. K. J. Maynard, A. D. Johnson, S. P. Daley and S. T. Ceyer, Faraday Discuss. Chem. Soc. **91**, 437 (1991).

22. A. D. Johnson, Ph. D. Thesis, Massachusetts Institute of Technology, 1991.

23. H. P. Steinruck, A. Winkler and K. D. Rendulic, Surf. Sci. **152/153**, 323 (1985).

24. Q. Y. Yang, Ph. D. Thesis, Massachusetts Institute of Technology, 1989.

25. D. A. McQuarrie and P. A. Rock, *General Chemistry*, New York: W. H. Freeman and Company, 1984.

26. I. N. Levine, *Molecular Spectroscopy*, New York: John Wiley & Sons, 1975.

27. M. A. Barteau, J. Q. Broughton and D. Menzel, Appl. Surf. Sci. **19**, 92 (1984).

28. B. Crawford, J. Chem. Phys. **20**, 977 (1952).

29. S. P. Daley, Ph. D. Thesis, Massachusetts Institute of Technology, 1994.

30. H. Ibach and S. Lehwald, J. Vac. Sci. Technol. **18**, 625 (1981).

31. Q. Y. Yang, K. J. Maynard, A. D. Johnson and S. T. Ceyer, J. Chem. Phys. **102**, 7734 (1995).

32. P. K. Wang, C. P. Slichter and J. H. Sinfelt, J. Phys. Chem **89**, 3606 (1985).

33. I. J. Malik, M. E. Brubaker, S. B. Moshin and M. Trenary, J. Chem. Phys. **87**, 5554 (1987).

34. P. W. Sutton and L. F. Dahl, J. Am. Chem. Soc. **89**, 261 (1967).

35. K. G. Lloyd, B. Roop, A. Campion and J. M. White, Surf. Sci. **214**, 227 (1989).

36. F. Zeara and R. B. Hall, Surf. Sci. **180**, 1 (1987).

37. Z. M. Liu, X. L. Zhou, D. A. Buchanan, J. Kiss and J. M. White, J. Am. Chem. Soc. **114**, 2031 (1992).

38. E. M. Stuve and R. J. Madix, J. Phys. Chem. **89**, 105 (1985).

39. F. Zaera and N. Bernstein, J. Am. Chem. Soc. **116**, 4881 (1994).

40. J. Evans and G. S. McNulty, J. Chem. Soc. Dalton Trans. **1983**, 639.

41. G. Masetti and G. Zerbi, Spectrochimica Acta **26A**, 1891 (1970).

42. L. M. Sverdlov, M. A. Kovner and E. P. Krainov, *Vibrational Spectra of Polyatomic Molecules*, New York: Wiley, 1974.

43. L. L. Kesmodel, G. D. Waddill and J. A. Gates, Surf. Sci. **138**, 464 (1984).

44. J. A. Stroscio, S. R. Bare and W. Ho, Surf. Sci **148**, 499 (1984).

45. J. E. Parmeter, M. M. Hills and W. H. Weinberg, J. Am. Chem. Soc. **108**, 3563 (1986).

46. T. S. Marinova and P. K. Stefanov, Surf. Sci. **191**, 66 (1987).

47. F. Zaera and R. B. Hall, J. Phys. Chem. **91**, 4318 (1987).

48. J. Yoshinobu, T. Sekatani, M. Onchi and M. Nishijima, J. Phys. Chem. **94**, 4269 (1990).

49. M. M. Hills, J. E. Parmeter, C. B. Mullins and W. H. Weinberg, J. Am. Chem. Soc. **108**, 3554 (1986).

50. F. Zaera and R. B. Hall, J. Phys. Chem. **91**, 4318 (1987).

51. M. Nishijima, J. Yoshinobu, T. Sekitani and M. Onchi, J. Chem. Phys. **90**, 5114 (1989).

Chapter II

52. A. L. Backman and R. I. Masel, J. Phys. Chem. **94**, 5300 (1990).

53. B. E. Koel, J. E. Crowell, B. E. Bent, C. M. Mate and G. A. Somorjai, J. Phys. Chem. **90**, 2949 (1986).

54. J. Evans and G. S. McNulty, J. Chem. Soc. Dalton Trans. **1984**, 79.

55. J. A. Gates and L. L. Kesmodel, Surf. Sci. **124**, 68 (1983).

56. G. H. Hatzikos and R. I. Masel, Surf. Sci. **185**, 479 (1987).

57. M. M. Hills, J. E. Parmeter and W. H. Weinberg, J. Am. Chem. Soc. **109**, 597 (1987).

58. G. Socrates, *Infrared Characteristic Group Frequencies*, Chichester: John Wiley and Sons, 1980.

59. J. Evans and G. S. McNulty, J. Chem. Soc. Dalton Trans. **1983**, 639.

60. J. R. Durig, A. E. Sloan and J. D. Witt, J. Phys. Chem. **76**, 3591 (1972).

61. J. R. Durig, A. E. Sloan, J. W. Thompson and J. D. Witt, J. Chem. Phys. **60**, 2260 (1974).

62. R. G. Windham and B. E. Koel, J. Phys. Chem. **94**, 1489 (1990).

63. C. E. Anson, N. Sheppard, D. B. Powell, J. R. Norton, W. Fischer, R. L. Keiter, B. F. Johnson, J. Lewis, A. K. Bhattacharrya, S. A. Knox and M. L. Turner, J. Am. Chem. Soc. **116**, 3058 (1994).

CHAPTER III:
ATTEMPTS AT SYNTHESIS OF AN ETHYL SPECIES ADSORBED ON Ni(111)

I. Introduction

Previous studies have shown that hydrogen emerging from the bulk to the Ni(111) surface can hydrogenate adsorbed ethylene to ethane.[1] These studies also demonstrated that surface bound hydrogen does not hydrogenate adsorbed ethylene. The differences in the reactivity of bulk and surface hydrogen are understood in terms of different energetics and geometries of the hydrogen approach, as discussed in Chapter I.

Two hydrogen atoms must be added to ethylene to produce ethane. Therefore, there must be at least two steps in the mechanism of the hydrogenation reaction of adsorbed ethylene: conversion of ethylene to ethyl and ethyl to ethane. Although it is known that bulk hydrogen atoms are necessary for the hydrogenation of ethylene to ethane, the role bulk hydrogen plays in each mechanistic step from ethylene to ethane is uncertain. For example, the second step, addition of a hydrogen atom to ethyl to form ethane, may not require a bulk hydrogen atom. Instead, the process may proceed by reaction with surface hydrogen. Therefore, to complete the picture of the mechanism for ethylene hydrogenation by bulk hydrogen, the chemistry of the reaction intermediate, adsorbed ethyl, must be studied.

The synthesis and identification of an ethyl adsorbate has not been demonstrated previously on the Ni(111) surface. Therefore, a synthetic route to an adsorbed ethyl species must be discovered before its reactivity with bulk and surface hydrogen can be studied. The synthetic route must be selective such that the ethyl species is produced exclusively. The study of hydrogenation of an ethyl species in the presence of other hydrocarbons would not be ideal. For example, ethane coadsorbed with ethyl would complicate a study of the hydrogenation of ethyl to ethane. Also, the coadsorption of species other than hydrocarbons with an ethyl adsorbate may affect the reactivity of ethyl towards hydrogenation. Small concentrations of surface contaminants are known to significantly alter the chemical reactivity. Therefore, the ultimate goal of these experimental studies is to produce an adsorbed ethyl species 'cleanly', without either hydrocarbon or nonhydrocarbon coadsorbates.

This chapter describes many different attempts to synthesize an ethyl adsorbate. The results and discussion section starts with a description of attempts at adsorbed ethyl synthesis from dissociation of ethyl halides. Although dissociation of ethyl halides to produce an adsorbed ethyl species and an adsorbed halogen does not produce an ethyl 'cleanly', the identification of a ethyl adsorbate by vibrational spectroscopy even in the presence of a halide would be valuable because the vibrational spectrum of ethyl bound to Ni(111) is unknown. This information would lend additional support for identification of ethyl without coadsorbates. The discussion will then turn to attempts at ethyl production from ethylene and ethane. Many approaches were studied in the effort to convert these precursor molecules to adsorbed ethyl: thermal activation, irradiation with a xenon arc lamp, exposure to electrons, exposure to gas phase hydrogen atoms, reactions with bulk hydrogen, and translational activation.

II. Experimental

The experimental apparatus, nickel surface and analytical techniques have been described in Chapters I and II.

II.A. Ethyl Halides

Ethyl halides were used as precursor molecules for adsorbed ethyl synthesis. Ethyl iodide (99% - Aldrich) and ethyl bromide (99% - Aldrich), both liquid at room temperature, were used as received except for several freeze-pump-thaw cycles with liquid nitrogen to remove incondensable gases. Ethyl halides were introduced onto the crystal by exposure to a neat ethyl halide beam. The vapor pressure of the liquid at room temperature (2 psi and 7 psi for ethyl iodide and ethyl bromide, respectively) was used as the backing pressure for the molecular beam expansion. Because ethyl iodide is photosensitive, its exposure to light was minimized.

The coverages of the ethyl halides are measured by thermal desorption spectrometry. At low coverages of both ethyl halides, decomposition to ethylene at the surface is observed. The ethylene itself then either decomposes on or desorbs from the surface. Saturation coverage of the ethyl halide is defined as an exposure that yields only ethylene and hydrogen in the thermal desorption experiment. Desorption of the molecular ethyl halide is used as an indication of a multilayer coverage.

Multilayer coverages were only used in the measurement of electron energy loss spectra of multilayers. Multilayers of ethyl halides were not used in any attempts to synthesize an ethyl species.

II.B. Adsorbed Ethylene or Ethane

Ethylene and ethane are also used as precursor molecules in attempts at adsorbed ethyl synthesis. Ethylene and ethane are introduced to the surface by exposure of the surface to a molecular beam of the hydrocarbon seeded in argon. The coverage is measured using the ratio of the carbon to nickel Auger signals calibrated for absolute coverage as discussed previously in the experimental section of Chapter I.

II.C. Electrons and Gas Phase Hydrogen Atoms

Electrons and gas phase hydrogen atoms were used as reactants in attempts to convert adsorbed precursor molecules to adsorbed ethyl. Electrons incident on the surface are produced by thermionic emission from a hot tungsten filament as described in Chapter I. Gas phase hydrogen atoms were produced by molecular hydrogen dissociation over a hot tungsten filament as described in Chapter I.

II.D. Irradiation by a Xenon Arc Lamp

A 300 W Oriel arc lamp (model # 66084) with a ozone-free xenon lamp (Oriel model # 6258) is used for irradiation of ethyl bromide in an attempt to produce the ethyl adsorbate. The light is directed into the main chamber through the sapphire window closest to the electron energy loss spectrometer. The crystal is positioned just above the electron energy loss spectrometer directly facing the window during irradiation by the arc lamp. The intensity of the light is controlled by the combination of an iris and the focusing of the light. Since the irradiation warmed the crystal, attempts are made to illuminate the entire crystal without illuminating the crystal cold shield. Avoiding the illumination of the cold shield allows the light intensity on the surface to be as high as possible while maintaining low surface temperatures.

III. Results and Discussion

III.A. The Vibrational Spectrum of an Adsorbed Ethyl Species

The tool which will be used to identify an ethyl adsorbate is high resolution electron energy loss spectroscopy. Unfortunately, the vibrational spectrum of an ethyl species bound to Ni(111) is unknown. However, adsorbed ethyl has been observed previously by electron energy loss spectroscopy on a Pt(111) surface.[2] The vibrational frequencies observed in the study are shown in Table 3.1 along with the vibrational frequencies observed for a few gas phase ethyl halide molecules.[3,4] Also included in the table are vibrational frequencies observed for molecular ethyl bromide adsorbed on a Ni(111) surface. This spectrum has been measured in our lab and is shown in Figure 3.1. The coverage of molecular ethyl bromide is less than saturation. Also included in the Figure are the electron energy loss spectra of adsorbed ethyl bromide multilayers on the Ni(111) surface. The temperature of the surface

was 80 K during both the exposure to molecular ethyl bromide and the electron energy loss spectroscopy measurements.

The vibrational frequencies observed for adsorbed ethyl bromide are very similar to those of gas phase ethyl bromide molecules for both the less than saturation and multilayer coverages. Although electron energy loss spectroscopy does not have the resolution required to resolve all the features which are resolved in the infrared spectrum of gas phase ethyl bromide, every feature of the adsorbed species, with the exception of the C-Br stretch, matches well with that of the gas phase molecule. As is seen in Table 3.1, the C-Br stretch frequency is shifted, upon adsorption to the surface. This mode is 580 cm^{-1} in the gas phase spectrum and 520 cm^{-1} in the adsorbed molecule spectrum. The change in frequency upon adsorption is not unreasonable since the ethyl bromide molecule is likely bound to the surface through the bromine atom. The lowering of the frequency upon adsorption can be understood as a change in the force constant of the C-Br bond due to donation of electron density from the bromine atom to the nickel surface. The stretching frequency of the C-Br mode of multilayers of ethyl bromide is measured at 560 cm^{-1}, much closer to the gas phase value. The higher C-Br stretching frequency demonstrates the diminished interaction of the ethyl bromide with the surface when separated from the surface by layers of adsorbed molecules.

The electron energy loss features observed for adsorbed molecular ethyl bromide can be used as a guide for the features expected for an adsorbed ethyl species with the exception of the C-Br stretching feature. An adsorbed ethyl species will have a C-Ni bond rather than a C-Br bond. Chapter II showed typical carbon-nickel stretching frequencies to be in the 300 to 480 cm^{-1} range.

Mode	Sym.	Cl -CH_2CH_3	Br -CH_2CH_3	I -CH_2CH_3	Pt(111) -CH_2CH_3	Ni(111)-Br-CH_2CH_3
asym CH_2 str	A"	3012	3018	3015		3020
asym CH_3 str	A'	2983	2988	2973	2918	3020
asym CH_3 str	A"	2983	2988	2989		
sym CH_2 str	A'	2946	2937	2960	2918	2870
sym CH_3 str	A'	2890	2880	2972	2918	2870
CH_2 sciss	A'	1452	1451	1419	1450	1450
asym CH_3 def	A'	1452	1451		1430	1450
asym CH_3 def	A"	1452	1451	1437		
sym CH_3 def	A'	1389	1386	1377	1376	1400
CH_2 wag	A'	1287	1252	1203	1173	1240
CH_2 twist	A"	1244	1248	1201		
C-C str	A'	972	964	952	1022	960
CH_3 rock	A'	1080	1061	1052	941	1050
CH_3 rock	A"	972	964	1049		
CH_2 rock	A"	785	770	741		770
C-X str	A'	676	583	501	484	520
C-C-X def	A'	336	290	263		240
Torsion	A"	243	247	257		
Reference		Ref. 3	Ref. 3	Ref. 4	Ref. 2	Figure 3.1

Table 3.1 Observed vibrational frequencies for gas phase molecules and adsorbates with an ethyl structure. Units are in cm^{-1}.

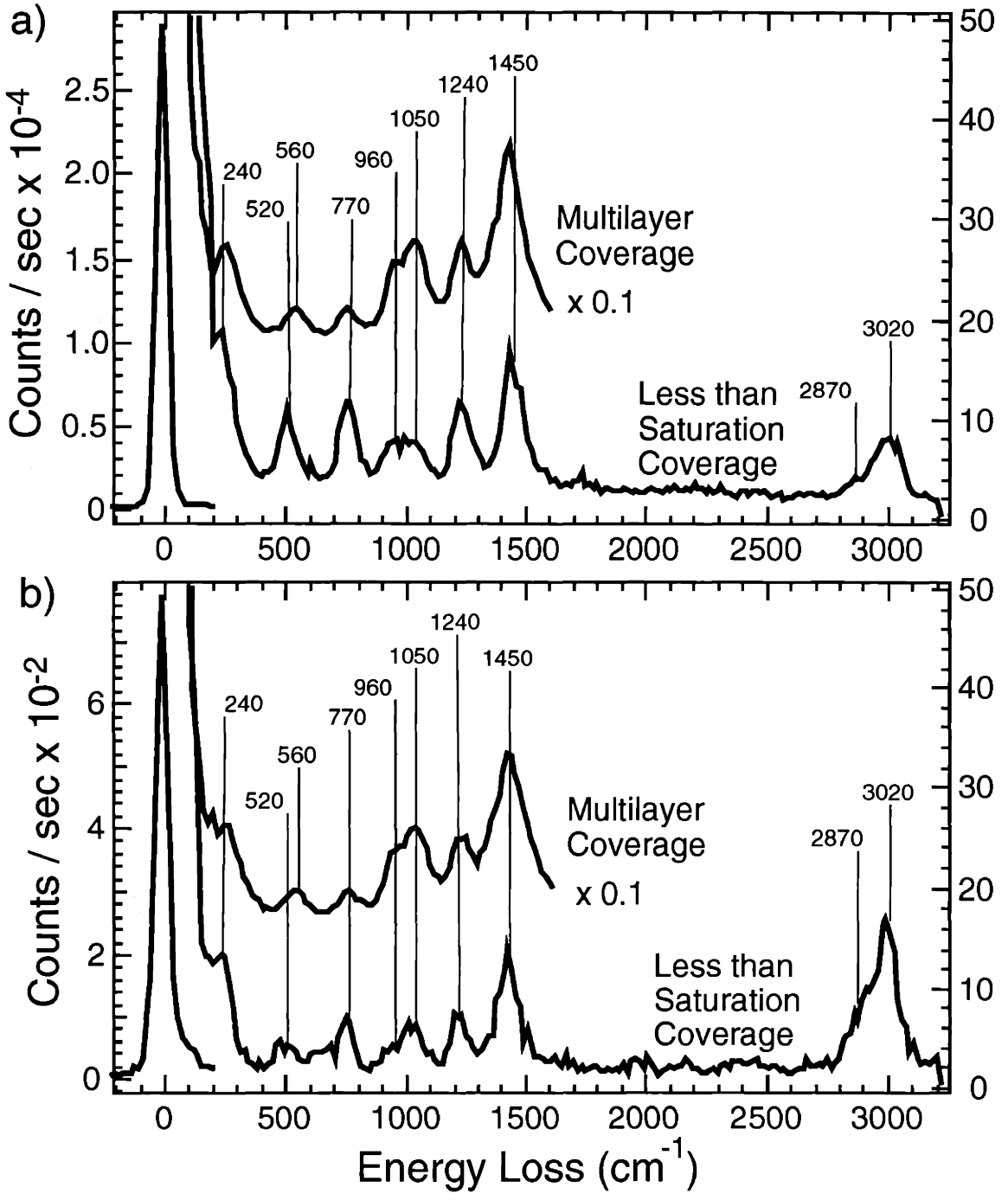

Figure 3.1. Electron energy loss spectra of adsorbed ethyl bromide at two coverages: multilayers and less than saturation. **a)** on-specular **b)** 10° off-specular

III.B. Attempts at Adsorbed Ethyl Synthesis with Ethyl Halides

Carbon-halogen bonds involving the heavier halogens are typically weaker than C-C and C-H bonds. For example, the C-Br bond strength is approximately 65 kcal/mol, while C-C and C-H bonds are greater than 100 kcal/mol.[5] Because of the weaker bonds, halogens are very often used as 'leaving groups' in the synthesis of organic molecules.[6] In analogous fashion, several attempts at producing ethyl adsorbed on a Ni(111) surface has used a halogen leaving group. The hope is to be able to break the carbon-halogen bond, form a carbon-surface bond, and leave the ethyl species intact.

The goal of the studies as a whole is to synthesize an ethyl adsorbate on a clean or hydrogen covered surface Ni(111) surface. Using an ethyl halide as a precursor to an absorbed ethyl species will not likely meet this goal because the halide is likely to remain on the surface after the synthesis steps. But, because alkyl halides seem promising precursors to an 'easy' synthesis of alkyl adsorbates, ethyl halides have been used in attempt to provide a ready source of an adsorbed ethyl species whose spectrum can then be measured. These spectra could then provide template for the identification of an adsorbed ethyl species produced from more difficult synthetic routes which would not involve ethyl halides.

III.B.1. Thermal decomposition of ethyl halides

One way to break a carbon-halogen bond is to thermally activate the carbon-halogen bond by heating the ethyl halide covered surface. Such a synthesis has been attempted. Figure 3.2 shows the electron energy loss spectrum of a surface covered with ethyl bromide after warming to 140 K and immediately cooling to 80 K, the temperature at which the electron energy loss spectrum was measured. The coverage of the ethyl bromide was less than saturation. The temperature of the surface during the exposure to ethyl bromide was 80 K.

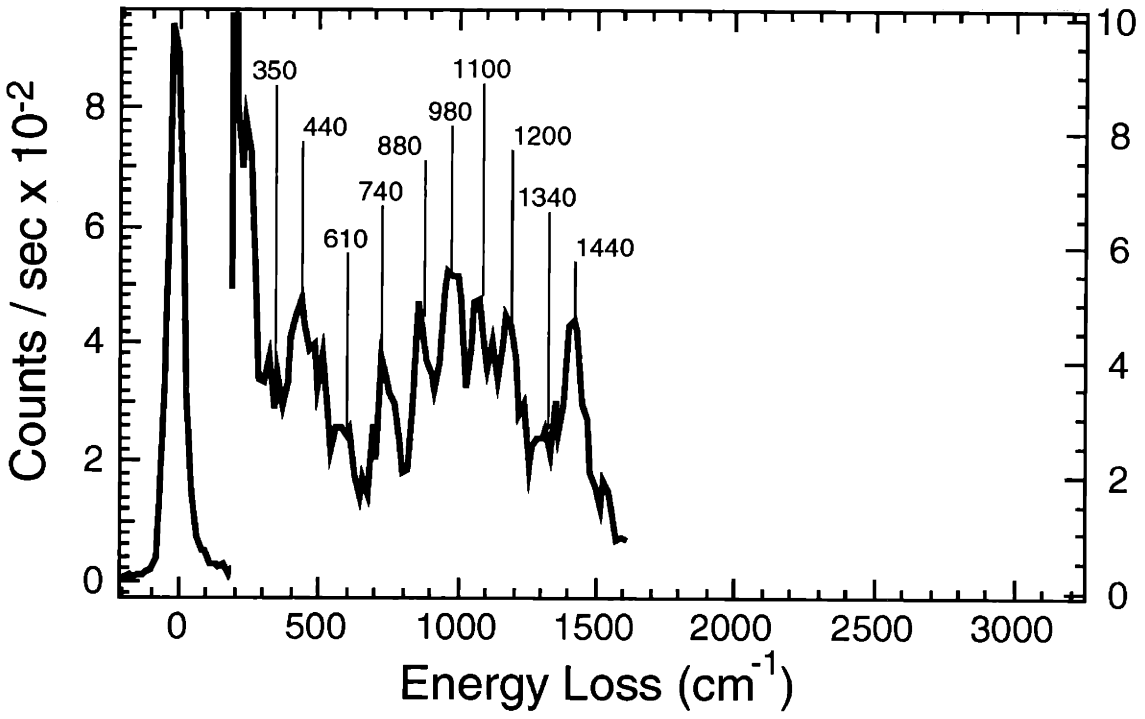

Figure 3.2. Electron energy loss spectrum measured 10° off-specular after heating an ethyl bromide covered surface to 140 K.

The spectrum is readily assigned to adsorbed ethylene. The vibrational spectrum of adsorbed ethylene has been shown previously in Figure 2.12 of Chapter II and the observed vibrational frequencies have been assigned previously.[1] Table 3.2 is a reproduction of the vibrational mode assignments for adsorbed ethylene. Comparison of the vibrational frequencies from the spectrum of the thermal decomposition of ethyl bromide with those from the spectrum of adsorbed ethylene shows a one to one correspondence. Every feature in the spectrum matches a vibrational feature of ethylene. Therefore, adsorbed ethyl bromide warmed to 140 K does indeed decompose to break the C-Br bond, but the observed decomposition product is not ethyl. Instead, ethylene is the thermal decomposition product.

Mode	C_2H_4
CH_2 str	3010, 2965
soft CH_2 str	2710
CH_2 sciss	1440, 1340
C-C str	1200
CH_2 wag	1100
CH_2 rock	980, 740
CH_2 twist	880
asym C-Ni str	610
sym C-Ni str	460
hindered rotation	350
hindered translation	250

Table 3.2. Observed vibrational frequencies in cm^{-1} for adsorbed ethylene on a Ni(111) surface. Taken from reference 1.

Adsorbed ethyl synthesis has also been attempted by decomposition of ethyl iodide. Figure 3.3 shows the electron energy loss spectrum of the surface after exposure to ethyl iodide. The temperature of the surface is held at 80 K during its exposure to ethyl iodide and the electron energy loss spectroscopy measurement. The crystal was not heated prior to the electron energy loss measurement.

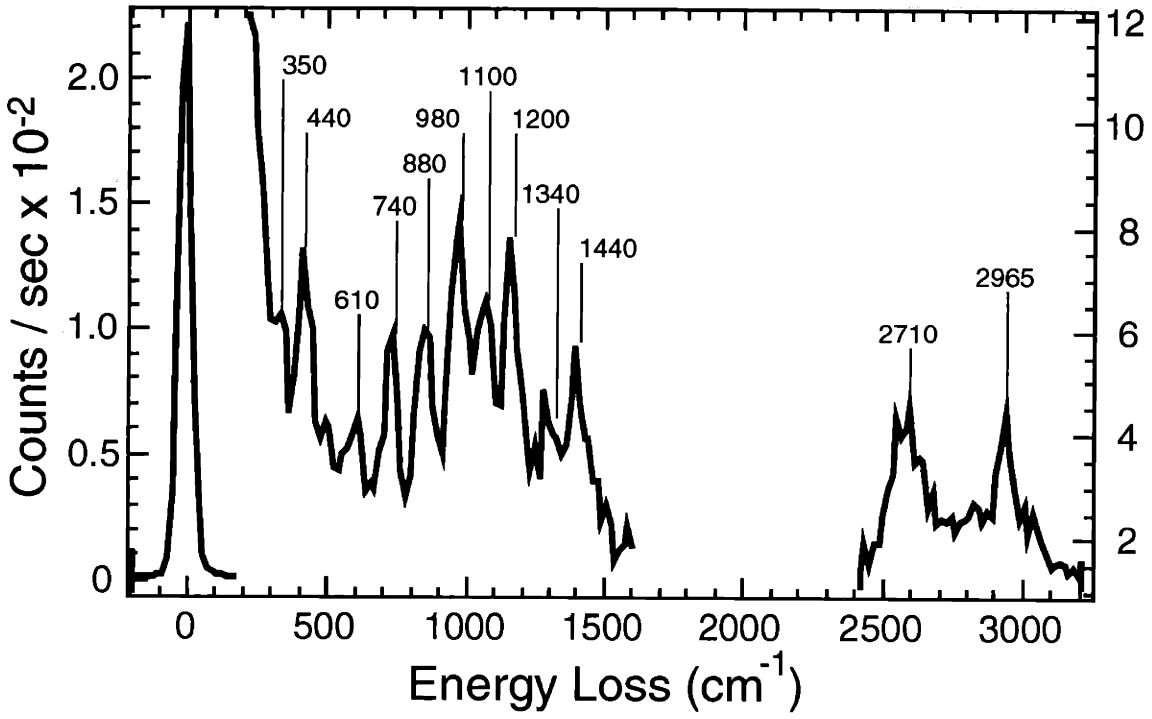

Figure 3.3. Electron energy loss spectrum measured 10° off-specular after exposure of a 80 K surface to ethyl iodide.

Again the electron energy loss spectrum is that of ethylene. Comparison of the vibrational features with those reported for adsorbed ethylene in Table 3.2 shows an excellent match. Even the 'soft C-H stretches' of the adsorbed ethylene are observed. Therefore, ethyl iodide decomposes to ethylene at 80 K. Note that this temperature for dissociation is lower than that observed for ethyl bromide. Ethyl bromide is observed to be stable at 80 K.

Neither ethyl bromide nor ethyl iodide thermal decomposition produces an adsorbed ethyl species on a clean Ni(111) surface. Both are observed to thermally decompose to ethylene. It appears that although the carbon-halogen bond can be thermally activated on the surface, the resulting ethyl species itself is not stable and its decomposition to ethylene is facile, even at 80 K.

III.B.2. Ethyl iodide on a hydrogen covered surface

Decomposition of adsorbed ethyl to ethylene produces an adsorbed hydrogen atom. Perhaps the ethyl species can be stabilized by blocking the surface sites available for dissociation of the ethyl species with surface bound hydrogen. Such an attempt to block the ethyl decomposition was made. A nearly hydrogen saturated Ni(111) surface is exposed to ethyl iodide. Figure 3.4 shows the electron energy loss spectra of a surface with 0.8 ML of adsorbed hydrogen or deuterium after exposure to ethyl iodide. The surface temperature during the ethyl iodide exposure and subsequent electron energy loss spectroscopy measurement was held at 80 K.

The spectra appear to be those of an ethyl species. By comparison to the spectra of adsorbed molecular ethyl bromide, the CH_2 rocking mode at 740 cm^{-1}, C-C stretch at 960 cm^{-1}, CH_2 wagging mode at 1160 cm^{-1}, and CH_2 scissors and an antisymmetric CH_3 deformation at 1450 cm^{-1} are expected to be the most intense features of an ethyl species, as is observed. Because surface hydrogen is known to exhibit features at 780 cm^{-1}, 950 cm^{-1} and 1160 cm^{-1} for coverages between 0.5 and 1.0 ML,[7] the same experiment has been repeated with a deuterated surface exposed to ethyl iodide to confirm that the 950 cm^{-1} and 1160 cm^{-1} features are those of the ethyl species. Isotopic labeling of the surface hydrogen shifts the Ni-D stretching modes to 560 cm^{-1}, 740 cm^{-1} and 850 cm^{-1}. However, features remain present at 950 cm^{-1} and 1180 cm^{-1} in the spectra of surface deuterium exposed to ethyl iodide indicating these features are attributable to ethyl iodide. The intensities of these features relative to the 1450 cm^{-1} feature, also match the intensities observed in the electron energy loss spectra of adsorbed molecular ethyl bromide, with 1450 cm^{-1} being the strongest feature of the ethyl species. Also, the CH_3 rocking mode at 1020 cm^{-1} is better resolved in the spectrum with surface deuterium because there is no overlap with the surface hydrogen feature at 950 cm^{-1}. The spectra of the surface species present after exposure of a hydrogen covered surface to ethyl iodide are consistent with an ethyl structure.

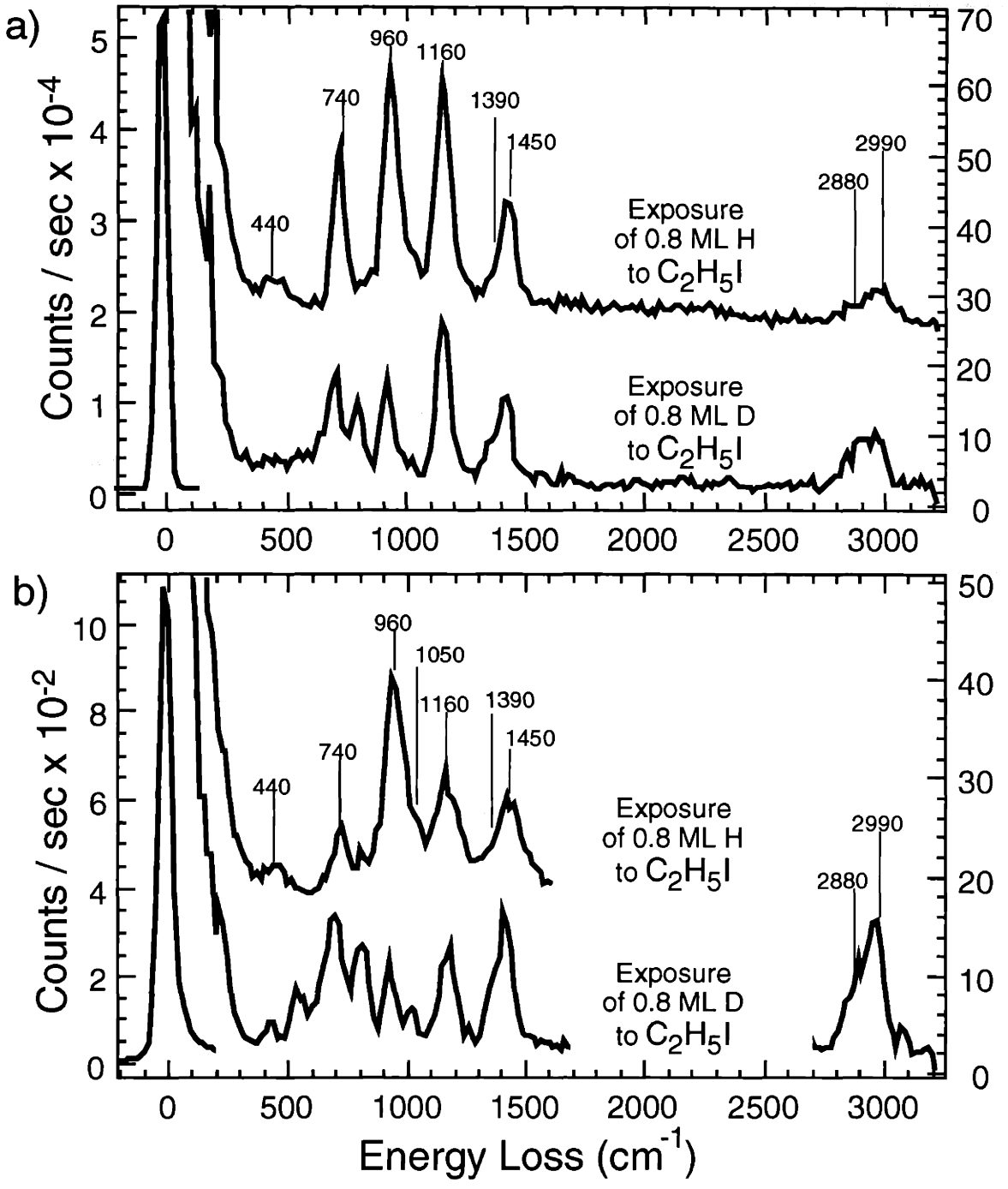

Figure 3.4. Electron energy loss spectra measured after exposure of a 0.8 ML hydrogen or deuterium covered surface to ethyl iodide. **a)** on-specular. **b)** 10° off-specular.

All the observed features, except for the 440 cm^{-1} feature, match very well with those of adsorbed molecular ethyl bromide. However, while it is clear from the electron energy loss spectra that an ethyl structure is still present, it is not clear whether the species is molecular ethyl iodide or whether the C-I bond has broken and an adsorbed ethyl species has been synthesized. As proposed earlier, adsorbed hydrogen is expected to inhibit the ethyl to ethylene conversion, but the adsorbed hydrogen could also inhibit the ethyl iodide to ethyl conversion by blocking the sites for the adsorption of the ethyl species. The key to knowing if the surface species is molecular ethyl iodide or adsorbed ethyl is the assignment of the 440 cm^{-1} feature. This feature could be the C-I stretch or a C-Ni stretch. A frequency of 440 cm^{-1} is within the typical range for C-Ni stretches of adsorbed hydrocarbons, but the C-I stretching frequency of molecular ethyl iodide adsorbed to Ni(111) is unknown.

To gain more information about the expected stretching frequency of the C-I bond of molecularly adsorbed ethyl iodide, the electron energy loss spectrum of multilayers of ethyl iodide has been measured. Figure 3.5 shows the spectrum.

The C-I stretch frequency of adsorbed multilayers of ethyl iodide is observed at 510 cm^{-1}, close to the gas phase value of 500 cm^{-1}. This is similar to what was seen for ethyl bromide. The multilayer frequency for the C-Br bond was 560 cm^{-1}, a small shift from gas phase value of 580 cm^{-1}. The C-Br stretching frequency shifts downward approximately 40 cm^{-1} in going from the multilayer coverage to the less than saturation coverage. Assuming an equal magnitude of shift in the C-I stretching frequency at less than saturation coverage, the C-I stretching frequency is expected to occur at 460 cm^{-1}. This value is very close to the observed frequency of 440 cm^{-1}. It is very difficult to tell if this feature is the C-I stretching mode or a C-Ni stretching mode. Therefore, from the electron energy loss spectra it is impossible to know if the species resulting from exposure of a 0.8 ML hydrogen covered surface to ethyl iodide is molecular ethyl iodide or if the C-I bond is broken and adsorbed ethyl has been synthesized.

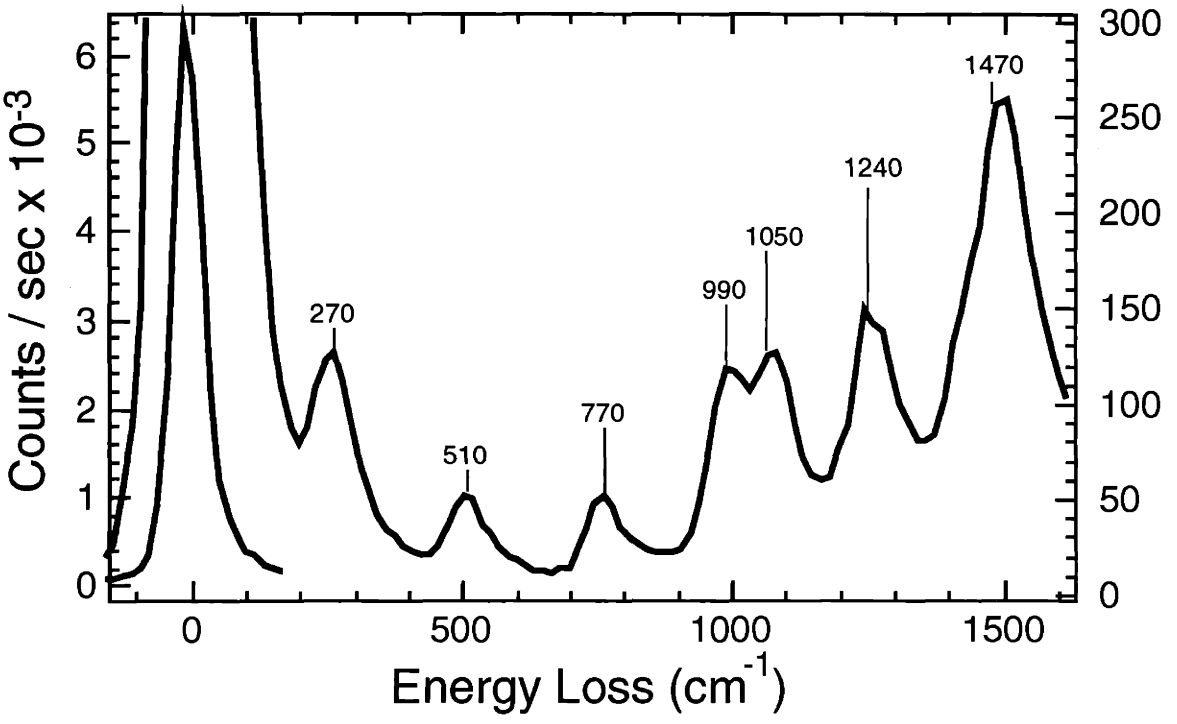

Figure 3.5. Electron energy loss spectrum measured in the specular direction of a multilayer coverage of ethyl iodide.

In an attempt to clarify if the C-I bond has broken, the system has also been studied by thermal desorption spectroscopy. Figure 3.6 shows a thermal desorption experiment after exposure of a 0.8 ML hydrogen covered Ni(111) surface to ethyl iodide. For comparison, the thermal desorption spectrum after exposure of a clean Ni(111) surface to the same amount of ethyl iodide has been measured. The results are shown in Figure 3.7.

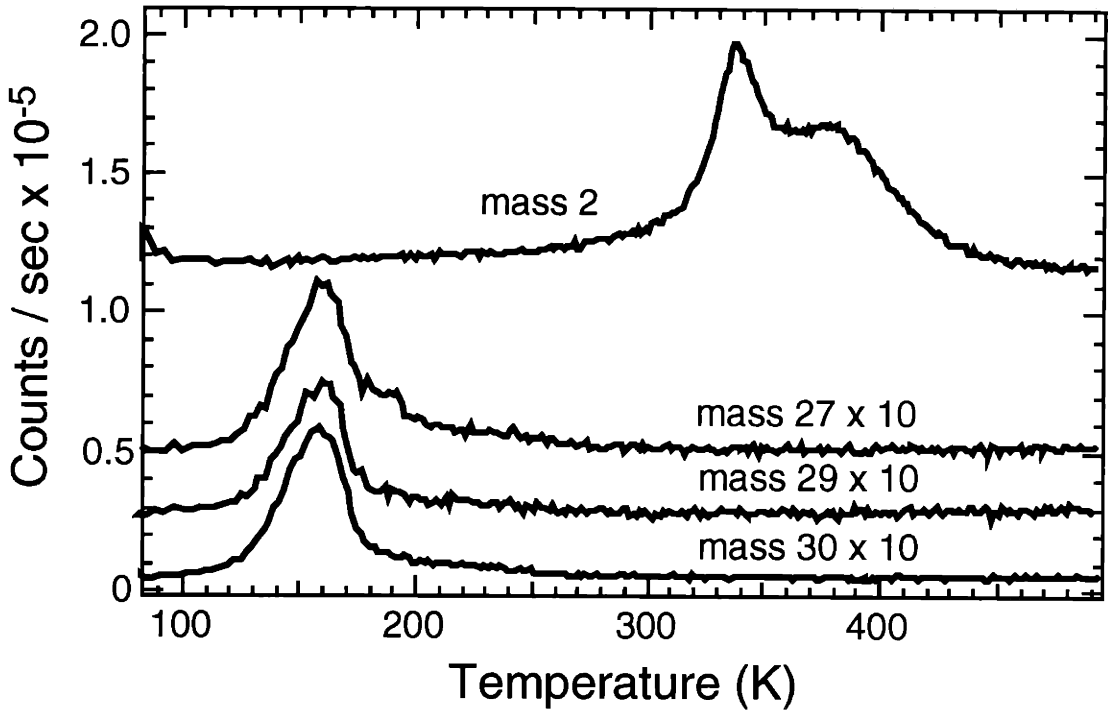

Figure 3.6. Thermal desorption spectrum measured after exposure of a 0.8 ML hydrogen covered surface to ethyl iodide at 80 K. The heating rate was 2 K/sec.

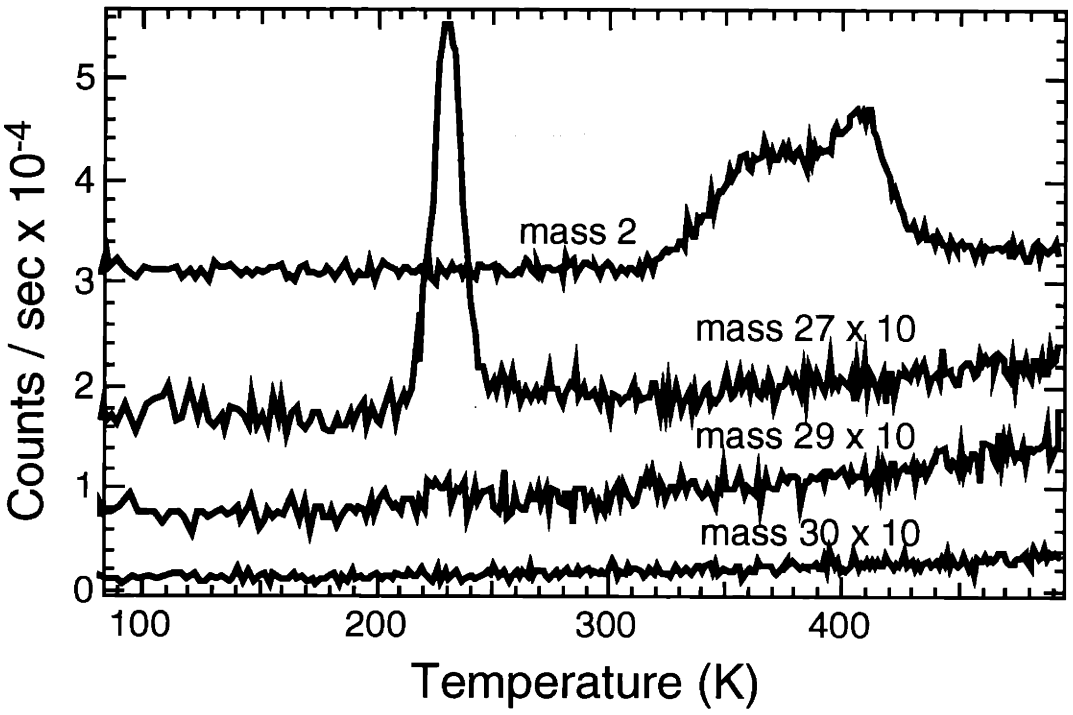

Figure 3.7. Thermal desorption spectrum measured after exposure to ethyl iodide at 80 K. The heating rate was 2 K/sec.

Dramatic differences are seen in the thermal desorption spectra from exposure of a hydrogen covered surface versus a clean surface to ethyl iodide. From the exposure of a clean surface to ethyl iodide, the only desorption features are in the mass 2 and mass 27 signals. The mass 27 desorption feature at 230 K is ethylene desorbing from the surface. Ethyl iodide and ethane are eliminated as desorption products because each cracks to mass 29 and mass 30, respectively, in addition to cracking to mass 27. Ethylene desorption is not surprising because ethyl iodide decomposes to ethylene at 80 K, as was shown in the electron energy loss spectra (Figure 3.3). In addition, previous studies have shown that ethylene coverages higher than 0.16 ML yield molecular ethylene desorption at approximately 200 K.[1] The same studies have also shown that any ethylene which does not desorb from the surface, dehydrogenates at the surface. The surface hydrogen, resulting from ethylene decomposition, recombinatively desorbs at higher temperatures. The mass 2 signal observed in Figure 3.6 is the recombinative desorption of surface hydrogen formed from ethylene decomposition.

The thermal desorption spectrum measured after exposure of a hydrogen covered surface to ethyl iodide shows very different results. Mass 29 and mass 30 thermal desorption features are observed in addition to the mass 27 desorption feature at 160 K. The mass 30 signal must be due to ethane desorption because ethyl iodide and ethylene cannot crack to mass 30. Therefore, ethane must be desorbing from the surface at approximately 160 K. In addition to mass 30, ethane also cracks to mass 29 and mass 27, the cracking pattern being approximately equal for all three masses. Therefore, mass 27, mass 29 and mass 30 features at 160 K can be assigned to desorbing ethane, but small amounts of desorbing ethylene and ethyl iodide cannot be eliminated without a quantitative analysis of these results. In fact, close inspection of the spectrum at mass 27 reveals another feature at 180 K which is not observed in the mass 29 and mass 30 signals. This feature is likely the desorption of ethylene.

The desorption of ethane from the surface suggests hydrogenation of an ethyl adsorbate by surface hydrogen in the presence of adsorbed iodine. It is not known if the ethyl

adsorbate is created during the thermal desorption experiment from decomposition of adsorbed molecular ethyl iodide or if ethyl iodide decomposes immediately upon exposure of the surface to ethyl iodide to yield the adsorbed ethyl species. Therefore, it cannot be determined if the electron energy loss spectra in Figure 3.4 are those of molecular ethyl iodide or an adsorbed ethyl species.

III.B.3. Irradiation of Adsorbed Ethyl Bromide

Synthesis of an adsorbed ethyl species on Pt(111) by irradiation of adsorbed ethyl chloride with ultraviolet light has been reported by K. G. Lloyd et. al.[2] A similar procedure was carried out on the ethyl bromide adsorbed to Ni(111) in an attempt to synthesize an adsorbed ethyl.

Unfortunately, irradiation of the crystal with the light from a xenon arc lamp heats the crystal. The temperature of the crystal during irradiation depends on the intensity of the light. The previous section demonstrated that ethyl bromide thermally decomposes to ethylene at 140 K. Therefore, the intensity of the arc lamp light was kept low to ensure that the crystal temperature did not exceed 140 K. As a consequence, long exposures of the ethyl bromide to the light of the arc lamp were necessary.

Figure 3.8 shows the electron energy loss spectra of two different experiments in which ethyl bromide was irradiated. The experiments differ only in the light intensity and therefore, the temperature of the surface at which irradiation took place, 90 and 110 K. The duration of the irradiation was one hour in both experiments. The electron energy loss spectrum of ethyl bromide exposed to the lower intensity light (resulting in the crystal heating to 90 K) looks identical to the spectrum of ethyl bromide without irradiation (Figure 3.1). The presence of a feature at 510 cm^{-1} indicates that the C-Br bond is still intact. A C-Ni bond is expected at a lower frequency.

The electron energy loss spectrum of ethyl bromide exposed to the higher intensity light (resulting in the crystal heating to 110 K) can again be assigned as adsorbed ethylene. All the frequencies observed are those of adsorbed ethylene (table 3.2). It is clear that ethyl bromide has decomposed to ethylene during the irradiation. What is not known is whether the C-Br bond was broken by absorption of the light or if the light merely heated the crystal and the C-Br bond was broken thermally. Although surface temperatures of 120 K were not observed to decompose ethyl bromide when this temperature was approached at 2 K/second, holding the surface for extended periods at lower temperatures could result in thermal decomposition. A control experiment of holding a ethyl bromide covered surface at 110 K for one hour could answer this question. But, since the goal of these experiments was to synthesize adsorbed ethyl and not to study the activation of C-Br bond of adsorbates by irradiation, this control experiment was not conducted.

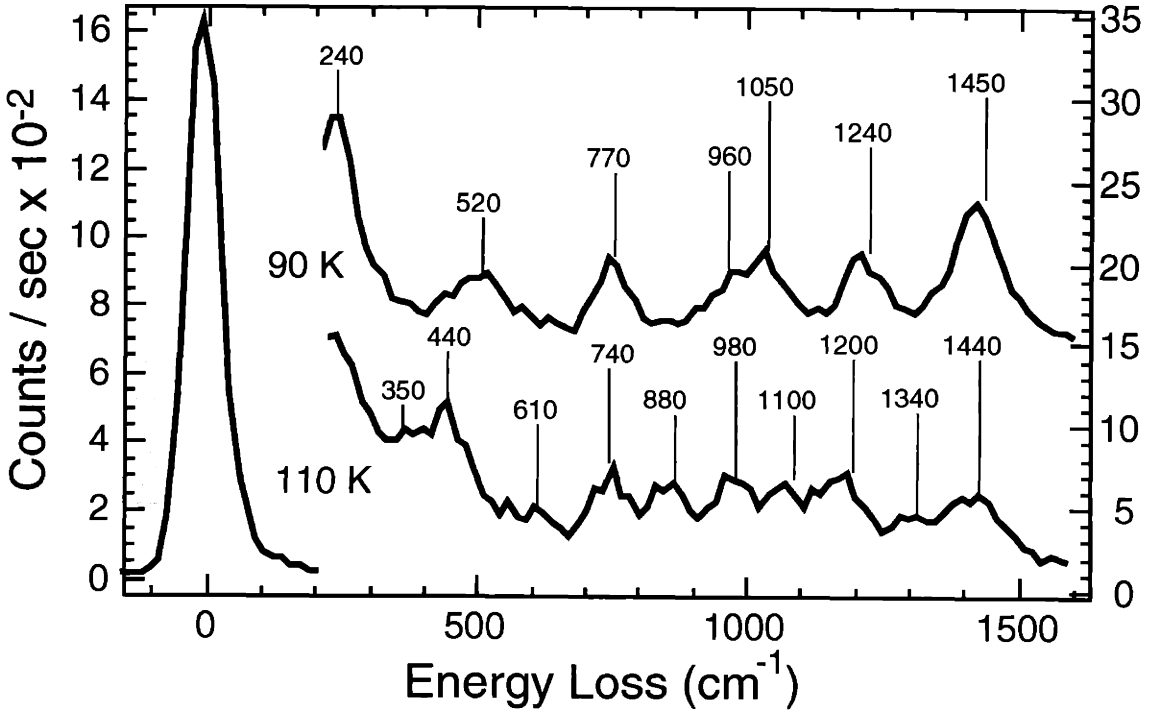

Figure 3.8. Electron energy loss spectra measured 10° off-specular after a one hour exposure of ethyl bromide to irradiation of a xenon arc lamp. The temperatures indicate the surface temperature during the irradiation.

Several other attempts to synthesize an ethyl species by irradiation of ethyl bromide were made at different light intensities and times of irradiation, but the results were always similar to one of the two experiments discussed. The electron energy loss spectra indicated the presence of either molecular ethyl bromide or ethylene.

III.B.4 Ethyl bromide exposure to electrons

Adsorbed ethyl bromide has also been exposed to electrons in an attempt to break the C-Br bond and leave the ethyl species intact and adsorbed to the surface. Figure 3.9 shows the electron energy loss spectra of adsorbed ethyl bromide after exposure to 20 eV electrons for five minutes with a current to the crystal of 3e-6 amps. The temperature of the surface prior to the electron bombardment was 80 K, but it warmed to 100 K during the bombardment due to radiative heating from the filament which created the incident electrons. Included in the Figure is an electron energy loss spectrum of a surface covered with adsorbed ethyl bromide which has been annealed at 100 K for five minutes.

The features observed in the electron energy loss spectrum of ethyl bromide after exposure to electrons can once again be assigned to adsorbed ethylene as listed in table 3.2. Therefore, exposure of ethyl bromide to 20 eV electrons has induced the decomposition of ethyl bromide to ethylene.

The control experiment of annealing the ethyl bromide for five minutes at 100 K showed no decomposition of the ethyl bromide. All the features observed are those of ethyl bromide. The surface temperature, 100 K, is the same reached during the electron bombardment and therefore the possibility of thermal decomposition of the adsorbed ethyl bromide during the electron exposure can be eliminated. The decomposition must be initiated by the incident electrons.

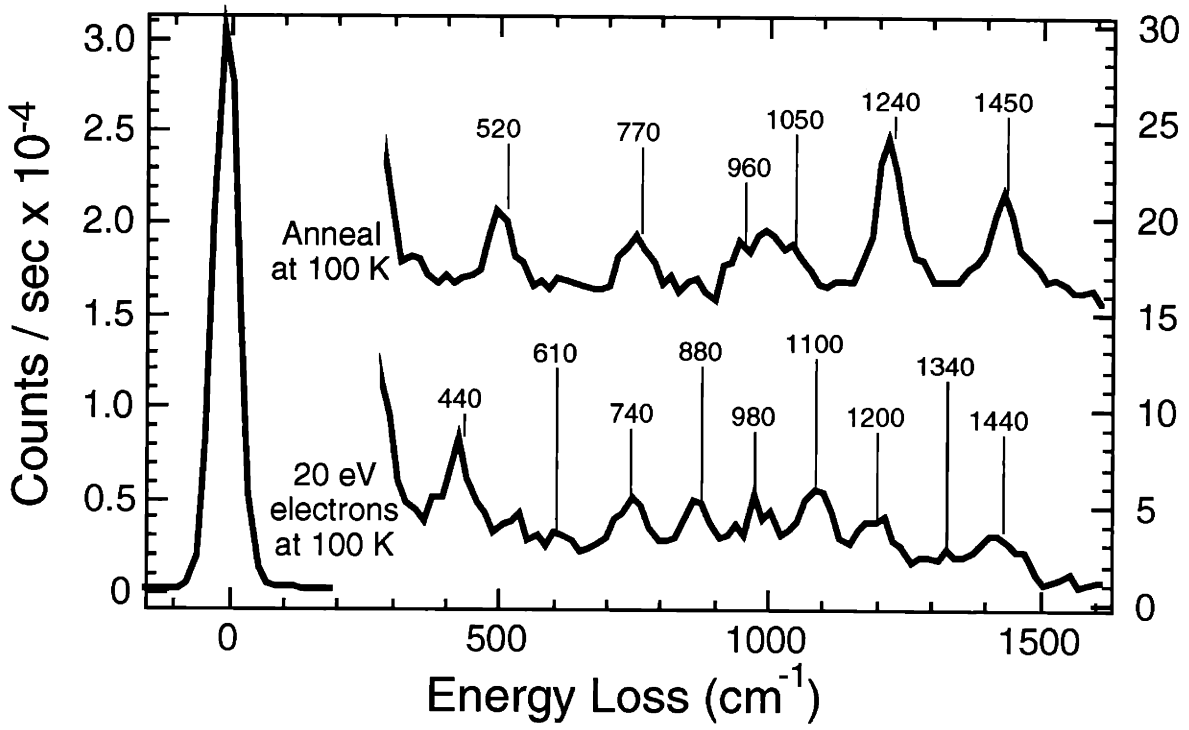

Figure 3.9. Electron energy loss spectra of ethyl bromide after annealing at 100 K for five minutes and ethyl bromide after exposure to 20 eV electrons for five minutes. The spectrum was measured 10° off-specular.

It is clear that the C-Br bond of adsorbed ethyl bromide is broken by the incident electrons, but the final product is once again ethylene, not adsorbed ethyl. It is reasonable that ethylene is formed by the decomposition of adsorbed ethyl. The conversion of adsorbed ethyl to ethylene could be a thermal process or an electron induced process. The next section will show that C-H bonds of adsorbed ethane can be activated by electron bombardment, but higher energy electrons (40 - 80 eV) are needed. Electrons at 20 eV are not observed to break a C-H bond of adsorbed ethane. This observation suggests that the 20 eV electrons in this experiments do not have enough energy to break a C-H bond. Therefore, the conversion of ethyl bromide to ethylene is initiated by the incident electrons, but decomposition of ethyl to ethylene is likely a thermal process. Regardless, the goal of synthesizing an adsorbed ethyl species has not been realized.

III.C. Attempts at Adsorbed Ethyl Synthesis from the Precursors Ethane and Ethylene

Even though it was envisioned that the synthesis of adsorbed ethyl from ethyl halides was relatively straightforward, none of the synthetic routes produced adsorbed ethyl species. The only experiment which could have produced an adsorbed ethyl species, an exposure of a 0.8 ML hydrogen covered surface to ethyl iodide, was ambiguous. Molecular ethyl iodide could not be differentiated from an adsorbed ethyl species because the 440 cm^{-1} feature could not be definitively assigned as a C-I or C-Ni stretch. Synthesis of adsorbed ethyl from ethylene and ethane would avoid this complication since neither of these hydrocarbons have this low frequency intramolecular mode and neither have a vibrational spectrum similar to that of adsorbed ethyl. Although the synthesis routes may be more difficult experimentally, the identification of the ethyl species will likely be easier. Furthermore, if the surface chemistry of adsorbed ethyl is to be investigated on a Ni(111) surface, a reaction scheme to form the ethyl species without the use of ethyl halides must be developed. The structure of ethylene and ethane are closest to that of ethyl and therefore, these hydrocarbons serve as the best precursors to adsorbed ethyl. Several methods for the synthesis of adsorbed ethyl from ethylene and ethane have been attempted.

III.C.1 Electron induced dissociation of adsorbed ethane

The activation of a C-H bond of ethane by electron impact has been attempted for the purpose of synthesizing an adsorbed ethyl species. Figure 3.10 is the electron energy loss spectra of 0.21 ML ethane after exposure to 80 eV electrons. The duration of the electron exposure is 15 minutes with an electron current to the crystal of 1.6×10^{-6} amps. The crystal temperature prior to the electron exposure is 70 K, but increases to 85 K during the exposure due to radiative heating from the filament used as the source of incident electrons. The crystal is immediately cooled to 70 K and held there for the electron energy loss measurements.

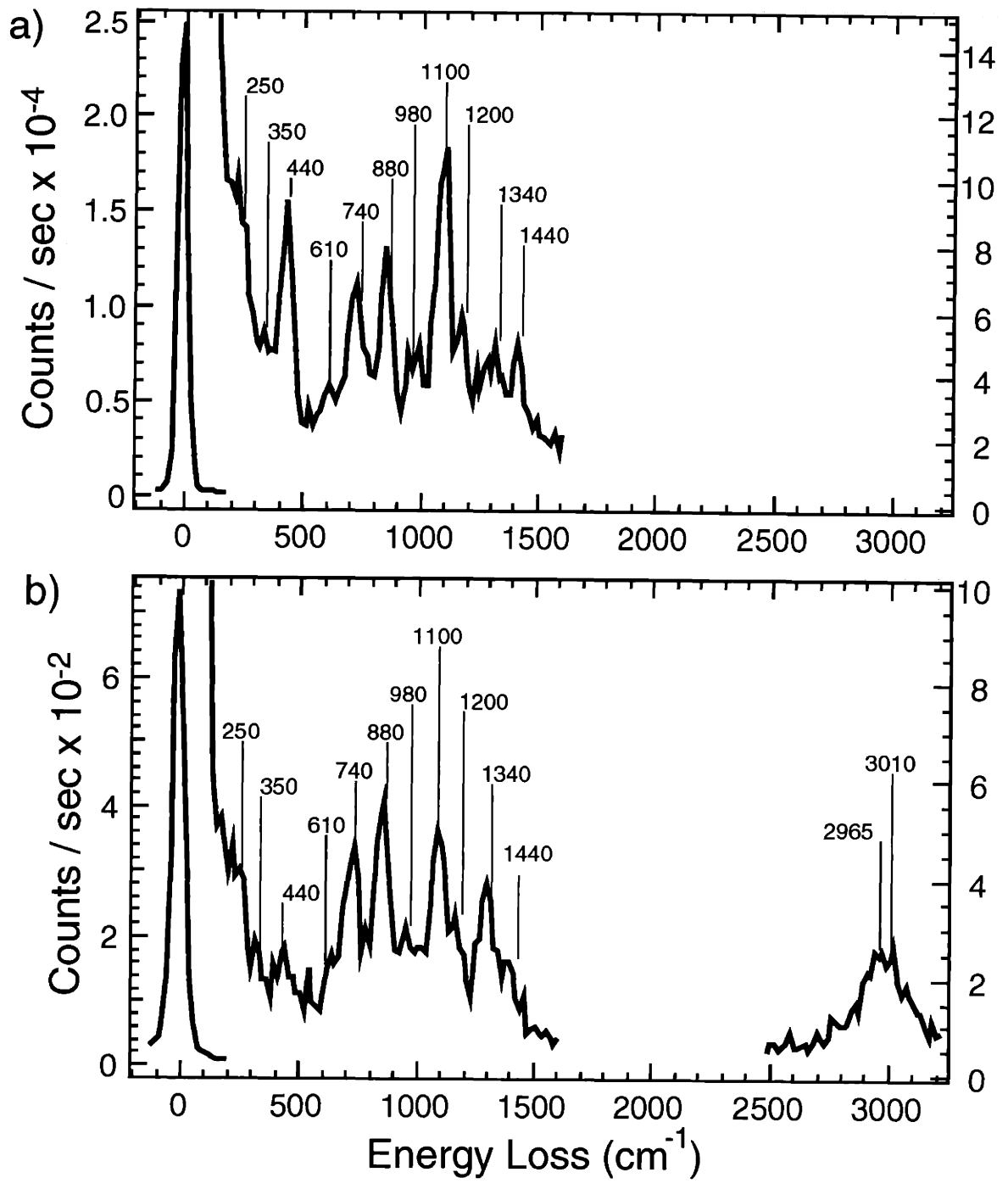

Figure 3.10. Electron energy loss spectra measured after exposure of 0.21 ML ethane to 80 eV electrons for 15 minutes at a surface temperature of 85 K. **a)** on-specular. **b)** 10° off-specular.

Figure 2.13 in Chapter II showed the spectra of adsorbed ethane. The features in the electron energy loss spectra after exposure to electrons are not those of adsorbed ethane. The spectra are instead consistent with adsorbed ethylene. Again, all the features match those previously assigned to ethylene (Table 3.2). In addition, the dipole activity of the features are consistent with that of adsorbed ethylene. The symmetric C-Ni stretch, the CH_2 wag, and the symmetric CH_2 scissors exhibit the strongest dipole activity, with the rest of the features displaying little or no dipole activity. Therefore, exposure of adsorbed ethane to 80 eV electrons produces ethylene, not ethyl.

This same experiment has been performed at lower crystal temperatures in an attempt to prevent the thermal decomposition of ethyl to ethylene. Figure 3.11 shows the electron energy loss spectrum after 80 eV electron bombardment to 0.21 ML adsorbed ethane. The duration of the electron exposure is 15 minutes with an electron current to the crystal of 1.4×10^{-6} A. The crystal temperature prior to the electron exposure is 10 K, but warmed to 40 K during the exposure due to radiative heating from the electron source filament. The crystal is immediately cooled to 10 K and held there for the electron energy loss measurements.

The frequencies of the features in the electron energy loss spectra are again characteristic of adsorbed ethylene. The intensities and dipole activities do not agree exactly with those of adsorbed ethylene, but the coadsorption of surface hydrogen with a hydrocarbon has been observed previously to result in different intensities and dipole activities. Chapter I discussed the observed change in the intensity of modes of adsorbed acetylene upon coadsorption with hydrogen. Once again, attempts to synthesize adsorbed ethyl have resulted in the production of adsorbed ethylene. The C-H bond of ethane is broken by exposure to the electrons, but the resulting ethyl species itself decomposes, breaking another C-H bond to produce ethylene.

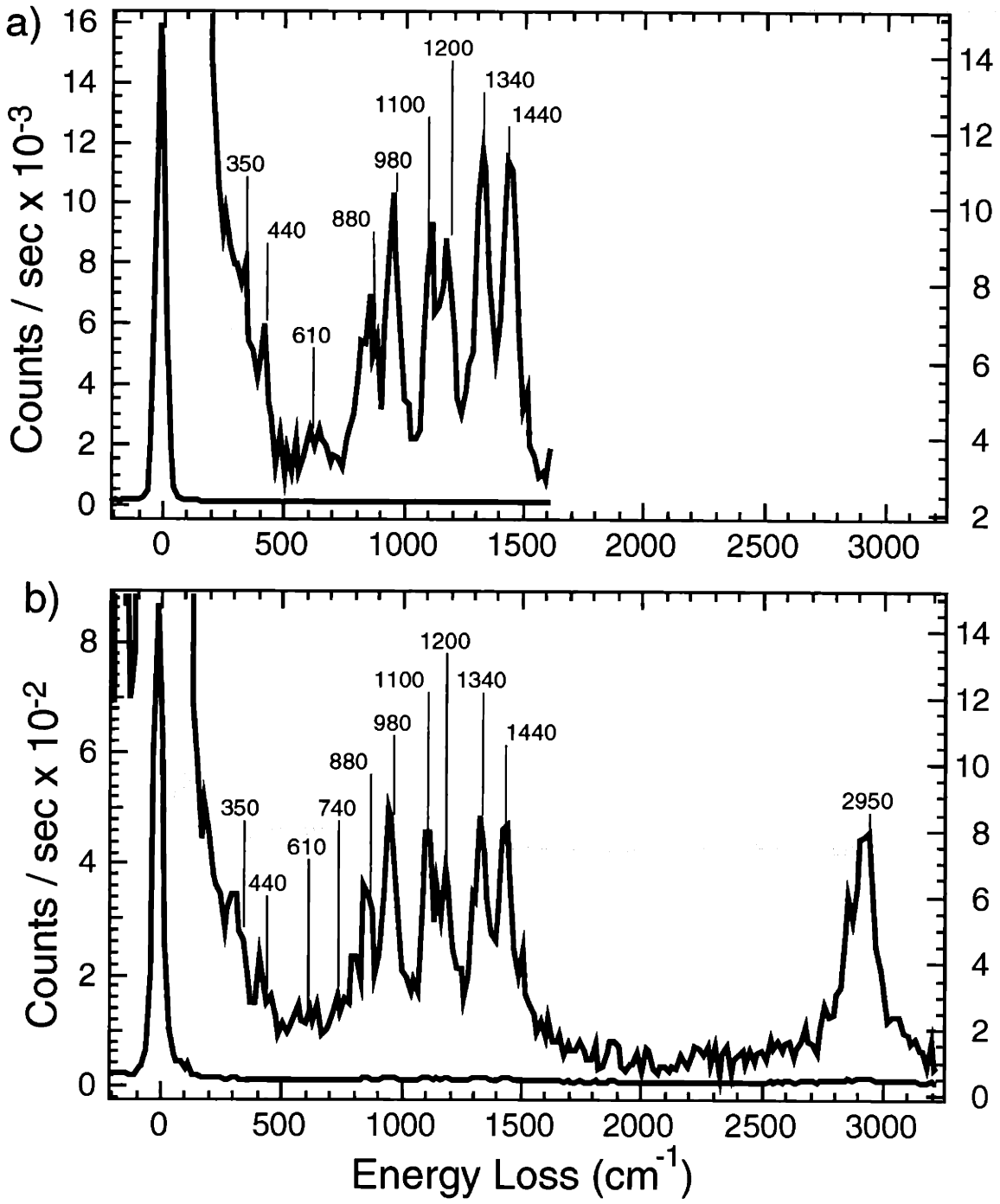

Figure 3.11. Electron energy loss spectra measured after a 15 minute exposure of 0.21 ML ethane to 80 eV electrons at a surface temperature of 40 K. **a)** on-specular. **b)** 10° off-specular.

The decomposition of ethyl to ethylene could be a thermal process or it could be induced by the incident electrons. In the latter case, there should be a build up in the concentration of the ethyl species before the ethyl species itself is converted to ethylene by electron impact dissociation. That is, the spectra of ethane after short exposures to electrons should be of that ethyl and ethane. However, the absence of ethyl features in the electron energy loss spectra suggests that the decomposition of ethyl to ethylene in not induced by electron impact. It must be pointed out, however, that this argument assumes that the cross sections for breaking the C-H bond of ethane and ethyl are equal. If electrons break the C-H bond of ethyl more efficiently than ethane, then there would not be a build up of the ethyl concentration since the ethane to ethyl conversion would be the rate determining step. Although the lack of any adsorbed ethyl suggests the decomposition of the ethyl species to ethylene during electron bombardment of adsorbed ethane is thermally activated, the process of electrons efficiently breaking the C-H bond of ethyl to produce ethylene cannot be excluded. More information on the relative cross sections for electron induced dissociation of C-H bonds in ethane and ethyl would be needed to do so.

III.C.2. H atom addition to and abstraction from adsorbed ethylene and ethane

Adsorbed ethyl synthesis has also been attempted by exposure of ethylene and ethane to gas phase hydrogen atoms. Chapter I has discussed the reactivity of gas phase hydrogen atoms extensively. Both addition of gas phase hydrogen atoms to adsorbed hydrocarbons and abstraction of hydrogen atoms from adsorbed hydrocarbons have been demonstrated. Therefore, exposure of adsorbed ethylene or ethane to gas phase hydrogen atoms could conceivably produce an ethyl species. However, no adsorbed ethyl was detected in the electron energy loss spectra. In fact, adsorbed hydrocarbon exposure to gas phase hydrogen atoms was shown to produce adsorbed ethylidyne.

Although no ethyl is detected in the electron energy loss spectra following exposure of adsorbed hydrocarbons to gas phase hydrogen atoms, the ethyl species can be inferred to be present during the reaction of gas phase hydrogen atoms with adsorbed ethane. In the conversion of ethane to ethylidyne, the first step must be abstraction of a hydrogen atom from adsorbed ethane to produce ethyl. The fact that no ethyl is detected in the electron energy loss spectra suggests that this first step is the rate limiting step. Any ethyl formed is efficiently converted to ethylidyne by the mechanism discussed in Chapter I or to ethane by addition of a gas phase hydrogen atom.

The presence of adsorbed ethyl can also be inferred in the reactions of gas phase hydrogen atoms with adsorbed ethylene. Ethane is observed by mass spectrometric measurements to desorb from the surface during the hydrogen atom exposure. The conversion of ethylene to ethane must go through the ethyl intermediate. But electron energy loss spectra of experiments in which the reaction of gas phase hydrogen atoms with adsorbed ethylene was stopped before completion do not show any ethyl features. Only ethylene and ethylidyne features are observed. Therefore, the coverage of ethyl present on the surface is too low to stand out against ethylene and ethylidyne or the ethyl species decomposes on the surface to produce ethylene before the electron energy loss spectroscopy measurement.

Mass spectrometric measurements at different hydrogen atom fluxes support the notion that ethyl is not stable at surface temperatures as low as 80 K. Figure 3.12 shows the mass 27 and mass 30 mass spectrometer signals during two different exposures of 0.25 ML adsorbed ethylene to two hydrogen atom fluxes, one an order of magnitude higher than the other. The sequence of the experiment was the same as was detailed in Chapter I. The high sloping signal background observed in the Figures is not due to a surface desorption process. The background signal has been discussed previously in Chapter I as due to reactions in the ionization region of the mass spectrometer. The maxima observed in the mass spectrometer signals immediately after the hydrogen atom filament is turned on are a result of hydrocarbon

desorption from the crystal surface. The only difference in spectra shown in Figure 3.12 are the molecular hydrogen pressure employed during the hydrogen atom exposures, $2x10^{-5}$ torr in Figure 3.12 (a) and $2x10^{-6}$ torr in Figure 3.12 (b). Less hydrogen dissociates on the hydrogen atom filament at lower molecular hydrogen pressures and therefore, the flux of hydrogen atoms on the surface is lower at lower molecular hydrogen pressures. The most significant difference in the exposures at the two fluxes is the absence of a maximum in the mass 30 signal when the lower hydrogen atom flux is directed at the crystal. Since the mass 30 signal is a measure of the ethane production, no hydrogenation of the adsorbed ethylene to ethane is taking place at the lower hydrogen atom flux. In contrast, a large mass 30 signal (ethane) is seen in the higher hydrogen atom flux experiment.

This observation is consistent with the thermal decomposition of an ethyl species. The hydrogenation of adsorbed ethylene to ethane must go through the ethyl intermediate. One hydrogen atom from the gas phase adds to the ethylene to form adsorbed ethyl. The ethyl can then react with another gas phase hydrogen atom to form ethane which subsequently desorbs from the surface and is detected in the mass spectrometer. However, if a gas phase hydrogen atom does not add to the adsorbed ethyl soon enough, the ethyl can undergo a different reaction, thermal decomposition to ethylene. The competition between the two processes of the adsorbed ethyl species depends on the flux of the gas phase hydrogen atoms. At high flux, the hydrogenation of the ethyl is significant and ethane is observed, but at low fluxes the thermal decomposition of ethyl to ethylene dominates, and no ethane is observed.

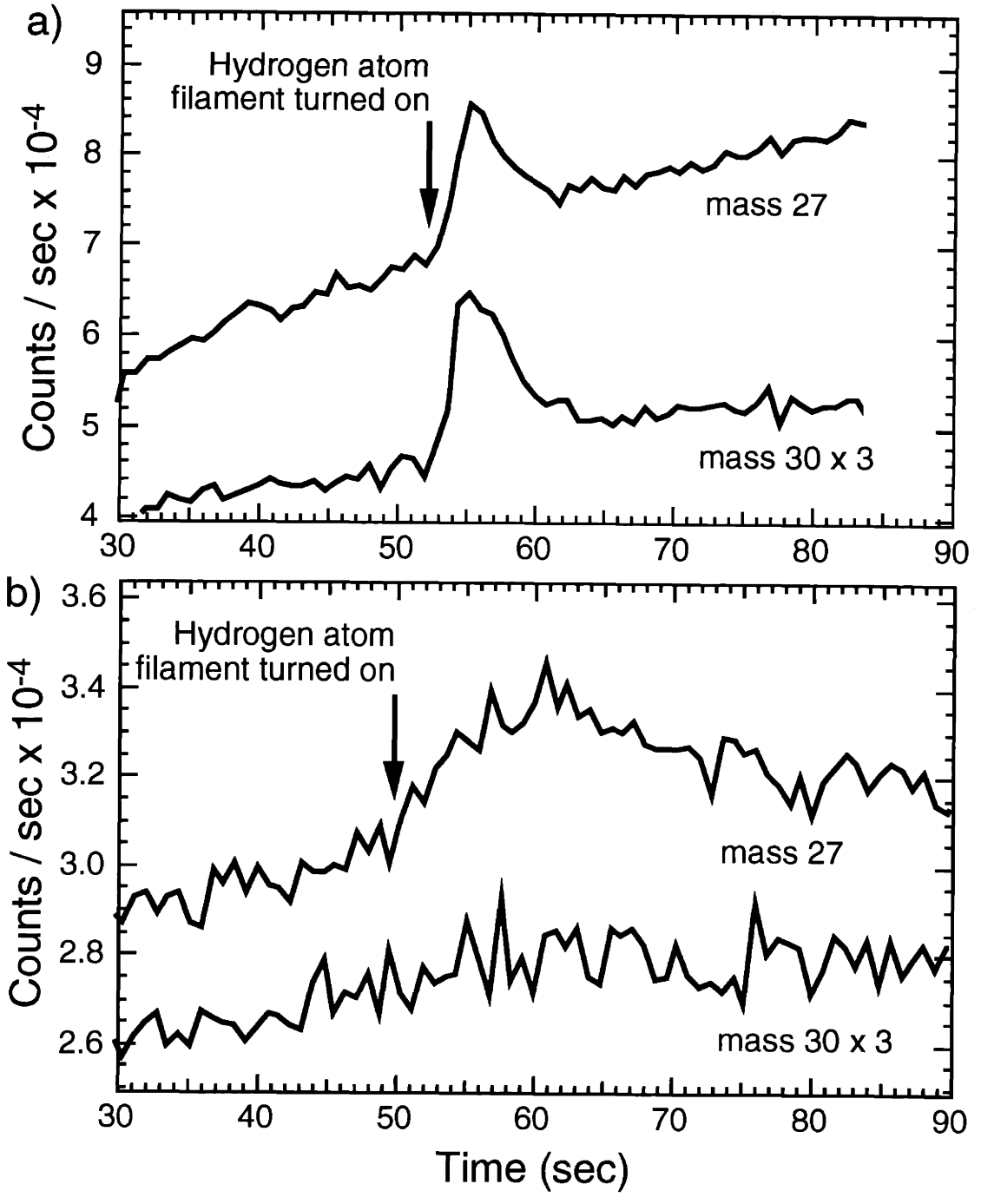

Figure 3.12. Mass spectrometric measurements during exposure of 0.25 ML adsorbed ethylene to gas phase hydrogen atoms. **a)** Molecular hydrogen pressure of $2x10^{-5}$ torr during the hydrogen atom exposure. **b)** Molecular hydrogen pressure of $2x10^{-6}$ torr during the hydrogen atom exposure.

III.C.3. Reaction of bulk hydrogen with adsorbed ethylene

Hydrogen emerging from the bulk to a Ni(111) surface has been demonstrated in previous studies to hydrogenate ethylene to ethane.[1] Hydrogenation of ethylene to ethane must involve an ethyl intermediate. Experiments have been performed in an attempt to trap the adsorbed ethyl intermediate. The experimental procedure is as follows. Bulk hydrogen is produced by exposure of the surface to gas phase hydrogen atoms. The surface hydrogen is subsequently removed from the surface by a 30 minute exposure to a 140 kcal/mol Xe beam at an incident angle of 40° from the surface normal.[8,9] After the Xe bombardment, the surface is exposed to ethylene. The crystal is then heated to the temperature at which hydrogen emerges from the bulk to the surface. The surface is immediately cooled to 80 K and the electron energy loss spectra were measured.

Figure 3.13 shows the electron energy loss spectra of 0.4 ML of bulk hydrogen and 0.25 ML of adsorbed ethylene after warming the crystal to 163 K. The features in the electron energy loss spectra are characteristic of ethylene as is observed by comparison to the frequencies for adsorbed ethylene shown in table __. No ethyl features can be observed amidst the ethylene features.

Experiments using different amounts of bulk hydrogen and adsorbed ethylene were attempted. The temperature to which the surface is warmed was also varied. In all cases the results are the same. The electron energy loss spectra showed only features characteristic of ethylene. An ethyl species could possibly be present, but the dominant features of ethylene obscure its identification. Two other possibilities remain. One explanation is that the addition of the first hydrogen atom to ethylene could be the rate determining step. Once the ethyl is formed, the second step to form ethane is facile and therefore, there is no build up of the adsorbed ethyl concentration. The other explanation is that the adsorbed ethyl species formed by bulk addition to ethylene is not stable, and it decomposes to ethylene before its electron energy loss spectrum can be measured.

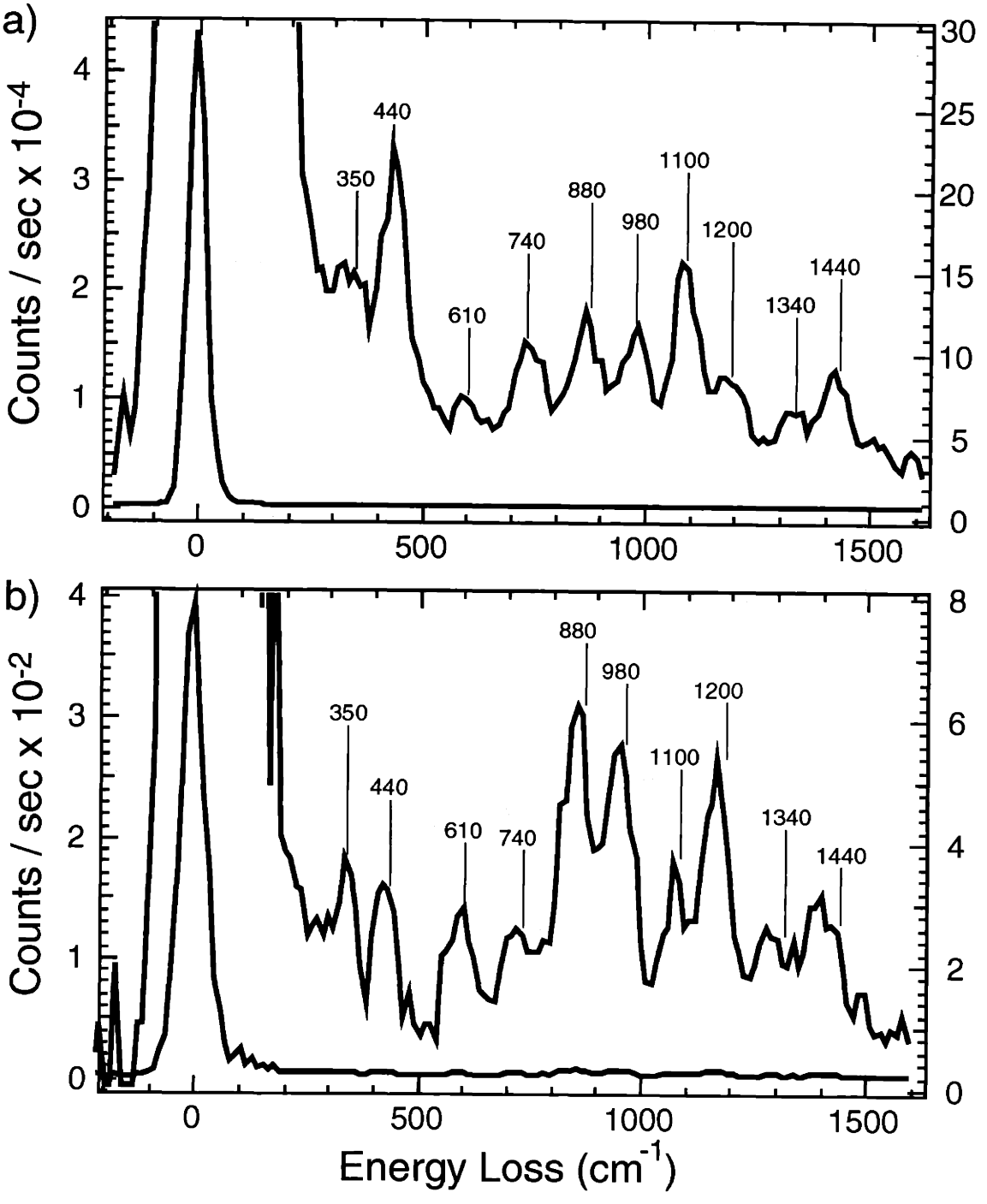

Figure 3.13. Electron energy loss spectra of 0.4 ML bulk hydrogen and 0.25 ML adsorbed ethylene after heating the crystal to 163 K. **a)** on-specular **b)** 10° off-specular

III.C.4. Translational activation of ethane

The synthesis of an adsorbed ethyl species has also been attempted by exposure of the surface to high translational energy ethane molecules. This technique has been successfully employed in the synthesis of methyl adsorbates by translational activation of methane.[10] Figure 3.14 shows the electron energy loss spectra after a 10 minute exposure of the surface to ethane molecules with an average translational energy of 35 kcal/mol, formed by an adiabatic expansion of 2% ethane/He at 600 K. The temperature of the surface was held at 90 K during the ethane exposure. After the ethane exposure, the crystal was cooled to 80 K, the temperature at which the electron energy loss spectra were measured.

Again, the electron energy loss spectral features are those of ethylene. All the features in the spectra match those previously assigned to adsorbed ethylene shown in Table 3.2. Also, the symmetric C-Ni stretch at 440 cm^{-1}, CH_2 wag at 1100 cm^{-1} and the symmetric CH_2 scissors at 1440 cm^{-1} are dipole active as is observed for adsorbed ethylene. Therefore, exposure of the surface to high translational energy ethane molecules has resulted in adsorbed ethylene.

Because the temperature of the nozzle during the expansion is high (600 K), there exists the possibility that ethane thermally decomposes in the nozzle to hydrocarbons such as ethylene which will stick to the surface during its exposure to the beam. This possibility can be tested by exposing the surface to a beam of ethane which has been formed by expansion from hot nozzle, but does not have enough translational energy to cause translational activation. Experiments have been performed in which the surface has been exposed to a molecular beam created by expansion of 2% ethane/argon at 700 K. The translational energy of ethane in this beam is lower (10 kcal/mol) due to the heavier seed gas used. No ethylene features or any hydrocarbon features are observed by electron energy loss spectroscopy after the exposure. Therefore, the adsorbed ethylene observed in Figure 3.14 must be due to translational activation of ethane and not thermal decomposition of ethane in the nozzle.

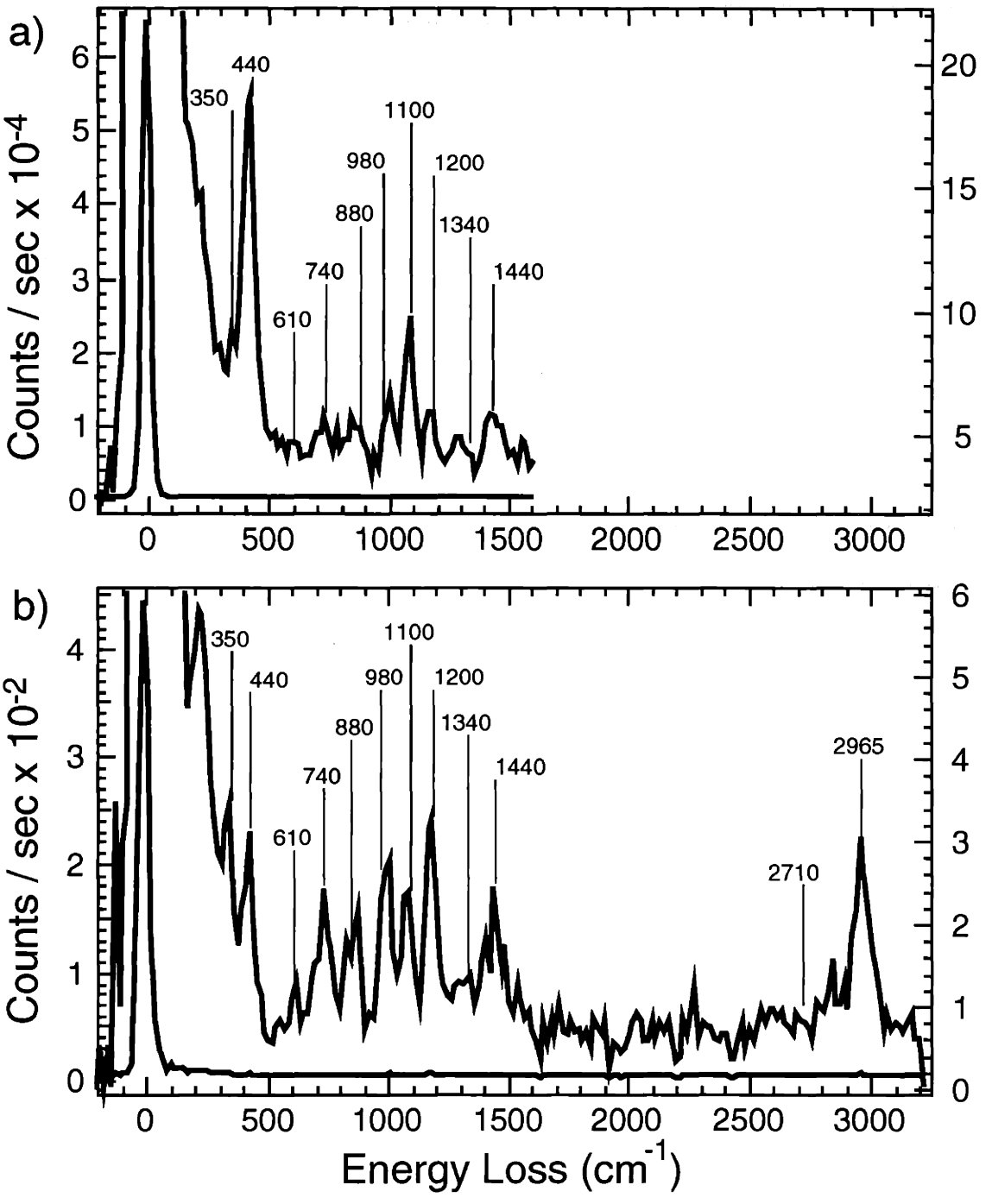

Figure 3.14. Electron energy loss spectra measured after a 10 minute exposure of a 90 K surface to a 35 kcal/mol ethane molecular beam. **a)** on-specular **b)** 10° off-specular.

Ethane must lose two hydrogen atoms to yield ethylene. It has been shown that the high energy of the incident ethane molecule breaks at least one C-H bond upon collision with the surface. What is unclear is if the second C-H bond is broken due to the incident translational, or if the adsorbed ethyl species undergoes thermal decomposition to produce ethylene. If the ethyl to ethylene conversion is a thermal process, then a lower surface temperature could inhibit the conversion.

However, it is not feasible to prevent the thermal decomposition of the ethyl species by lowering the surface temperature in this experiment. At temperatures lower than 90 K, ethane sticks to the surface. Adsorbed ethane blocks the sites necessary for the translational activation of the incident ethane. Exposures of a 80 K surface to ethane molecules with 35 kcal/mol translational energy does not form a measurable amount of ethylene. The electron energy loss spectra after the exposure show only features of adsorbed ethane. Electron energy loss spectra were measured again, after raising the crystal temperature to remove the adsorbed ethane, but no hydrocarbon vibrational features were observed. Also, no carbon was present on the surface as evidenced by the carbon Auger signal.

IV. Conclusions

The goal of the experiments described in this chapter was to develop a synthesis for an isolated adsorbed ethyl species. None of the attempts to reach this goal have been successful. Electron energy loss spectroscopy showed that the only identifiable adsorbates at the end of each experimental attempt to produce an adsorbed ethyl species were the reactant molecule or ethylene. Some of the experiments may have produced a small fraction of adsorbed ethyl, but the spectroscopic features of the initial reactant or the ethylene product obscured its identification. Even if ethyl were present in these studies, these synthetic schemes are useless as a source of an ethyl species for the study of its surface chemistry unless a mechanism for removing the coadsorbates is developed.

The fact that so many of the attempted synthetic routes to an ethyl species yielded ethylene suggests that the ethyl species is not a stable adsorbate on Ni(111). That is, it appears that the barrier for thermal decomposition of adsorbed ethyl to adsorbed ethylene and surface hydrogen is very low or nonexistent. Of course, if no barrier exists for ethyl decomposition, it will never be able to be isolated. However, if a small barrier does exist, the ethyl species should be able to be stabilized by lower surface temperatures. Therefore, further ethyl synthesis attempts should be performed at the lowest surface temperature attainable (10 K). To do so, reaction techniques for adding hydrogen atoms to ethylene or activating a C-H bond of ethyl must be developed which do not heat the surface.

V. References

1. S. P. Daley, Ph. D. Thesis, Massachusetts Institute of Technology, 1994.
2. K. G. Lloyd, B. Roop, A. Campion, and J. M. White, Surface Sci. **214,** 227-239 (1989).
3. T. Shimanouchi, Tables of Molecular Vibrational Frequencies, Natl. Std. Ref. Data Ser., Natl. Bur. Std. (US) **39** (1962)
4. J. R. Durig, J. W. Thompson, V. W. Thyagason, J. D. Witt, J. Molec. Struc. **24,** 41-58 (1975).
5. D. A. McQuarrie and P. A. Rock, *General Chemistry*, New York: W. H. Freeman and Company, 1984.
6. S. H. Pine, *Organic Chemistry*, New York: McGraw-Hill Book Company, 1987.
7. Q. Y. Yang, Ph. D. Thesis, Massachusetts Institute of Technology, 1989.
8. A. D. Johnson, S. P. Daley, A. L. Utz, and S. T. Ceyer, Science **257**, 223 (1992).
9. A. D. Johnson, Ph. D. Thesis, Massachusetts Institute of Technology, 1991.

10. Q. Y. Yang, K. J. Maynard, A. D. Johnson, and S. T. Ceyer, J. Chem. Phys. **102**, 7734 (1995).

CHAPTER IV:
DESIGN OF A MOLECULAR BEAM-SURFACE SCATTERING AND SURFACE ANALYSIS INSTRUMENT

I. Introduction

Our research group currently uses two experimental apparatuses for the study of gas-surface interactions. One of these apparatuses couples supersonic molecular beams with a rotatable line-of-sight triply-differentially pumped mass spectrometer and is well suited to interrogate the gas phase reaction products of a gas-solid interaction by identifying and measuring the translational energy and angular distributions of the molecules which desorb or scatter from the surface.[1,2] The other apparatus is well suited to identify and determine the structure of the adsorbed intermediates and adsorbed reaction products of a gas-surface interaction through surface spectroscopic techniques, vibrational spectroscopy in particular.[3,4] Ideally, the capabilities of both apparatuses would be incorporated in one instrument so that both the gas phase and adsorbed reaction products of the gas-surface interaction could be characterized. However, the combination of supersonic molecular beams, a line-of-sight differentially pumped mass spectrometer and several surface spectroscopic analytical techniques into one experimental apparatus has not been achieved previously.

This chapters describes the design of an experimental apparatus which combines supersonic molecular beams, a differentially pumped mass spectrometer, and several surface spectroscopic analytical techniques for the study of gas-surface interactions. Included in the design of the new apparatus are two supersonic molecular beam sources. Motivation for using supersonic molecular beams to supply gas molecules to a surface for study of the gas-surface dynamics has been discussed extensively in previous works.[1,2,4,5] One of the molecular beams of this apparatus is designed to rotate around the scattering position of the crystal relative to the triply-differentially pumped detector. Simultaneous rotation of the source and the crystal will allow the angular distribution of the scattered molecules to be measured. Rotation of the source will allow the reaction dynamics to be studied as a function of the incident angle. Rotation of the molecular beam source rather than the triply-differentially pumped detector is a major difference from the apparatus previously designed.[1]

The advantage of this design is that it is easier to couple a laser beam to a stationary detector than it would be to a rotatable detector. Coupling of a laser beam to the detector is desirable to be able to ionize molecules with laser light through multi-photon ionization (MPI). MPI with tunable laser light allows ionization of specific rotational-vibrational states of gas phase molecules. Therefore, by measuring the relative number of molecules in each rotational-vibrational state, the internal energy distributions of desorbing and scattering gas molecules can be determined. The translational energy of specific rotational-vibrational states can be determined by measuring the time it takes for the ionized molecules to travel a known distance to the detector through a field free region. In addition to photoionization through MPI, slight modification of the detector allows ionization of gas molecules through electron impact. In this configuration, the detector can be used to measure the angular and translational energy distributions of molecules which desorb or scatter from the surface, similar to the apparatus currently in use.[1,2] The ability of the detector of this apparatus to measure all the parameters of the desorbing or scattering molecules such as the rotational energy, the vibrational energy, the translational energy and the angular distributions will provide a powerful tool for probing the gas phase reaction products of the gas-surface interaction.

In addition to the line-of-sight detector, the apparatus design includes several surface spectroscopic analytical tools. The experimental apparatus currently in use has shown the combination of Auger electron spectroscopy (AES), low energy electron diffraction (LEED) and high resolution electron energy loss spectroscopy (HREELS) to be successful in identifying and determining the structure of adsorbates.[6-8] The new experimental apparatus design includes these surface analytical tools and adds x-ray photoelectron spectroscopy (XPS) and reflection adsorption infrared spectroscopy (RAIRS). AES is an elemental analysis technique. Because it is sensitive to all elements except hydrogen and helium, AES is useful for verifying the purity of the crystal surface. AES is sensitive to surface contaminants down to a coverage of approximately 0.01 ML.[10] In addition to determining surface purity, AES can be used to

measure the relative coverage of surface adsorbates because the AES signal is proportional to the surface concentration. XPS is also an elemental analysis technique and can be used in a similar manner as AES. However, XPS has the advantage of the ability to distinguish the chemical environment of the element by detecting small changes in the binding energy of the core electrons of the element.[9] Low energy electron diffraction (LEED) uses back scattering of electrons to determine long-range ordering of the surface atoms or adsorbates. HREELS and RAIRS are surface vibrational spectroscopic techniques. These techniques are certainly the most powerful surface spectroscopies of the apparatus because analysis of vibrational spectra can lead to a molecular identification of an adsorbate and determination of its structure. Two different vibrational spectroscopies have been included in the design of the apparatus because they complement each other. Each has its advantages. RAIRS has the advantage of spectral resolution. A resolution of less than 5 cm^{-1} full width of half maximum linewidths is typical for RAIRS. Although the resolution of HREELS is very dependent on the spectrometer employed, it is typically much larger, in the 40 - 60 cm^{-1} range. Therefore, RAIRS can resolve spectral features which would be superimposed in HREEL spectra. Also, the higher resolution allows the vibrational frequency of the feature to be more precisely determined.

An advantage of HREELS over RAIRS is the sensitivity.[10] Consider the RAIRS measurement. The light intensity reflected from the surface decreases when the frequency of the light matches the absorption frequency of the adsorbate. The reflectivity of metal surfaces in the spectral region of interest is close to unity and a small deviation from unity is very difficult to detect. HREELS, on the other hand, does not have this difficulty. In HREELS, the signal is measured by counting the electrons which have lost energy to the vibrations at the surface. The electrons which have not lost energy to the surface are counted at a different energy, the incident energy. Therefore, the background is near zero. It is easier to detect a small increase in a signal from near zero (HREELS) than it is to measure a small decrease from a large signal (RAIRS). HREELS also benefits in its sensitivity over RAIRS due to the fact that the cross section for

vibrational excitation by interaction with an electron is two orders of magnitude larger than that by interaction with light.[11]

Another difference in RAIRS and HREELS is the selection rules. In RAIRS, the mechanism for excitation is a dipolar interaction. Chapter II discusses the excitation of surface vibrations through the dipole scattering mechanism. Only transitions to totally symmetric modes are dipole allowed. Therefore, RAIRS can only detect totally symmetric vibrations. In HREELS, excitation occurs through dipolar scattering in addition to another excitation mechanism , impact scattering.[10] Impact scattering does not have the strict selection rule which allows only totally symmetric modes to be observed. Therefore, more vibrational modes of the adsorbate can be detected by HREELS. This could be considered a disadvantage of RAIRS; fewer modes can be detected by it. However, the selection rule is also an advantage because it identifies the symmetry of the modes observed by RAIRS to be totally symmetric. Chapter II shows that HREELS can also identify the modes which are totally symmetric by comparison of the intensities of the features measured in the specular direction to those measured out of the specular direction. However, in some cases the identification is ambiguous because some modes are excited by both the dipolar and impact scattering mechanisms. The confirmation of the mode symmetry provided by RAIRS would remove that ambiguity.

In summary, the new experimental apparatus will be able to probe many different aspects of a gas-surface interaction. Molecular beams are used to prepare the reactant gas molecules with a well defined energy and incident direction and therefore, the reactivity can be studied as a function of these parameters. The combination of surface spectroscopic techniques with the line-of-sight detector allows the reactivity of the incident beam to be monitored by measuring both the adsorbed and the gas phase reaction products. The coverage, surface order, identity, and structure of the adsorbed intermediates and products of the gas-surface interaction can be characterized through AES, XPS, LEED, HREELS, and RAIRS. The identity, translational energy, rotational energy, vibrational energy, and angular distributions of the gas

phase products of the gas-surface interaction can be characterized by the line-of-sight detector. The combination of these complimentary techniques into one apparatus will provide a powerful experimental system for probing gas-surface dynamics.

This chapter describes the design of the important components of the experimental apparatus. At the present time, the primary welded assembly of the apparatus which consists of an ultrahigh vacuum chamber, triply-differentially pumped detector chambers, a singly-differentially pumped detector chamber, the second stage of the stationary molecular beam source and the source stage of the rotatable molecular beam source is being fabricated. The design of inserts and chambers which are not directly welded to the primary welded assembly have not been completed. Also, final decisions about components such as spectrometers, manipulators, pumps, gate valves, traps, etc. have not been made. This work does include discussion of some of the required aspects of the inserts, chambers and components to help facilitate their design and integration into the primary welded assembly, but these descriptions are meant only to be schematic.

II. External Layout of the Primary Welded Assembly

A brief discussion of the external layout of the primary welded assembly of the apparatus will help to facilitate the later discussion of the internal layout of the apparatus. Figure 4.1 shows the Top view of the welded assembly of the experimental apparatus and also labels each side of the apparatus, Detector, Access, Front and Source. These labels are used throughout the discussion in this chapter. Figures 4.2, 4.3, 4.4 and 4.5 show the side views of the primary welded assembly of the experimental apparatus. The apparatus is oriented such that the Top side of the primary welded assembly is facing upward. Therefore, the vertical directions referred to in this chapter are directions toward and away from the Top side and horizontal directions are directions toward the side walls of the primary welded assembly.

Each flange on the welded assembly has been numbered. Tables 4.1, 4.2, 4.3, 4.4 and 4.5 list the flanges and include the description and the proposed purpose for the flange. The apparatus was designed for some degree of flexibility and therefore, the purpose of a few flanges is duplicated.

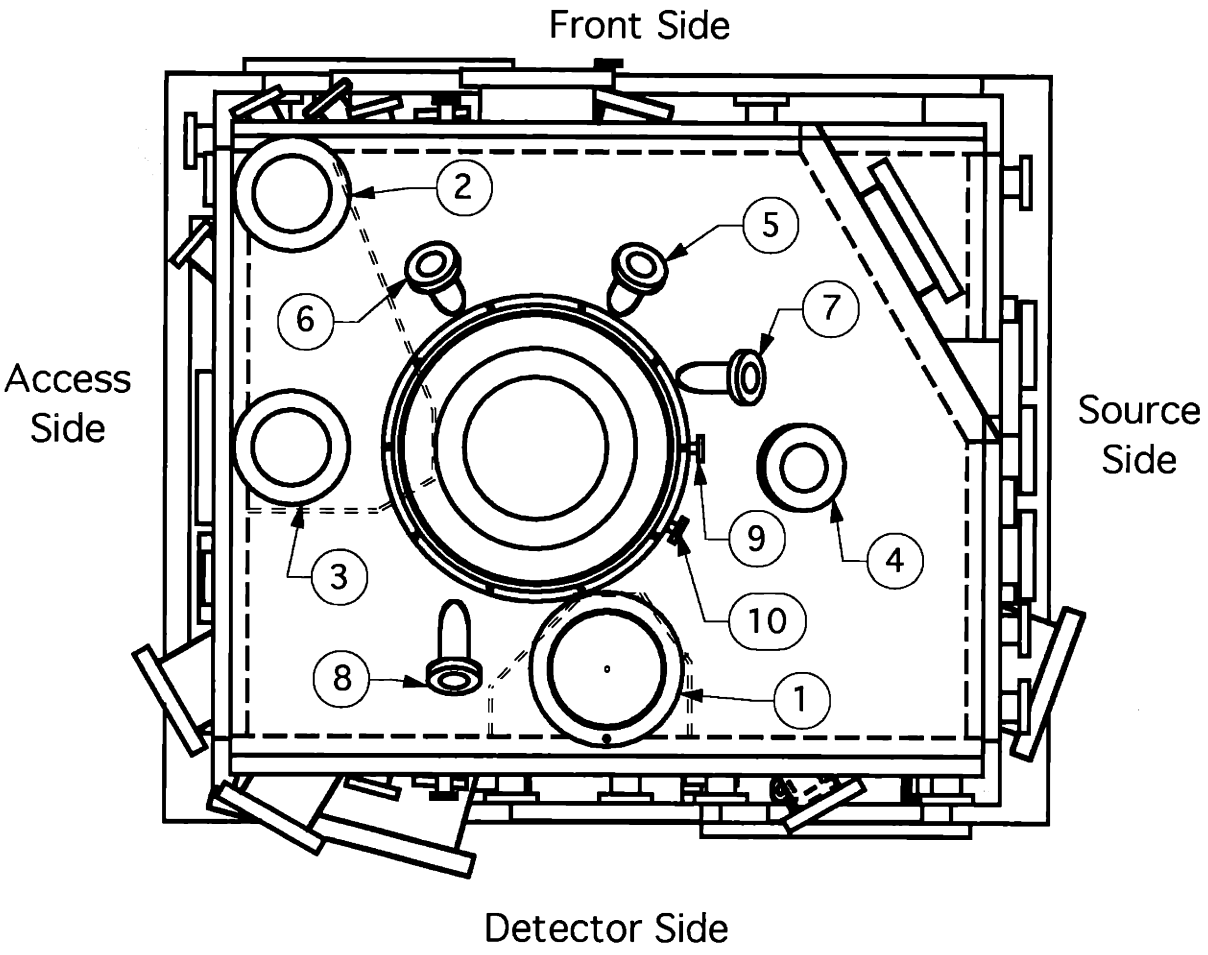

Figure 4.1. External layout of the Top side of the primary welded assembly.

Top Side		
Flange #	Purpose	Description
1	Ionizer	8 Special
2	Turbo pump	6 conflat
3	Access flange	6 CF-tapped
4	Laser window	4.5 CF-tapped
5	Ion gun	2.75 CF-tapped
6	Ion gun	2.75 CF-tapped
7	X-ray source	2.75 CF-tapped
8	Window	2.75 CF-tapped
9	Differential pumping	1.33 CF-tapped
10	Differential pumping	1.33 CF-tapped

Table 4.1. Flanges on the Top side of the primary welded assembly.

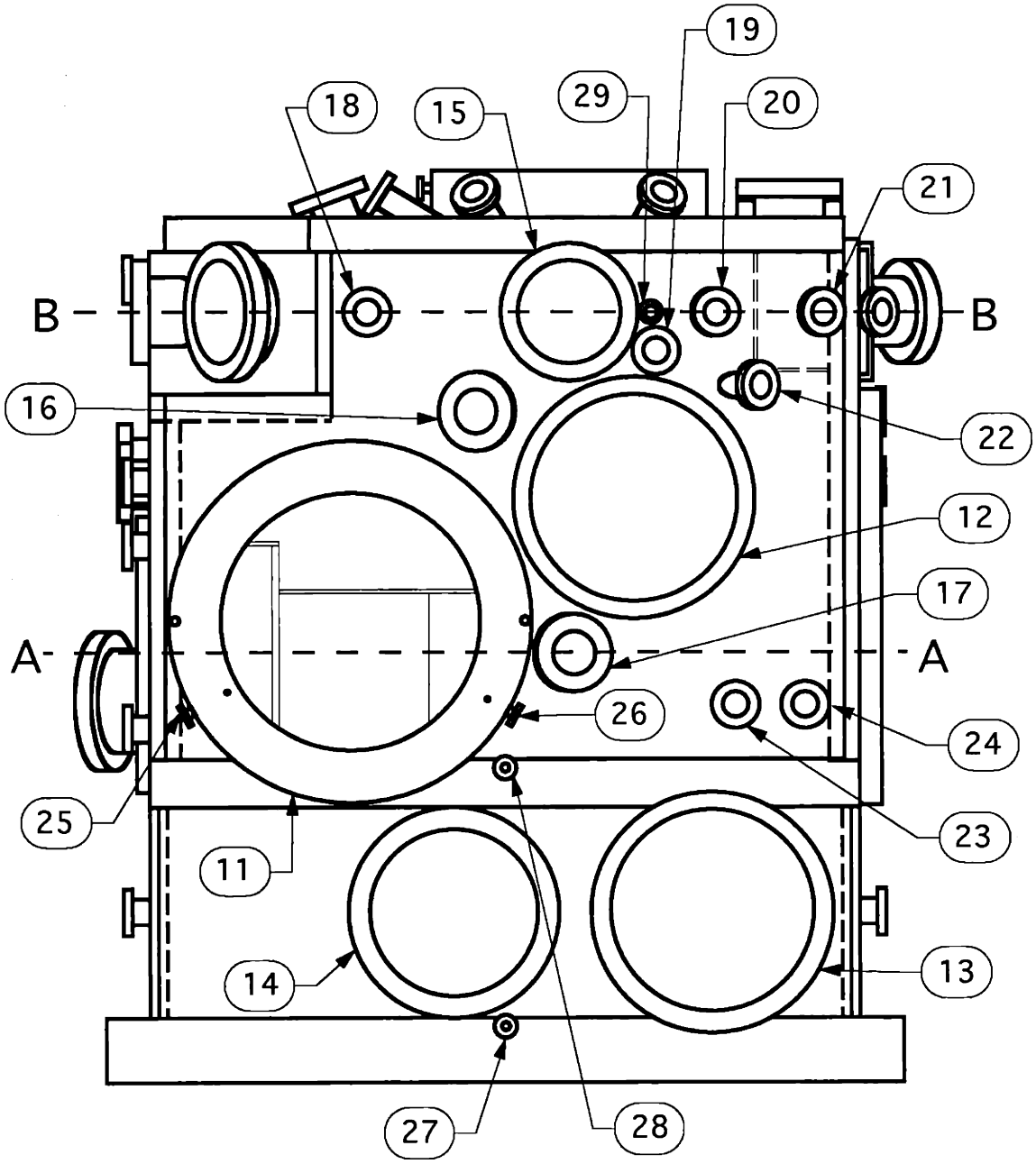

Figure 4.2. External layout of the Front side of the primary welded assembly. Dashed lines A-A and B-B indicate the beam scattering and surface spectroscopy heights, respectively.

Front Side		
Flange #	Purpose	Description
11	21" Access flange	21 teflon-tapped
12	EELS	14 conflat
13	Source pump	14 O-ring-tapped
14	Access flange	12.25 O-ring
15	Auger	8 conflat
16	Window	4.5 CF-tapped
17	Window	4.5 CF-tapped
18	Ion gauge, lamps	2.75 conflat
19	I R Window	2.75 CF-tapped
20	Window	2.75 CF-tapped
21	Window	2.75 CF-tapped
22	I R Window	2.75 CF-tapped
23	Ion gauge, lamps	2.75 conflat
24	Ion gauge, lamps	2.75 conflat
25	Differential pumping	1.33 CF-tapped
26	Differential pumping	1.33 CF-tapped
27	Differential pumping	1.33 CF-tapped
28	Differential pumping	1.33 CF-tapped
29	Laser Window	1.33 CF-tapped

Table 4.2. Flanges on the Front side of the primary welded assembly.

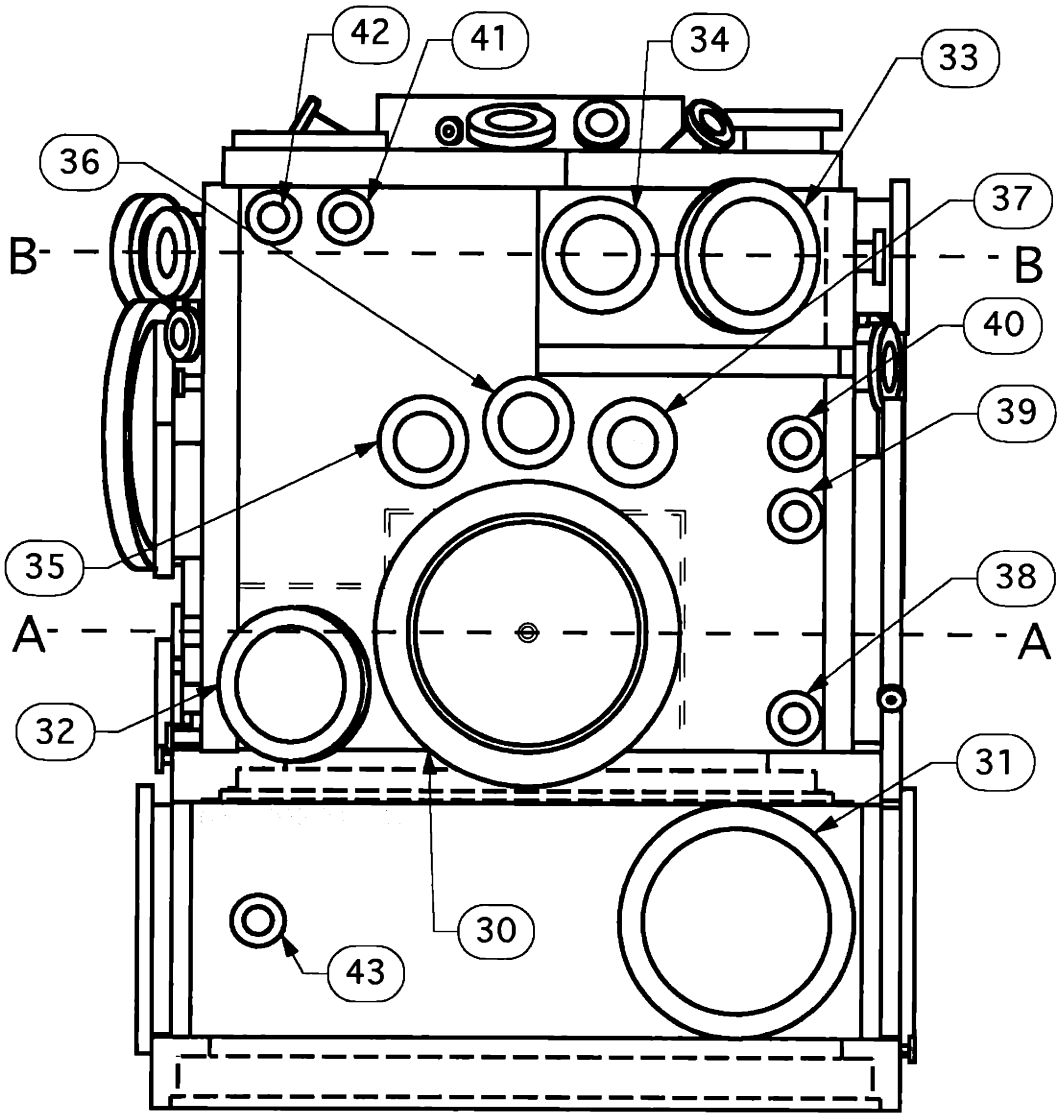

Figure 4.3. External layout of the Source side of the primary welded assembly. Dashed lines A-A and B-B indicate the beam scattering and surface spectroscopy heights, respectively.

Source Side		
Flange #	Purpose	Description
30	Source	16 Special
31	Access flange	12.25 O-ring
32	1st Stage DP	8 conflat
33	LEED	8 conflat
34	Window	6 CF-tapped
35	Feedthroughs	4.625 conflat
36	H or K source	4.625 conflat
37	Window	4.5 conflat
38	Rough pump	2.75 conflat
39	Heating feedthrough	2.75 conflat
40	Leak valve	2.75 conflat
41	Heating feedthrough	2.75 conflat
42	Heating feedthrough	2.75 conflat
43	Ion gauge	2.75 conflat

Table 4.3. Flanges on the Source side of the primary welded assembly.

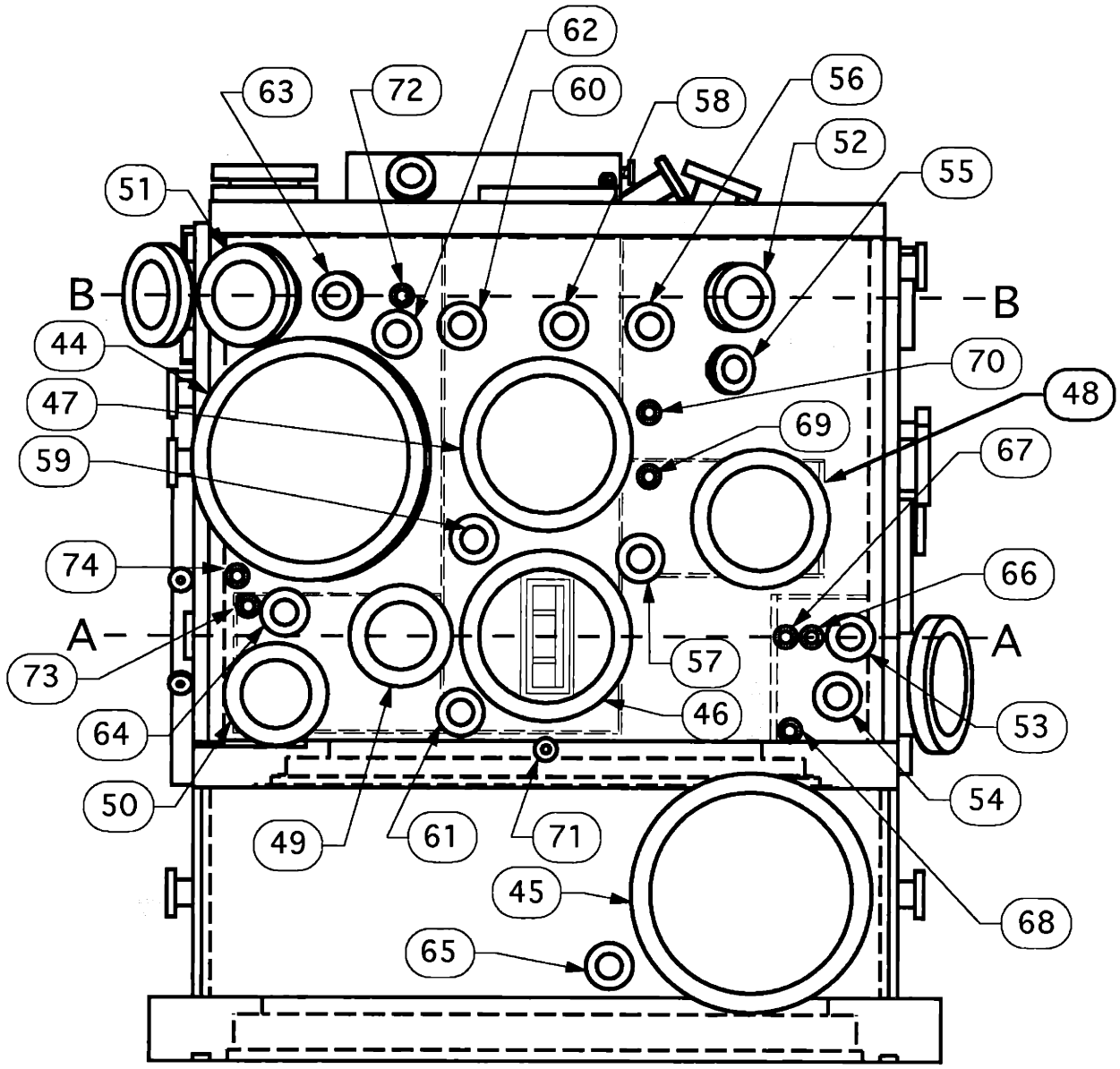

Figure 4.4. External layout of the Detector side of the primary welded assembly. Dashed lines A-A and B-B indicate the beam scattering and surface spectroscopy heights, respectively.

Detector Side		
Flange #	Purpose	Description
44	Main chamber pump	14 conflat
45	Source pump	14 O-ring
46	Quad. mass spec.	10 Special
47	Access to detector	10 conflat
48	Turbo (1st)	8 conflat
49	Chopper motor	6 CF-tapped
50	Chopper turbo	6 conflat
51	Window	6 CF-tapped
52	Window	4.5 CF-tapped
53	LED/PD feedthrough	2.75 conflat
54	Ion gauge	2.75 conflat
55	I R Window	2.75 CF-tapped
56	Roughing flange (2nd)	2.75 conflat
57	Ion gauge 1st-det	2.75 CF-tapped
58	Roughing flange (2nd)	2.75 conflat
59	Elec. feedthrough	2.75 CF-tapped
60	Ion gauge	2.75 conflat
61	Electrical feedthrough	2.75 CF-tapped
62	I R Window	2.75 CF-tapped
63	Window	2.75 CF-tapped
64	Ion gauge	2.75 CF-tapped
65	Ion gauge	2.75 conflat
66	Laser	1.33 CF-tapped
67	Beam valve	1.33 CF-tapped
68	Chopper stop	1.33 CF-tapped
69	Roughing flange (1st)	1.33 CF-tapped
70	Roughing flange (1st)	1.33 CF-tapped
71	Diff. pumping	1.33 CF-tapped
72	Laser window	1.33 CF-tapped
73	Roughing flange (chop)	1.33 CF-tapped
74	Roughing flange (chop)	1.33 CF-tapped

Table 4.4. Flanges on the Detector side of the primary welded assembly.

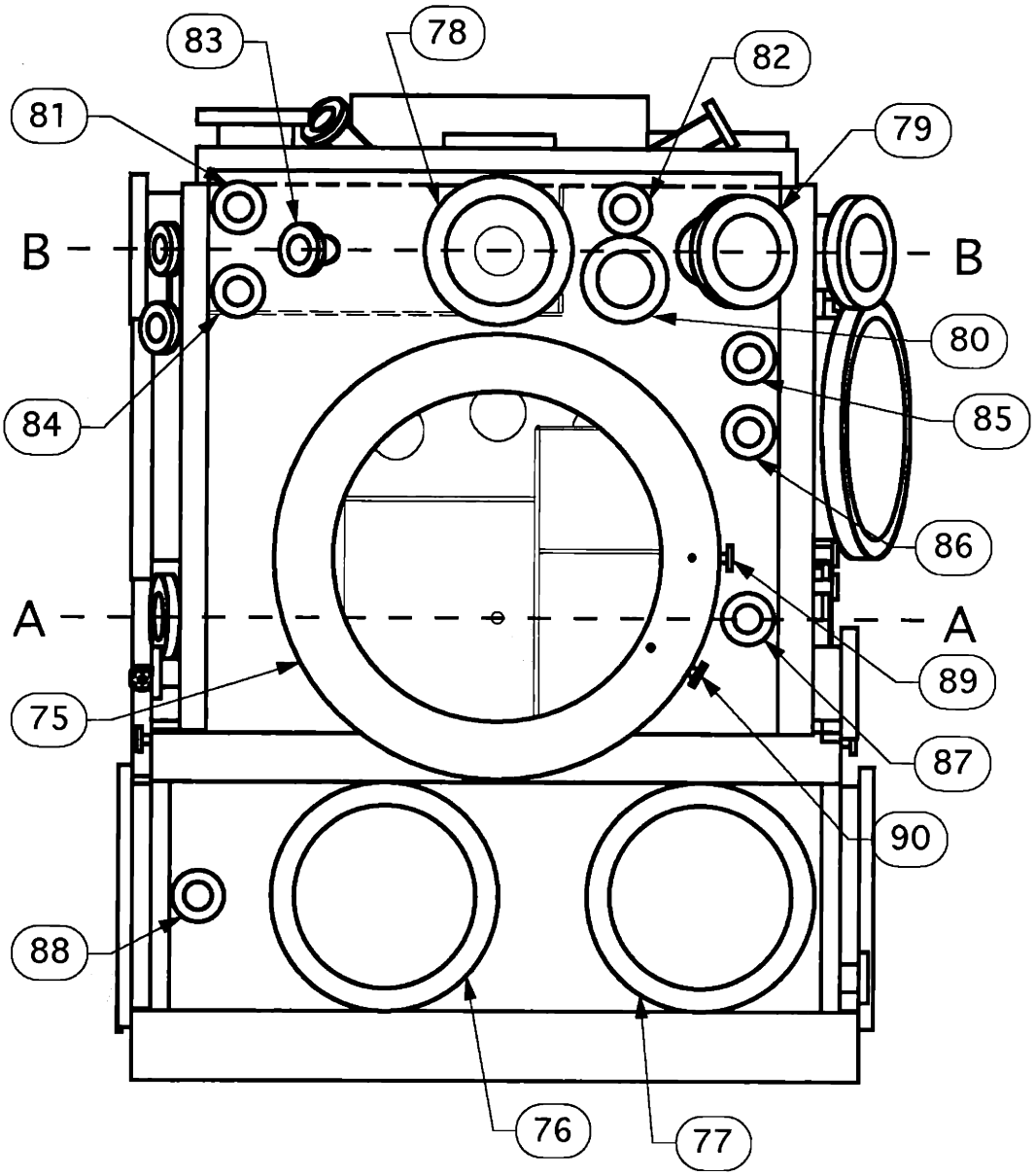

Figure 4.5. External layout of the Access side of the primary welded assembly. Dashed lines A-A and B-B indicate the beam scattering and surface spectroscopy heights, respectively.

Access Side		
Flange #	Purpose	Description
75	Access flange	24 special
76	Access flange	12.25 O-ring
77	Access flange	12.25 O-ring
78	Quad detector	8 Special
79	LEED viewport	6 CF-tapped
80	H-atom source	4.625 CF-tapped
81	Ion gauge	2.75 CF-tapped
82	Feedthrough	2.75 CF-tapped
83	Window	2.75 CF-tapped
84	Ionizer feedthrough	2.75 CF-tapped
85	Ion gauge, lamps	2.75 conflat
86	Ion gauge, lamps	2.75 conflat
87	PD/LED feedthrough	2.75 CF-tapped
88	Ion gauge	2.75 conflat
89	Diff. pumping	1.33 CF-tapped
90	Diff. pumping	1.33 CF-tapped

Table 4.5. Flanges on the Access side of the primary welded assembly.

III. Main Chamber

The chamber that houses the crystal and the electron spectrometers for surface analysis is an ultrahigh vacuum (UHV) chamber and is referred to as the main chamber. The main chamber area is defined by the outer walls of the primary welded assembly with the exception of the lower section, referred to as the rotatable source chamber, as shown in Figure 4.8. The chambers interior to the external walls are referred to as the single stage detector, triple stage detector, and the second stage of the stationary source as shown in Figures 4.6 and 4.7 . The shape of the main chamber is a rectangular box of inner dimensions 30.5" x 37.5" x 29.375" with the exception of the cutout angled corner where the LEED flange (#33) is located. A portion of the inner volume of the main chamber is taken up by the internal chambers.

The large size of the main chamber is necessary because a rotatable source is incorporated into the design of the apparatus. This molecular beam source rotates inside the main chamber and therefore, the main chamber must be larger than the volume swept out by its rotation. The large number of surface spectroscopic tools also mandates a large chamber because almost all of the spectrometers which are of considerable size are mounted within the main chamber.

Eight 304L stainless steel plates combine to form the main chamber. Type 304L stainless steel is used because it is low in carbon content and therefore produces less carbon monoxide, one of the two main contaminants of an UHV chamber, than other types of stainless steel. Prior to the fabrication of the primary welded assembly, the plates are baked at 1050° C for 16 hours in a vacuum furnace to remove some of the hydrogen, the other main contaminant of an UHV chamber, from the stainless steel. The thickness of the plates varies: the Detector and Top plates are 2", the Access and Source plates are 1.75", the Front plate is 1.5", and the Bottom plate is 2.625". When under vacuum, the chamber wall will deflect inward due to the pressure differntial. The different thicknesses of these plates reflect the different requirements for the alignment for the flanges which are welded to each of these plates. For example,

alignment of the rotatable molecular beam source and the quadrupole mass spectrometer is critical for beam scattering experiments and therefore the plates to which the beam source and the detector are attached, the Detector and Bottom plates, are quite thick. Alignment of the Auger spectrometer with the rest of the chamber is not as critical and therefore, the plate to which it attaches, the Front plate, is not as thick. The calculated deflections of the plates are 0.0005", 0.0012", 0.0025", 0.0012", 0.0012" and 0.0011" for the Bottom, Top, Front, Access, Source and Detector sides, respectively. All the plates are designed with notched edges to help ensure proper alignment of the plates during welding. The welding of the plates is done on the inside of the chamber to prevent occlusions of air which can lead to virtual leaks.[12]

The final machining of the primary welded assembly is performed after all welding and heat treatments to eliminate the possible structural distortion of the assembly caused by the extreme heating of the plates. The position and alignment of several of the flanges are critical for beam scattering experiments. These flanges include the ionizer flange (#1), the stationary source flange (#30) and the quadrupole mass spectrometer flange (#46). The alignment of the rotatable lid to which the sample manipulator will be mounted and the rotatable molecular beam source assembly is also critical. The position and alignment of these flanges are described in the following sections of this chapter.

Several tapped holes are machined on the inside of the plates which make up the main chamber. Some of these holes are designed to mount heating lamps for baking of the chamber. The other holes are designed to hold magnetic shielding which will line the entire interior of the main chamber. Magnetic shielding is necessary because the trajectories of the low energy electrons employed in high resolution electron energy loss spectroscopy are affected by magnetic fields. The details of the heating lamps and the magnetic shielding will be provided in future work.

III.A. Sample manipulation

Several different positions within the main chamber must be accessible by the crystal. A long stroke bellows manipulator, mounted vertically, is used to translate the crystal in the vertical direction. The lowest and highest heights the crystal must attain are the beam scattering height and the surface spectroscopy height, respectively, which are indicated in Figures 4.2, 4.3, 4.4 and 4.5. The distance between these two heights is 19.675". Therefore, the manipulator design must accommodate a translation of approximately 20". The manipulator should also be capable of small horizontal translations, approximately ±0.5", to allow for precise positioning of the crystal with respect to the chamber and the surface sensitive spectrometers. It is also necessary to be able to translate the crystal horizontal distances greater than one inch. To accommodate this horizontal translation, the manipulator is mounted eccentrically on a rotatable flange. This flange, referred to as the rotating lid flange, is the large unnumbered flange shown on the Top of the apparatus in Figure 4.1. The lid is a differentially pumped teflon sealed rotatable flange which is a duplicate design of a lid currently in use.[4] The manipulator is mounted 3.75" off the center of rotation of the rotatable lid. Therefore, rotation of the lid by 180° translates the crystal horizontally by 7.5". The dashed circular line shown in Figure 4.6 indicates the path on which the crystal translates upon rotation of the lid.

III.B. Surface Spectroscopies

The flanges which are important for the surface spectroscopies are detailed in the following sections. The crystal positions for of each the spectroscopies are also discussed.

III.B.1. Auger electron spectroscopy

The Auger electron spectrometer is mounted on a 8" OD conflat flange (#15) on the Front side wall of the primary welded assembly. The Auger flange has been designed for a Physical Electronics double pass cylindrical mirror analyzer spectrometer (model # 15-255G). The distance from the face of the flange to the crystal position is 16.03". The horizontal cross

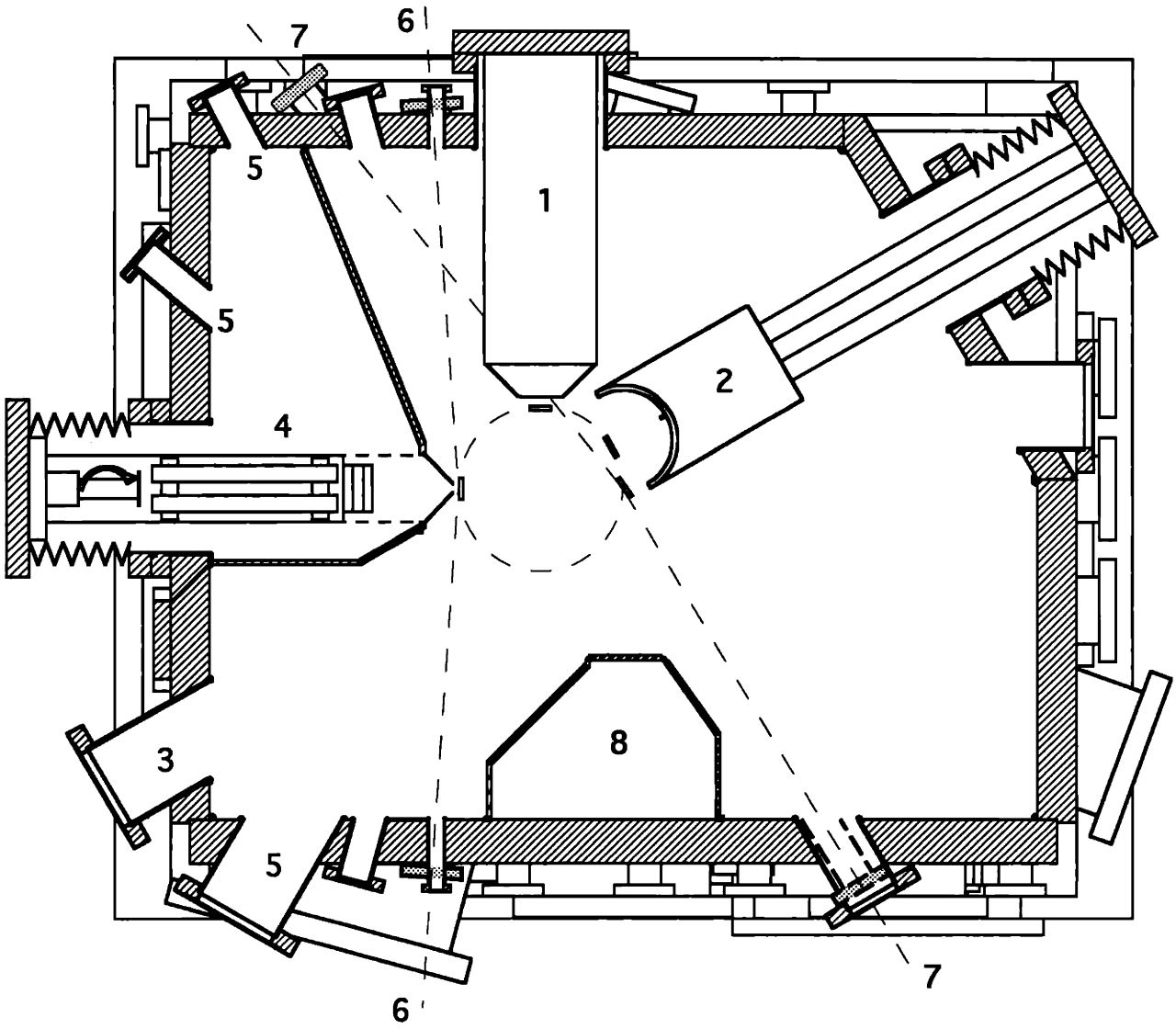

Figure 4.6. Cross sectional view at the surface spectroscopy height. 1) cylindrical mirror analyzer for Auger and XPS measurements; 2) low energy electron diffraction (LEED) spectrometer; 3) window for viewing LEED patter; 4) singly-differentially pumped detector mass spectrometer; 5) windows for viewing translation of cone extension; 6) pair of IR windows for reflection absorption infrared spectroscopy; 7) pair of IR windows for reflection absorption infrared spectroscopy; 8) second differential pumping stage of the triply-differentially pumped detector.

section at the surface spectroscopy height in Figure 4.6 shows the Auger spectrometer and the position of the crystal for Auger analysis.

III.B.2. X-ray photoelectron spectroscopy

The double pass cylindrical mirror energy analyzer is used to measure the kinetic energy of the emitted electrons during x-ray photoelectron spectroscopy (XPS) experiments. Therefore, only an x-ray source is needed for XPS measurements. Flange #7 is designed to mount the x-ray source. The bore of this flange is directed to the position of the crystal when it is directly in front of the double pass cylindrical mirror energy analyzer. The distance from the flange face to the crystal position is 13.25". This relatively long dimension will be an important issue when deciding which x-ray source to purchase since the x-ray intensity at the crystal is inversely proportional to square of the distance between the x-ray source and the surface.

III.B.3. Low energy electron diffraction

Flange #33, an 8" OD conflat, is designed to mount a low energy electron diffraction (LEED) spectrometer. The design allows for any spectrometer that will fit through the bore of the 8" OD conflat. Figure 4.6 includes a schematic of the position for the LEED spectrometer. The distance from the flange face to the LEED crystal position is 19.58". Since no commercially available spectrometer extends from the mounting flange this far, the spectrometer will have to be adapted to extend this distance. The LEED spectrometer shown in the figure is mounted on a translational stage. The translational stage is necessary to move the spectrometer back when it not in use. The crystal position for molecular beam scattering is below the LEED crystal position and since the crystal manipulator is mounted from above, the LEED spectrometer will need to be translated back towards its flange in order for the crystal to able to access the scattering position. Note that a translation stage is not needed for the Auger spectrometer because there is no need for the crystal to access positions directly below the

Auger crystal position. The window opposite the LEED spectrometer (flange #79) is used for viewing the LEED pattern on the spectrometer.

III.B.4. Reflection absorption infrared spectroscopy

The spectrometer used for reflection absorption infrared spectroscopy (RAIRS) is external to the primary welded assembly. The infrared radiation enters the chamber through a window, scatters from the surface, and exits the chamber through another window. Two different crystal positions for RAIRS have been included in the design and are shown in Figure 4.6. Therefore, there are two pairs of IR windows: one pair is flanges #19 and #62 and the other pair is #22 and #55. It is noted that these flanges and RAIRS crystal positions are not at the surface spectroscopy height shown in Figure 4.6. Flanges # 19 and # 62 are 2.25" and flanges # 22 and # 55 are 4.25" below the surface spectroscopy height. The bore of these pairs of flanges which mount the windows are directed at the surface making an angle of 172° with respect to each other and yield a grazing angle of 4° for the incident and reflected IR beams. Grazing incident and reflection angles maximize the sensitivity of RAIRS to surface vibrations.[13]

III.B.5 High resolution electron energy loss spectroscopy

The spectrometer used for high resolution electron energy loss spectroscopy (HREELS) bolts to a 14" OD conflat flange (#12) on the Front side wall of the primary welded assembly. The distance from the face of the flange to the center of the crystal position for the HREELS measurement is 15.75". Most commercially available spectrometers have sample position to flange distances which are shorter than 15.75", and therefore, the spectrometer will have to be adapted to extend farther into the chamber. The EELS spectrometer is not shown in Figure 4.6 because it is not positioned at the surface spectroscopy height shown in the figure. However, the horizontal position of the crystal for an EELS measurement is the same as that shown for the

differentially pumped thermal desorption experiment which is described in the next section, and the vertical position is 10.75" below the surface spectroscopy height.

IV. Singly-Differentially Pumped Detector

The singly-differentially pumped detector chamber is welded to the Access side wall on the inside of the main chamber at the surface spectroscopy height as shown in Figure 4.6. This detector chamber houses a quadrupole mass spectrometer and is designed for differentially pumped thermal desorption experiments. In a thermal desorption experiment, a mass spectrometer monitors the partial pressure of a gas as a function of the crystal temperature. Raising the crystal temperature causes adsorbates to desorb from the surface into the gas phase. Thus, the increase in the partial pressure is a measure of the desorption rate of adsorbates from the crystal. Ideally, only the crystal is heated during the experiment such that desorption of molecules from other surfaces does not take place, but in practice, it is impossible not to heat surfaces close to the crystal surface or those in thermal contact with it. Desorption from surfaces other than the crystal surface complicates thermal desorption measurements if it contributes to the partial pressure of the gas of interest.

A differentially pumped thermal desorption experiment minimizes the detection of the background desorption from surfaces other than from the crystal. This is achieved by placing the mass spectrometer in a chamber separate from the main chamber in which the crystal is housed with its own pumping. The crystal is placed directly in front of a small aperture between the chambers. As the crystal is heated and molecules desorb from the surface, the flux of molecules from the main chamber into the detection chamber through the aperture is dominated by molecules which have desorbed directly from the surface. The partial pressure of gases which have desorbed from surfaces other than the crystal is lower in the single stage detector chamber than the main chamber because only the molecules desorbing from the crystal are in the line-of-sight of the aperture. Molecules which do not impinge on the aperture are

deflected and pumped away by the main chamber pump. Only a small effusive background from the main chamber into the single differentially pumped chamber is present.

Figure 4.6 shows a cone shaped insert which extends from the single stage detector into the main chamber. The aperture between the main chamber and the singly-differentially pumped chamber is machined onto the front of this cone insert. Also shown in the figure is the crystal position during a differentially pumped thermal desorption measurement. Because the crystal must be able to access positions directly below that used for differentially pumped thermal desorption, it will be necessary to translate the cone insert back towards the single stage detector chamber when it is not in use. One solution to this translation is attaching the cone to the mass spectrometer and translating the whole assembly with an exterior bellows design as is shown in Figure 4.6. Another solution is to translate just the cone extension itself. The access flange into the single differentially pumped chamber (#3) could be used for the motion feedthrough for this translation. Several windows are strategically positioned for viewing the translation of the cone extension insert.

The singly-differentially pumped detector chamber can be used for an additional type of thermal desorption experiment because the ability to cross a laser beam with the desorbing molecules has been included in the design of the primary welded assembly. The laser radiation is used for ionization of desorbing molecules through multi-photon ionization (MPI). By ionizing specific rotational-vibrational states through MPI, the internal state distributions of the desorbing molecules can be detected. The setup is similar to that used in the MPI geometry of the triply-differentially pumped detector except only one differential pumping stage is incorporated. Two 1.33" OD conflat flanges (#29 and #72) which are directed 1" in front of the crystal when it is in the differentially pumped thermal desorption position are used for the laser beam windows, one for the entrance of the beam to the chamber and the other for its exit.

The single stage detector chamber is constructed from two 3/16" and one 1/4" thick stainless steel plates. The front plate which is positioned away from the Access side wall is

thicker to allow sufficient material for precision machining of circular locating steps on each side of the 2.626" circular opening between this chamber and the main chamber. The cone extension inserts into this opening. The steps are machined exactly parallel to the face of the quadrupole mass spectrometer mounting flange (#78). In addition, the opening is machined to be exactly concentric to the bore of the quadrupole mass spectrometer mounting flange. There are also eight through tapped holes equally spaced on a 2.973" bolt circle for permanent mounting of the cone extension, if it is decided that its translation is unnecessary.

There are four flanges on the Access side wall of the primary welded assembly that lead into this chamber. Three of these flanges are 2.75" OD conflat flanges: #81 is used for an ion gauge, #83 is used for a window, and #84 is used for electrical feedthroughs for the mass spectrometer. The fourth flange (#78) is a special flange similar to the Balzers DN100ISO. It is an aluminum wire seal flange which allows for better alignment than conflat flanges. The quadrupole mass spectrometer bolts to this flange.

Two flanges access this chamber through the Top side wall of the primary welded assembly. They are both 6" OD conflat flanges. Flange #2 mounts the pump, a Balzers TPU 330 l/s turbomolecular pump, for this chamber while the other flange (#3) is used as an access into the singly-differentially pumped detector chamber. It can also serve as a mount for a translation stage feedthrough as discussed earlier.

One conflat flange comes through the Front side wall of the primary welded assembly into the single stage differential pumping chamber. It is a 2.75" OD conflat and is used as a window for viewing the translation of the cone extension insert.

V. Molecular Beam Scattering

Figure 4.7 is a cross sectional schematic at the molecular beam height showing the beam scattering arrangement. Shown in the figure are the rotatable molecular beam source, stationary

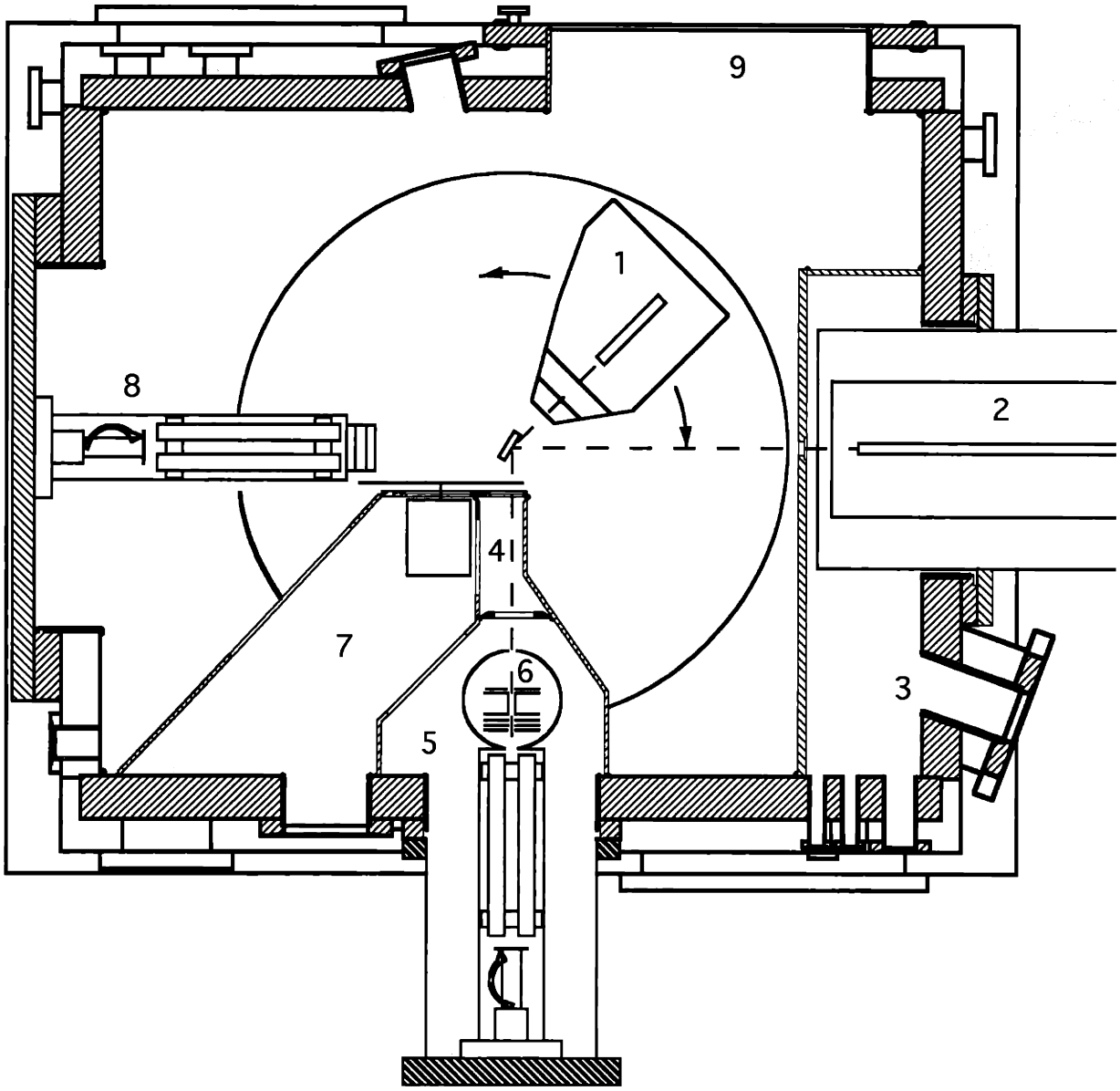

Figure 4.7. Cross sectional view at the molecular beam scattering height. 1) rotational source; 2) stationary source; 3) second differential pumping stage of the stationary source; 4) first differential pumping stage of triply-differentially pumped detector; 5) mass spectrometer and second differential pumping stage of triply-differentially pumped detector; 6) ionizer and third differential pumping stage of triply-differentially pumped detector; 7) chopper chamber; 8) main chamber mass spectrometer; 9) access flange to main chamber.

molecular beam source, the triply-differentially pumped detector and the main chamber mass spectrometer. Each component is described separately.

V.A. Rotatable Molecular Beam Source

The rotatable molecular beam source assembly is designed to enter the main chamber through the large opening in the Bottom Plate. A schematic diagram is shown in Fig 4.8. A section of the rotatable source assembly extends upward from the Bottom Plate Mating Flange into the main chamber. The molecular beam exits the rotatable source assembly from this section at the beam height. All three differential pumping stages are present in this section. The source pumping stage extends downward through the Bottom Plate Mating Flange. The area between the Bottom and Base Plates is the source pumping stage of the rotatable molecular beam source. A diffusion pump mounted on the side of this chamber provides pumping for this chamber. The first differential pumping and second differential pumping stages extend downward through the Bottom Plate Mating Flange, the source pumping stage, and the Base Plate Mating Flange to flanges attached to the Base Plate Mating Flange. The diffusion pumps for the first and second stages bolt to flanges which go through the Base Plate Mating Flange into the first and second stages. Details of the rotatable beam source assembly will be described in future work.

To allow for rotation of the rotatable source assembly while maintaining vacuum, the seals between the Base Plate Mating Flange and Base Plate and Bottom Plate Mating Flange and Bottom Plate are spring loaded teflon seals. The design of the sealing surfaces of the Base Plate and Bottom Plate Mating Flanges is similar in design to the teflon flanges shown in Figure 4.9. The Bottom Plate Mating Flange is sealed with three teflon seals. The combination of the three teflon seals with two differential pumping stages allows a UHV seal against atmospheric pressures. The first and second stage pumpout grooves are connected through the Bottom Plate

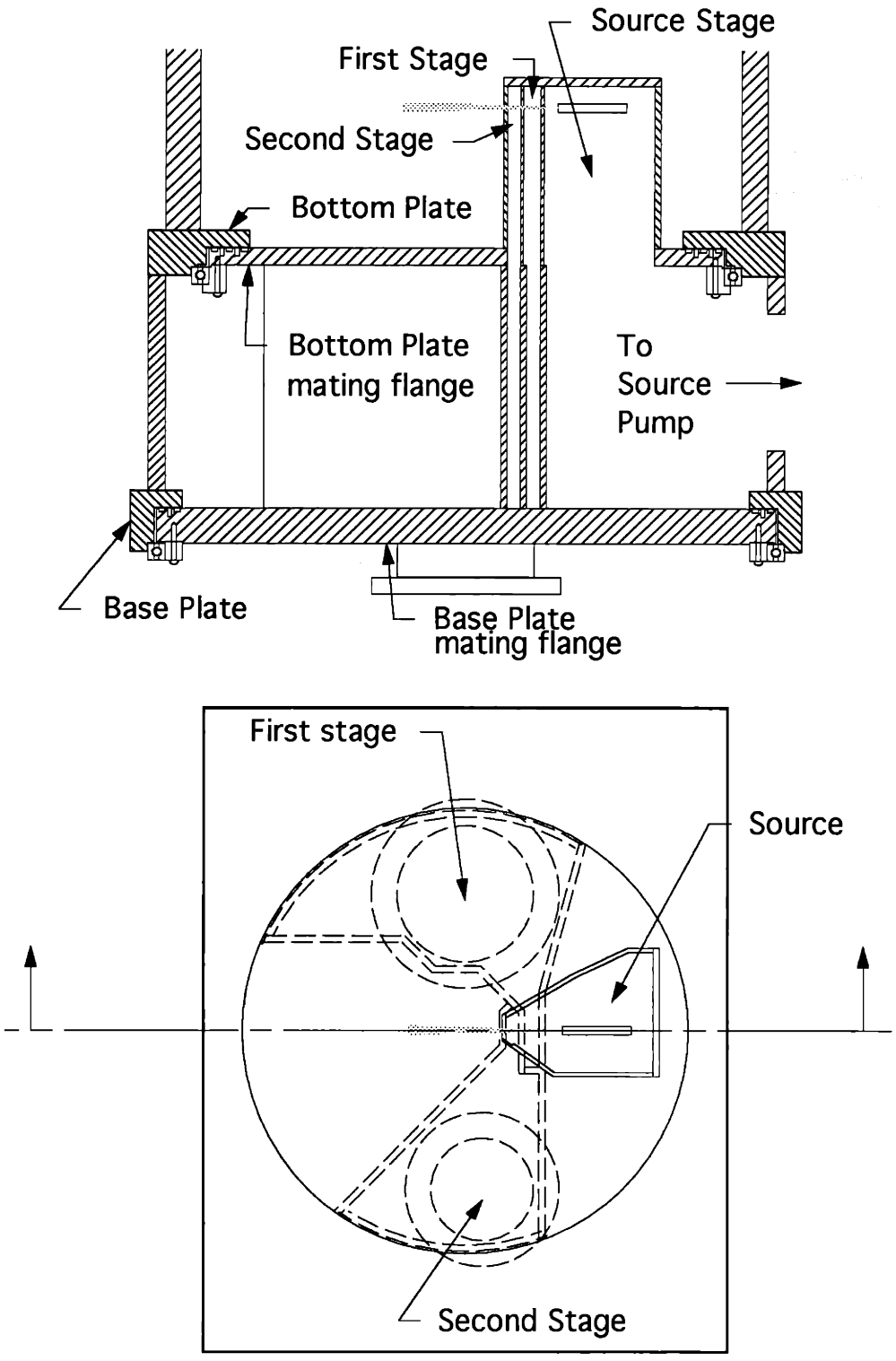

Figure 4.8. Rotatable source assembly.

to conflat flanges #71 and #28 respectively. The area between the Bottom Plate and Base Plate is the source pumping stage of the rotatable molecular beam source. This chamber is not designed to operate at UHV. Therefore, only two teflon seals and one differential pumping stage are needed to seal this chamber with respect to atmosphere. A bore through the Base Plate connects conflat flange #27 to the differential pumping groove.

Alignment of the rotatable source assembly with the primary welded assembly is critical. The source must rotate around the crystal scattering position in a horizontal plane which is perpendicular to the triply-differentially pumped detector. This alignment is achieved by the precision machining of the locating step in the Bottom Plate into which the bearings that support the rotatable source assembly are inserted. This locating step is machined such that its bore precisely intersects the bore of the flange with mounts the stationary source and the flange which mounts the mass spectrometer of the triply-differentially pumped detector. The surface of the locating step is machined exactly perpendicular to the flange which mounts the mass spectrometer of the triply-differentially pumped detector.

Pumping of the source stage of the rotatable molecular beam source is achieved through either or both of the 14" o-ring sealed flanges (#13 and #45). There are four more o-ring sealed flanges which enter the source pumping stage (#14, #31, #76, and #77). These flanges serve as access to the source pumping stage and are especially important in assembly of the rotatable source and the primary welded assembly. There is one more flange leading into this chamber (#65). This 2.75" OD conflat flange is used as an ion gauge port.

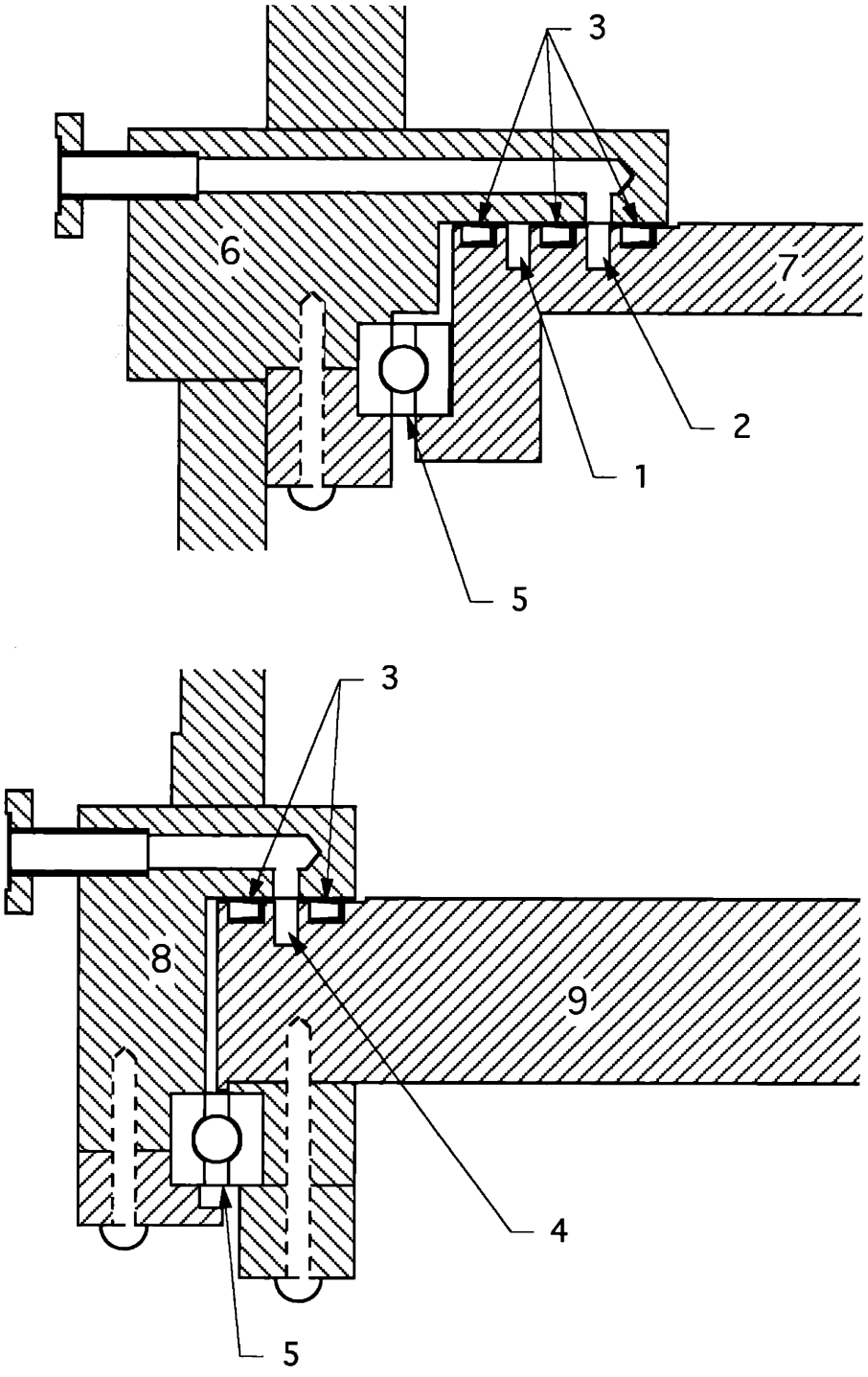

Figure 4.9. Cross section of the Bottom and Base Plates and their mating flanges. 1) first differential pumping groove of the Bottom Plate Mating Flange; 2) second differential pumping groove of the Bottom Plate Mating Flange; 3) spring loaded teflon seals; 4) first differential pumping groove of the Bottom Plate Mating Flange; 5) precision mounted bearings; 6) Bottom Plate; 7) Bottom Plate Mating Flange; 8) Base Plate; 9) Base Plate Mating Flange.

V.B. Stationary Molecular Beam Source

The stationary molecular beam source assembly couples to the Source side wall of the primary welded assembly. The design of the stationary source is similar to a molecular beam source described previously.[4] The source assembly consists of three separate stages, the source pumping stage, the first differential pumping stage, and the second differential pumping stage. The second differential pumping stage is part of the primary welded assembly and therefore, is described here. Details of the source and first differential pumping stages can be found elsewhere.

The internal chamber welded to the lower portion of the Source side wall and extending into the main chamber is referred to as the second differential stage of the stationary molecular beam source. It can be seen in the horizontal cross section at the beam scattering level shown in Figure 4.7. This chamber serves as the last differential pumping stage of the stationary molecular beam. Housed in this chamber are a chopper wheel, LED/photodiode for the chopper, a chopper wheel stopper, and a molecular beam valve.

The molecular beam chopping wheel is used for time-of-flight spectrometry which enables characterization of the translational energy of the molecular beam. As a small slit in the chopping wheel aligns itself with the molecular beam, a short pulse of gas travels onward into the main chamber and is finally detected by a mass spectrometer. The LED/photodiode pair signal the moment at which the molecular beam passes through the slit in the chopper wheel. The time it takes for the pulse of molecules to travel from the chopper to the detector is measured. This time along with the length of the flight path is used to calculate the velocity of the molecules in the beam. The motor for the chopper wheel is housed in the first stage of the molecular beam source and therefore, will be described elsewhere.

When chopping of the molecular beam is not desired, the slit in the chopping wheel must be positioned so as to allow the beam to pass through it. A chopper stopper enables

manual positioning of the chopping wheel and holds the chopping wheel in place. The chopper stopper is similar to that previously designed.[4]

The second differential stage of the stationary molecular beam source is constructed out of five stainless steel plates which are sufficiently thick to withstand an atmospheric pressure differential without warping. This feature is desirable so that the stationary source can be vented without venting the ultrahigh vacuum main chamber. Four of these plates are 1/4" thick stainless steel and the fifth plate, the front plate which is the largest plate, is 3/8" thick stainless steel. The front plate is thicker because the opening between the main chamber and this chamber is precision machined onto this plate. A thicker plate provides more material for the final machining.

The second differential stage is not designed to maintain UHV. Therefore, the welds are not full penetration welds, eliminating the need to chamfer the plates which make up the second stage and to premachine welding reliefs on the main chamber walls. The welding is performed on the main chamber side of the plates to prevent virtual leaks into the UHV main chamber.

This chamber is accessed through flanges on the Source side wall and the Detector side wall of the primary welded assembly. The 16" OD flange (#30) on the source side wall is the stationary source flange onto which the source and first stage assembly of the stationary molecular beam source will bolt. The horizontal distance from the surface of this flange to the crystal at the scattering position is 21.250". To ensure alignment of the stationary source with respect to the triply-differentially pumped detector, the surface of this flange is machined to be exactly perpendicular to the detector quadrupole mass spectrometer flange surface. The bore of this flange is also precision machined so that it intersects precisely the rotational axis of the rotatable molecular beam source and the mass spectrometer flange. In addition, a 0.18" deep locating step is machined onto the flange to ensure concentricity of the mating source flange with this bore. The other flange entering this chamber through the Source side wall is an 8" OD

conflat flange which serves as the pumping port. This flange is angled away from the source flange to allow room for the second stage gate valve, cold trap, and diffusion pump.

Five conflat flanges access this chamber through the Detector side wall of the primary welded assembly. The two 2.75" OD conflats (#53 and #54) are designed for the LED/photodiode electrical feedthroughs and an ion gauge. The remaining flanges are 1.33" OD conflats. Flange #66 is designed as a possible window for a laser beam. This flange is at the molecular beam height and therefore, allows the capability of crossing the molecular beam with a laser beam. The other flange at the molecular beam height (#67) is for the molecular beam valve. The molecular beam valve serves two purposes. One purpose is to isolate the stationary beam source chamber from the main chamber, permitting one to be vented while keeping the other under vacuum. The other purpose served by the molecular beam valve is to position different size orifices in front of the molecular beam, thus defining the cross section of the molecular beam introduced into the main chamber. The beam valve design is a duplicate of that previously designed and is currently in use.[4] The last flange into the second differential stage is used for the chopper wheel stopper discussed previously.

An important feature of the second differential stage design is the precision machined opening between the second differential stage and the main chamber. The beam valve insert fits tightly into this opening which is bored to be concentric with the stationary source flange. A locating step around the bore is precision machined to be parallel to and concentric with the source flange. A tight fit of the insert assures alignment of the collimating slit mounted on the insert with the rest of the stationary molecular beam source. The surface around the opening is spot faced to ensure a good sealing surface for the beam valve.

V.C. Main Chamber Quadrupole Mass Spectrometer

The main chamber quadrupole mass spectrometer has several functions. Its most critical function is time-of-flight detection of the stationary source molecular beam which requires the

mass spectrometer to be precisely aligned with the stationary source. Figure 4.7 shows the position of the main chamber mass spectrometer. It is mounted eccentrically on the flange which mates the large access flange (#75). The access flange face is precision machined to be parallel to the stationary beam source flange. A locating step and a dowel pin hole on this flange ensure positional and rotational alignment, respectively, with the stationary source flange. The quadrupole mass spectrometer must be attached to the mating flange precisely. The design of the mating flange will be discussed in future work.

Another function of the main chamber mass spectrometer is a detector of the partial pressure of gases in a thermal desorption experiment. It can also be used for residual gas analysis and as a detector for helium leak detection.

V.D. Triply-Differentially Pumped Detector

The chambers on the Detector side wall of the primary welded assembly comprise what is referred to as the triply-differentially pumped mass spectrometer detector. This detector is used to measure the translational energy and angular distributions of mass-selected molecules desorbing or scattering from the surface. The translational energy distributions are measured using a time-of-flight technique in which the beam entering the detector is mechanically modulated. Collimating slits between the differential pumping stages of the detector define the acceptance angle into the detector. The angle between the normal to the crystal surface and the detector defines the detection angle. Different detection angles can be accessed by rotation of the crystal, allowing the angular distribution of the desorbing or scattering products to be measured.

Four separate compartments make up the triply-differentially pumped detector. Three of these compartments are welded into place and are described in this work: the chopper chamber, the first differential pumping stage, and the second differential pumping stage. The

fourth compartment, the third differential pumping stage, bolts into place from above on flange #1 and will be discussed elsewhere.

Ten plates combine to form these chambers. All except two of the plates are 1/8" and 3/16" thick stock. The remaining two plates, the plate between the main chamber and the first and chopper stages and the plate between the first stage and second stage, are 5/16" and 1/4" stock, respectively. Openings machined in these plates are precision aligned. Since it is impossible to weld a plate into place precisely, the machining of these openings are deferred until after all welding and a high temperature anneal of the whole apparatus. The extra thickness of these plates gives ample material for the final machining.

The detector stages and chopper chamber need to attain ultrahigh vacuum pressures and therefore, all welds involving this chambers are full penetration welds. To help accommodate full penetration welds, the detector plates are chamfered to a thickness of 1/16" at the point of welding, and welding reliefs are machined into the main chamber walls where the detector chamber walls meet the main chamber wall. Welding reliefs are produced by machining two grooves 1/16" deep and 1/8" wide, with only a 1/16" strip of material remaining on the main chamber walls. Therefore, at the point of contact, there is only 1/16" thick material on the both the main chamber and the detector wall plates. Figure 4.10 shows a drawing of a chamfered plate and a welding relief.

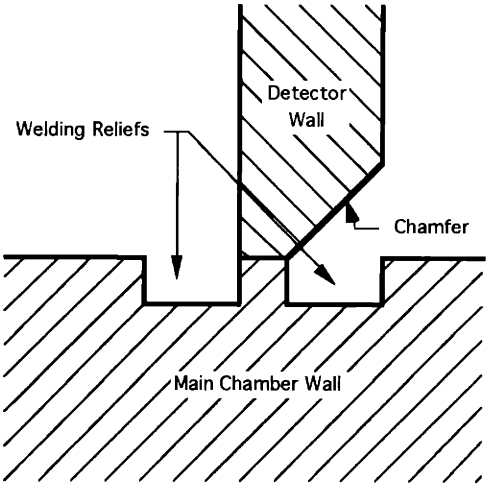

Figure 4.10. Schematic showing a chamfered detector wall and welding reliefs machined on the main chamber wall.

V.D.1. Chopper chamber

The compartment on the access side of the triply-differentially pumped detector is referred to as the chopper chamber. The purpose of this chamber is to differentially pump the chopper motor because it will outgas when in use. The chopper motor is mounted on the insert plate which attaches to the opening between the chopper chamber and the main chamber. The shaft of the chopper motor extends through this insert so that the chopper wheel is in the main chamber and the chopper motor is in the chopper chamber.

There are four conflat flanges through the Detector side wall of the primary welded assembly leading to the chopper chamber: two 6" OD; one 2.75" OD and one 1.33" OD. The 1.33" conflat flange (#73) is used for rough pumping of the chopper chamber. The 2.75" flange (#64) is used for an ion gauge. A Balzers TPU 330 l/s turbomolecular pump attaches to one of the 6" conflat flanges(#50). The other 6" conflat (#49) is used for the electrical feedthroughs and the water cooling lines for the chopper motor.

In addition to these flanges, there are several openings between the chopper chamber and the adjacent chambers. These openings are sealed by close fits of the cover or insert plates. These seals are not leak tight but are sufficient for seals between two ultrahigh vacuum

chambers. The opening through the front plate to the main chamber is precision aligned with respect to the quadrupole detector flange (#46). The front face of this plate is also precision machined to be 2.000" from the crystal scattering position and parallel to the face of the quadrupole detector flange. Alignment of the insert plate to which the chopper motor is mounted is ensured by a 0.093" deep locating step. Twenty-two 6^{32} through tapped holes are used for mounting of the front chopper plate. Details of this insert plate will be discussed elsewhere. The positions of the other openings in this chamber are not crucial and are machined in the plates prior to assembly.

V.D.2. First differential pumping stage

The first differential pumping stage of the detector is the chamber closest to the scattering position as shown in Figure 4.7. The chamber extends up and then flares out toward the Detector side wall of the primary welded assembly. The flared portion of the first stage allows a higher conductance and space for the first stage pump to be attached. The bottom plate of the flared portion is 3.5" above the beam height so as to allow space for rotation of the rotatable source underneath it.

Similar to the chopper chamber, there are access holes to this compartment from within the main chamber, chopper chamber and second stage. Two of these openings need precision alignment: the one from the main chamber to the first differential pumping stage and one from the first differential pumping stage to the second differential pumping stage. Discussion of the opening between the first and second stages is discussed in the next section.

The opening between the main chamber and the first differential pumping stage holds an insert plate onto which a collimation slit is machined. Alignment of the insert is assured by the 0.093" deep locating step and a tight fit in the precision machined opening. The collimation slit in the insert defines the acceptance angle of the detector. The insert is held in place by nine 6^{32} through tapped holes.

There are three conflat flanges through the detector side wall of the primary welded assembly to the first differential pumping stage: one 8" OD, one 2.75" OD and one 1.33" OD. Similar to the chopper chamber, the 1.33" conflat (#69) is used for rough pumping of the first stage. The 2.75" conflat (#57) mounts an ion gauge. The 8" conflat (#48) is used for pumping of the first differential stage by a Balzers TPU 330 l/s turbomolecular pump. Since the inlet flange on this pump is on a 6" OD conflat, a reducing flange must be used. The larger than necessary flange was incorporated to make the first differential pumping stage more accessible from outside the apparatus.

V.D.3. Second differential pumping stage

The last compartment welded into the triply-differentially pumped detector is the second differential pumping stage. This chamber is located between the first differential pumping stage and the Detector side wall of the primary welded assembly and extends from the bottom plate of the detector chamber to the Top wall of the primary welded assembly. The chamber extends to the main chamber Top wall because the third differential detector stage (ionization stage) mounts onto flange #1 and extends through the second stage down to the beam height and below.

Five conflat flanges and one specially machined flange on the Detector side wall of the primary welded assembly lead into the second differential pumping stage. The 10" OD conflat (#47) is an access port into the second stage from outside the apparatus. There are four 2.75" OD conflats, flange #58 is used for rough pumping of the second differential pumping stage, flanges #59 and #61 serve as electrical feedthroughs for the mass spectrometer, and flange #60 is used as a port for an ion gauge. The special flange (#46) is used to mount the quadrupole mass spectrometer. The flange design is similar to the DN160ISO flange manufactured by Balzers, an aluminum wire seal flange. This type of flange allows for better alignment than a conflat type flange. The face of this flange is precision machined exactly perpendicular to the face of the stationary source flange at a horizontal distance of 17.906" from the axis of rotation

of the rotatable source. The bore of this flange is machined to intersect the bore of stationary source flange and the axis of rotation of the rotatable source. A 0.385" deep locating step is machined on the flange to assure proper alignment of the third differential pumping stage with the quadrupole mass spectrometer assembly.

As mentioned earlier, flange #1 extends through the Top plate of the primary welded assembly into this chamber. It is also a aluminum wire-sealed flange. Again, this type of flange is used because of its superior alignment capabilities. The third differential pumping stage bolts to this flange. This flange is smaller than the quadrupole mounting flange, but is similar to the Balzers DN100ISO flange. The face of the flange is machined exactly perpendicular to the quadrupole mounting flange at a vertical distance of 26.125" above the scattering height. The bore of this flange is located exactly 11.500" from the axis of rotation of the rotatable source in the horizontal direction. A precision locating step is counterbored to ensure positional alignment and a 1/4" dowel pin hole is machined into the flange to provide rotational alignment of the mounted flange. Details of the ionization assembly will be provided in a future thesis.

There are openings from this chamber to the main chamber, chopper chamber, and the first differential pumping stage. Only one of these opening is precision machined. It is the opening between the first and second stages. An insert onto which the collimation slit between the first and second differential stages is machined fits tightly into this opening. The back side (toward the main chamber Detector side wall) of this plate is spot faced to be exactly parallel to the face of the quadrupole mounting flange, 10.249" from it. Again, a locating step is also machined at this opening to assure alignment of the collimation slit insert. Eighteen 6^{32} through tapped holes are used to secure the insert in place.

V.D.4. Multi-Photon Ionization Detection

In addition to the capability of electron impact ionization, the detector chamber has been designed to incorporate the capability of photoionization of molecules scattered or desorbed from the surface. The ionizing radiation will enter the chamber through a window mounted on the 4.5" OD conflat flange (# 4) which enters through the Top wall of the primary welded assembly. The bore of this flange is directed to a position in between the crystal scattering position and the front face of the welded assembly of the detector. Figure 4.11 shows a schematic drawing of the detector in the MPI configuration. A compartment is bolted onto the front plate of the detector. Note that this removable compartment encases both the openings through the front plate of the detector to the chopper chamber and the first differential pumping chamber. The opening from the chopper chamber to the removable compartment is left open, allowing the chopper chamber to be used as a differential pumping stage during MPI experiments. A collimation aperture on the front of the removable compartment defines the acceptance angle of the MPI detector. A second compartment, which holds a second collimating aperture and is referred to as the ionization and field-free drift region, bolts into the opening between the compartment and the first differential pumping chamber. Molecules whose trajectories are not directly aligned with the second collimation aperture do not enter the ionization and field-free drift region and are pumped away through the chopper chamber. Molecules which do enter the ionization region will intersect the laser beam. Holes in the removable compartment and the ionization and field-free drift region compartment allow the laser radiation to enter from above and exit each compartment from below. Molecules which are not ionized are pumped away by any of the first, second, and third stage pumps. The ionized molecules drift down the field free region until they are detected by a channeltron or multichannel plates which are secured into place using the tapped holes surrounding the opening between the first and second stages pumping stages.

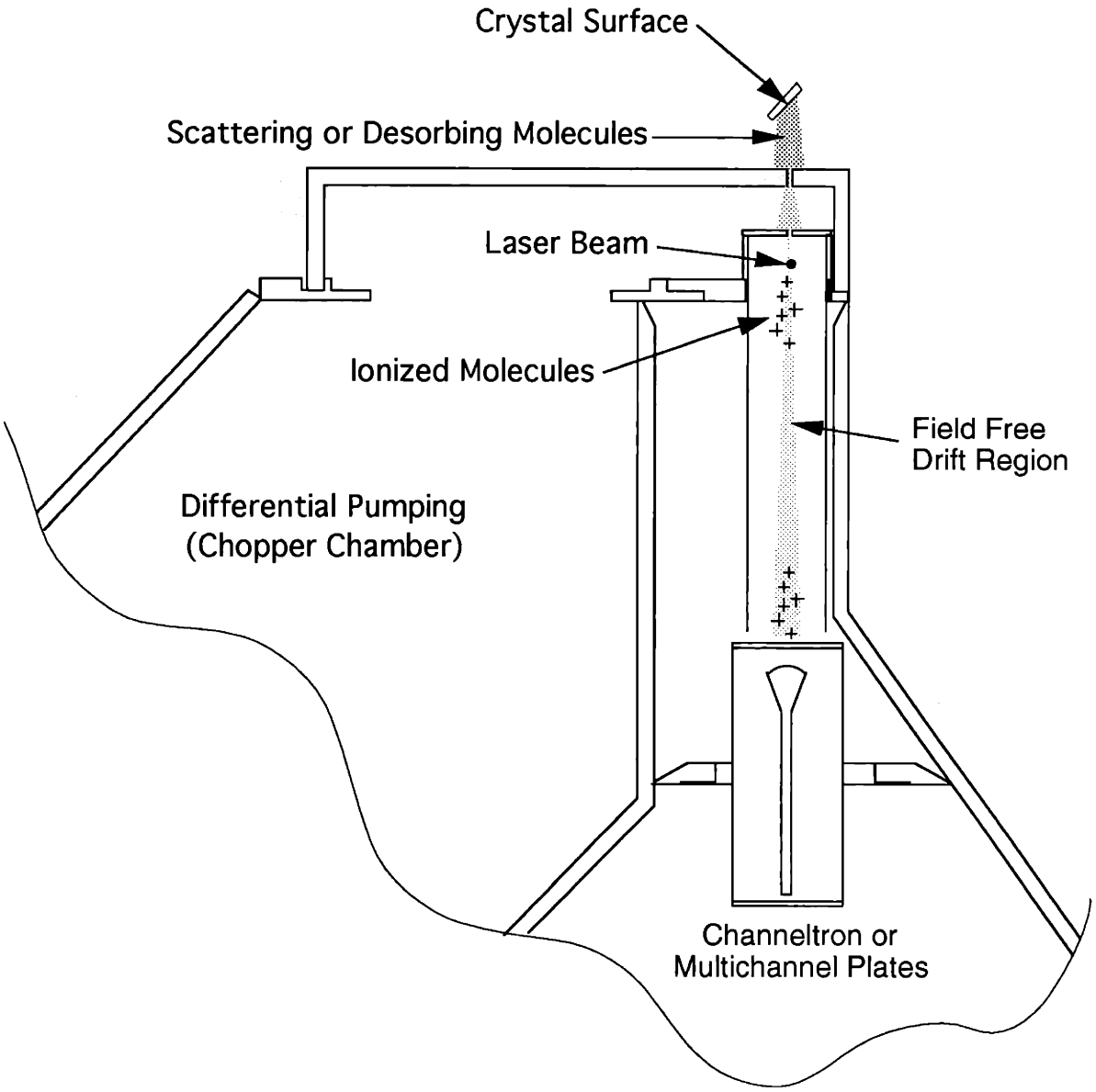

Figure 4.11. Schematic drawing showing the detector in the MPI configuration.

VI. References

1. M. McGonigal, Ph. D. Thesis, Massachusetts Institute of Technology, 1989.
2. M. T. Schulberg, Ph. D. Thesis, Massachusetts Institute of Technology, 1990.
3. S. L. Tang, Ph. D. Thesis, Massachusetts Institute of Technology, 1985.
4. M. B. Lee, Ph. D. Thesis, Massachusetts Institute of Technology, 1987.
5. B. W. Rossiter and R. C. Baetzold, ed., *Investigations of Surfaces and Interfaces-Part A*, Physical Methods of Chemistry Series, 2nd ed., Vol IXA, New York: John Wiley & Sons, 1993.
6. J. D. Beckerle, Q. Y. Yang, A. D. Johnson and S. T. Ceyer, Surf. Sci. **195**, 77 (1988).
7. Q. Y. Yang, A. D. Johnson, K. J. Maynard and S. T. Ceyer, J. Am. Chem. Soc. **111**, 8748 (1989).
8. Q. Y. Yang, K. J. Maynard, A. D. Johnson and S. T. Ceyer, J. Chem. Phys. **102**, 7734 (1995).
9. A. Zangwill, *Physics at Surfaces*, Cambridge: University Press, 1988.
10. H. Ibach and D. L. Mills, *Electron Energy Loss Spectroscopy and Surface Vibrations*, New York: Academic Press, 1982.
11. H. Ibach, Surf. Sci. **66**, 56 (1977).
12. J. H. Moore, C. C. Davis and M. A. Coplan, *Building Scientific Apparatus*, Reading: Addison-Wesley Publishing Co., 1989.
13. R. G. Greenler, J. Chem. Phys. **44**, 310 (1966).